STRUCTURAL AND SPECTROSCOPIC INVESTIGATIONS OF HALOGENO COMPLEXES OF IRIDIUM(III) AND IRIDIUM(IV)

A thesis
submitted in partial fulfilment
of the requirements for the Degree
of
Doctor of Philosophy in Chemistry
in the
University of Canterbury

by

D.A. Rankin

University of Canterbury
1978

ACKNOWLEDGEMENTS

I would like to thank my two supervisors of studies, Dr J.E. Fergusson and Professor B.R. Penfold, for their invaluable advice and guidance throughout this work. Also, I would like to thank my fellow postgraduate students and members of the staff of the University of Canterbury who have given me advice and assistance in this work. Finally, my thanks go to my parents and my wife who have encouraged me in furthering my studies. I acknowledge the financial assistance provided by a Teaching Fellowship at this University for part of my course of study.

CONTENTS

ABSTRACT

This thesis reports the results of some structural and spectroscopic studies performed on a number of crystalline chloro and bromoiridate(III) and (IV) complexes. The crystal and molecular structures of $K_3[IrCl_6]$, $K_3[IrCl_6]H_2O$, $(NH_4)_3[IrCl_6]H_2O$, $Rb_3[IrBr_6]H_2O$, $Cs_2[IrCl_5(H_2O)]$ and $[N(CH_3)_4]_3[Rh_2Br_9]$ have been determined using single crystal X-ray diffraction methods. Infrared and Raman, ultraviolet-visible and nuclear quadrupole resonance spectroscopic studies of these and other halogenoiridate(III) and (IV) complexes have been undertaken. In studying the preparative chemistry of Ir(III) halogeno compounds, and the interrelation of these with Ir(IV) compounds, the new complexes $A_3[Ir_2X_9]$ (A = univalent cation, X = Cl, Br) have been isolated.

Unit cell parameters and space groups have been determined for most of the complexes prepared using both single crystal and powder X-ray diffraction techniques, and isomorphism between these complexes has been studied and compared with stoichiometrically related complexes of other transition metal ions. The influence of the cations on the formation of particular structures for the complex salts has been discussed. A notable feature of the structures of halogenoiridate(III) compounds reported is the distortion of the halogenoiridate(III) anions from their ideal molecular point symmetry. This contrasts with the regular octahedral symmetry retained by the

hexahalogenoiridate(IV) anions in their $A_2[MX_6]$ salts. The cause of this distortion has been attributed to crystal packing effects.

Low frequency infrared spectroscopic studies have been performed on all the complexes isolated and observed spectra have been interpreted with the aid of factor group analyses. This has proved useful in explaining the complexity of many of the observed spectra.

Previously reported nuclear quadrupole resonance data on a number of hexachloroiridates(III) have been reinterpreted in the light of the structures determined in this work and a further study has been made of the structural phase transitions that some of these complexes undergo below room temperature. The reported nuclear quadrupole resonance data are consistent with the reported structures and give further evidence for the unsymmetrical crystal environment and distortion of the hexachloroiridate(III) anions in the solid state.

The diffuse reflectance spectra of a number of crystalline halogenoiridate(III) and (IV) complexes are also reported and interpreted.

ABBREVIATIONS

IR	infrared
R	Raman
L.A.	Refers to a low frequency infrared spectrum recorded at 179 K
RES.	resolution
P D F Card No.	Identification number of card contained in the X-ray Powder Data File published by the American Society for Testing Materials
Me_4N	tetramethylammonium
Et_4N	tetraethylammonium

LIST OF FIGURES

LIST OF TABLES

CHAPTER 1

INTRODUCTION

The halogeno complexes of iridium(III) and iridium(IV) have been studied intermittently over the past eighty years and include kinetic studies of species formed in aqueous solutions and spectroscopic and structural studies of a number of compounds in the solid state. The majority of structural and spectroscopic studies have been confined to the cubic hexahalogenoiridate(IV) salts of stoichiometry $A_2[IrX_6]$ (A = univalent cation, X = Cl, Br) and a few isolated spectroscopic studies have been reported for hexahalogenoiridate(III) complexes. No comprehensive study of the structures of the halogenoiridate(III) complexes has been reported.

The halogenometallate(III) complexes of rhodium and ruthenium on the other hand have been studied in more depth, and a number of crystal structures reported of salts which contain the ions $[MX_6]^{3-}$ (X=Cl,Br)[1-4,14] $[MCl_5(H_2O)]^{2-}$ [5-8,14], $[MCl_4(H_2O)_2]^{-}$ [8-10,14] and $[M_2X_9]^{3-}$ (X = Cl,Br)[8;11-14] where M = Ru, Rh together with univalent cations. A similar chemistry of osmium is almost entirely lacking.

In this thesis the preparative, structural and spectroscopic studies are reported on a number of halogenoiridate(III) and (IV) complexes containing the $[IrX_6]^{3-}$ (X = Cl, Br), $[IrCl_5(H_2O)]^{2-}$, $[Ir_2X_9]^{3-}$ (X = Cl,Br), $[IrCl_6]^{2-}$

species with univalent cations such as K^+, NH_4^+, Rb^+, Cs^+ and $N(CH_3)_4^+$ (and in one case a trivalent cation, $[Co(NH_3)_6]^{3+}$). The work is divided into three major sections preparative, structural and spectroscopic and a review of previous work (where applicable) is presented in each chapter prior to a discussion of the present results.

The preparation of iridium(III) and iridium(IV) halogeno complexes is discussed in Chapter 2. The majority of complexes isolated were prepared by reported methods although in some cases some reported compounds have not been confirmed or have been incorrectly formulated. A number of new diiridate(III) complexes of stoichiometry $A_3[Ir_2X_9]$ (X = Cl, Br; A = univalent cation) have been isolated.

In Chapters 3 and 4 the single crystal X-ray diffraction crystal structures of some representative structural types of the halogenoiridate(III) and (IV) complexes have been determined. The structures of $K_3[IrCl_6]$, $K_3[IrCl_6]H_2O$, $(NH_4)_3[IrCl_6]H_2O$, $Rb_3[IrBr_6]H_2O$, $Cs_2[IrCl_6]$, $Cs_2[IrCl_5(H_2O)]$ and $[N(CH_3)_4]_3[Rh_2Br_9]$ are reported as well as structural data on other halogenoiridate(III) and (IV) complexes. The structural types of these complexes, their isomorphism to related transition metal ion complexes and the distortions of their anions away from ideal molecular point symmetry in the solid state are discussed in each chapter. A discussion of some structural aspects of salts containing the diiridate (III) $[Ir_2X_9]^{3-}$ (X = Cl,Br) species and other related tervalent transition metal ion complexes is presented in Chapter 4, primarily to establish the presence or absence

of Ir-Ir bonding in the diiridate(III) anion (such metal-metal bonding is found in the complex ditungstate(III) anion, $[W_2Cl_9]^{3-}$).

The Chapters 5,6 and 7 are devoted to a discussion of results of far infrared and Raman spectra, nuclear quadrupole resonance spectra (including a reinterpretation of previous data), and ultraviolet-visible spectra respectively. Extensive use has been made of the structural data reported in Chapters 3 and 4 to interpret the vibrational and nuclear quadrupole resonance spectra.

In Chapter 8 a brief review is given of some aspects of the present results particularly in relation to the properties of other halogenometallate(III) and (IV) and dimetallate(III) complexes.

The experimental procedures in X-ray structure determinations and the physical methods used in the present work are detailed in Chapter 9. An appendix consists of the structure factor tables for the seven crystal structures determined.

CHAPTER 2

THE PREPARATION OF IRIDIUM(III) AND IRIDIUM(IV) HALOGENO-METALLATE COMPLEXES

2.1 INTRODUCTION

A number of iridium(III) and iridium(IV) halogenometallate complexes have been reported in the literature since the first reports in the 1800's. A brief survey of the preparation of the halogenoiridate(III) and (IV) complexes will be presented followed by a discussion of aspects of halogeno-iridate(III) preparative chemistry that have arisen out of the present work. The preparative details are given at the end of the chapter.

2.2 A BRIEF SURVEY OF THE PREPARATIONS OF IRIDIUM(III) AND (IV) HALOGENO COMPLEXES

The preparations of a number of hexachloroiridate(IV) salts of univalent cations with stoichiometries $A_2[IrCl_6]6H_2O$ (A = Li, Na) and $A_2[IrCl_6]$ (A = K, NH_4, Rb, Cs) were reported in the early 1900's[15,16,17,18,19].

Both the lithium and sodium salts were prepared by chlorination of a mixture of iridium metal and their respective alkali metal chloride salt at 300°C and extraction of the product in water. The remaining salts were prepared by the replacement of sodium in $Na_2[IrCl_6]6H_2O$ with other

cations. More recently reported preparations of hexachloroiridates(IV) use the same routes[20-27] or with slight modifications. A number of salts containing complex organic cations have also been prepared from $(NH_4)_2[IrCl_6]$[28]. Aquation of the $[IrCl_6]^{2-}$ anion has been observed, but to date no salts of the species formed in solution have been reported[29]. The species in solution have also been prepared by oxidation of corresponding iridate(III) aqua complexes.

Hexachloroiridate(III) salts $A_3[IrCl_6]$ (A = Na, K, NH_4), $A_3[IrCl_6]12H_2O$ (A = Li, Na), $A_3[IrCl_6]H_2O$ (A = K, NH_4, Rb, Cs) have been prepared by a number of workers[2, 16, 19, 21, 24, 25, 30, 31, 32, 33] primarily by reduction of the corresponding hexachloroiridates(IV) using a variety of reducing agents (e.g. ferrous ions[30], oxalate ions[24,25,34], aqueous hydrogen sulphide[21,35] and other reducing agents[21, 24, 36, 37, 31, 38, 39]) or by metathesis from potassium or sodium hexachloroiridate(III) salts and the appropriate ACl salts. The pentachloroaquairidate(III) salts $A_2[IrCl_5(H_2O)]$ (A = K, NH_4, Rb, Cs) have been isolated from the reduction of hexachloroiridates(IV) with oxalate[24,25,16] and with N,N' dimethylpiperazine[31]. The formation of the pentachloroaqua species in preference to the hexachloroiridate (III) ion is dependent on reaction conditions (e.g. the concentration of the chloride ions, age of the solutions, method of recrystallisation of the complex) and is essentially independent of the reducing agent used. A number of aquation and anation studies have been made on the $[IrCl_6]^{3-}$ anion and aquation products of this anion[24,29,39,40,41,42,43] but

although the $[IrCl_5(H_2O)]^{2-}$ and $[IrCl_4(H_2O)_2]^-$ species have been characterised in solution only salts of the pentachloroaquairidate(III) species have been isolated. The complex $[N(CH_2CH_2NH_3)_3][IrCl_6]3H_2O$ has been prepared by reacting $IrCl_3 3H_2O$ with 6M HCl and $[N(CH_2CH_2NH_3)_3]Cl_3$ [44]. It is reported[32,33,45] that chlorination of a mixture of NaCl and Ir metal at 800°C produces $Na_3[IrCl_6]$ and followed by extraction in water produces the efflorescent dodecahydrate $Na_3[IrCl_6]12H_2O$ which on standing gives the decahydrate $Na_3[IrCl_6]10H_2O$ (which is also produced by exposing hygroscopic $Na_3[IrCl_6]$ to a moist atmosphere[16]). Other workers have reported that chlorinations over the temperature range 300°C to 625°C produce $Na_2[IrCl_6]$[16,46] which when crystallised from water gives $Na_2[IrCl_6]6H_2O$. While the preparation of an Ir(III) salt by a chlorination procedure appears unusual, it should be noted that the reaction was carried out at a higher temperature and furthermore other iridium(III) compounds (e.g. $\alpha IrCl_3$, $\beta IrCl_3$, $IrBr_3$) are prepared by direct combination of elements at 600°C[23, 46, 47, 48, 49, 50]. The compound $Na_3[IrCl_6]$ could be produced in a disproportionation reaction similar to that postulated to explain the thermal decomposition of $K_2[IrCl_6]$ [27] above 600°C.

$$\text{i.e. } 3K_2[IrCl_6] \xrightleftharpoons{\Delta} 2K_3[IrCl_6] + Ir + 3Cl_2$$

In some cases the preparation of Ir(IV) complexes was assured as for example in the preparation of $Na_2[IrCl_6]$ [22],

extraction of the chlorinated Ir/NaCl mixture was achieved using HCl and Cl_2 gas which would oxidise any Ir(III) to Ir(IV) and hence give $Na_2[IrCl_6]6H_2O$ as the product.

A number of hexabromoiridate(III) salts have been reported[20, 34, 36, 44, 51, 52, 53] with the following stoichiometries $Na_3[IrBr_6]12H_2O$, $K_3[IrBr_6]$, $K_3[IrBr_6]4H_2O$, $A_3[IrBr_6]H_2O$ (A = Rb, Cs) and $[N(CH_2CH_2NH_3)_3][IrBr_6]H_2O$. These complexes have been prepared by four routes; reduction of a hexabromoiridate(IV) complex[36], treatment of iridium hydroxide compounds with HBr and an appropriate counter cation bromide salt[52], bromination[a] by HBr solution of hexachloroiridate(III) analogues[51,53] and in the case of $[N(CH_2CH_2NH_3)_3][IrBr_6]H_2O$ treatment of a potassium oxalate complex with the counter cation $N(CH_2CH_2NH_3)_3Cl_3$ salt in 9M HBr[44]. Pentabromoaquairidates(III) of K^+ and Rb^+ have been isolated by aquation of their respective hexabromoiridate (III) complexes[52]. Delépine-Tard[52] has reported the isolation of a complex salt $Cs_5[Ir_3Br_{14}]2H_2O$, postulated to contain a triiridate(III) anionic species composed of three edge shared $[IrBr_6]$ octahedra.

Blue hexabromoiridate(IV) salts of K^+, NH_4^+, Rb^+, Cs^+ have been reported and their preparations have normally involved exhaustive treatment of their corresponding hexachloroiridate(IV) complexes with HBr solutions[53,54] Some hexabromoiridate(IV) salts of complex organic cations

[a] Use of the word "bromination" here and in the following text refers to treatment with 63% or 48% HBr (not to treatment with bromine).

have been prepared by oxidation of $IrBr_3$ (with the appropriate quaternary ammonium halide in a solution of benzene) by atmospheric oxygen[28].

2.3 RESULTS AND DISCUSSION OF PREPARATIVE AND SOLUTION CHEMISTRY OF IRIDIUM(III) AND (IV) HALOGENOMETALLATES

2.3.1 The Preparation of Complexes in the Present Work

Other than the use of cation exchange, the preparations of the majority of salts of iridium(III) and (IV) complexes prepared in this work were achieved using reported methods. Potassium oxalate was used extensively to effect the reduction of Ir(IV) to Ir(III), and cation exchange was used in the preparation of NH_4^+, Rb^+ and Cs^+ chloro and bromo iridate salts from the potassium salts. This avoided otherwise complicated procedures required to remove unwanted cations or prepare complexes in the presence of other cations. It should be pointed out that while reported preparations were used, the complexity of the reactions and mixtures of products was not obvious from reported details. A diagrammatic summary of the compounds isolated, preparative routes and interrelations are given in Figure 2.3.1.

A number of compounds or reaction routes reported previously could not be confirmed in the present work. The complex $K_3[IrCl_6]3H_2O$[35,51] could not be isolated, and the preparative method[37] reported (very briefly) for

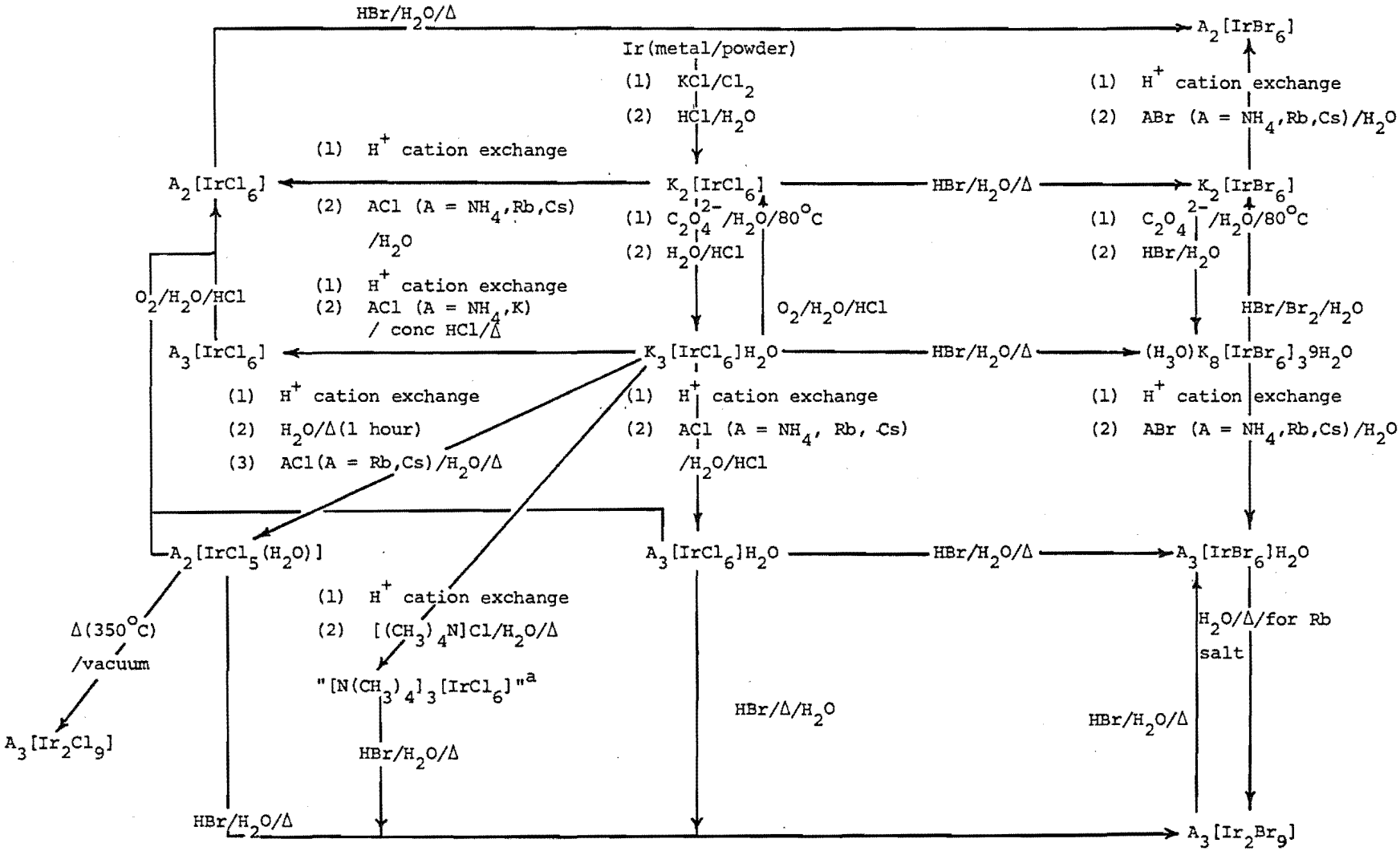

[a] Unknown composition (not isolated).

Figure 2.3.1: Diagrammatic Description of the Preparations and Interrelations of Ir(IV) and (III) Halogeno Complexes

$K_2[IrCl_5(H_2O)]$ (by the reduction of $K_2[IrCl_6]$ with ethanol) yielded $K_3[IrCl_6]H_2O$ only. This is not surprising in view of the chloride ion concentration (4M HCl) used in the reaction. However, the powder photograph of the compound obtained by the authors[37] (PDF 22-826) is nearly identical to that of $K_2[RhCl_5(H_2O)]$ (PDF 22-842) suggesting that the compound isolated was in fact $K_2[IrCl_5(H_2O)]$. Also attempts to reproduce the preparations of $K_2[IrCl_5(H_2O)]$ [25] and $(NH_4)_2[IrCl_5(H_2O)]$[24] by oxalate reduction in aqueous solutions of hexachloroiridate(IV) salts failed, and in each case $K_3[IrCl_6]H_2O$ and $(NH_4)_3[IrCl_6]H_2O$ was obtained. The salt $Cs_2[IrCl_5(H_2O)]$ isolated and characterised by Delépine[16] and suggested by Birnbaum[31] on the basis of analytical data to be a monohydrate (i.e. $Cs_2[IrCl_5(H_2O)]H_2O$) has been found in the present study to be $Cs_2[IrCl_5(H_2O)]$. No hydrated pentachloroaqua salts were found.

A compound described previously as $K_3[IrBr_6]3H_2O$[55] and $K_3[IrBr_6]4H_2O$[52] has now been characterised as $(H_3O)K_8[IrBr_6]_3 9H_2O$ by its isomorphism to a rhodium analogue[4]. The hydroxonium cation in this complex was confirmed by a pH measurement (pH = 3.0 for a solution 0.0013 M in $(H_3O)K_8[IrBr_6]_3 9H_2O$) on an aqueous solution of the compound. As for the rhodium analogue[4] it was assumed no appreciable hydrolysis of the $[MBr_6]^{3-}$ (M = Ir,Rh) species occurred during the period of recording the pH. The salt $K_3[IrBr_6]$[34,53] was not confirmed in the present work, repeated attempts to prepare it by reported methodsalways produced $(H_3O)K_8[IrBr_6]_3 9H_2O$

Attempts to obtain $K_3[IrBr_6]$ by recrystallisation of $(H_3O)K_8[IrBr_6]_3 9H_2O$ from HBr solutions at different concentrations again always produced the starting material. Finally, neither of the salts $K_2[IrBr_5(H_2O)]H_2O$ or $Rb_2[IrBr_5(H_2O)]$ [52] could be isolated by methods described.

The failure to produce some of the above complexes is probably due to incorrect formulations in some cases (especially for some of the complexes reported in the earlier literature, e.g. $K_3[IrBr_6]3H_2O$ or $K_3[IrBr_6]4H_2O$ [52] now reformulated as $(H_3O)K_8[IrBr_6]_3 9H_2O$), but in others the failure probably reflects the complex nature of the solution chemistry of iridium(III) and (IV) halogeno complexes where slight variations in concentrations would alter the product obtained. Fine[56,57] and Broszkiewicz[58] have studied spectroscopically the species present in HCl solutions of $[IrCl_6]^{2-}$ that are responsible for the various colour changes that can be induced by varying conditions of pH, chloride ion concentration, age and temperature. They have produced evidence for the existence of polymeric aggregates (containing hydroxo ligands)in solution even at low pH. However, Fine[56,57] has found that aqueous solutions of $[IrCl_6]^{2-}$ freshly prepared from salts, generally remain stable (i.e. in the form of $[IrCl_6]^{2-}$) for a period of at least 2 hours which is considerably more time than is required to achieve reduction and cation exchange procedures used in the preparations. Ir(IV) solutions have also been reported to undergo spontaneous redox reactions to produce Ir(III)

salts[16,57,59] . This has been observed in this work and will be discussed in Section 2.3.2 below. The other major factor affecting attempts to isolate Ir(III) compounds in the present work is the competition between aquation and anation reactions of the various halogeno species present in solution. The aquation (and reverse anation reaction of the product) of $[IrCl_6]^{3-}$ can be expressed by the equilibrium (equation (2.3.1))

$$[IrCl_6]^{3-} + H_2O \rightleftharpoons [IrCl_5(H_2O)]^{2-} + Cl^- \quad . \qquad (2.3.1)$$

This equilibrium offers an explanation for the failure to prepare both K^+ and NH_4^+ pentachloroaqua salts in the present work. For example $(NH_4)_2[IrCl_5(H_2O)]$ is reported to be slightly more soluble than $(NH_4)_3[IrCl_6]H_2O$ (15.4g/100 ml compared with 10.5 g/100 ml at 19°C [16]) and if $(NH_4)_3[IrCl_6]H_2O$ crystals appeared first there would be less chance of obtaining $(NH_4)_2[IrCl_5(H_2O)]$ from the solution. A similar explanation could apply for the potassium salt. Equation (2.3.1) and related aquation reactions also offer an explanation for the reported impurities present in some commercially available Ir(III) salts[60].

With such competing reactions as well as redox reactions it has proved difficult at times to obtain entirely pure Ir(III) complexes and as outlined above impossible to produce some reported Ir(III) complexes. However, as will be discussed in Section 2.3.4 it has been possible

to isolate most compounds in a reasonably pure state (see Table 2.3.1).

2.3.2 Preparation of Complexes Containing the Diiridate(III) Anions, $[Ir_2Cl_9]^{3-}$ and $[Ir_2Br_9]^{3-}$

The new compounds $A_3[Ir_2Cl_9]$ (A = Rb, Cs) and $A_3[Ir_2Br_9]$ (A = Rb, Cs, $[N(CH_3)_4]$ have been prepared in this work.

The rubidium and caesium salts of tri-μ-chlorohexachlorodiiridate(III) have been prepared by a method similar to that used for analogous rhodium(III) compounds[14] . The K, NH_4, Rb, and Cs pentachloroaqua salts of Rh(III)[14] , Cr(III)[14] and Ru(III)[13] undergo an irreversible dimerisation reaction when heated to about 350°C. The reaction for the iridium complexes was followed by means of differential thermal analysis (DTA) and the DTA curves presented in Figure 2.3.2 indicate that endothermic reactions occurred for $Rb_2[IrCl_5(H_2O)]$ and $Cs_2[IrCl_5(H_2O)]$ at 300°C and 310°C respectively leading to the formation of the diiridate(III) compounds. The reaction may be described by equation (2.3.2) or (2.3.3).

$$3[IrCl_5(H_2O)]^{2-} \xrightarrow{\Delta} [Ir_2Cl_9]^{3-} + [IrCl_6]^{3-} + 3H_2O\uparrow \qquad (2.3.2)$$

$$\text{or} \quad 2[IrCl_5(H_2O)]^{2-} \xrightarrow{\Delta} [Ir_2Cl_9]^{3-} + Cl^- + 2H_2O\uparrow \qquad (2.3.3)$$

The residue obtained was washed with distilled water to remove

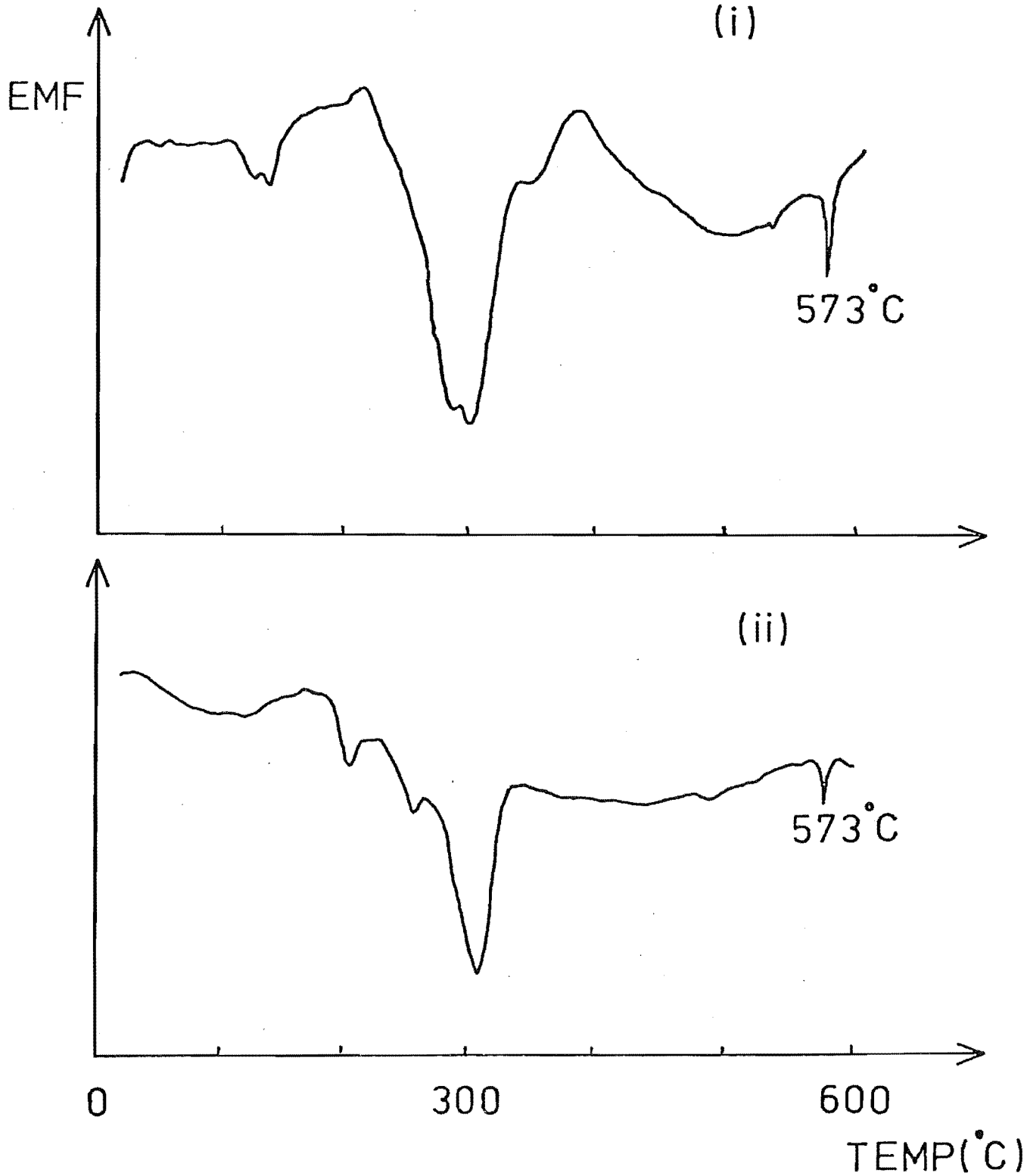

Figure 2.3.2 : High temperature differential thermal analysis (DTA) curves for (i) $Rb_2[IrCl_5(H_2O)]$ and (ii) $Cs_2[IrCl_5(H_2O)]$ (ice water (0°C) and the phase transition in quartz (573°C) are used to calibrate the spectra).

the $A_3[IrCl_6]$ or ACl contaminant. Low frequency infrared spectra suggest that the washing process was only partially successful (see Section 5.5) and also suggest equation (2.3.2) is the most likely course of the thermal decomposition.

Rubidium, caesium and tetramethylammonium tri-μ-bromo-hexabromodiiridate(III) complexes were prepared by exhaustive bromination of either the hexachloro or pentachloroaquoiridate(III) salts. In the case of the Rb^+ and Cs^+ salts the reaction product often consisted of a mixture of the bromodiiridate(III) and hexabromoiridate (III) salts, and in some instances no dimetallate salt was produced at all. In order to obtain pure samples of the bromodiiridate salts small hexagonal crystals of these compounds were separated by hand from the product mixture with the aid of a binocular microscope. Attempts to recrystallise the $[Ir_2Br_9]^{3-}$ salts from HBr solutions led to some formation of hexabromoiridate(III) salts. This presumably arises from a ready interconversion of the diiridate(III) anion and its monoiridate(III) components according to the equation (2.3.4).

$$[Ir_2Br_9]^{3-} + 3Br^- \rightleftharpoons 2[IrBr_6]^{3-} \qquad (2.3.4)$$

A reasonable yield of dimetallate(III) product could be obtained by ensuring a high Ir(III) species concentration in the HBr solution from which the material was recrystallised. The dimeric Rb^+ and Cs^+ salts were found to be insoluble in dichloromethane and glacial acetic acid and only very

slightly soluble in dimethylsulphoxide and acetonitrile and attempts to recrystallise the compounds from the latter two organic solvents also failed to produce crystals large enough for a single crystal X-ray diffraction study.

The rubidium salt, $Rb_3[Ir_2Br_9]$, was also obtained by heating under reflux a sample of $Rb_3[IrBr_6]H_2O$ in deionised water, over a period of six hours. An insoluble material appeared which was identified as $Rb_3[Ir_2Br_9]$. This is in accord with the overall equation (2.3.4) above (as can be seen from the sum of reactions (2.3.5) and (2.3.6) below) and would suggest that formation of the diiridate species may also occur via aquated intermediates.

$$\text{i.e. } 2[IrBr_6]^{3-} + 2H_2O \rightleftharpoons 2[IrBr_5(H_2O)]^{2-} + 2Br^- \qquad (2.3.5)$$

$$2[IrBr_5(H_2O)]^{2-} \rightleftharpoons [Ir_2Br_9]^{3-} + Br^- + 2H_2O \qquad (2.3.6)$$

$$[Ir_2Br_9]^{3-} + 3Rb^+ \rightarrow Rb_3[Ir_2Br_9]\downarrow \qquad (2.3.7)$$

In this scheme an important driving force for the preparation of the diiridate(III) salt could be its high lattice energy [61] as is evident in its low solubility. Further evidence for the reactions (2.3.5)-(2.3.7) comes from a study of $Cs_3[Ir_2Br_9]$ in water. A sample of this compound which dissolved after boiling in deionised water had a visible absorption spectrum with a maximum at 415 nm. The absorption spectrum of $[IrBr_6]^{3-}$ in deionised water (measured immediately after dissolution) contains two

bands at 377 nm and 438 nm while after boiling for one hour has only one absorption maximum at 415 nm, suggesting the same product as obtained from the diiridate(III) salt.

In view of the existence of the diiridate(III) anion $[Ir_2Br_9]^{3-}$ it is possible that the complex $Cs_5[Ir_3Br_{14}]2H_2O$ reported by Delépine-Tard[52] contains $Cs_3[Ir_2Br_9]$ contaminated with $Cs_3[IrBr_6]H_2O$.

2.3.3 The Problem of Oxidation Occurring in the Preparation of Iridium(III) Complexes

In addition to the equilibrium found between hexabromoiridate(III) and nonabromodiiridate(III) complexes, oxidation of Ir(III) was also encountered. For example when a stream of air was used to facilitate solvent evaporation from solutions containing Ir(III) chloro species it was found that considerable oxidation was occurring leading to the formation of Ir(IV) compounds (equation (2.3.8)).

$$4[IrCl_6]^{3-} + 4H^+ + O_2 \rightarrow 4[IrCl_6]^{2-} + 2H_2O \qquad (2.3.8)$$

This reaction has been postulated previously in both acidic and neutral aqueous solutions[16, 28, 56, 59]. In basic media (pH > 11) Fine[57] has found that the reverse reaction (equation (2.3.9)) occurs with the liberation of oxygen.

$$2[IrCl_6]^{2-} + 2OH^- \rightarrow 2[IrCl_6]^{3-} + \tfrac{1}{2}O_2 + H_2O \qquad (2.3.9)$$

In both neutral and acidic media Cabral[59] and Fine[56] have suggested that equation (2.3.9) can be represented as an equilibrium reaction and explains the partial oxidation for example of $Na_3[IrCl_6]$ in 12M HCl[56], complete oxidation occurs with aging or heating the solution. Standard reduction potentials[62] give $E^o = 0.209V$ for the reaction described by equation (2.3.8).

The atmospheric oxidation process was probably largely responsible for the presence of Ir(IV) impurities in the prepared Ir(III) compounds. For example, the presence of $K_2[IrBr_6]$ impurities in $(H_3O)K_8[IrBr_6]_3 9H_2O$, which was observed using a binocular microscope as small blue-black octahedra on the large green crystals of the Ir(III) salt, was also detected when the ultraviolet-visible absorption spectrum was measured in deionised water. As well as the two expected absorption bands of the $[IrBr_6]^{3-}$ species the spectrum contained peaks that were exactly the same as those found for the $[IrBr_6]^{2-}$ species obtained by dissolving $K_2[IrBr_6]$ in deionised water. Although calculations using predetermined extinction coefficients revealed that the $[IrBr_6]^{3-}$ solution in fact contained no more than 1% (in terms of concentration) of $[IrBr_6]^{2-}$, the absorbance values of the absorption bands were all of the same order of magnitude because of the high extinction coefficients of the charge transfer bands of the $[IrBr_6]^{2-}$ species.

It was found that during the reaction

$$[IrCl_6]^{3-} + 6Br^- \rightarrow [IrBr_6]^{3-} + 6Cl^- \qquad (2.3.10)$$

using commercially available HBr solution some oxidation of Ir(III) occurred, the oxidant in this case being the small amounts of bromine dissolved in the HBr solution.

$$2[IrCl_6]^{3-} + Br_2(aq) \rightarrow 2Br^- + 2[IrCl_6]^{2-} \qquad (2.3.11)$$

$$[IrCl_6]^{2-} + 6HBr \xrightarrow{\Delta} [IrBr_6]^{2-} + 6HCl \qquad (2.3.12)$$

Standard reduction potentials[62] predict a spontaneous reaction for equation (2.3.11) $E^{\circ} = 0.067V$. The formation of $[IrBr_6]^{3-}$ may occur before oxidation (shown in equation (2.3.11)) and assuming oxidation of the $[IrBr_6]^{3-}$ can still take place the overall result will be the same. When hydrobromic acid purified by removal of bromine was used in the reactions oxidation was not observed. Furthermore, addition of small amounts of bromine to aqueous solutions of $[IrCl_6]^{3-}$ or $[IrBr_6]^{3-}$ produced the corresponding $[IrCl_6]^{2-}$ and $[IrBr_6]^{2-}$ complexes immediately.

2.3.4 Characterisation of Complexes

Preparations of complexes in this work often resulted in mixtures of products and to obtain pure samples and identify components of these mixtures a number of physical

and structural techniques were employed. Previously reported preparations usually gave a good idea as to what products could be expected from certain reactions and the following procedure for characterisation of products was used.

A sample of crystals of the same morphology, as viewed with a binocular microscope, was collected and a powder diffraction photograph taken of a portion of the sample. From the remaining sample a single crystal (where possible) was selected for both precession and Weissenberg X-ray diffraction studies in order to determine unit cell dimensions and other crystal data. In conjunction with measured densities and powder diffraction photographs and in some cases complete single crystal X-ray structure determinations, the stoichiometry of the complexes could normally be readily assigned.

All of the green Ir(III) halogenoiridate complexes prepared in this work (except the $[Co(NH_3)_6]^{3+}$ salts for which no Rh(III) analogues are yet reported) have isomorphous Rh(III) counterparts[8] and extensive use has been made of powder photographs of these complexes[63] in characterisation of the Ir(III) analogues. Hexahalogenoiridates(IV) isolated crystallise in the cubic space group Fm3m and could be identified from reported powder diffraction patterns. When these were not available powder photographs could be identified as being those of the face centred cubic system on the basis of $\sin^2\theta/\sin^2\theta_1$ ratios (see page 102)for all observed

reflections and their similarity in terms of line positions to related isostructural complexes. The notable simplicity of the powder photographs of these compounds and their colour also helped in characterisation of these Ir(IV) salts.

Because of the limitations of powder photography in the characterisation of complexes and to provide further crystal data compounds have been studied using single crystal X-ray diffraction techniques wherever possible. This provided unit cell data, the stoichiometry of the complex (via density measurements) and helped determine any isomorphism (or isostructural relationships) between compounds. Full single crystal X-ray structure determinations have been made for some compounds which allows precise determination of their stoichiometry and that of isomorphous (or isostructural) compounds. In cases where suitable single crystals of compounds could not be obtained X-ray powder diffractometry was used on well defined crystalline material to determine unit cell parameters and again assist in characterisation of the complexes.

The principal means by which the compounds studied in this work have been characterised are listed in Table 2.3.1. More complete structural information on these complexes is given in Chapters 3 and 4 and complementary spectroscopic data is given in Chapters 5 and 7.

Characterisation of these complexes by the above means was adopted because of the unreliability of halide analyses that were attempted (gravimetric determination

Table 2.3.1: Complexes Prepared and the Principal Means of Characterisation

Technique / Complex	Powder Photography (P.D.F. card no.)	X-ray Powder Diffractometry	Single Crystal X-ray Diffraction Study	Single Crystal X-ray Structure Determination
Ir(IV) Complexes	$K_2[IrCl_6]$ (25-648)			
	$(NH_4)_2[IrCl_6]$ (25-37)			$Cs_2[IrCl_6]$
	$Rb_2[IrCl_6]$ (18-1111)			
	$K_2[IrBr_6]$			
	$(NH_4)_2[IrBr_6]$			
	$Rb_2[IrBr_6]$ (18-1110)			
	$Cs_2[IrBr_6]$			
Monoiridate(III) Complexes			$(NH_4)_3[IrCl_6]$	$K_3[IrCl_6]$
			$Rb_3[IrCl_6]H_2O$	$K_3[IrCl_6]H_2O$
		$[Co(NH_3)_6][IrCl_6]$	$Cs_3[IrCl_6]H_2O$	$(NH_4)_3[IrCl_6]H_2O$
		$[Co(NH_3)_6][IrBr_6]$	$Rb_2[IrCl_5(H_2O)]$	$Cs_2[IrCl_5(H_2O)]$
			$(H_3O)K_8[IrBr_6]_3 9H_2O$	$Rb_3[IrBr_6]H_2O$
			$(NH_4)_3[IrBr_6]H_2O$	
			$Cs_3[IrBr_6]H_2O$	
Diiridate(III) Complexes		$Rb_3[Ir_2Cl_9]$		
		$Cs_3[Ir_2Cl_9]$		
		$Rb_3[Ir_2Br_9]$		
		$Cs_3[Ir_2Br_9]$		
		$[N(CH_3)_4]_3[Ir_2Br_9]$		

with Ag^+ ions). Furthermore with experimental errors in these analyses of ± 2% (of the analysis percentage) it was not possible to significantly distinguish between different complexes. These problems are illustrated by examining analytical figures reported in Table 2.3.2 for a number of caesium salts.

Table 2.3.2: Analytical Data for Caesium Halogenoiridate Salts.

Compound	% Theoretical	% Cl Found
$Cs_3[IrCl_6]H_2O$	25.89	
$Cs_3[IrCl_6]$	26.47	
$Cs_2[IrCl_5(H_2O)]$	27.13	25.99,24.60,23.06
$Cs_3[Ir_2Cl_9]$	28.95	
$Cs_2[IrCl_6]$	31.71	29.50,28.14

Pure samples of compounds for spectroscopic and other studies were obtained by using the preparations that follow (Section 2.5) and by collecting crystals contained in the products of the same morphology (with the aid of a binocular microscope). The crystals so obtained (thus allowing removal of unwanted impurities or other crystalline products) were then identified using powder photography. In only a few instances e.g. the preparation of tri-μ-chloro-hexachlorodiiridate(III) and cobaltic(III) hexaammine halogenoiridates(III) was this kind of procedure not possible

as large single crystals were not obtained because of the mode of preparation. In these cases the preparations were designed to minimise the presence of impurities in the final product. Thus, in the majority of cases the presence of Ir(IV) impurities in prepared Ir(III) complexes (or other unwanted Ir(III) complexes) caused no problems as their physical removal from crystalline products meant a reasonably pure sample of most compounds could be obtained.

2.5 PREPARATIONS

Chemical reagents used in the following preparations were commercially available and all but HBr solutions were used without further purification. HBr was purified by removal of dissolved bromine by standing the solution over red phosphorus for twenty four hours and distilling off a constant boiling fraction (48% HBr) at 126°C [64]. When stored in a stoppered dark glass bottle this solution was still free from bromine after two months.

Cation exchange was achieved using a glass column (20 mm internal diameter) with a scintered glass bed containing Dowex 50 W-X8 Cation Exchange Resin to a depth of 90 mm. The column was used in a "prepared" activated hydrogen ion form, prepared by passing 200 mls of 1 M HCl slowly through the column and washing the column with deionised water until acid free.

Products obtained in the following preparations were collected by filtration, washed with acetone and ether and air dried.

Potassium Hexachloroiridate(IV), $K_2[IrCl_6]$

Iridium metal powder (1g) and AR KCl (2g) were intimately mixed and heated in a silica glass boat in a silica tube to 650°C in a tube furnace. A stream of chlorine gas (3 mls/second) was passed over the sample at all times and the temperature was maintained at 650°C for at least one hour[20-26].

The cold residue was extracted (by boiling for five minutes) three times with successive additions of 70 mls of 4 M HCl. After the third extraction the HCl solution would normally be relatively clear. Remaining insoluble material was largely unreacted iridium metal. The combined extracts were then evaporated to 60 mls using an airstream to facilitate evaporation and the solution set aside for crystallisation. Red black crystals were obtained, filtered, washed with acetone and ether, and air dried (yield approximately 60%).

Salts of the Hexachloroiridate(IV) Anion, $A_2[IrCl_6]$ ($A = NH_4$, Rb, Cs)

The salt $K_2[IrCl_6]$ (0.2 g) dissolved in the minimum quantity of deionized water was added to a protonated cation exchange column and the effluent "$H_2[IrCl_6]$" collected. Stoichiometric quantities (2:1 mole ratio of cation to "$H_2[IrCl_6]$") of the appropriate counter cation chloride or carbonate salt dissolved in a minimum quantity of water was added to the effluent. The relatively insoluble Rb^+ and Cs^+ salts formed immediately on mixing, while concentration of the solution was necessary for the ammonium

salt. The compounds were collected, washed and dried as above.

Both $Rb_2[IrCl_6]$ and $Cs_2[IrCl_6]$ were also isolated as by products in the preparations of $Rb_3[IrBr_6]H_2O$ and $Cs_3[IrBr_6]H_2O$ (from atmospheric oxidation).

Potassium Hexabromoiridate(IV), $K_2[IrBr_6]$

Two grams of $K_2[IrCl_6]$ was treated with 50 mls of 63% HBr solution (or 48% HBr solution) and boiled to near dryness. This process was repeated twice. After the third evaporation a further 60 mls of HBr solution was added and the solution evaporated to 20 mls. On cooling the purple product crystallised. The compound was characterised using powder photography (its photograph being similar to that of isostructural $Rb_2[IrBr_6]$, PDF 18-1110).

Salts of the Hexabromoiridate(IV) Anion, $A_2[IrBr_6]$ ($A = NH_4$, Rb, Cs)

The three salts were obtained in an identical manner to the corresponding $A_2[IrCl_6]$ salts, using bromide ABr salts. The salt $Rb_2[IrBr_6]$ was characterised by the reported powder diffraction pattern (PDF 18-1110). The salts $(NH_4)_2[IrBr_6]$ and $Cs_2[IrBr_6]$ were characterised by comparison of their powder photographs to that of isostructural $Rb_2[IrBr_6]$.

These compounds can also be prepared by exhaustive treatment with HBr solution of their corresponding hexachlorometallate analogues $A_2[IrCl_6]$.

Potassium Hexachloroiridate(III) Monohydrate, $K_3[IrCl_6]H_2O$

The complex $K_2[IrCl_6]$ (2g) was heated to near boiling in 60 mls of water to which was added the calculated amount of $K_2C_2O_4.H_2O$ dissolved in water. During reduction CO_2 was evolved and the solution changed colour from brown to yellow-green. A small additional amount of oxalate salt was added to ensure complete reduction. The solution was heated to near dryness and the residue taken up with gentle heat in a minimum quantity of 2 M HCl and set aside for crystallisation. Green crystals which normally appeared after a few days were filtered washed with acetone and ether and air dried.

Salts of Hexachloroiridate(III) Anion, $A_3[IrCl_6]H_2O$ ($A = NH_4$, Rb, Cs)

An aqueous solution of $K_3[IrCl_6]H_2O$ (0.2g) was added to a prepared cation exchange column and the effluent collected. The stoichiometric quantity (3:1) of the required counter cation salt (either chloride or carbonate salt) dissolved in a minimum volume of water was added to the column effluent. The solution was heated to near dryness and the residue redissolved, with gentle heating, in a minimum of 2 M HCl. Green crystals normally appeared in 2 to 5 days.

The quantities used in these preparations can be scaled. However, care must be taken that the capacity of the cation exchange resin is not exceeded. In one preparation of $(NH_4)_3[IrCl_6]H_2O$, a salt of mixed cation content resulted (see Section 3.4.2) presumably because of incomplete cation exchange. This may have arisen from saturation of the column with cations, or an excessive elution rate.

Potassium Hexachloroiridate(III), $K_3[IrCl_6]$ and Ammonium Hexachloroiridate(III), $(NH_4)_3[IrCl_6]$

A sample of $K_3[IrCl_6]H_2O$ (or $(NH_4)_3[IrCl_6]H_2O$) was dissolved with gentle heating in concentrated HCl. In the case of the potassium salt green crystals of anhydrous $K_3[IrCl_6]$ were obtained after a period of 2 to 3 days by slow evaporation of the solvent. For $(NH_4)_3[IrCl_6]$ the HCl solution was evaporated off more rapidly by warming the solution to approximately 35°C. Flat plate-like green crystals appeared once the majority of the solvent had been removed.

Both of the above compounds were characterised by single crystal X-ray diffraction studies in conjunction with a detailed X-ray structure determination of $K_3[IrCl_6]$ (see Section 3.2).

Hexaamminecobaltic(III) Hexachloroiridate(III), $[Co(NH_3)_6][IrCl_6]$

A solution of $K_3[IrCl_6]H_2O$ (0.2g) was eluted on a prepared cation exchange column. The calculated amount

(in a 1:1 mole ratio) of $[Co(NH_3)_6]Cl_3$ dissolved in a minimum quantity of water was added to the column effluent. The yellow brown product precipitated immediately.

Rubidium Pentachloroaquairidate(III), $Rb_2[IrCl_5(H_2O)]$ and Caesium Pentachloroaquairidate(III), $Cs_2[IrCl_5(H_2O)]$

A solution of $K_3[IrCl_6]H_2O$ (0.2g) was eluted in a protonated cation exchange column. A solution of RbCl or Rb_2CO_3 (2:1 moles of Rb^+ to $K_3[IrCl_6]H_2O$) was then added to the effluent and the solution evaporated to near dryness. The residue obtained was boiled gently for 1 hour in 50 mls of water and the solution then decreased in volume to about 0.5 mls. On cooling the green crystalline product would appear.

The complex $Cs_2[IrCl_5(H_2O)]$ was prepared in the same manner but using CsCl instead of RbCl.

To obtain reasonable yields of both complex salts preparations are best attempted so as to produce about 2g of product as the products are relatively soluble.

Rubidium Tri-μ-chlorohexachlorodiiridate(III), $Rb_3[Ir_2Cl_9]$ and Caesium Tri-μ-chlorohexachlorodiiridate(III), $Cs_3[Ir_2Cl_9]$

A sample of crystalline $Rb_2[IrCl_5(H_2O)]$ (or $Cs_2[IrCl_5(H_2O)]$) was heated in a porcelain boat under vacuum at 350°C for 2 hours. The residue was cooled under vacuum, placed in 10 ml of distilled water when cool, stirred vigorously and left to stand for 30 minutes. The insoluble green material was then filtered at the pump, washed with acetone and ether and air dried.

Hydronium Potassium Hexabromoiridate(III) Nonahydrate, $(H_3O)K_8[IrBr_6]_3 9H_2O$

A solution of $K_2[IrBr_6]$ (2.4g) was brought near to boiling point and a solution containing the calculated quantity of $K_2C_2O_4.H_2O$ added in small portions. After evolution of CO_2 gas had ceased the green solution was evaporated down to about 10 mls and set aside to crystallise. Large green crystals were obtained after 2 to 3 days.

This compound can also be prepared by exhaustive bromination of $K_3[IrCl_6]H_2O$ in a manner analogous to the preparation of $K_2[IrBr_6]$ from $K_2[IrCl_6]$.

Salts of the Hexabromoiridate(III) Anion, $A_3[IrBr_6]H_2O$ ($A = NH_4$, Rb, Cs)

These compounds were prepared in a manner similar to that of $A_3[IrCl_6]H_2O$ salts but using $(H_3O)K_8[IrBr_6]_3 9H_2O$ as a starting material and bromide salts of the respective counter cations. The three compounds form green needle-like crystals.

Hexaamminecobaltic(III) Hexabromoiridate(III), $[Co(NH_3)_6][IrBr_6]$

This was prepared using the same method as for $[Co(NH_3)_6][IrCl_6]$ but with $(H_3O)K_8[IrBr_6]_3 9H_2O$ as the starting material.

Rubidium Tri-μ-bromohexabromodiiridate(III), $Rb_3[Ir_2Br_9]$

Method 1. 0.5 grams of $Rb_3[IrBr_6]H_2O$ was dissolved in 35 mls of distilled water and the solution refluxed for 6 hours. During this prolonged heating insoluble material was produced. After cooling this brown material was filtered washed with acetone and ether and air dried. The compound was identified as $Rb_3[Ir_2Br_9]$ from powder photographs and was identical to that diiridate(III) product obtained by the following preparative route.

Method 2. A sample of $Rb_3[IrCl_6]H_2O$ (or $Rb_2[IrCl_5(H_2O)]$ was exhaustively brominated using freshly distilled HBr solution as in the preparation of $K_2[IrBr_6]$ from $K_2[IrCl_6]$. After the third heating to near dryness the residue was redissolved in a minimum of boiling 48% HBr solution and set aside to crystallise. The product obtained was often a mixture of $Rb_3[Ir_2Br_9]$ and $Rb_3[IrBr_6]H_2O$. This could be ascertained by examination of the product under a microscope as $Rb_3[Ir_2Br_9]$ forms small hexagonal plates and $Rb_3[IrBr_6]H_2O$ forms long needle-like crystals. In some cases this method did yield pure $Rb_3[Ir_2Br_9]$.

Caesium Tri-μ-bromohexabromodiiridate(III), $Cs_3[Ir_2Br_9]$

This complex was prepared by bromination of $Cs_3[IrCl_6]H_2O$ or $Cs_2[IrCl_5(H_2O)]$ in the same manner as Method 2 for $Rb_3[Ir_2Br_9]$ This method also produced a mixture of $Cs_3[Ir_2Br_9]$ and $Cs_3[IrBr_6]H_2O$ products and again the difference in crystal morphology allowed physical separation of the two compounds

for characterisation of $Cs_3[Ir_2Br_9]$ by powder photography and an X-ray powder diffractometer study.

If a good yeild of the dimeric compound is obtained in this preparation (as judged by the presence of small hexagonal crystals) the product should be filtered immediately to prevent interconversion of $[Ir_2Br_9]^{3-}$ to $[IrBr_6]^{3-}$.

Tetramethylammonium Tri-μ-bromohexabromodiiridate(III), $[N(CH_3)_4]_3[Ir_2Br_9]$

This complex was prepared by exhaustive bromination of the compound "$[N(CH_3)_4]_3[IrCl_6]$" obtained by addition of a solution of $[N(CH_3)_4]Cl$ to the column effluent obtained from elution of a solution of $K_3[IrCl_6]H_2O$ on a cation exchange column. The compound was characterised by powder photography and a powder X-ray diffractogram.

Reclaimation of residues

Aqueous residues were evaporated to dryness and the solid heated in a stream of air to 700°C for one hour. The cooled material was treated with boiling water* to remove soluble alkali metal halide salts leaving a black material which contained iridium metal (PDF 6-0598) and other compounds probably oxides of iridium. This material could then be chlorinated (as for the iridium metal) to produce $K_2[IrCl_6]$.

* If the aqueous solution became intensely coloured (e.g. from $[IrCl_6]^{2-}$ compounds) initial heating to 700°C was repeated.

CHAPTER 3

STRUCTURAL STUDIES - PART 1. THE CRYSTAL STRUCTURES OF POTASSIUM HEXACHLOROIRIDATE (III), POTASSIUM HEXACHLOROIRIDATE (III) MONOHYDRATE, AMMONIUM HEXACHLOROIRIDATE (III) MONOHYDRATE AND RUBIDIUM HEXABROMOIRIDATE (III) MONOHYDRATE AND RELATED HEXAHALOGENOIRIDATES (III)

3.1 INTRODUCTION

In this chapter the crystal structures of four hexahalogenoiridate (III) salts and a number of other hexahalogenoiridate (III) compounds studied in this thesis will be discussed. The crystal structures reported have been satisfactorily solved using intensity data collected on an automatic Hilger and Watts four circle diffractometer. To avoid unnecessary repetition of experimental methods and procedures involved in data collection and structure analysis common to all four crystal structures, these techniques are discussed in detail in Chapter 9 and can be referred to for clarification of any methods or procedures mentioned.

Each crystal structure will be discussed under the headings; results of preliminary studies, structure solution and refinement, and finally a description of the structure.

No problems were encountered in the determination of the crystal structures of the potassium hexachloroiridate (III)

salts. However, in the case of ammonium hexachloroiridate (III) monohydrate, an initial attempt at structure elucidation failed using data that were collected on what was later found to be a twinned crystal. Data were then collected on an isomorphous compound, rubidium hexabromoiridate (III) monohydrate (the fourth structure discussed in this chapter), and the structure was solved satisfactorily. Intensity data were then recollected on a non-twinned $(NH_4)_3[IrCl_6]H_2O$ crystal, and using the isomorphism between this and the $Rb_3[IrBr_6]H_2O$ structure, the crystal structure of the former compound was finally refined. The remaining sections of this chapter deal with the characterisation of the crystal structures of the other hexahalogenometallate salts studied in this thesis and a general discussion of the distortion from pure octahedral (O_h, m3m) symmetry found in the hexahalogenoiridate (III) anions in these compounds in the solid state.

3.2 THE CRYSTAL STRUCTURE OF POTASSIUM HEXACHLOROIRIDATE (III), $K_3[IrCl_6]$

3.2.1 Preliminary Study and Data Collection

A preliminary study carried out using Buerger precession and Weissenberg photographic techniques established the crystal system as triclinic. The space group was either P1 or $P\bar{1}$. A Delaunay reduction was carried out on the triclinic

cell, but the cell as chosen was found to be completely reduced. Relevant crystal data are given in Table 3.2.1.

A small crystal of suitable quality for data collection was then mounted in a random orientation on a four circle diffractometer. Relevant experimental parameters for data collection and processing are given in Table 3.2.2. Refined cell dimensions obtained were

$$a = 12.631(2)\text{Å},\ b = 7.029(1)\text{Å},\ c = 7.027(1)\text{Å}$$
$$\alpha = 116.12(2)^{\circ},\ \beta = 91.21(9)^{\circ},\ \gamma = 106.88(9)^{\circ}$$

The intensities of 2465 reflections in the hemisphere of reciprocal space $h \geqslant 0$, $-9 \leqslant k, \ell \leqslant 9$ were measured out to a Bragg angle of 27.2° (MoKα radiation). Automatic attenuation was required for a small number of very intense reflections whose count rates exceeded 8000 counts per second.

1550 reflections (0.63 of the total number recorded) such that $F_{obs}^2 \geqslant 3\sigma(F_{obs}^2)$ were finally obtained and these were used in the following structure analysis and refinement.

3.2.2 Structure Solution and Refinement

A three dimensional Patterson synthesis revealed possible locations at (0,0,0) and (0.5, 0, 0.5) for two iridium atoms and indicated the correct space group was $P\bar{1}$. With the iridium atoms located on the special positions

Table 3.2.1: Crystal Data for $K_3[IrCl_6]$

Formula	$K_3[IrCl_6]$
Formula weight	522.224
Crystal system	triclinic
Space group	$P\bar{1}$ (C_i^1, No. 2)
a	12.631(2)Å
b	7.029(1)Å
c	7.027(1)Å
α	116.12 (7)°
β	91.21 (9)°
γ	106.88 (9)°
V	527.8 $Å^3$
z	2
d calculated	3.286 gcm^{-3}
measured	3.284(6) gcm^{-3}
F(000)	472
μ(MoKα)	159.47 cm^{-1}

Table 3.2.2: Experimental Parameters for $K_3[IrCl_6]$ Data Collection.

Temperature	$25^{\circ}C(\pm 1^{\circ}C)$
Radiation	$MoK\alpha(\lambda = 0.7107\text{Å}$ for $MoK\bar{\alpha})$
Scan range	0.80° (0.01° steps)
Scan time	60 seconds
Total background time	30 seconds
Bragg angle limit	27.2°
Incident beam collimator (diameter)	1.0mm
Diffracted beam collimator (diameter)	5.0 mm
Tube take-off angle	3°
Crystal dimensions (maximum)	0.15 mm x 0.23 mm x 0.10 mm
Crystal volume	0.004249 mm^3
Mosaicity	0.15°
Total independent reflections	2465
Reflections used in refinement	1550 (such that $F^2_{obs} \geqslant 3\sigma(F^2_{obs})$)
Ratio observations to variables	1550:90
in least squares refinements	$\approx$ 17:1
Range of transmission factors	0.2739(for 001) - 0.1035(for 3-73)
Weighting parameter p	0.05

suggested by the Patterson map, a trial least squares refinement, with both atoms given isotropic temperature parameters, produced a residual of 0.41. A difference electron density map calculated at this stage revealed six independent chlorine atomic positions, completing the octahedral coordination of chlorine atoms in both the $[IrCl_6]^{3-}$ anions at (0,0,0) and (0.5,0,0.5). Further least squares refinements, again with all atoms isotropic, saw the R factor drop to 0.27. A further difference electron density map revealed positions for 3 potassium atoms. However, after further refinement (all atoms isotropic), where the residual dropped to 0.18, a difference electron density map showed regions of unacceptably high residual density around the iridium atom at (0,0,0).

To clarify this anomaly, least squares refinement was repeated including the 2 iridium atoms, 3 potassium atoms and the chlorine atoms associated with the iridium atom at (0.5, 0, 0.5) but excluding the chlorine atoms associated with the iridium atoms at (0,0,0). All atoms were given isotropic temperature factors. This refinement produced a residual of 0.17 and more significantly, the difference electron density map at this stage revealed two choices of orientation of the $[IrCl_6]^{3-}$ anions located at (0,0,0). The relative heights of those peaks attributed to the chlorine atoms indicated that both orientations were equally favourable.

After the data set had been corrected for absorption, using a numerical technique, least squares refinement was continued, including in the model 3 full weight chlorine

atoms, 6 half weight chlorine atoms, 2 iridium atoms and 3 potassium atoms. After 3 cycles of refinement (all atoms isotropic) the residual, R, dropped to 0.11. A further difference electron density map indicated disorder at 2 of the chosen potassium ion sites and with this taken into account the following model was refined to convergence. It contained two anisotropic iridium atoms each at positions of point symmetry $\bar{1}$. Around the first at (0,0,0) were a disordered octahedral grouping of chlorine atoms generated by two independent sets of three isotropic atoms Cl(1), Cl(2), Cl(3) and Cl(1A), Cl(2A), Cl(3A) each of half weight. Around the second iridium atom at (0.5, 0, 0.5) was an ordered octahedral grouping of chlorine atoms generated by an independent set of three (anisotropic) atoms. There was one full weight potassium ion (K(1)) vibrating anisotropically and two sets of two half weight potassium ions with isotropic temperature factors (K(2), K(3), K(2A), K(3A)). Included in this final refinement were corrections for anomalous dispersion (for the iridium and chlorine atoms) and an extinction parameter to account for a number of strong low angle reflections where F_{obs} was found to be systematically lower than F_{calc}.

After 4 cycles of refinement the model converged with no changes in parameters being greater than 0.01 of their associated estimated standard deviations. The residual, R, was 0.039, the weighted residual, R_w was 0.050. The standard error of an observation of unit weight was 1.634. The weighting scheme was shown, by analysis of

errors over ranges of structure factor magnitudes, sin θ/λ and indices to be quite satisfactory.

The model, at convergence, showed satisfactory temperature factors for all the disordered atoms and it was on this basis that the choice of occupancy factors for the disordered atom sites was chosen and left at 0.5. A list of final atomic parameters are recorded in Table 3.2.3 and final observed and calculated structure factors are listed in Appendix A.

3.2.3 Description of the Structure

Figure 3.2.1 gives an illustration of the unit cell contents of $K_3[IrCl_6]$. The labelling scheme is that used for the atomic coordinates reported in Table 3.2.3. Figure 3.2.2 gives a stereoscopic view of the unit cell, viewed down an axis perpendicular to the ab face of the unit cell as for Figure 3.2.1.

The unit cell contains two independent octahedral $[IrCl_6]^{3-}$ anions, one located at (0.5, 0, 0.5) and one disordered and located at the origin. Both anions have point symmetry $C_i(\bar{1})$. The separations between the disordered pairs of chlorine atoms in the disordered anion at (0,0,0) are as follows; Cl(1)-Cl(1A) 1.953(8)Å, Cl(2)-Cl(3A) 1.318(10)Å, Cl(3)-Cl(2A) 1.322(10)Å. Reflecting the disorder of the $[IrCl_6]^{3-}$ anion at (0,0,0) is the disorder of the potassium ion over the sites K(2), K(3), K(2A) and K(3A). This can be seen by examination of the non bonding contacts reported in Tables 3.2.4 and 3.2.5 for atoms in $K_3[IrCl_6]$. Essentially

Table 3.2.3 : Positional and Thermal Parameters for $K_3[IrCl_6]$

Atom	x	y	z	U or U_{11}	U_{22}	U_{33}	U_{12}	U_{13}	U_{23}
Ir(1)	0.0	0.00	0.0	0.0145(4)	0.0119(4)	0.0134(4)	0.0036(3)	0.0024(3)	0.0058(3)
Ir(2)	0.5	0.0	0.5	0.0149(4)	0.0132(4)	0.0150(4)	0.0032(3)	0.0021(3)	0.0083(3)
Cl(1)	-0.0004(5)	-0.048(1)	0.312(1)	0.024(1)					
Cl(2)	0.1481(6)	-0.346(1)	0.188(1)	0.028(1)					
Cl(3)	-0.1417(6)	0.165(1)	0.100(1)	0.032(2)					
Cl(1A)	-0.0002(5)	-0.311(1)	0.0494(9)	0.021(1)					
Cl(2A)	-0.1475(6)	0.040(1)	0.198(1)	0.030(1)					
Cl(3A)	0.1420(6)	0.243(1)	0.307(1)	0.029(1)					
Cl(4)	0.6164(3)	0.2379(6)	0.3790(6)	0.022(2)	0.032(2)	0.038(2)	0.004(1)	0.006(1)	0.027(1)
Cl(5)	0.6098(5)	-0.235(1)	0.395(1)	0.073(4)	0.067(3)	0.196(7)	0.058(3)	0.091(4)	0.100(4)
Cl(6)	0.3901(5)	-0.215(1)	0.1555(7)	0.072(3)	0.105(4)	0.028(2)	-0.059(3)	-0.028(2)	0.038(2)
K(1)	0.4009(4)	0.2615(9)	0.1391(9)	0.036(2)	0.095(9)	0.101(4)	0.009(2)	0.003(2)	0.080(3)
K(2)	0.1809(5)	-0.272(1)	0.3218(9)	0.026(1)					
K(3)	-0.1847(6)	-0.381(1)	0.331(1)	0.030(1)					
K(2A)	0.1805(5)	-0.140(1)	0.4531(9)	0.026(1)					
K(3A)	-0.1843(5)	0.485(1)	0.197(1)	0.029(1)					

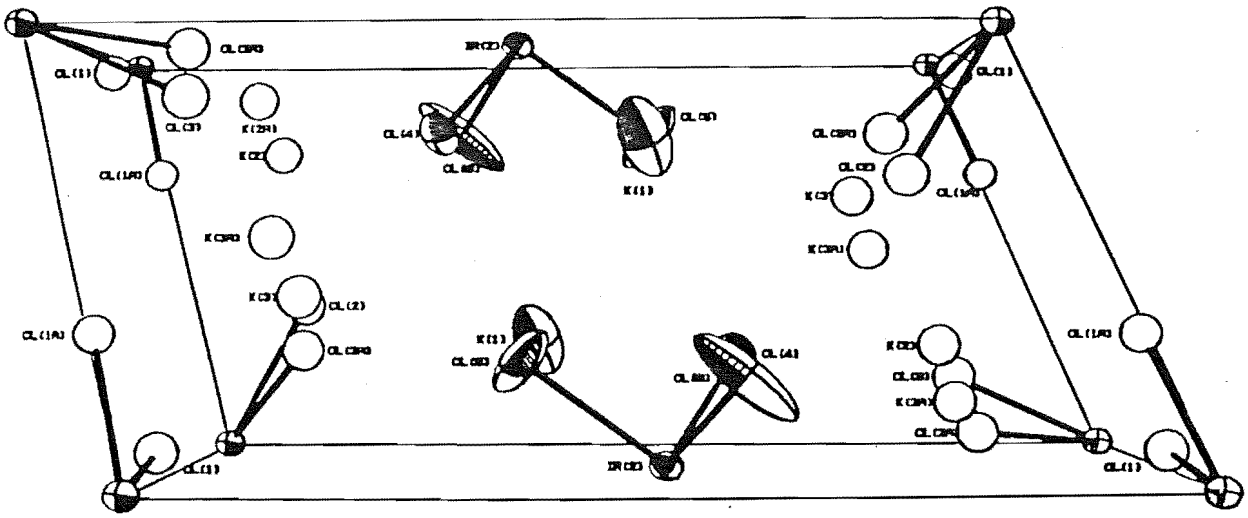

Figure 3.2.1: Projection diagram of the unit cell contents of $K_3[IrCl_6]$ viewed down an axis perpendicular to the ab face.

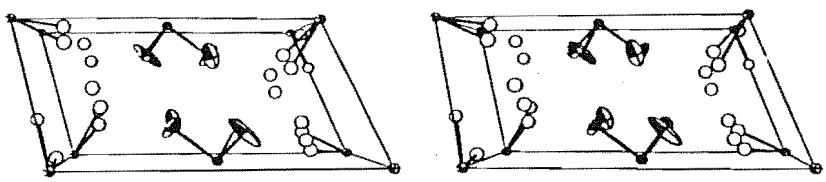

Figure 3.2.2: Stereoscopic view of the unit cell contents of $K_3[IrCl_6]$.

Table 3.2.4: Bond Lengths (Å) and Angles (degrees) in the $[IrCl_6]^{3-}$ Anion in $K_3[IrCl_6]$.

(a) Bond lengths for disordered anions at (0,0,0)

Ir-Cl(1)	2.360(6)	Ir-Cl(1A)	2.360(6)
Ir-Cl(2)	2.363(7)	Ir-Cl(2A)	2.355(7)
Ir-Cl(3)	2.361(7)	Ir-Cl(3A)	2.366(7)
Mean [a]	2.361(4)		

(b) Bond lengths for anion at (½,0,½), including bond lengths corrected for riding motion.

Uncorrected values		Corrected values	
Ir-Cl(4)	2.357(3)	Ir-Cl(4)	2.365(3)
Ir-Cl(5)	2.342(4)	Ir-Cl(5)	2.389(5)
Ir-Cl(6)	2.343(4)	Ir-Cl(6)	2.391(4)
Mean	2.347	Mean	2.382

(c) Angles

Cl(1)-Ir-Cl(2)	89.9(2)	Cl(1A)-Ir-Cl(2A)	90.0(2)
Cl(1)-Ir-Cl(3)	90.5(2)	Cl(1A)-Ir-Cl(3A)	90.5(2)
Cl(2)-Ir-Cl(3)	93.8(2)	Cl(2A)-Ir-Cl(3A)	93.8(2)
Cl(1)-Ir-Cl(1A)	48.9(2)		
Cl(1)-Ir-Cl(2A)	59.8(2)		
Cl(1)-Ir-Cl(3A)	58.6(2)		
Cl(4)-Ir-Cl(5)	89.2(2)		
Cl(4)-Ir-Cl(6)	89.2(2)		
Cl(5)-Ir-Cl(6)	89.0(3)		

[a] Estimated standard deviations (e.s.d.'s) for mean bond lengths were calculated from the expression $\sigma=\sum_{i=1}^{i=N}((\ell_i-\bar{\ell})^2/(N-1))^{\frac{1}{2}}$ where ℓ_i is the i^{th} bond length and $\bar{\ell}$ is the mean bond length.

Table 3.2.5: Potassium Ion Contacts (Å) less than 3.4Å in $K_3[IrCl_6]$.

K(1)...Cl(4)	3.255(5)		
...Cl(6)	3.364(9)		
...Cl(5)	3.367(9)		
...Cl(6)	3.391(8)		
...Cl(5)	3.392(9)		
K(2)...K(2A)	0.979(8)		
...Cl(2)	2.317(9)	K(2A)...Cl(2A)	2.320(9)
...Cl(1A)	2.821(8)	...Cl(1)	2.822(9)
...Cl(6)	2.904(9)	...Cl(5)	2.907(9)
...Cl(1A)	3.119(8)	...Cl(1)	3.106(9)
...Cl(2A)	3.139(9)	...Cl(1A)	3.137(8)
...Cl(1)	3.148(9)	...Cl(2)	3.138(9)
...Cl(4)	3.162(7)	...Cl(4)	3.169(7)
...Cl(3A)	3.253(10)	...Cl(3)	3.259(10)
...K(3A)	3.280(9)	...K(3)	3.277(9)
K(3)...K(3A)	0.997(8)		
...Cl(3A)	2.276(9)	K(3A)...Cl(3)	2.279(9)
...Cl(1)	2.836(9)	...Cl(1A)	2.828(9)
...Cl(5)	3.033(8)	...Cl(6)	3.035(8)
...Cl(3)	3.098(10)	...Cl(3A)	3.093(9)
...Cl(1)	3.142(9)	...Cl(1A)	3.142(9)
...Cl(1A)	3.158(9)	...Cl(1)	3.157(9)
...Cl(4)	3.243(7)	...Cl(4)	3.249(7)
...K(2A)	3.277(9)	...K(2)	3.280(9)
...Cl(2)	3.294(9)	...Cl(2A)	3.299(10)
...Cl(2A)	3.390(9)	...Cl(2)	3.388(9)

potassium ions K(2) and K(3A) are within satisfactory non bonding contacts with the $[IrCl_6]^{3-}$ anion at (0,0,0) containing chlorine atoms Cl(1A), Cl(2A) and Cl(3A). Likewise potassium ions K(2A) and K(3) show satisfactory non bonding contacts with the $[IrCl_6]^{3-}$ anion (at the same site) containing chlorine atoms Cl(1), Cl(2) and Cl(3). For any other combinations this is not the case. Thus in a sense, the structure is composed of a random array of two types of unit cells, one containing one of the disordered octahedra at (0,0,0) and a suitable set of the disordered K^+ ions (and the remaining unit cell contents), and the other containing the other set of disordered K^+ ions and the other orientation of the octahedral $[IrCl_6]^{3-}$ anion at (0,0,0)(with the remainder of the unit cell contents i.e. the potassium ions K(1) and the $[IrCl_6]^{3-}$ octahedron at (0.5,0,0.5)).

Even with this description of the crystal structure there are still four K^+ ... Cl contacts that are somewhat small. These involve the disordered K^+ ions K(2), K(2A), K(3) and K(3A) and the disordered chlorine atoms Cl(1) and Cl(1A). The average of the four close contacts (reported in Table 3.2.5 is 2.827(7)Å. The ionic radii for K^+ and Cl^- respectively are 1.33Å and 1.81Å respectively. This means non bonding contacts should be at least of the order of 3.14Å. These "short" interactions in the solid state offer an explanation as to why the disordered anions located at (0,0,0) show significantly greater distortion from octahedral symmetry than does the ordered anion at

(0.5, 0, 0.5), where such close approaches are not found.

Bond lengths and bond angles for the $[IrCl_6]^{3-}$ anions in $K_3[IrCl_6]$ are listed in Table 3.2.4. The Ir-Cl bond lengths for the disordered anion at (0,0,0) in the unit cell and the ordered anion at (0.5, 0, 0.5) do not differ significantly from one another. The bond lengths compare favourably with those reported in α and β-$IrCl_3$[47,65], both compounds containing distorted $[IrCl_6]$ octahedra, where Ir-Cl bond lengths vary from 2.31 Å to 2.42 Å. However, in both the $[IrCl_6]^{3-}$ anions at (0,0,0) and (0.5,0,0.5), significant departures from O_h structural symmetry in terms of bond angle departures from 90° are found.

Table 3.2.6 contains a list of root-mean-square amplitudes of vibration of the anisotropic atoms along the three principal axes of their respective thermal ellipsoids. Two of the three independent chlorine atoms in the $[IrCl_6]^{3-}$ anion at (0.5, 0, 0.5) are apparently undergoing considerable anisotropic motion with the larger components of their displacement at right angles to their respective Ir-Cl bond vectors. This would imply librational motion of these anions, or alternatively could be interpreted as a disordering of chlorine positions on a smaller scale than that for the other anions. Bond lengths corrected assuming a simple riding motion model for the two chlorine atoms showing large anisotropic motion (where the chlorine atoms are assumed to ride on the heavy iridium atoms) show poor agreement with those bond lengths of the anions located at (0,0,0), their mean being 2.390(2)Å compared with 2.361(4)Å

Table 3.2.6: Root-Mean-Square Components (Å) of the Thermal Vibration Ellipsoids of Selected Atoms Along their Principal Axes and Angles (degrees) between these Principal Axes of the Anisotropic Chlorine Atoms and their Respective Ir-Cl Bond Vectors in $K_3[IrCl_6]$.

Atom	Axis 1	Angle	Axis 2	Angle	Axis 3	Angle
Ir(1)	0.108(2)		0.116(2)		0.124(2)	
Ir(2)	0.103(2)		0.121(2)		0.131(2)	
Cl(4)	0.116(6)	4(4)	0.158(5)	93(6)	0.211(5)	87(3)
Cl(5)	0.130(8)	24(7)	0.174(7)	114(7)	0.466(8)	92(1)
Cl(6)	0.113(8)	177(6)	0.162(7)	87(6)	0.472(8)	89(1)
K(1)	0.183(6)		0.190(6)		0.363(6)	

for the latter. Their average when not corrected is significantly shorter at 2.343(1)Å. This disagreement between average corrected bond length and average bond length for the chlorine atoms in the $[IrCl_6]^{3-}$ anions at (0.5, 0, 0.5) and (0,0,0) indicates that the apparent librational motion of the anions at (0.5, 0, 0.5) is not well described by the simple riding model and suggests that it is probably due to a slight disordering.

3.3 THE CRYSTAL STRUCTURE OF POTASSIUM HEXACHLOROIRIDATE (III) MONOHYDRATE, $K_3[IrCl_6]H_2O$

3.3.1 Preliminary Study and Data Collection

A preliminary study on the title compound confirmed the earlier reported isomorphism of this compound[2] with the analogous rhodium compound. It crystallises in the orthorhombic space group Pbcn. This was uniquely determined from systematic absences in zero and upper level photographs recorded on a Buerger precession camera using Ni filtered CuKα radiation. Relevant crystal data is given in Table 3.3.1.

Table 3.3.2 lists relevant experimental parameters and others used during data collection and processing. Refined cell constants obtained were as follows:

$a = 12.436(3)Å$, $b = 15.682(3)Å$, $c = 12.072(2)Å$, $\alpha=\beta=\gamma=90^{o}$.

Table 3.3.1: Crystal Data for $K_3[IrCl_6]H_2O$

Formula	$K_3[IrCl_6]H_2O$
Formula weight	540.239
Crystal system	orthorhombic
Space group	Pbcn (D_{2h}^{14}, No. 60)
a	12.436(3)Å
b	15.682(3)Å
c	12.072(2)Å
α,β,γ	90^o
V	2354 Å^3
z	8
d calculated	3.05 gcm^{-3}
measured	3.20(5) gcm^{-3}
F(000)	1968
μ(MoKα)	143.13

Table 3.3.2: Experimental Parameters for $K_3[IrCl_6]H_2O$ Data Collection.

Temperature	$25^{\circ}C(\pm 1^{\circ}C)$
Radiation	MoKα(λ=0.7107 for MoKᾱ)
Scan range	0.60° (in 0.01° steps)
Scan time	60 seconds
Total background time	30 seconds
Bragg angle limit	28°
Incident beam collimator (diameter)	1.0 mm
Diffracted beam collimator (diameter)	5.0 mm
Tube take-off angle	3°
Crystal dimensions (maximum)	0.25mm x 0.44mm x 0.24mm
Crystal volume	0.01735 mm^3
Mosaicity	0.23°
Total independent reflections	2791
Reflections used in refinement	1845 (such that $F^2_{obs} \geqslant 3\sigma (F^2_{obs})$)
Ratio observations to variables in least squares refinements	1845:95 $\approx$ 19:1
Range of transmission factors	0.1127 (for 0 2 15) to 0.0717 (for 0 6 0)
No. of equivalent forms of data	1
Weighting parameter p	0.05

Using Zr filtered MoKα radiation, the intensities of 2791 reflections were measured in the positive octant of reciprocal space (such that h, k, $\ell \geq 0$) to a Bragg angle of 28^{o}. Attenuation was required for a few intens low angle reflections and empirically determined attenuation factors were applied in data reduction.

1845 reflections (0.66 of the total number collected) with $F_{obs}^{2} \geq 3\sigma(F_{obs}^{2})$ were finally obtained for use in subsequent structure analysis and least squares refinements.

3.3.2 Structure Solution and Refinement

Use of trial atomic coordinates from the isomorphous $K_3[RhCl_6]H_2O$ structure [2, 3] in a least squares refinement did not lead to satisfactory convergence. Thus the parameters for atoms other than iridium were established *ab initio* based on phasing by the iridium atom alone. Six chlorine atomic positions at satisfactory bonding distances to the iridium atom were determined from a difference electron density synthesis. Least squares refinement of these atomic coordinates, with all atoms isotropic, yielded a residual, R, of 0.18. A further difference Fourier map at this stage revealed suitable atomic positions of the remaining three potassium atoms and one oxygen atom in the asymmetric unit. Least squares refinement of all positional parameters and isotropic thermal parameters finally yielded a residual of 0.062.

Following corrections for absorption final full matrix least squares refinements were completed with all

atoms, except for the oxygen atom, assigned anisotropic thermal parameters. Corrections for anomalous dispersion for iridium and chlorine atoms were also included but no extinction parameter was refined as examination of F_{calc} and F_{obs} for strong low angle reflections showed no systematic discrepancies. The final cycles of refinement saw the model converge at a residual of 0.035, with a weighted residual, R_w, of 0.043. The standard error in an observation of unit weight was 1.124. A final difference Fourier synthesis revealed a flat difference map. The highest peak of 1.9 electrons/$Å^3$ (located close to the iridium atom) was considerably smaller than that identified with an oxygen atom whose peak in a previous difference map was 7.2 electrons/$Å^3$. An analysis of errors produced after this final refinement indicated the original choice of p factor (0.05) yielded a satisfactory weighting scheme. Final atomic coordinates and thermal parameters for $K_3[IrCl_6]H_2O$ and isomorphous $K_3[RhCl_6]H_2O$ (from reference 2) are listed in Tables 3.3.3(a) and 3.3.3(b). Calculated and observed structure factors for data used in final refinement are recorded in Appendix B.

3.3.3 Description of the Structure

Figure 3.3.1 gives a perspective view of the unit cell contents of $K_3[IrCl_6]H_2O$. Figure 3.3.2 shows a stereoscopic view of the unit cell contents.

As for the isomorphous structure of $K_3[RhCl_6]H_2O$ (a second independent determination of whose structure has

Table 3.3.3(a): Positional Parameters for $K_3[IrCl_6]H_2O$ and Isomorphous $K_3[RhCl_6]H_2O$

Atom	Parameter	$K_3[IrCl_6]H_2O$	$K_3[RhCl_6]H_2O$ [a]	Atom	Parameter	$K_3[IrCl_6]H_2O$	$K_3[RhCl_6]H_2O$ [a]
Ir	x	0.21529(3)	0.21481(8)	Cl(6)	x	0.2867(2)	0.2861(3)
	y	0.37092(2)	0.12890(7)		y	0.2441(2)	0.2551(2)
	z	0.05731(9)	0.05731(9)		z	-0.0201(2)	-0.0193(2)
Cl(1)	x	0.3481(2)	0.3472(3)	K(1)	x	0.1079(2)	0.1087(3)
	y	0.3665(2)	0.1337(2)		y	0.4249(2)	0.0752(2)
	z	0.1981(2)	0.1988(3)		z	0.3843(2)	0.3838(3)
Cl(2)	x	0.1421(2)	0.1417(3)	K(2)	x	0.2688(3)	0.2686(3)
	y	0.4958(2)	0.0045(2)		y	0.1673(2)	0.3329(2)
	z	0.1341(2)	0.1340(3)		z	0.2331(2)	0.2334(3)
Cl(3)	x	0.0983(2)	0.0987(3)	K(3)	x	0.4634(3)	0.4635(3)
	y	0.2928(2)	0.2065(2)		y	0.3354(2)	0.1643(2)
	z	0.1683(2)	0.1675(3)		z	0.4739(3)	0.4729(3)
Cl(4)	x	0.3288(2)	0.3278(3)	O	x	0.0898(8)	0.0894(9)
	y	0.4548(2)	0.0452(2)		y	0.0698(7)	0.4309(7)
	z	-0.0577(2)	-0.0580(3)		z	0.1658(9)	0.1654(10)
Cl(5)	x	0.0780(2)	0.0783(3)				
	y	0.3718(2)	0.1282(2)				
	z	-0.0778(2)	-0.0778(3)				

[a] The y coordinates of all atoms in $K_3[RhCl_6]H_2O$ are related to those in $K_3[IrCl_6]H_2O$ by a transformation of (0.5 -y'), where y' is the y coordinate of an atom in the rhodium structure.

Table 3.3.3(b): Thermal Parameters for $K_3[IrCl_6]H_2O$

Atom	U(or U_{11})	U_{22}	U_{33}	U_{12}	U_{13}	U_{23}
Ir	0.0169(2)	0.0191(2)	0.0147(2)	0.0047(2)	0.0025(2)	0.0001(2)
Cl(1)	0.030(1)	0.039(2)	0.032(1)	0.006(1)	-0.010(1)	-0.002(1)
Cl(2)	0.033(1)	0.024(1)	0.026(1)	0.008(1)	0.003(1)	-0.006(1)
Cl(3)	0.032(1)	0.031(1)	0.029(1)	0.000(1)	0.010(1)	0.005(1)
Cl(4)	0.033(2)	0.040(2)	0.033(1)	-0.001(1)	0.010(1)	0.011(1)
Cl(5)	0.026(1)	0.035(1)	0.026(1)	0.007(1)	-0.004(1)	-0.003(1)
Cl(6)	0.036(2)	0.030(1)	0.030(1)	0.016(1)	0.004(1)	-0.007(1)
K(1)	0.037(1)	0.029(1)	0.029(1)	0.001(1)	-0.004(1)	0.003(1)
K(2)	0.078(2)	0.036(1)	0.034(2)	0.020(2)	-0.022(2)	-0.003(1)
K(3)	0.044(2)	0.059(2)	0.071(2)	-0.011(2)	0.019(2)	0.009(2)
O	0.058(3)					

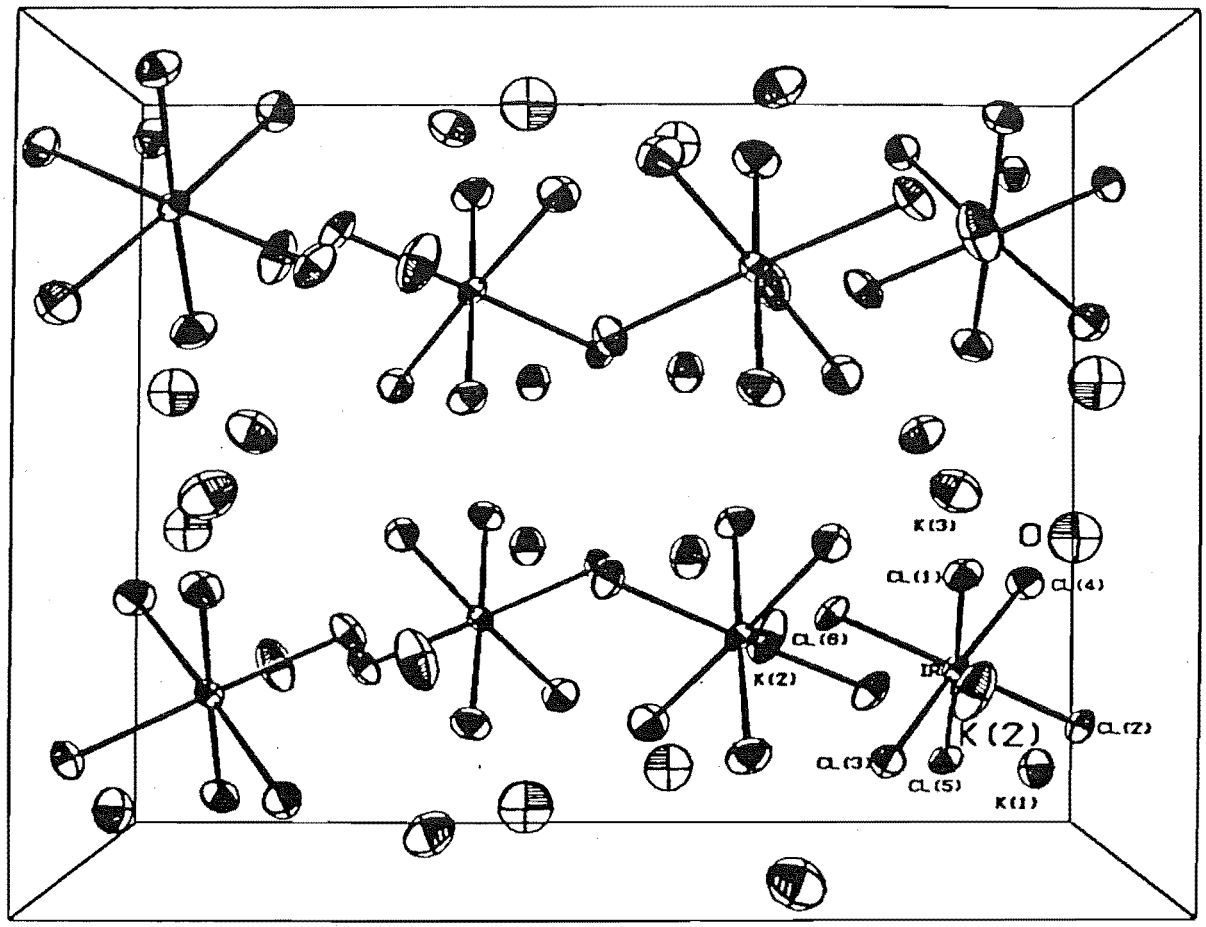

Figure 3.3.1: Projection diagram of the unit cell contents of $K_3[IrCl_6]H_2O$ viewed down an axis parallel to the c axis.

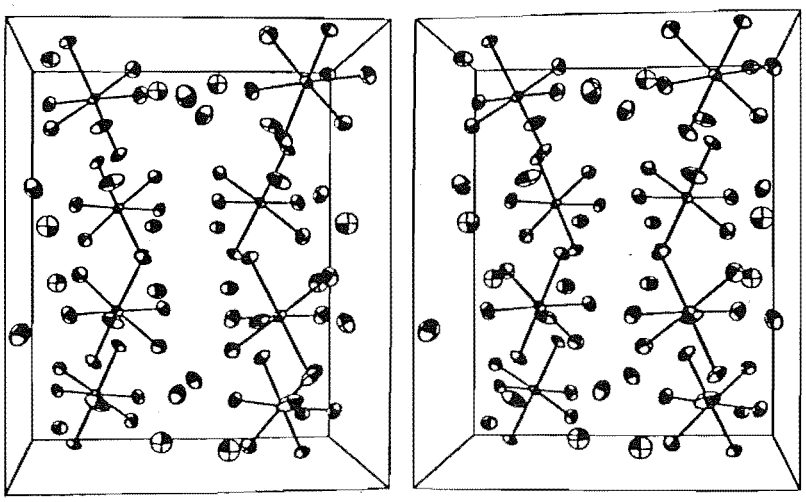

Figure 3.3.2: Stereoscopic view of the unit cell contents of $K_3[IrCl_6]H_2O$.

been reported recently[3], the structure consists of discrete octahedral $[IrCl_6]^{3-}$ anions arranged in chains throughout the unit cell with K^+ ions and water molecules occupying the channels between them.

As can be seen from Table 3.3.4, which lists bond lengths and angles in the anions of the two isomorphous structures, the $[IrCl_6]^{3-}$ anion shows similar distortion to the $[RhCl_6]^{3-}$ anion. However, although the bond angles are the same for both anions (within experimental error), the Rh-Cl bond lengths in the $[RhCl_6]^{3-}$ anion are significantly shorter than their respective counterparts in the $[IrCl_6]^{3-}$ anion. This presumably reflects the small differences in the ionic radii of the component Rh^{3+} and Ir^{3+} ions. The anions are located on sites of C_1 symmetry (i.e. no symmetry at all). The range of bond lengths in the $[IrCl_6]^{3-}$ anions in $K_3[IrCl_6]H_2O$, from 2.327(3)Å to 2.376(3)Å, is large compared to those ranges found in similar anions in $(NH_4)_3[IrCl_6]H_2O$ and $K_3[IrCl_6]$ (2.341(2)Å to 2.368(2)Å and 2.342(4)Å to 2.366(7)Å respectively) and far exceeds the limit of error in an individual bond. In both $K_3[IrCl_6]H_2O$ and $K_3[RhCl_6]H_2O$, the Ir(Rh)-Cl(3) bond is particularly short (2.327(3)Å and 2.302(4)Å respectively) especially when the Ir-Cl(3) bond length is compared with mean values found for $[IrCl_6]^{3-}$ anions in other structures (normally close to 2.360Å).

Table 3.3.5 lists root-mean-square components of vibration ellipsoids of the anisotropic atoms and reveals the major displacement in the vibrating chlorine atoms occurs at right

Table 3.3.4: Bond Lengths (Å) and Angles (degrees) in the $[MCl_6]^{3-}$ Anion in $K_3[IrCl_6]H_2O$ and Isomorphous $K_3[RhCl_6]H_2O$.

(a) Bonds

	Uncorrected	Corrected[a]		Uncorrected
Ir-Cl(1)	2.373(3)	2.383(3)	Rh-Cl(1)	2.364(4)
Ir-Cl(2)	2.351(3)	2.358(3)	Rh-Cl(2)	2.337(4)
Ir-Cl(3)	2.327(3)	2.336(3)	Rh-Cl(3)	2.302(4)
Ir-Cl(4)	2.376(3)	2.387(3)	Rh-Cl(4)	2.366(4)
Ir-Cl(5)	2.360(3)	2.367(3)	Rh-Cl(5)	2.345(4)
Ir-Cl(6)	2.369(3)	2.378(3)	Rh-Cl(6)	2.352(4)
Mean	2.359	2.368		2.344

(b) Angles

	(M=)Ir	(M=)Rh		(M=)Ir	(M=)Rh
Cl(1)-M-Cl(2)	90.6(1)	90.6(1)	Cl(2)-M-Cl(6)	179.2(1)	179.2(1)
Cl(1)-M-Cl(3)	90.4(1)	90.0(1)	Cl(3)-M-Cl(4)	177.6(1)	177.5(1)
Cl(1)-M-Cl(4)	91.2(1)	91.8(1)	Cl(3)-M-Cl(5)	87.1(1)	87.3(1)
Cl(1)-M-Cl(5)	177.4(1)	177.3(1)	Cl(3)-M-Cl(6)	91.1(1)	91.0(1)
Cl(1)-M-Cl(6)	89.8(1)	89.8(1)	Cl(4)-M-Cl(5)	91.4(1)	90.9(1)
Cl(2)-M-Cl(3)	88.2(1)	88.3(1)	Cl(4)-M-Cl(6)	90.7(1)	90.8(1)
Cl(2)-M-Cl(4)	89.9(1)	89.9(1)	Cl(5)-M-Cl(6)	90.3(1)	90.1(1)
Cl(2)-M-Cl(5)	89.3(1)	89.5(1)			

[a] Bond lengths corrected for thermal motion using a riding model.

Table 3.3.5: Root-Mean-Square Components (Å) of the Thermal Vibration Ellipsoids of Selected Atoms along their Principal Axes and Angles (degrees) between these Principal Axes of the Anisotropic Chlorine Atoms and their Respective Ir-Cl Bond Vectors in $K_3[IrCl_6]H_2O$.

Atom	Axis 1	Angle	Axis 2	Angle	Axis 3	Angle
Ir	0.109(1)		0.125(1)		0.152(1)	
Cl(1)	0.143(4)	9(4)	0.187(4)	99(5)	0.215(4)	91(3)
Cl(2)	0.126(5)	11(4)	0.172(4)	81(4)	0.193(4)	85(3)
Cl(3)	0.140(5)	16(4)	0.175(4)	81(6)	0.204(4)	102(3)
Cl(4)	0.138(5)	168(2)	0.192(4)	93(4)	0.224(4)	78(2)
Cl(5)	0.145(4)	159(10)	0.162(4)	71(10)	0.200(4)	97(4)
Cl(6)	0.113(5)	166(2)	0.182(4)	89(3)	0.2218(4)	103(2)
K(1)	0.159(4)		0.177(4)		0.197(4)	
K(2)	0.149(5)		0.179(4)		0.306(4)	
K(3)	0.167(5)		0.255(4)		0.285(5)	

Table 3.3.6: Selected Interatomic Distances (Å) less than 3.5 Å in $K_3[IrCl_6]H_2O$

K(1)...Cl(6)	3.174(4)	K(3)...O	2.830(11)
...Cl(5)	3.243(4)	...Cl(1)	3.170(4)
...Cl(2)	3.247(4)	...Cl(3)	3.184(5)
...Cl(2)	3.290(4)	...Cl(4)	3.348(5)
...Cl(2)	3.309(4)	...Cl(5)	3.349(5)
...Cl(3)	3.332(4)	...Cl(6)	3.352(4)
...Cl(3)	3.357(4)	...Cl(6)	3.467(5)
...Cl(5)	3.390(4)		
...Cl(4)	3.405(4)	O...K(2)	2.820(11)
		...K(3)	2.830(11)
K(2)...O	2.820(11)	...O	3.020(21)
...Cl(3)	2.997(4)	...Cl(1)	3.304(11)
...Cl(5)	3.036(4)	...Cl(4)	3.399(11)
...Cl(2)	3.144(4)	...Cl(3)	3.498(11)
...Cl(6)	3.293(4)	...Cl(3)	3.498(11)
...Cl(6)	3.293(4)		
...Cl(1)	3.304(4)	Angles‡ O-O-Cl(1)	95.3(2
...Cl(6)	3.360(4)	Cl(4)-O-Cl(3)	121.9(3
...Cl(4)	3.394(5)		
Cl(1)...Cl(3)	3.334(4)	Cl(5)...Cl(3)	3.229(4)
...Cl(6)	3.348(4)	...Cl(2)	3.310(4)
...Cl(2)	3.358(4)	...Cl(6)	3.352(4)
...Cl(4)	3.393(4)	...Cl(4)	3.388(4)
Cl(2)...Cl(3)	3.256(4)	Cl(4)...Cl(6)	3.377(4)
...Cl(4)	3.341(4)		
Cl(3)...Cl(6)	3.353(4)		

‡ Angles between atoms close to the oxygen atom of the water molecule. These sets of angles could give an indication of possible hydrogen atomic sites attached to the oxygen atom, where long range favourable $H^{\delta+}$...Cl(or O)$^{\delta-}$ interactions would mean hydrogen atoms lie along these inter-atomic vectors.

angles to their respective Ir-Cl bond vectors. Corrections to Ir-Cl bond lengths, assuming a simple riding motion model were therefore made. The maximum change as a result of this correction was 0.011 Å.

No non bonding contacts between K^+ ions and oxygen or chlorine atoms within the structure (listed in Table 3.3.6) are smaller than expected. No evidence of hydrogen bonding of the water of crystallisation hydrogen atoms to either oxygen or chlorine atoms was found in the analysis of the structure primarily because no hydrogen atomic positions were located. All distances between the water molecule oxygen atom and other atoms were greater than 3.0 Å (except for two close approaches to K^+ ions). However, as shown in Table 3.3.6, there are two sets of atomic positions, Cl(1) and O, and Cl(3) and Cl(4) which form suitable angles of approximately 104^o around the water molecule oxygen atom. The water molecules could thus be oriented in the crystal lattice with hydrogen atoms pointing towards one of these combinations of centres.

3.4 THE CRYSTAL STRUCTURE OF AMMONIUM HEXACHLOROIRIDATE (III) MONOHYDRATE, $(NH_4)_3[IrCl_6]H_2O$

3.4.1 Preliminary Study and Data Collection

Preliminary studies indicated the space group of this compound was Pnma, or the non-centric equivalent, $Pna2_1$. Relevant crystal data are given in Table 3.4.1.

Table 3.4.1: Crystal Data for $(NH_4)_3[IrCl_6]H_2O$

Formula	$(NH_4)_3[IrCl_6]H_2O$ (see Section 3.4.3)
Formula weight	477.049
Crystal system	Orthorhombic
Space group	Pnma (D_{2h}^{16}, No. 62)
a	12.229(2) Å
b	7.011(1) Å
c	14.088(2) Å
α, β, γ	90°
V	1207 $Å^3$
z	4
d calculated	2.62 gcm^{-3}
measured	2.61(1) gcm^{-3}
F(000)	888
μ (MoKα)	129.59 cm^{-1}

3.4.1(a): Attempts at Data Collection on a Twinned Crystal

The first attempt at solving this structure using intensity data collected on the diffractometer failed. This was later found to be a direct result of severe twinning present in the crystal used for data collection.

The problem of twinning in these crystals was not clarified until the second data collection was attempted. The twinning involved two crystallites sharing a common face but misaligned from one another along this face normally by an angle of the order of one degree. As all the crystals isolated and examined by a microscope showed this habit a decision was made to attempt data collection from a twinned crystal.

A suitable twinned crystal, composed of approximately equal volumes of both crystallites was mounted and examined on a four-circle diffractometer. Using suitably large scan ranges (2^{o}) four circle setting angles were determined for 12 high angle reflections in the usual manner, and the following refined cell dimensions obtained

$a = 12.206(7)$ Å, $b = 6.944(6)$ Å, $c = 14.140(9)$ Å,
$\alpha=\beta=\gamma=90^{o}$.

When data collection was attempted a fundamental problem was encountered. It was found that for some reflections the usual scanning technique for data collection

(i.e. the θ-2θ scan technique in bisecting mode geometry) detected no intensity at all during a scan of the reflection, even when the scan range was of the order of 2^{o}. However, for this same reflection, a ω scan (θ held constant) produced a total integrated count considerably above background levels having encountered the two reflections from the crystallites satisfactorily.

This problem could not be overcome and any attempt to collect data on such a crystal would give an erroneous data set. Thus, attempts to collect data on a twinned crystal were abandoned and efforts were directed towards physical separation of the twin components.

3.4.1(b): Actual Data Collection

To obtain a suitable crystal for data collection, large crystals were grown and the two components of the twin physically separated by cutting. A clean fragment of the desired dimensions was produced and preliminary precession photographs confirmed that the specimen was a true single crystal.

The cell dimensions were refined in the usual fashion to produce

$$a = 12.229(2)\ \text{Å},\quad b = 7.011(1)\ \text{Å},\quad c = 14.088(2)\ \text{Å},$$
$$\alpha = \beta = \gamma = 90^{o}.$$

These cell dimensions are significantly different to those obtained for the twinned crystals examined previously and

furthermore, their errors are smaller.

The intensities of 2475 reflections were measured in the octant of reciprocal space defined by h, k, $\ell \geqslant 0$ to a Bragg angle of 31° (MoKα radiation) using the θ-2θ scan technique. Relevant experimental parameters used in data collection and processing are summarised in Table 3.4.2. No attenuation of any reflections was required.

1645 reflections (0.66 of the total number collected) such that $F_{obs}^{2} \geqslant 3\sigma(F_{obs}^{2})$ were finally obtained for use in subsequent least squares refinement.

3.4.2 Structure Solution and Refinement

With a suitable scale factor established for the data set by a trial least squares refinement of positional and thermal parameters of the iridium atom located in the asymmetric unit, full matrix least squares refinement was attempted using coordinates (and isotropic thermal parameters) obtained from the isomorphous rubidium hexabromoiridate (III) monohydrate structure (Section 3.5). 3 cycles of refinement produced a residual of 0.076.

Following corrections for absorption, using an analytical method, 3 cycles of least squares refinement were executed with four chlorine atoms and the iridium atom given anisotropic temperature factors (with suitable constraints) and the remaining three nitrogen atoms and oxygen atom left with isotropic thermal parameters. An R factor of 0.036 resulted.

Table 3.4.2: Experimental Parameters for $(NH_4)_3[IrCl_6]H_2O$ Data Collection.

Temperature	$24^{\circ}C$ ($\pm$ $1^{\circ}C$)
Radiation	MoKα (λ=0.7107Å for MoK$\bar{\alpha}$)
Scan range	0.72 (0.01° steps)
Scan time	144 seconds
Total background time	72 seconds
Bragg angle limit	31°
Incident beam collimator	1 mm (diameter)
Diffracted beam collimator	5 mm (diameter)
Tube take off angle	3°
Crystal dimensions	0.4 mm x 0.2 mm x 0.2 mm
Crystal volume	0.00436 mm^3
Mosaicity	0.25°
Total independent reflections	2475
Reflections used in refinement	1645 (such that $F^2_{obs} \geqslant 3\sigma (F^2_{obs})$)
Ratio observations to variables in least squares refinements	1645:59 $\approx$ 27:1
Range of transmission factors	0.3697 (for 111) to 0.2637 (for 200)
No. of equivalent forms of data	1
Weighting parameter p	0.05

At this stage of refinement it was noted that the temperature factor of one of the nitrogen atoms (N(1)) was anomalously low at 0.0114 compared with 0.0507 and 0.0380 for the other two nitrogen atoms and 0.0633 for the oxygen atom. This was attributed to the presence of potassium ions on this nitrogen atom site, as was suggested by a potassium Atomic Absorption analysis and a nitrogen elemental analysis on the bulk sample of crystals from which the crystal under study was selected. A pH measurement also suggested that the N(1) site also contained a substantial proportion of oxygen atoms (arising from H_3O^+ ions).

In the final structural model, isotropic temperature factors were fixed for a potassium atom (U_{iso} = 0.0279) and a nitrogen atom (U_{iso} = 0.0380) both located on the original N(1) site and with the constraint on their variable occupancy factors that the total occupancy factor was 1.0. The chosen potassium and nitrogen atom temperature factors were obtained from average values from the $K_3[IrCl_6]$ structure (Section 3.2) and the remaining two isotropic nitrogen atoms in the present analysis. Anisotropic thermal parameters were assigned to all other atoms. Subsequent full matrix least squares refinement (with extinction and anomalous dispersion corrections included) produced a residual of 0.029 and a weighted residual of 0.042 at convergence. The standard error of an observation of unit weight was 1.252. The weighting scheme appeared to be satisfactory.

A difference electron density synthesis at this stage revealed no major features and the positions of highest density were near nitrogen and oxygen atom sites. No self-consistent sets of hydrogen atom sites for the NH_4^+ cations or H_2O water molecule could be found although a number of resolved peaks in the difference map were at distances from oxygen and nitrogen atoms corresponding to hydrogen bond lengths.

The atomic coordinates and thermal parameters obtained from the final least squares refinements are listed in Table 3.4.3. Observed and calculated structure factor magnitudes for the data used in final refinement are listed in Appendix C.

3.4.3 Description of the Structure

Satisfactory solution of this structure has confirmed the isomorphism between the $Rb_3[IrBr_6]H_2O$ and $(NH_4)_3[IrCl_6]H_2O$ structures. The one problem encountered in this analysis concerning the disorder of one of the NH_4^+ cation sites deserves further comment. Because the K^+ ionic radius is somewhat smaller than that of the NH_4^+ cation (1.33 Å compared with 1.43 Å), occupancy of an NH_4^+ site by a K^+ ion will not expand the lattice. The final refined occupancy factor of the N(1) site by a nitrogen atom was 0.79. This does not compare very favourably with occupancy factors of 0.36 and 0.30 obtained from Atomic Absorption spectroscopy and nitrogen elemental analyses respectively. However, the site occupancy factors will have

Table 3.4.3: Positional and Thermal Parameters for $(NH_4)_3[IrCl_6]H_2O$.

Atom	x	y	z	U(or U_{11})	U_{22}	U_{33}	U_{12}	U_{13}	U_{23}
Ir	0.27524(3)	0.25	-0.09476(2)	0.0277(2)	0.0237(2)	0.0205(1)	0.0	-0.0005(1)	0.0
Cl(1)	0.3650(2)	0.25	0.0520(1)	0.043(1)	0.064(1)	0.0243(9)	0.0	-0.0072(8)	0.0
Cl(2)	0.1865(2)	0.25	-0.2441(2)	0.042(1)	0.063(1)	0.0261(8)	0.0	-0.0089(9)	0.0
Cl(3)	0.3963(1)	0.0159(2)	-0.1521(1)	0.0515(9)	0.0356(7)	0.0408(8)	0.0132(7)	0.0053(7)	-0.0026(7)
Cl(4)	0.1556(2)	0.0146(3)	-0.0363(1)	0.0532(9)	0.0445(8)	0.0449(8)	-0.0184(8)	0.0075(7)	0.0018(7)
N(1)(K,N)	0.1077(7)	0.25	-0.4635(5)	0.0279(K)	0.0380(N)[a]				
N(2)	0.0561(6)	-0.25	0.1451(5)	0.016(3)	0.136(9)	0.018(3)	0.0	-0.001(3)	0.0
N(3)	0.3315(8)	0.25	0.2790(5)	0.068(6)	0.031(3)	0.020(3)	0.0	0.009(3)	0.0
O	0.0590(9)	0.25	0.1571(6)	0.087(7)	0.107(8)	0.041(4)	0.0	-0.009(5)	0.0

[a]The final refined occupancy factors for N and K on site N(1) were

N 0.786(8)

K 0.214

The error associated with the refined occupancy factor of the nitrogen atom (as obtained from the variance-covariance matrix) is not particularly meaningful as the temperature factors chosen for the disordered K and N atoms on the site N(1) may not be the real temperature factors of these atoms. Furthermore, the presence of oxygen atoms (from hydronium ions) on this site has not been accounted for.

large errors (see footnote(a) Table 3.4.3). Furthermore, the composition of the single crystal under study may be quite different to that of the bulk sample. The possibility of H_3O^+ cations also present on the N(1) site has not been allowed for in the present model. The ionic radius of this cation would be expected to be of the same order of the NH_4^+ cation and thus have little effect on the crystal lattice. In essence therefore, the solved crystal structure is that of $(NH_4)_3[IrCl_6]H_2O$, although it would perhaps be more appropriate on the basis of the present structural analysis to label the title compound $(NH_4)_{2.8}K_{0.2}[IrCl_6]H_2O$.

The two sets of atomic coordinates for $(NH_4)_3[IrCl_6]H_2O$ (Table 3.4.3) and $Rb_3[IrBr_6]H_2O$ (Table 3.5.3) do show significant differences for certain parameters. However, the same relative orientations and positions of the $[IrCl_6]^{3-}$ and $[IrBr_6]^{3-}$ octahedral anions and the same relative positions of the remaining ions and water molecules in the unit cell are retained in both structures. A projection diagram of the unit cell contents of $(NH_4)_3[IrCl_6]H_2O$, with an asymmetric unit labelled, is given in Figure 3.4.1. Figure 3.4.2 contains a stereoscopic view of the unit cell contents for this compound.

A number of other features in the structure of $(NH_4)_3[IrCl_6]H_2O$ reflect the isomorphism of this compound to $Rb_3[IrBr_6]H_2O$. The $[IrCl_6]^{3-}$ anions are located on mirror planes at y=1/4, 3/4 in the unit cell and show significant distortion from ideal octahedral symmetry.

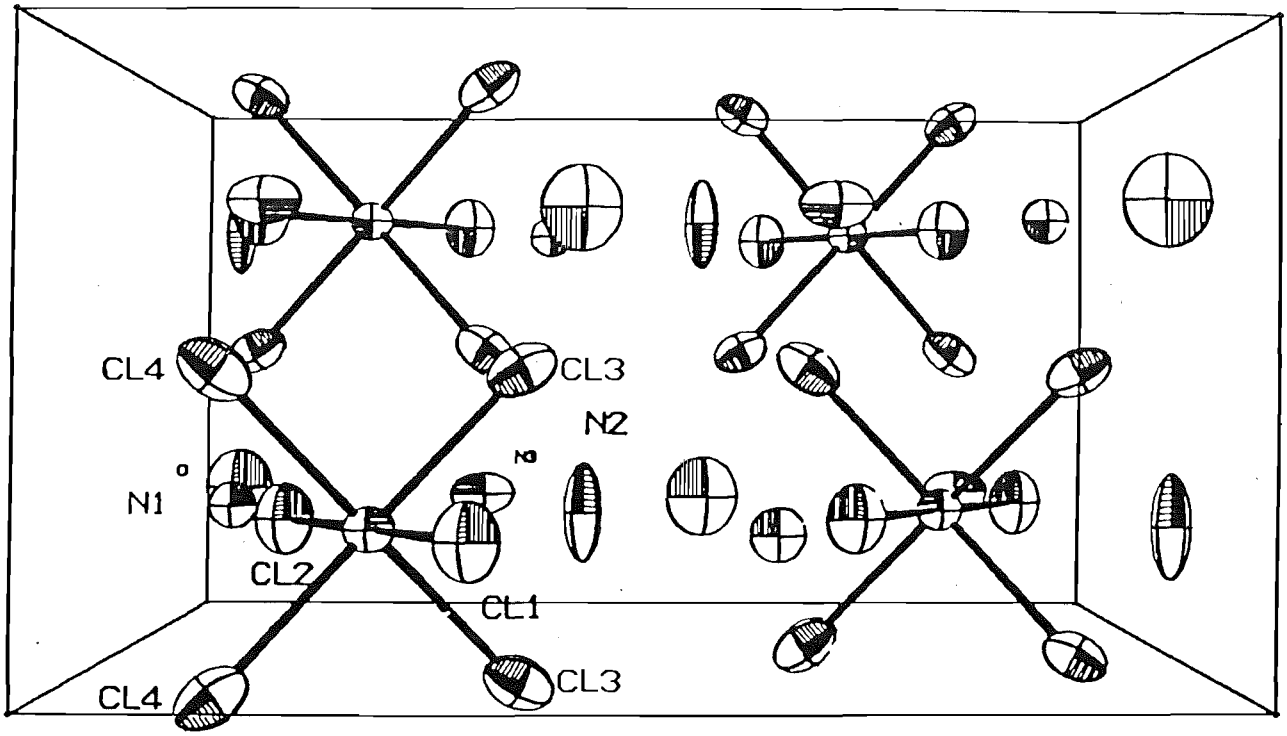

Figure 3.4.1: Projection diagram of the unit cell contents of $(NH_4)_3[IrCl_6]H_2O$ viewed down an axis parallel to the c axis.

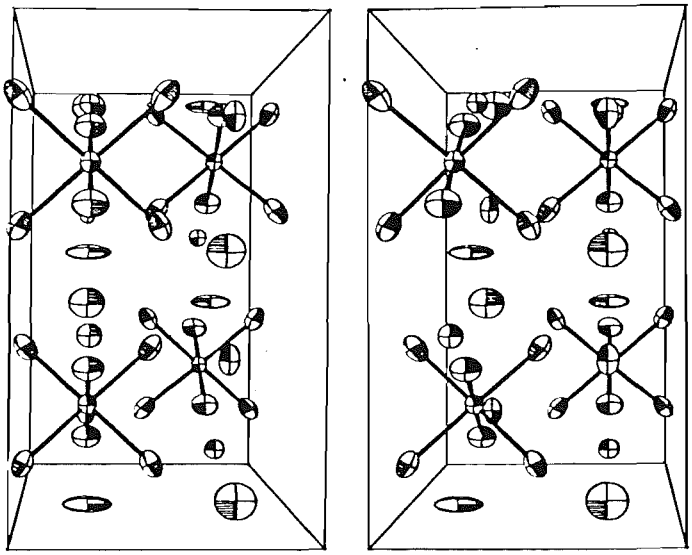

Figure 3.4.2: Stereoscopic view of the unit cell contents of $(NH_4)_3[IrCl_6]H_2O$

Table 3.4.4 contains a list of bond lengths and bond angles between the iridium and chlorine atoms in the $[IrCl_6]^{3-}$ anion in $(NH_4)_3[IrCl_6]H_2O$. The bond angles reported in this table show the same measure of distortion relative to idealized octahedral symmetry as do those angles found for the $[IrBr_6]^{3-}$ anion in $Rb_3[IrBr_6]H_2O$ (see Table 3.5.4). Also shown in Table 3.4.4 are a series of corrected bond lengths (i.e. those evaluated where a correction for thermal motion is made). The root-mean-square components of the anisotropic thermal vibration ellipsoids for atoms in $(NH_4)_3[IrCl_6]H_2O$ are given in Table 3.4.5. As for $Rb_3[IrBr_6]H_2O$, the largest anisotropic thermal motion of the chlorine atoms (Br atoms in the latter case) is at right angles to the Ir-Cl bond vector for the respective atoms. The thermal motion of atoms N(2) and N(3) and the oxygen atom in $(NH_4)_3[IrCl_6]H_2O$ also shows close resemblance to that for atoms Rb(2) and Rb(3) and the oxygen atom in $Rb_3[IrBr_6]H_2O$. In both cases the major component of anisotropic motion is at right angles to the mirror planes on which these atoms are located.

The mean bond lengths in the $[IrCl_6]^{3-}$ anion, both those calculated for and without correction made for the riding model are within the range observed for the same anions in $K_3[IrCl_6]$ and $K_3[IrCl_6]H_2O$. No non bonding contacts in $(NH_4)_3[IrCl_6]H_2O$ (summarised in Table 3.4.6) are found to be significantly less than those expected on the basis of ionic or Van der Vaals radii.

Table 3.4.4: Bond Lengths (Å) and Angles (degrees) in the $[IrCl_6]^{3-}$ Anions in $(NH_4)_3[IrCl_6]H_2O$

(i) Bond lengths

Ir-Cl(1)	2.341(2)		
Ir-Cl(2)	2.368(2)		
Ir-Cl(3)	2.353(2)	Ir-Cl(5)[a]	2.353(2)
Ir-Cl(4)	2.355(2)	Ir-Cl(6)[a]	2.355(2)
Mean	2.354(8)		

(ii) Corrected bond lengths

Ir-Cl(1)	2.354(2)		
Ir-Cl(2)	2.380(2)		
Ir-Cl(3)	2.365(2)	Ir-Cl(5)[a]	2.365(2)
Ir-Cl(4)	2.369(2)	Ir-Cl(6)[a]	2.369(2)
Mean	2.367(8)		

(iii) Angles

Cl(1)-Ir-Cl(2)	179.32(9)	Cl(3)-Ir-Cl(4)	91.27(7)
Cl(1)-Ir-Cl(3)	90.47(6)	Cl(3)-Ir-Cl(5)	88.44(9)
Cl(1)-Ir-Cl(4)	89.01(6)	Cl(3)-Ir-Cl(6)	179.41(6)
Cl(1)-Ir-Cl(5)	90.47(6)	Cl(4)-Ir-Cl(5)	179.41(6)
Cl(1)-Ir-Cl(6)	89.01(6)	Cl(4)-Ir-Cl(6)	89.0(1)
Cl(2)-Ir-Cl(3)	89.04(6)	Cl(5)-Ir-Cl(6)	91.27(7)
Cl(2)-Ir-Cl(4)	91.47(6)		
Cl(2)-Ir-Cl(5)	89.04(6)		
Cl(2)-Ir-Cl(6)	91.47(6)		

[a] Cl(5) and Cl(6) are symmetry related atoms of Cl(3) and Cl(4) respectively.

Table 3.4.5: Root-Mean-Square Components (Å) of the Thermal Vibration Ellipsoids of Selected Atoms along their Principal Axes and Angles (degrees) between these Principal Axes of the Anisotropic Chlorine Atoms and their Respective Ir-Cl Bond Vectors in $(NH_4)_3[IrCl_6]H_2O$.

Atom	Axis 1	Angle	Axis 2	Angle	Axis 3	Angle
Ir	0.1431(5)		0.1541(5)		0.1665(5)	
Cl(1)	0.148(3)	9(2)	0.212(3)	99(2)	0.254(3)	90.0(0)
Cl(2)	0.149(1)	176(2)	0.215(3)	86(2)	0.251(3)	90.0(0)
Cl(3)	0.163(2)	10(1)	0.205(2)	87(2)	0.244(2)	81(1)
Cl(4)	0.166(2)	90(1)	0.215(2)	56(2)	0.262(2)	34(2)
N(2)	0.125(12)		0.138(11)		0.368(13)	
N(3)	0.136(10)		0.176(10)		0.265(11)	
O	0.197(11)		0.298(12)		0.328(12)	

Table 3.4.6: Selected Interatomic Contacts (Å) less than 3.5 Å in $(NH_4)_3[IrCl_6]H_2O$

N(1)[a]	...Cl(1)	3.219(9)	Cl(1)	...Cl(3)	3.333(2)
	...Cl(2)	3.238(8)		...Cl(4)	3.292(3)
	...Cl(3)	3.246(7)			
	...Cl(3)	3.469(7)	Cl(2)	...Cl(3)	3.310(3)
				...Cl(4)	3.382(3)
N(2)	...Cl(2)	3.278(8)			
	...Cl(3)	3.346(6)	Cl(3)	...Cl(3)[b]	3.283(3)
	...Cl(4)	3.385(6)		...Cl(4)	3.366(3)
	...Cl(4)	3.431(7)			
			Cl(4)	...Cl(4)[b]	3.301(4)
N(3)	...O	2.92(2)			
	...Cl(4)	3.199(6)			
	...Cl(1)	3.224(7)			
	...Cl(3)	3.489(8)			
O	...N(3)	2.92(2)			
	...Cl(3)	3.316(7)			
	...N(4)	3.398(8)			

[a] Site containing potassium atom (occupancy factor of 0.21) and nitrogen atom (occupancy factor 0.79) to give a total occupancy factor of 1.0.

[b] symmetry related atoms

3.5 THE CRYSTAL STRUCTURE OF RUBIDIUM HEXABROMOIRIDATE (III) MONOHYDRATE, $Rb_3[IrBr_6]H_2O$

3.5.1 Preliminary Study and Data Collection

A preliminary study carried out on green needle-like crystals of this compound established the space group to be Pnma (or the non-centric equivalent, in terms of extinctions, $Pna2_1$). Relevant crystal data for this compound is given in Table 3.5.1.

A crystal suitable for data collection was chosen. Refined cell parameters as follows were finally obtained.

$a = 12.768(2)$ Å, $b = 7.391(1)$ Å, $c = 14.982(2)$ Å,
$\alpha = \beta = \gamma = 90^{\circ}$.

Intensity data for 2060 reflections were collected in two equivalent octants of reciprocal space defined by $h,k,\ell \geqslant 0$ and $h \leqslant 0$; $k,\ell \geqslant 0$ out to a Bragg angle of 23° (MoKα radiation). Relevant experimental data for data collection and processing is given in Table 3.5.2. No attenuation of any reflections was required.

1283 reflections with $F_{obs}^2 \geqslant 3\sigma(F_{obs}^2)$ were finally obtained for use in subsequent structure analysis and least squares refinements. This number represented 0.62 of the total number of reflections whose intensities were measured. The two equivalent sets of data were not averaged in the initial stages of structure solution. They were, however, averaged after absorption corrections had been made.

Table 3.5.1: Crystal Data for $Rb_3[IrBr_6]H_2O$

Formula	$Rb_3[IrBr_6]H_2O$
Formula Weight	946.049
Crystal system	orthorhombic
Space group	Pnma (D_{2h}^{16}, No. 62)
a	12.768(2) Å
b	7.391(1) Å
c	14.982(2) Å
α,β,γ	90^{o}
V	1413 $Å^3$
z	4
d calculated	4.46 g cm^{-3}
measured	> 3.33 g cm^{-3}
F(000)	1632
μ(MoKα)	358.05 cm^{-1}

Table 3.5.2: Experimental Parameters for $Rb_3[IrBr_6]H_2O$ Data Collection

Temperature	$25^{\circ}C (\pm 1^{\circ}C)$
Radiation	MoKα (λ = 0.7107 Å for MoK$\bar{\alpha}$)
Scan Range	0.60°
Scan time	120 seconds
Total background time	60 seconds
Bragg angle limit	23°
Incident beam collimator	1 mm (diameter)
Diffracted beam collimator	5 mm (diameter)
Tube take off angle	3°
Crystal dimensions	0.2 mm x 0.23 mm x 0.13 mm
Crystal volume	0.006563 mm^3
Mosaicity	0.15°
Total independent reflections	1071
Reflections used in refinement	550 such that $F^2_{obs} \geqslant 3\sigma(F^2_{obs})$
Ratio observations to variables	550:62
in least squares refinements	≈ 9:1
Range of transmission factors	0.07063 (for -1018) to 0.007513 (for 123)
No. equivalent forms of data	2 (hkℓ and $\bar{h}$kℓ)
Weighting parameter p	0.05

3.5.2 Structure Solution and Refinement

A three dimensional Patterson synthesis revealed possible atomic positions of the iridium and bromine atoms in the unit cell. Vector concentrations in the Patterson map[226] indicated the correct space group was Pnma. However, unsatisfactory initial refinements using such coordinates saw recourse to direct methods as a means of structure solution. Two E-maps produced by the automatic centrosymmetric direct methods option in SHELX76 (see § 9.2) were carefully analysed. The more favourable of the two (by statistical criteria), revealed satisfactory atomic positions for an iridium atom, four independent bromine and three rubidium atoms.

Trial least squares refinements of the positional parameters of the iridium atom and four bromine atoms (with all the atoms given isotropic thermal parameters) produced a residual, R, of 0.31. A difference fourier synthesis at this stage of refinement returned the same three locations for the rubidium atoms produced by the direct methods solution to the structure. A further three cycles of least squares refinement were then executed with one iridium atom, four bromine and three rubidium atoms all assigned isotropic thermal parameters. This produced a residual of 0.155.

All atoms were assigned anisotropic thermal parameters, some with constraints associated with occupancy of special positions, and full matrix least squares refinement continued.

A further 3 cycles produced a residual of 0.119. A difference electron density map calculated at this stage revealed the location of the remaining oxygen atom arising from the water molecule present in the crystal lattice.

Before further refinement the two equivalent forms of data were corrected for absorption using an analytical method and were then averaged. The spread of correction factors applied to the data set is very large and reflects the two "different" orientations of the crystal in the X-ray beam during data collection of the two equivalent forms. Certainly the range is much greater than that expected for a data set where only one unique form of data had been collected.

Further full matrix least squares refinements with all atoms anisotropic produced an R factor of 0.054. The temperature factor of the oxygen atom was rather large at this stage and some large residual density remained near the iridium atom in the difference electron density synthesis calculated for this model. Close examination of the magnitude of observed and calculated structure factors indicated an extinction correction was required and final full matrix least squares refinement with this and corrections for anomalous dispersion included saw the model converge at a residual of 0.053 with a weighted residual of 0.053. The weighting scheme appeared to be satisfactory at this stage.

The full matrix least squares refinements above were completed using the SHELX76 programme package and as a

comparison, these refinements were repeated using the local least squares refinement programme, CUCLS76. Exactly the same number of variables was used in these refinements including an extinction parameter. Convergence of the model using CUCLS76 produced a residual of 0.054 with a weighted residual of 0.060. The weighting scheme appeared to be satisfactory and the error in an observation of unit weight was 1.182. The positional and thermal atomic parameters for one of these refinements are given in Table 3.5.3.

The refinements using the SHELX76 and CUCLS76 programmes produce atomic and thermal parameters which lay within the range of one standard deviation of each other. The difference in the residual is not significant and the larger difference between the weighted residual is a result of the slightly different weighting schemes used in the two programmes.

A final list of observed and calculated structure factors is listed in Appendix D.

3.5.3 Description of the Structure

A projection diagram of the unit cell contents for $Rb_3[IrBr_6]H_2O$ is illustrated in Figure 3.5.1. Figure 3.5.2 gives a stereoscopic view of the unit cell contents.

The structure is isomorphous to that of $(NH_4)_3[IrCl_6]H_2O$. It contains distorted $[IrBr_6]^{3-}$ anions located on mirror planes at y = 1/4, 3/4 with two of the bromine atoms in each anion also lying on the mirror plane. The three rubidium

Table 3.5.3: Positional and Thermal Parameters for $Rb_3[IrBr_6]H_2O$.

Atom	x	y	z	U(or U_{11})	U_{22}	U_{33}	U_{12}	U_{13}	U_{23}
Ir	0.2742(2)	0.25	-0.0976(1)	0.027(1)	0.024(1)	0.0234(9)	0.0	-0.0008(8)	0.0
Br(1)	0.3625(4)	0.25	0.0502(3)	0.041(3)	0.062(3)	0.028(3)	0.0	-0.007(2)	0.0
Br(2)	0.1855(4)	0.25	-0.2464(3)	0.040(3)	0.062(3)	0.033(3)	0.0	-0.012(2)	0.0
Br(3)	0.3979(3)	0.0137(5)	-0.1533(2)	0.051(3)	0.041(2)	0.042(2)	0.013(2)	0.007(2)	-0.001(2)
Br(4)	0.1519(3)	0.0126(5)	-0.0408(2)	0.053(2)	0.050(2)	0.047(2)	-0.020(2)	0.009(2)	0.001(2)
Rb(1)	0.1106(4)	0.25	-0.4644(3)	0.045(3)	0.047(3)	0.032(2)	0.0	-0.004(2)	0.0
Rb(2)	0.0584(5)	-0.25	0.1458(4)	0.039(4)	0.182(8)	0.036(3)	0.0	-0.001(3)	0.0
Rb(3)	0.3281(3)	0.25	0.2737(4)	0.163(8)	0.059(4)	0.045(3)	0.0	0.025(4)	0.0
O	0.063(5)	0.25	0.155(3)	0.10(4)	0.23(7)	0.06(3)	0.0	0.02(4)	0.0

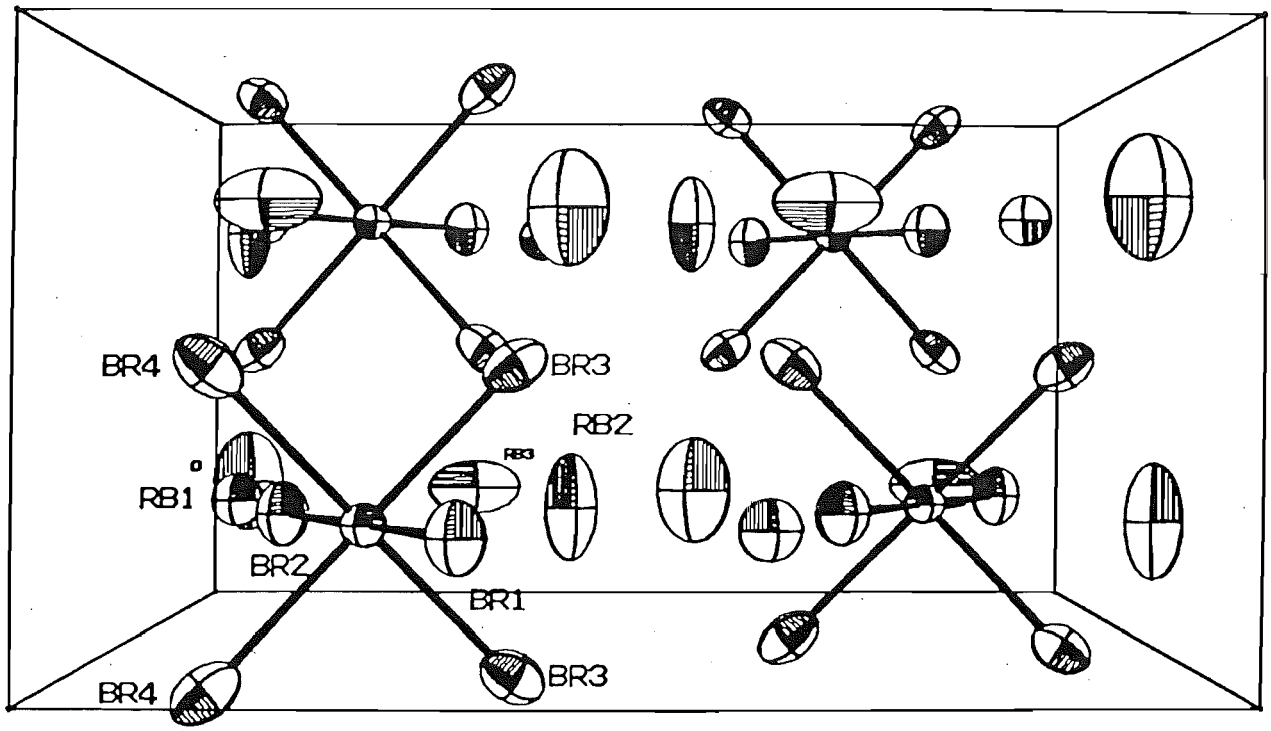

Figure 3.5.1: Projection diagram of the unit cell contents of $Rb_3[IrBr_6]H_2O$ viewed down an axis parallel to the c axis.

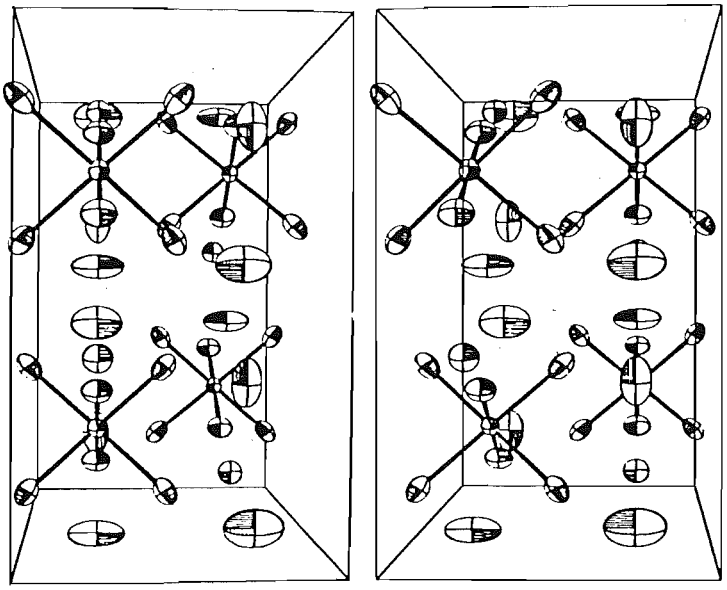

Figure 3.5.2: Stereoscopic view of the unit cell contents of $Rb_3[IrBr_6]H_2O$.

atoms and water molecule in the asymmetric unit also lie on these mirror planes, the remaining four bromine atoms in each anion are on general positions. The distortion in the anions is small with bond angles showing significant departure from ideal octahedral angles (of 90°) but the bond lengths remaining essentially the same. Bond lengths and bond angles for the anions are reported in Table 3.5.4. The averaged bond length of the iridium bromine bond of 2.496(4)Å is close to that reported for the rhodium bromine bond length of 2.50 Å found in the $[RhBr_6]^{3-}$ anion in $(H_3O)K_8[RhBr_6]_3 9H_2O$.

Root-mean-square components of thermal displacement of atoms in $Rb_3[IrBr_6]H_2O$, and for the bromine atoms the angles between the principal axes of their thermal ellipsoids and their respective iridium bromine bond vectors, are given in Table 3.5.5. The largest displacements of the bromine atoms in anisotropic vibration occur at right angles to the Ir-Br bond vectors as expected. Corrected bond lengths taking into account this thermal motion of the bromine atoms are shown in Table 3.5.4. No significant differences from the uncorrected bond lengths are found.

Interatomic contacts between bromine, rubidium and oxygen atoms less than 3.7 Å are given in Table 3.5.6. These show no contacts significantly less than those expected on the basis of the sum of ionic radii for the various ions concerned.

No hydrogen atoms were included in the present refinements and their positions remain undetermined.

Table 3.5.4: Bond Lengths (Å) and Bond Angles (degrees) in the $[IrBr_6]^{3-}$ Anion in $Rb_3[IrBr_6]H_2O$.

(i) Bond lengths

Ir-Br(1)	2.486(5)		
Ir-Br(2)	2.500(5)		
Ir-Br(3)	2.499(4)	Ir-Br(5)[a]	2.499(4)
Ir-Br(4)	2.498(4)	Ir-Br(6)[a]	2.498(4)
Mean	2.497(5)		

(ii) Corrected bond lengths

Ir-Br(1)	2.497(5)		
Ir-Br(2)	2.512(5)		
Ir-Br(3)	2.510(4)	Ir-Br(5)	2.510(4)
Ir-Br(4)	2.512(4)	Ir-Br(6)	2.512(4)
Mean	2.509(6)		

(iii) Bond angles

Br(1)-Ir-Br(2)	179.9(2)	Br(3)-Ir-Br(4)	91.0(1)
Br(1)-Ir-Br(3)	90.6(1)	Br(3)-Ir-Br(5)	88.7(2)
Br(1)-Ir-Br(4)	88.9(1)	Br(3)-Ir-Br(6)	179.4(2)
Br(1)-Ir-Br(5)	90.6(1)	Br(4)-Ir-Br(5)	179.4(2)
Br(1)-Ir-Br(6)	88.9(1)	Br(4)-Ir-Br(6)	89.2(2)
Br(2)-Ir-Br(3)	89.3(1)	Br(5)-Ir-Br(6)	91.0(1)
Br(2)-Ir-Br(4)	91.2(1)		
Br(2)-Ir-Br(5)	89.3(1)		
Br(2)-Ir-Br(6)	91.2(1)		

[a] Br(5) and Br(6) are symmetry related atoms of Br(3) and Br(4) respectively.

Table 3.5.5: Root-Mean-Square Components (Å) of Thermal Displacements of Atoms and Angles (degrees) between the Principal Axes of these Vibration Ellipsoids and the Ir-Br vectors for Bromine Atoms in $Rb_3[IrBr_6]H_2O$.

Atom	Axis 1	Angle	Axis 2	Angle	Axis 3	Angle
Ir	0.152(3)		0.156(3)		0.164(3)	
Br(1)	0.157(8)	3(7)	0.209(8)	93(7)	0.250(7)	90.00
Br(2)	0.155(8)	169(5)	0.221(7)	101(5)	0.249(6)	90.00
Br(3)	0.172(6)	4(5)	0.206(5)	96(2)	0.248(5)	87(3)
Br(4)	0.172(6)	176(3)	0.219(5)	88(5)	0.270(5)	87(2)
Rb(1)	0.175(7)		0.216(8)		0.217(7)	
Rb(2)	0.189(8)		0.199(9)		0.427(9)	
Rb(3)	0.201(8)		0.243(8)		0.410(10)	
O	0.23(7)		0.33(7)		0.48(8)	

Table 3.5.6: Selected Interatomic Contacts (Å) less than 3.7 Å in $Rb_3[IrBr_6]H_2O$.

Rb(1)...Br(2)	3.404(7)	Br(1)...Br(4)	3.489(6)
...Br(1)	3.418(7)	...Br(3)	3.543(6)
...Br(3)	3.438(5)		
...Br(3)	3.679(6)	Br(2)...Br(3)	3.514(6)
		...Br(4)	3.571(6)
Rb(2)...Br(2)	3.460(9)		
...Br(3)	3.525(7)	Br(3)...Br(3)[a]	3.493(7)
...Br(4)	3.572(7)	...Br(4)	3.564(5)
...Br(4)	3.607(7)		
...Br(2)	3.647(9)	Br(4)...Br(4)[a]	3.509(8)
Rb(3)...O	3.183(63)		
...Br(1)	3.377(8)		
...Br(4)	3.399(7)		
...Br(3)	3.650(9)		
O...Rb(3)	3.183(63)		
...Br(3)	3.511(5)		
...Br(4)	3.599(5)		

[a] symmetry related atoms

3.6 THE CRYSTAL STRUCTURES OF RELATED HEXAHALOGENOMETALLATES

Preliminary X-ray diffraction photographic studies carried out on single crystals on a number of other hexahalogenometallates prepared in this work have revealed isomorphism of compounds both with structures reported in this work and with structures reported in the literature. A summary of unit cell parameters and other crystal data is given in Table 3.6.1.

Before examining this material some comments will be made on the use of single crystal and powder X-ray diffraction studies to determine isomorphism between compounds as both these techniques have been used extensively in this work.

Single crystal studies yield by far the most detailed and conclusive information on isomorphism between compounds short of complete structural analyses. Zero and upper level precession or Weissenberg photographs permit determination of unit cell parameters and space groups as well as a visual check on relative intensities of reflections for compounds suspected of being isomorphous (or being isostructural). Powder photography on the other hand, is less informative. Except in simple cases (e.g. cubic compounds), cell parameters and space group data are not readily extractable and only where compounds have similar cell dimensions will the powder photographs of two isomorphous compounds appear identical (although reflection intensities will differ). Thus, powder photography has only been used to suggest isomorphism between compounds in

Table 3.6.1: Crystal Data for Iridium (III) Hexahalogenometallates[a]

Compound	Space Group	Anion Site Symmetry	a(Å)	b(Å)	c(Å)	α(°)	β(°)	γ(°)	d_m (gcm^{-3})	d_c (gcm^{-3})
$K_3[IrCl_6]$	$P\bar{1}$	$C_i(\bar{1})$	12.631(2)	7.029(1)	7.027(1)	116.12(2)	91.21(9)	106.88(9)	3.284(6)	3.286
$(NH_4)_3[IrCl_6]$	$P\bar{1}$	$C_i(\bar{1})$	12.602(30)	7.226(20)	7.502(20)	119.18(50)	91.60(50)	106.70(50)	2.86(5)	2.72
$K_3[IrCl_6]H_2O$	Pbcn	$C_1(1)$	12.436(3)	15.682(3)	12.072(2)	90	90	90	3.20(5)	3.05
$(NH_4)_3[IrCl_6]H_2O$	Pnma	$C_s(m)$	12.229(2)	7.011(1)	14.088(2)	90	90	90	2.61(1)	2.62
$Rb_3[IrCl_6]H_2O$	Pnma	$C_s(m)$	12.276(30)	7.016(20)	14.157(30)	90	90	90	3.02(5)	3.04
$Cs_3[IrCl_6]H_2O$	Pnma	$C_s(m)$	12.554(30)	7.200(20)	14.833(30)	90	90	90	>3.3	4.07
$[Co(NH_3)_6][IrCl_6]$	Pa3	$C_{3i}(\bar{3})$	11.169(3)	11.169(3)	11.169(3)	90	90	90	-	-
$(H_3O)K_8[IrBr_6]_3 9H_2O$	Pbam	$C_s(m), C_i(\bar{1})$	15.259(30)	16.523(30)	9.304(20)	90	90	90	>3.3	5.33
$(NH_4)_3[IrBr_6]H_2O$	Pnma	$C_s(m)$	12.672(30)	7.390(20)	14.951(30)	90	90	90	>3.3	3.53
$Rb_3[IrBr_6]H_2O$	Pnma	$C_s(m)$	12.768(2)	7.391(1)	14.982(2)	90	90	90	>3.3	4.46
$Cs_3[IrBr_6]H_2O$	Pnma	$C_s(m)$	13.060(30)	7.529(20)	15.744(30)	90	90	90	>3.3	4.67
$[Co(NH_3)_6)[IrBr_6]$	Pa3	$C_{3i}(\bar{3})$	11.600(4)	11.600(4)	11.600(4)	90	90	90	-	-
$Na_3[IrCl_6]10H_2O$[b]	$R\bar{3}m$	unknown	16.677	16.677	16.677	100.02	100.02	100.02	2.29	2.22

[a] All data (except for $[Co(NH_3)_6][IrCl_6]$ and $[Co(NH_3)_6][IrBr_6]$] from single crystal X-ray diffraction studies.

[b] From reference[32].

the present study where powder photographs are nearly identical.

In some cases, powder photographs of compounds suggested to be isomorphous by single crystal studies, bear no resemblance to one another. This occurs for example for the compounds $(NH_4)_3[IrCl_6]H_2O$ and $Rb_3[IrBr_6]H_2O$, and arises from the large differences in the relative magnitudes of structure factors and cell dimensions as a consequence of the different anions and cations present in the compounds. It may be more correct to refer to such compounds as isostructural, in contrast to the usual definition of isomorphous, which refers to the situation where an anion or cation (or component atom of an anion or cation) is replaced by a counterpart of a similar size (e.g. in the isomorphous structures of $K_3[RhCl_6]H_2O$ and $K_3[IrCl_6]H_2O$ where the tervalent Rh^{3+} and Ir^{3+} ions both have ionic radii of about 0.68 Å).

In the following sections the determination of the isomorphous or isostructural nature of various compounds is largely made on the basis of single crystal X-ray diffraction photographic studies. With the space group, cell parameters and intensity data determined in these studies, isomorphism between compounds can be determined with a reasonable degree of certainty. However, it should be remembered that although both powder and single crystal diffraction studies may indicate compounds are isomorphous or isostructural, the only conclusive means by which such hypotheses can be verified is full crystal structure analysis of the compounds in question.

3.6.1 Ammonium Hexachloroiridate (III), $(NH_4)_3[IrCl_6]$

This compound was found to be isomorphous to $K_3[IrCl_6]$ and must therefore, contain distorted $[IrCl_6]^{3-}$ anions on sites of $\bar{1}$ symmetry. The measured density of the compound was in agreement with that calculated on the basis of the cell dimensions determined from zero level precession photographs using CuKα radiation. Its powder photograph differed considerably in appearance from that of $K_3[IrCl_6]$, indicating the major influence on relative intensities and positions (Bragg angles) of reflections of substituting the relatively heavy K^+ for NH_4^+. Powder photographs also show $K_3[RhCl_6]$ is isomorphous to $K_3[IrCl_6]$. Powder photographs of the compound $K_3[RuCl_6]$, whose X-ray powder diffraction spectrum has been published[13], are similar to those of $K_3[IrCl_6]$ and these compounds could be isomorphous. No single crystals of $K_3[RuCl_6]$ were available to check this hypothesis.

3.6.2 Rubidium Hexachloroiridate (III) Monohydrate and Caesium Hexachloroiridate (III) Monohydrate, $Rb_3[IrCl_6]H_2O$ and $Cs_3[IrCl_6]H_2O$

Preliminary studies on both of the compounds revealed each crystallised in the space group Pnma (or the non centric equivalent, in terms of extinctions, $Pna2_1$) and with dimensions similar to those of $(NH_4)_3[IrCl_6]H_2O$. On these grounds it was concluded that all three compounds are probably isostructural and hence must contain $[IrCl_6]^{3-}$

anions located on sites of m symmetry. It is of interest to note that powder photographs of these compounds differed considerably in appearance, again a result of the very different diffracting power of the three cations and differences in the unit cell dimensions. This is illustrated in Table 3.6.2 where 2θ values for powder photographs (and approximate relative intensities of reflections) of $(NH_4)_3[IrCl_6]H_2O$, $Cs_3[IrCl_6]H_2O$ and $Rb_3[IrBr_6]H_2O$ show large variations in line positions (and intensities) although these compounds are isostructural. These salts are also isomorphous to their $A_3[RhCl_6]H_2O$ (A = NH_4, Rb, Cs) analogues. The rhodium(III) and iridium(III) salts with the same cation show almost identical powder photographs, indicating a close similarity between cell dimensions and therefore the ionic radii of the Ir^{3+} and Rh^{3+} ions in the compounds of these two metal ions.

3.6.3 Hexaammine cobaltic(III) Hexachloroiridate(III) $[Co(NH_3)_6][IrCl_6]$

Single crystals of this compound were not isolated and hence no density measurement was made. The simplicity of the X-ray powder diffraction photograph of this compound implied it crystallised in a cubic space group. A check on the lines appearing in the powder photograph revealed they were in fact consistent with a primitive cubic space group. This was achieved by evaluating $\sin^2\theta$ values for

Table 3.6.2: Theoretical 2θ (mm) Values and Relative Intensities[a] of Strong Low Angle Reflections of $(NH_4)_3[IrCl_6]H_2O$, $Cs_3[IrCl_6]H_2O$ and $Rb_3[IrBr_6]H_2O$ using CuKα ($K\bar{\alpha}$, λ = 1.5418Å) Radiation and a Debye-Scherrer Powder Camera of Radius 57.30 mm.

	$(NH_4)_3[IrCl_6]H_2O$		$Cs_3[IrCl_6]H_2O$	$Rb_3[IrBr_6]H_2O$	
hkℓ	2θ	I/I_o	2θ	2θ	I/I_o
002	12.57	41	11.93	11.81	23
011	14.11	50	13.67	13.36	30
200	14.49	80	14.11	13.87	39
102	14.51	86	13.87	13.71	55
211	20.28	44	19.69	19.30	13
013	22.79	63	21.81	21.47	38
004	25.29	41	24.00	23.76	8
020	25.41	68	27.73	24.08	56
311	26.06	53	25.34	24.86	32
104	26.33	38	25.04	24.77	8
213	27.11	56	26.07	25.65	24
123	32.71	49	31.56	30.91	1
322	36.12	89	35.03	34.29	43
024	36.15	29	34.73	34.08	7
031	39.07	32	37.98	36.98	15
033	43.24	47	41.84	40.84	23
040	52.19	100	50.72	49.32	100

[a] Determined for $(NH_4)_3[IrCl_6]H_2O$ and $Rb_3[IrBr_6]H_2O$ from intensity data (from single crystals) measured on a four circle diffractometer.

the reflections observed and determining the ratio $\sin^2\theta/\sin^2\theta_1$, where θ_1 is the Bragg angle of the lowest Bragg angle reflection observed. From these ratios, $N(\equiv(h^2+k^2+\ell^2))$ can be determined and with a knowledge of the h,k,ℓ combinations allowed for the primitive, face and body centred cubic space groups, the above assignment was made.

A survey of the literature revealed a number of related compounds of the above stoichiometry have been reported including hexaammine metallates of chromium, cobalt and rhodium with hexahalogenometallates of thallium, antimony, chromium and iron[66, 67, 68, 69, 70, 71, 72, 73] These compounds and relevant crystal data are listed in Table 3.6.3. All of the complex salts are reported to crystallise in the cubic space group Pa3 (No. 205) except one compound, hexaamminecobaltic(III) hexachloroantimonate (III), $[Co(NH_3)_6][SbCl_6]$.[68]

$[Co(NH_3)_6][SbCl_6]$ is said to crystallise in the orthorhombic space group Pbca (as determined by the systematic absenses 0kℓ, k=2n+1; h0ℓ, ℓ = 2n+1; hk0, h = 2n+1) with cell dimensions

$$a = 11.50(3)\ \text{Å},\ b = 11.53(3)\ \text{Å},\ c = 11.51(2)\ \text{Å},$$
$$\alpha = \beta = \gamma = 90^{\circ}.$$

The authors of this report make no mention of the other stoichiometrically related compounds previously reported and it would appear, for a number of reasons, that the structure could in fact be of the normal cubic space group

Table 3.6.3: Unit Cell Constants[a] for Hexaamminemetallate (III) Hexahalogenometallate (III) Compounds

Compound	Crystal class	Space group	z	a (Å)	Reference
$[Co(NH_3)_6][CrCl_6]$	cubic	Pa3	4	11.17	66
$[Cr(NH_3)_6][CrCl_6]$	cubic	Pa3	4	11.30	66
$[Rh(NH_3)_6][CrCl_6]$	cubic	Pa3	4	11.24	66
$[Co(NH_3)_6][FeCl_6]$	cubic	Pa3	4	11.22(4)	67
$[Cr(NH_3)_6][FeCl_6]$	cubic	Pa3	4	11.33	66
$[Co(NH_3)_6][IrCl_6]$	cubic	primitive	-	11.169(3)	this work
$[Co(NH_3)_6][SbCl_6]$	orthorhombic	Pbca	4	11.50(3)[b]	68
$[Co(NH_3)_6][SbCl_6]$	cubic	Pa3	4	11.48	69
$[Co(NH_3)_6][TlCl_6]$	cubic	Pa3	4	11.40	70
$[Co(NH_3)_6][IrBr_6]$	cubic	primitive	-	11.600(4)	this work
$[Co(NH_3)_6][TlBr_6]$	cubic	Pa3	4	11.77	70

a The two choices of reported unit cells (cubic or orthorhombic) for these compounds both have inter axial angles of 90° (i.e. $\alpha=\beta=\gamma=90^\circ$).

b The two remaining cell dimensions for the orthorhombic structure of $[Co(NH_3)_6][SbCl_6]$ are b = 11.53(3) Å, c = 11.51(2) Å.

c Crystal structures were determined in these cases from single crystal X-ray diffraction studies. Otherwise cell dimension data has been obtained from powder photographs. The cell data reported for the Ir(III) complexes studied in this work were evaluated from X-ray powder diffractograms.

(Pa3) type.' The systematic absences observed are consistent with the cubic space group Pa3. The axial cell dimensions are all equivalent (within experimental error) and their mean is of the correct magnitude for a cubic cell dimension analogous to those for related compounds. More importantly, the anions and cations in the reported structure on sites of $\bar{1}$ symmetry, are located in exactly that spatial arrangement for the cubic structures. This means that the coordinates reported for the component atoms of the two ion types in the compound correspond to those reported for the cubic structure. Furthermore Martineau and Milne[69] have reported $[Co(NH_3)_6][SbCl_6]$ to be isostructural with $[Co(NH_3)_6][TlCl_6]$ with a cubic cell dimension of 11.48 Å.

Thus, although no accurate determination of the crystal structure of a compound of the cubic structural type has been made to date (data in reference 70 was measured from films and no R factors were produced), the simplicity of powder photographs of apparently isomorphous compounds and the at least partial success of the cubic structure determination[70] lend support to the assertion that all these compounds probably crystallise in the cubic space group Pa3.

On the basis of the simple X-ray powder diffraction pattern and the determination of suitable cell dimensions (see Table 3.6.3 and Section 9.3.5(ii)) of the correct magnitude, the compound $[Co(NH_3)_6][IrCl_6]$ is assumed to crystallise in the cubic space group Pa3. This confers $\bar{3}$ site symmetry on both the $[IrCl_6]^{3-}$ and $[Co(NH_3)_6]^{3+}$ ions.

In the crystal structures of $[Co(NH_3)_6][SbCl_6]$ and $[Co(NH_3)_6][TlCl_6]$ reported to date, the hexachlorometallate ions have shown significant distortion from octahedral (O_h) symmetry. This distortion from $O_h(m3m)$ symmetry involves deformation only of interbond angles, as, for $\bar{3}$ symmetry of the $[IrCl_6]^{3-}$ anion to be retained, the bond lengths must all be the same. The compound $[Co(NH_3)_6][IrBr_6]$ also crystallises in the primitive cubic crystal class. The cell dimensions of this complex are within permissible limits, being smaller than those of $[Co(NH_3)_6][TlBr_6]$ as expected on the basis of the larger ionic radius of the Tl^{3+} ion.

3.6.4 Hydronium Potassium Hexabromoiridate (III) Nonahydrate, $(H_3O)K_8[IrBr_6]_3 9H_2O$

Crystals of this compound were found to crystallise in the orthorhombic space group Pbam with cell dimensions

$a = 15.259(30)$ Å, $b = 16.523(30)$ Å, $c = 9.304(20)$ Å, $\alpha=\beta=\gamma=90^{o}$.

The rhodium analogue, $(H_3O)K_8[RhBr_6]_3 9H_2O$,[4] crystallises in the same space group with cell dimensions

$a = 15.32(2)$ Å, $b = 16.63(2)$ Å, $c = 9.30(1)$ Å, $\alpha=\beta=\gamma=90^{o}$.

The two compounds are probably isomorphous. Their powder photographs are almost identical. The reported structure of the rhodium complex by Coetzer et al.[4] reveals $[RhBr_6]^{3-}$ octahedral anions (showing significant distortion from perfect octahedral geometry) located on two crystallographically distinct sites, one of symmetry $\bar{1}$ and the other of site symmetry m. The potassium ions surrounding these two types of $[RhBr_6]^{3-}$ anion have different spatial distributions.

3.6.5 Ammonium Hexabromoiridate (III) Monohydrate and Caesium Hexabromoiridate (III) Monohydrate, $(NH_4)_3[IrBr_6]H_2O$ and $Cs_3[IrBr_6]H_2O$

As for the corresponding hexachloroiridates, these compounds were both found to be isomorphous to $Rb_3[IrBr_6]H_2O$ and each salt is isomorphous to its rhodium analogue. The powder photographs of the three compounds do not give any indication of isomorphism between the compounds. All three compounds crystallise in the orthorhombic space group Pnma and their similar cell dimensions indicate their isomorphism with the series of hexachlorometallate salts of iridium and rhodium. The solved crystal structures of $Rb_3[IrBr_6]H_2O$ and $(NH_4)_3[IrCl_6]H_2O$ confirm this.

3.7 DISCUSSION OF THE CRYSTAL STRUCTURES OF HEXAHALOGENOMETALLATES OF IRIDIUM (III)

One of the notable features of the preceeding structures and structural types in which the iridium (III) hexahalogeno-

metallates crystallise, is the presence of $[IrX_6]^{3-}$ (X = Cl,Br) anions showing significant distortion from true octahedral symmetry. This is in direct contrast to iridium (IV) hexahalogenometallates (which will be discussed in the following chapter), which crystallise in the space group Fm3m, and where the octahedral $[IrX_6]^{2-}$ (X = Cl, Br) anions are located on sites of O_h(m3m) symmetry and which therefore show no distortion from ideal octahedral symmetry. Possible reasons for the distortion of the $[IrX_6]^{3-}$ anions in the compounds studied in this work will be considered following a discussion of the crystal structural types in which these compounds form.

3.7.1 Comments on the Crystal Structures of $K_2[IrCl_6]$ and $K_3[IrCl_6]$

(i) Structural Considerations; Comparison with Fluoro Analogues

A large number of hexafluorometallate complexes, primarily of first row transition metals, of stoichiometry $A_2[MF_6]$, $A_3[MF_6]$ and $A_2B[MF_6]$ (where A,B are univalent cations, M metals such as Fe, Co, Ni, Co, V in either the trivalent or tetravalent oxidation state) have been found to crystallise in the cubic space group Fm3m. Compounds of stoichiometry $A_2[MF_6]$ are isomorphous to the $K_2[PtCl_6]$ type structure and those of stoichiometry $A_3[MF_6]$ or $A_2B[MF_6]$ retain the same space group and locate the additional cations (A or B) on sites (0,0,½) and symmetry related

equivalents. Figure 3.7.1 contains diagrams of unit cells for both structural types.

Some structural aspects of the two compounds $Cs_2[CoF_6]$ and $Cs_3[CoF_6]$ will now be discussed primarily to elucidate reasons as to why the stoichiometrically related compounds $K_2[IrCl_6]$ and $K_3[IrCl_6]$ do not both crystallise in the same cubic space group Fm3m. Table 3.7.1 contains some relevant structural data.

Table 3.7.1: Structural Data for Cobalt (IV), Iridium (IV) and Cobalt (III) Hexahalogenometallates

Compound	a (Å)	u	M-X[a] distance (Å)	$X^-...A^+$[b] distance (Å)	$A^+...A^+$ distance (Å)
$Cs_2[CoF_6]$	8.905	0.2212	≈1.97	3.492	4.453
$Cs_3[CoF_6]$	9.22	0.2137	≈1.97	3.703,2.650	4.61,3.992
$K_2[IrCl_6]$	9.7189	0.2374(9)	2.307	3.439	4.860

[a] M = Co, Ir; X = F, Cl [b] A = Cs,K

The cell dimensions reflect expected expansion of the $Cs_2[CoF_6]$ lattice when a further caesium cation is added to the lattice in forming $Cs_3[CoF_6]$. With this change in the lattice a number of interatomic distances decrease as shown in Table 3.7.1.

With $K_2[IrCl_6]$ and $K_3[IrCl_6]$, the $[IrCl_6]^{n-}$ anions have larger dimensions than those of their hexafluorometallate counterparts. This arises primarily from the increase in the

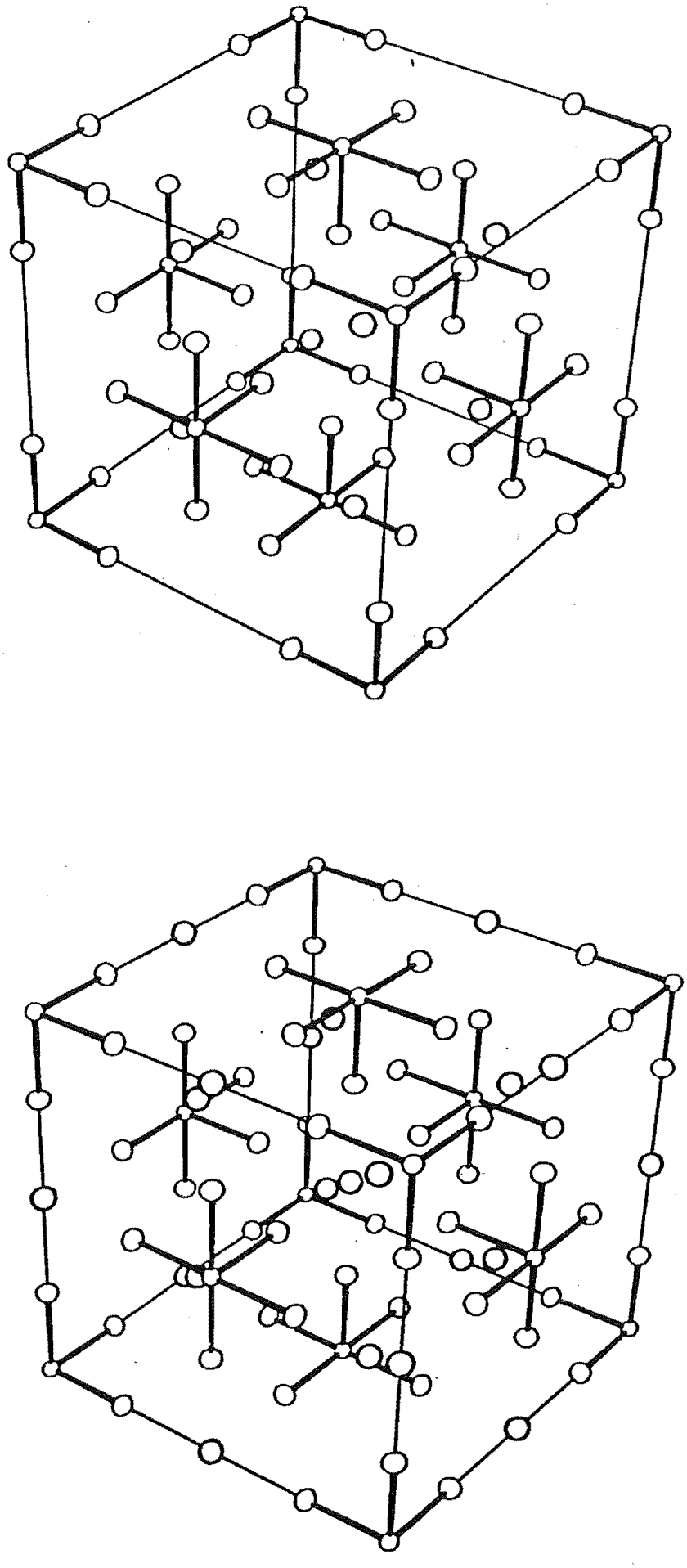

Figure 3.7.1: Projection diagrams of the unit cell contents of the $A_2[MF_6]$ (upper figure) and $A_3[MF_6]$ (lower figure) structural types viewed close to a body diagonal.

size of the halogen atoms bonded to the transition metal ion and to a lesser degree from the slightly larger central metal ion. In order to accommodate a further K^+ ion at a site such as $(0,0,\frac{1}{2})$ (to give $K_3[IrCl_6]$ and maintain the Fm3m space group) the cell dimensions for $K_2[IrCl_6]$ must expand to something of the order of 10.25Å. This would give $K^+...Cl^-$ contacts of 2.818 Å and 3.626 Å and relatively large $K^+...K^+$ interactions of 4.438 Å and 5.125 Å. However, compared with the $Cs_2[CoF_6]$ and $Cs_3[CoF_6]$ system, the increases are proportionally larger for $K_2[IrCl_6]$ and $K_3[IrCl_6]$, and the lattice arrangement would contain a great deal of space and be less stable than the more economical packing arrangement found in the triclinic space group $P\bar{1}$. Examination of the data in Table 3.2.5 reveals overall shorter distances for attractive interactions between Cl atoms and K^+ ions as well as expected shorter $K^+...K^+$ repulsive interactions. The more important point however, is that the packing arrangement is now considerably more space filling than the arrangement suggested for the cubic form of $K_3[IrCl_6]$.

Thus the relative sizes of the anion and cation make formation of $K_3[IrCl_6]$ in the cubic space group Fm3m (analogous to $Cs_3[CoF_6]$) unlikely.

(ii) Lattice Energy Considerations

As a means of gauging the energetically preferred packing arrangement of ions in $K_3[IrCl_6]$ in either the cubic Fm3m or triclinic $P\bar{1}$ crystal space groups some simple

point charge model lattice energy calculations were attempted.

Two simple point charge models are available for the calculation of lattice energies.[74] The Born-Landé equation sums ion interactions throughout the lattice, making use of a constant for a particular crystal structure type, the Madelung constant, and the smallest anion-cation distance, r_o. This is given in equation (3.7.1)

$$U = - \frac{N_A A z^2 e^2}{4\varepsilon_o r_o \pi} (1 - \frac{1}{n}) \qquad (3.7.1)$$

where N_A is Avagadro's number

A the Madelung constant

z the highest common factor of the anion and cation charges

n Born exponent, experimental derived value

ε_o 8.854×10^{-12} Fm^{-1}

r_o smallest anion-cation approach.

e electronic charge

The more general (and more approximate) Kapustinskii equation[75], which makes no assumption about the space group in which the compound forms, uses the ionic radii of the component ions in the lattice. This is given by equation (3.7.2)

$$U = \frac{N_A A e^2 v z_c z_a}{8\pi \quad \varepsilon_o (r_a + r_c)} (1 - \frac{1}{n}) \qquad (3.7.2)$$

where A is the Madelung constant for NaCl

z_a, z_c charges on the anions and cations respectively

r_a, r_c ionic (or thermochemical) radii of the anions and cations respectively

v the total number of ions in the stoichiometric molecule

other variables (constants) are as defined in equation (3.7.1)

When n = 9, equation (3.7.2) reduces to equation (3.7.3) when numerical constants are evaluated.

$$U = 108.0\ v\ \frac{z_a z_c}{r_c + r_a}\ kJ\ mol^{-1} \qquad (3.7.3)$$

Both the Born-Landé equation and Kapustinski equation yield lattice energies to within 5% of those correct values calculated by the Born-Haber cycle for simple alkali metal halide ionic compounds (e.g. NaCl).

The present study therefore, involved calculation of the "true" lattice energy for $K_3[IrCl_6]$ via the Kapustinskii equation and comparison of this value with that calculated for $K_3[IrCl_6]$ assuming it crystallises in the cubic $Cs_3[CoF_6]$ cubic structure. Calculations were also made for $K_2[IrCl_6]$.

Using equation (3.7.1) evaluation of the lattice energy is facile for $K_2[IrCl_6]$(whose Madelung constant is known, 5.03878[74]). However, the Madelung constant for $K_3[IrCl_6]$, assuming a $Cs_3[CoF_6]$ type structure, is not known and was therefore calculated from first principles.

A simple computer algorithm was written to perform this calculation. However, the algorithm used gave poor convergence of lattice summations. The Madelung constant calculated for $K_2[IrCl_6]$ (4.63635) was still 8% lower than the theoretical value for this antifluorite lattice (5.03878). Thus, associated with this poor convergence, there is an error attached to the evaluated lattice energies for the $K_3[IrCl_6]$ cubic structure and this could be as much as $\pm$ 10% of the calculated values recorded in Table 3.7.2. However discussion of the results of these approximate calculations is still meaningful.

The results of calculations are summarised in Table 3.7.2. The first section of the table gives data for calculations of the lattice energy of $K_2[IrCl_6]$ by both the Born-Landé method and by the Kapustinskii method. In the latter method a number of plausible ionic radii of the $[IrCl_6]^{2-}$ anion are considered, as the thermochemical radius of this anion is not accurately known. The second section of the table gives calculated lattice energies for the hypothetical cubic $K_3[IrCl_6]$ structure. These calculations, using the Born-Landé method, are executed for a range of cubic unit cell dimensions (within which the hypothetical cubic unit cell dimensions will lie) using the Madelung constant function calculated in this work. Calculations of the actual lattice energy of $K_3[IrCl_6]$ using the Kapustinskii equation completes this table.

The lattice energy calculated for $K_2[IrCl_6]$ by the Born-Landé expression is close to that calculated by the

Table 3.7.2: Results of Calculations of Lattice Energies for $K_2[IrCl_6]$ and $K_3[IrCl_6]$ by the Born-Landé and Kapustinskii Methods.

Compound	Calculation Method	Cubic Cell Constant (Å)	$[IrCl_6]^{n-}$ ionic radii (Å)	Madelung Constant (or Madelung Constant function)	U(Lattice Energy, kJ mol^{-1})
$K_2[IrCl_6]$	Born-Landé	9.7189[a]		5.03878	-1505
	Kapustinskii		4.28[c]		-1176
	"		3.78[d]		-1291
	"		3.28[e]		-1431
$K_3[IrCl_6]$	Born-Landé	9.7189[b]		1.46131[f]	-2030
	"	9.9189		1.43185	-1989
	"	10.1189		1.40354	-1950
	"	10.3189		1.37634	-1912
	"	10.5189		1.35017	-1876
	"	10.9189		1.30071	-1807
	Kapustinskii		4.30[c]		-2343
	"		3.80[d]		-2571
	"		3.30[e]		-2798

[a] $K_2[IrCl_6]$ cell data was obtained from reference

[b] The cubic cell dimensions listed for $K_3[IrCl_6]$ give a range of values within which the correct dimension of this hypothetical structure would lie.

[c] Calculated using the sum of ionic radii (Ir^{4+} 0.66 Å, Ir^{3+} 0.68 Å, Cl^- 1.81 Å)

[d] Intermediate value

[e] Calculated using the sum of the covalent radii (Ir^{4+} 1.30 Å, Ir^{3+} 1.32 Å, Cl 0.99 Å). All ionic and covalent radii data are from reference 77 .

[f] The values listed henceforth in this column are of the calculated Madelung constant function. The value of n (see equations (3.7.1) and (3.2.2) in all these calculations (10.5) was evaluated using the formulae suggested by reference 74 .

Kapustinskii equation where the ionic radius of the $[IrCl_6]^{2-}$ anion is 3.28Å (see Table 3.7.2). The implication is that for evaluation of the correct lattice energy for this compound by use of Kapustinskii's equation, the correct ionic radius of the $[IrCl_6]^{2-}$ (or $[IrCl_6]^{3-}$ anion for $K_3[IrCl_6]$ as the anions have a similar size) anion is closer to 3.3 Å than 4.3 Å and may be even smaller than the former value. This could suggest significant covalent bonding is present in the $[IrCl_6]^{2-}$ anion. The radius of 3.3 Å is in agreement with thermochemical ionic radii calculated for $Co(NH_3)_6^{2+}$ (2.6 Å) and $Co(H_2O)_6^{2+}$ (2.34 Å) from thermal data and use of Kapustinskii's equation.

With the ionic radius of the $[IrCl_6]^{3-}$ anion chosen at 3.3 Å, the lattice energy for $K_3[IrCl_6]$ calculated using the Kapustinskii equation is -2800 kJ mol^{-1}. If the $[IrCl_6]^{3-}$ thermochemical radius is smaller, then this lattice energy will be larger. Calculation of the lattice energy of $K_3[IrCl_6]$ (assuming the compound retains the $Cs_3[CoF_6]$ cubic structure) yields a value of -1930 kJ mol^{-1} for a cubic cell edge of 10.25 Å. This value, even allowing for an error of $\pm$ 10% in the calculated figure, is significantly lower than that predicted by the Kapustinskii equation.

This approximate analysis then, is consistent with the observation that $K_3[IrCl_6]$ does not crystallise in the cubic space group Fm3m in the $Cs_3[CoF_6]$ structural type. The analysis also gives a semi empirical basis to

the discussions in the previous section concerning the poor space filling characteristics shown by K^+ and $[IrCl_6]^{3-}$ ions in such a cubic structure.

3.7.2 Comments on the Crystal Structures of $A_3[IrCl_6]H_2O$ (where A=K, NH_4, Rb, Cs), $A_3[IrBr_6]H_2O$ (where A = NH_4, Rb, Cs) and $(H_3O)K_8[IrBr_6]_3 9H_2O$.

The isomorphism of the NH_4^+, Rb^+, Cs^+ salts of the series of compounds $A_3[IrCl_6]H_2O$ and $A_3[IrBr_6]H_2O$, with the ionic radii of the cations being 1.43 Å, 1.48 Å, and 1.67 Å respectively, and those of $[IrCl_6]^{3-}$ and $[IrBr_6]^{3-}$ showing a difference in ionic radii of approximately 0.3 Å, reflects the "accommodating" nature of the particular spatial arrangement of ions in this space group. This means that with satisfactory increases in cell dimensions (see Table 3.6.1) reflecting the placement of larger cations or anions in the unit cell, the non bonded contacts between the various ions and water molecules still remain satisfactory and do not require a change of spatial arrangement of the ions to give a more favourable energetically higher packing scheme for the ions.

Both the sodium and potassium salts of the hexachloroiridate (III) and potassium salts of the hexabromoiridate (III) ions do not crystallise in the same space group as their NH_4^+, Rb^+ or Cs^+ counterparts. $K_3[IrCl_6]H_2O$ adopts a new spatial arrangement of the ions in the space group Pbcn. This probably results from some critical minimum cation size (in the Pnma space group arrangement of ions)

having been reached with the smaller potassium cation (radius 1.33 Å). Thus the lattice has changed to an energetically more favourable structurally different form. $Na_3[IrCl_6]10H_2O$ similarly crystallises in a different space group, in this case the rhombohedral space group $R\bar{3}m$. The same situation occurs for $(H_3O)K_8[IrBr_6]_3 9H_2O$, where again the smaller size of the potassium ion means the $[IrBr_6]^{3-}$ anions no longer crystallise in the space group Pnma, with overall stoichiometry of the compound being $K_3[IrBr_6]H_2O$. Thus the compound crystallises in the space group Pbam with the compound showing a large degree of hydration which ensures adequate space filling of the unit cell of the crystal structure in which this compound forms.

3.7.3 Comparison of the Crystal Structures of $[Co(NH_3)_6][IrX_6]$, (X = Cl,Br)

Although crystallising in a cubic space group, the two types of ions in both these structures are located on sites of $C_{3i}(\bar{3})$ symmetry not of $O_h(m3m)$ symmetry. Assuming the compounds are isomorphous to their hexahalogeno-thallium analogues, one would expect both of the iridium compounds to show significant distortions of their respective anions from octahedral symmetry in the solid state.

The individual ions in $[Co(NH_3)_6][TlX_6]$(X=Cl,Br) structures are each surrounded by the counter ion in an octahedral fashion analogous to the structure of NaCl. Although for a point charge model the $[TlX_6]^{3-}$ ions must now be

surrounded by a spherically symmetric charge distribution (where +3 and -3 charges are assumed to be located on Co(III) and Ir(III) atom sites respectively), there are significant hydrogen bonding interactions in the solid state between the cobalt coordinated ammonia hydrogen atoms and the chlorine or bromine atoms coordinated to the thallium ions. These are probably responsible for the distortion of the $[TlCl_6]^{3-}$ and $[TlBr_6]^{3-}$ anions observed in the crystal structures of their respective hexaamminecobaltic(III) compounds. Such effects are also found in the reported structure of $[Co(NH_3)_6][SbCl_6]$, where the $[SbCl_6]^{3-}$ ions show significant distortion from octahedral symmetry.

It should be noted here that this distortion in the $[SbCl_6]^{3-}$ anion (of some bond angles by $0.7(2)^{\circ}$, $0.9(2)^{\circ}$ and $1.1(2)^{\circ}$ from 90°) is not a function of the lone pair in $[SbCl_6]^{3-}$ (from the total of seven valence electron pairs) occupying a coordination site. As has been shown in a Mössbauer study[78] and verified by other structural studies[79,80], the lone pair is probably occupying a spherically symmetric s orbital and therefore having no influence on the shape of the anion.

3.7.4 The Distortion in the Solid State of $[IrX_6]^{3-}$ (where X = Cl,Br) Anions in Iridium(III) Hexahalogenometallates

As the space groups in which tervalent iridium hexahalogenometallates form are non-cubic (except $[Co(NH_3)_6][IrX_6]$ where sites of the highest symmetry are $\bar{3}$) there is no crystallographically imposed requirement that the $[IrCl_6]^{3-}$ or $[IrBr_6]^{3-}$

anions need have perfect octahedral symmetry as is the case for the $[IrCl_6]^{2-}$ anion in cubic $K_2[IrCl_6]$. This does not rule out the possibility of the anions retaining idealised octahedral symmetry on sites of lower than O_h symmetry. However, in detailed structures of four halogenometallate complexes reported in preceeding sections, significant distortion of these anions from octahedral geometry was found. This distortion presumably arises from crystal packing effects, that is the unsymmetrical spatial arrangement of ions and water molecules and their repulsive and attractive non bonding interactions with one another result in distortion of the anions in the solid state. This naturally includes hydrogen bonding between suitable ions or water molecules of crystallisation in the crystal lattice and the electrostatic solid state forces between component ions and other constituents of the crystal lattice.

In a sense the stoichiometry of the complex is the reason for this distortion, as there appears to be no cubic space group in which compounds of the $A_3[IrX_6]H_2O$, $A_3[IrCl_6]$ or $[Co(NH_3)_6][IrX_6]$ stoichiometry may crystallise where the anions $[IrX_6]^{3-}$ could be located on sites of O_h (m3m) symmetry. The complex salt $Na_3[IrCl_6]10H_2O$ further emphasises this point. It crystallises in the rhombohedral system in the space group $R\bar{3}m$ (No. 166).[32] Thus tne assertion by Cresswell et. al.[2] that the presence of the water molecule was the prime factor causing distortion of the $[RhCl_6]^{3-}$ anions in $K_3[RhCl_6]H_2O$ is partially correct,

although the presence of this water molecule is not strictly required to ensure such distortion of anions will be present (as can be seen by consideration of $K_3[IrCl_6]$-H_2O and $K_3[IrCl_6]$). The important point is simply that there is a non spherically symmetric distribution of ions (or component atoms of these ions) around the anions in these compounds and that this distribution in itself is enough to cause the small distortions found.

The isomorphism between $K_3[IrCl_6]H_2O$ and $K_3[RhCl_6]H_2O$ lends support to this argument, as both compounds show the same distortion in the anions (although bond lengths differ significantly) and of course the same distribution of ions external to the $[MCl_6]^{3-}$ ions. Thus, the effect is not being caused by either the rhodium or iridium metal ion in these compounds. (It should be noted here that no Jahn-Teller effect (causing distortion of species because of orbital degeneracy present in the component metal ions) is possible in these d^6 diamagnetic low spin complexes).

3.8 SUMMARY

The single crystal X-ray diffraction studies completed for the hexahalogenometallates discussed in the present chapter have confirmed the isomorphism of a number of iridium (III) compounds both amongst themselves and with complexes of other transition metal ions. The characterisation of space groups and other crystal data in conjunction with

the crystal structures reported here have allowed determination of anion site symmetries of the hexahalogenometallate ions in various compounds. These data are required for a full discussion of spectroscopic studies (Raman, Infra-red and Nuclear Quadrupole Resonance) that have been completed on these compounds and reported on in Chapters 5 and 6.

The iridium (III) hexahalogenometallate anions present in the compounds studied in the solid state have all been found to be significantly distorted from ideal octahedral geometry. In general this distortion is not reflected in significantly different iridium halogen bond lengths in the individual anions but is present in interbond angles which always deviate significantly from the ideal angles of 90° or 180°. The reason for this distortion in the solid state has been attributed to crystal packing effects.

CHAPTER 4

STRUCTURAL STUDIES - PART 2. THE CRYSTAL STRUCTURES OF CAESIUM PENTACHLOROAQUAIRIDATE (III), CAESIUM HEXACHLORO-IRIDATE (IV), TETRAMETHYLAMMONIUM TRI-μ-BROMO-HEXA-BROMODIRHODATE (III) AND RELATED COMPOUNDS

4.1 INTRODUCTION

In the course of preparation and characterisation of iridium (III) hexahalogenometallates, a number of other halogeno compounds were isolated (see Chapter 2). The crystal structures of some of these compounds are now examined.

The crystal structure of $Cs_2[IrCl_5(H_2O)]$ has been found to be isomorphous to the reported structures of $Cs_2[RuCl_5(H_2O)]$ [5] and $Cs_2[RhCl_5(H_2O)]$ [7]. The crystal structure of $Cs_2[IrCl_6]$ is isomorphous to a wide ranging series of $A_2[MX_6]$ (A = univalent cation, M = tetravalent transition metal, X = halogen) transition metal complex fluoride, chloride and bromide salts crystallising in the cubic space group, Fm3m. The crystal structure of the rhodium compound, tri-tetramethylammonium tri-μ-bromo-hexabromodirhodate, has been solved in outline but the level of refinement achieved has been unsatisfactory. The structure of this compound was studied primarily because of its isomorphism to the analogous iridium complex, for which large enough crystals for a structure

determination could not be obtained. The crystal structures are discussed in the same format as those in Chapter 3.

Other compounds to be discussed later in the chapter have been examined using single crystal X-ray diffraction techniques, to determine space groups and cell dimension data to help characterise their respective structures. In some cases difficulty in obtaining large enough crystals for single crystal X-ray diffraction studies has meant X-ray powder diffraction has been resorted to.

This chapter will conclude with a discussion of the crystal structures of related pentachloroaqua salts, a brief mention of salts of the cubic $K_2[PtCl_6]$ type (in which the iridium (IV) analogues are included) and finally a discussion of structural aspects of salts containing the dimetallate $[M_2X_9]^{3-}$ anion (M-transition or non transition metal element, X-chlorine, bromine or iodine atom).

4.2 THE CRYSTAL STRUCTURE OF CAESIUM PENTACHLOROAQUAIRIDATE (III), $[Cs_2IrCl_5(H_2O)]$

4.2.1 Preliminary Study and Data Collection

Green needle-like crystals of this compound were found to crystallize in one of the three orthorhombic space groups Cmcm, $Cmc2_1$ or Ama2. This was deduced from a preliminary study completed on the compound using Weissenberg and precession photographic techniques.

Relevant crystal data are recorded in Table 4.2.1. Refined cell dimensions obtained were

$$a = 7.372(1)\text{Å},\ b = 17.283(3)\text{Å},\ c = 8.014(2)\text{Å},$$
$$\alpha = \beta = \gamma = 90^{\circ}.$$

These confirmed the isomorphism of the compound with both the rhodium[7] and ruthenium[5] analogues; their cell dimensions are reported in Table 4.5.1. The space group Cmcm (the standard setting equivalent of Amam reported for both $Cs_2[RhCl_5(H_2O)]$ and $Cs_2[RuCl_5(H_2O)]$) was therefore chosen for $Cs_2[IrCl_5(H_2O)]$.

The intensities of 1771 reflections, in two equivalent octants of reciprocal space ($h,k,\ell \geqslant 0$; $k \leqslant 0$, $h,\ell \geqslant 0$), were measured out to a Bragg angle of 30° using MoKα radiation. Relevant experimental and other parameters are recorded in Table 4.2.2. No attenuation was required for any reflections.

Initial structure analysis and refinement was carried out using the averaged data set (from the two equivalent forms) uncorrected for absorption. There were 382 reflections such that $F^2_{obs} \geqslant 3\sigma(F^2_{obs})$. Before final refinement absorption corrections were applied to the separate sets of reflections, using an analytical method, and the data reaveraged to produce 526 reflections with $F^2_{obs} \geqslant 3\sigma(F^2_{obs})$. The large range of absorption correction factors reflects a similar situation to that in the determination of the crystal structure of $Rb_3[IrBr_6]H_2O$, where two equivalent

Table 4.2.1: Crystal Data for $Cs_2[IrCl_5H_2O]$

Formula	$Cs_2[IrCl_5(H_2O)]$
Formula weight	653.290
Crystal system	Orthorhombic
Space group	Cmcm (D_{2h}^{17}, No. 63)
a	7.372(1)
b	17.283(3)
c	8.014(2)
α,β,γ	90^{o}
V	~~1012~~ 1021 $Å^3$
z	4
d calculated	4.29 gcm^{-3}
measured	> 3.33 gcm^{-3}
F(000)	1128
μ(MoKα)	204.09 cm^{-1}

Table 4.2.2: Experimental Parameters for $Cs_2[IrCl_5H_2O]$ Data Collection

Temperature	$23^{\circ}C$ ($\pm 1^{\circ}C$)
Radiation	MoKα (λ = 0.7107 Å for MoK$\bar{\alpha}$)
Scan range	0.60°
Scan time	120 seconds
Total background time	60 seconds
Bragg angle limit	30°
Incident beam collimator	1 mm (diameter)
Diffracted beam collimator	5 mm (diameter)
Tube take off angle	3°
Crystal dimensions	0.19 mm x 0.1 mm x 0.06 mm
Crystal volume	0.008713 mm^3
Mosaicity	0.18°
Total independent reflections	873
Reflections used in refinement	518 such that $F^2_{obs} \geqslant 3\sigma(F^2_{obs})$
Ratio observations to variables in least squares refinements	518:31 i.e. $\approx$ 16:1
Range of transmission factors	0.3145 (for 2-206) - 0.04560 (for 020)
No. equivalent forms of data	2 (hkℓ and h$\bar{k}\ell$)
Weighting parameter p	0.1

forms of data were also collected.

4.2.2 Structure Solution and Refinement

Full matrix least squares refinement was attempted with positional coordinates and isotropic thermal parameters obtained from the isomorphous $Cs_2[RuCl_5(H_2O)]$ structure reported by Hopkins et al.[5] Two cycles of refinement produced a residual of 0.103, clearly confirming the isomorphism between the two compounds. All atoms were then given anisotropic thermal parameters (with suitable constraints on thermal parameters of atoms on special positions) and refinement continued after corrections had been made for absorption. This model, which included corrections for anomalous dispersion for iridium, caesium and chlorine atoms, converged and produced a residual of 0.050 and a weighted residual of 0.067. The error in an observation of unit weight was 1.491. Analysis of the weighting scheme suggested a change in the p factor was desirable. This change (from 0.05 to 0.10) was made, the standard deviations of reflections re-evaluated, and the previous full matrix least squares refinements repeated (with an extinction parameter included). At convergence an R factor of 0.050 and a weighted R factor of 0.066 were produced. The error in an observation of unit weight was 0.953 and the weighting scheme was now found to be satisfactory.

A difference electron density map calculated for this final model had its largest peaks close to the iridium

atom but was otherwise featureless; there were no obvious peaks which could be ascribed to hydrogen atoms attached to the coordinated oxygen atom.

A list of final positional and thermal parameters is given in Tables 4.2.3(a) and (b) for $Cs_2[IrCl_5(H_2O)]$ and isomorphous $Cs_2[RuCl_5(H_2O)]$ and $Cs_2[RhCl_5(H_2O)]$. Calculated and observed structure factors for the data used in final least squares refinement are given in Appendix E.

4.2.3 Description of the Structure

Figure 4.2.2 contains a stereoscopic view of the unit cell contents of $Cs_2[IrCl_5(H_2O)]$. Figure 4.2.1 contains a projection view of the contents of the unit cell. Figure 4.2.3 shows the environment of the iridium atom in $Cs_2[IrCl_5(H_2O)]$.

The positional parameters listed in Table 4.2.3(a) for $Cs_2[IrCl_5(H_2O)]$, $Cs_2[RhCl_5(H_2O)]$ and $Cs_2[RuCl_5(H_2O)]$ confirm the isomorphism of the three complexes. The $[IrCl_5(H_2O)]^{2-}$ anions are located on sites of mm symmetry, with the oxygen, iridium and chlorine (Cl(1)) atoms forming a linear chain of atoms at the intersection of the two mirror planes at x = 0 and z = 1/4, 3/4 in the unit cell. The caesium atoms are located on the same type of site. As can be seen in Table 4.2.4, the $[MCl_5(H_2O)]^{2-}$ anion in all three complexes has distorted octahedral geometry and the metal atom is displaced out of the plane of the four Cl(2) atoms towards the Cl(1) atom by 0.05Å,

Table 4.2.3(a): Positional Parameters for $Cs_2[IrCl_5(H_2O)]$, $Cs_2[RuCl_5(H_2O)]$ and $Cs_2[RhCl_5(H_2O)]$

Atom	Parameter[b]	$Cs_2[IrCl_5(H_2O)]$	$Cs_2[RuCl_5(H_2O)]$[a]	$Cs_2[RhCl_5(H_2O)]$[a]
Ir(Ru,Rh)	x	0.0	0.0	0.0
	y	0.11392(6)	0.1153(1)	0.1142(1)
	z	0.25	0.25	0.25
Cs(1)	x	0.5	0.5	0.5
	y	-0.0305(1)	-0.0285(1)	-0.0301(1)
	z	0.25	0.25	0.25
Cs(2)	x	0.5	0.5	0.5
	y	0.2535(1)	0.2534(1)	0.2540(1)
	z	0.25	0.25	0.25
Cl(1)	x	0.0	0.0	0.0
	y	0.2479(4)	0.2490(4)	0.2472(3)
	z	0.25	0.25	0.25
Cl(2)	x	0.2231(5)	0.2222(6)	0.2225(4)
	y	0.1108(2)	0.1112(4)	0.1119(2)
	z	0.4594(5)	0.4605(6)	0.4582(3)
O	x	0.0	0.0	0.0
	y	-0.007(1)	-0.0064(20)	-0.0078(10)
	z	0.25	0.25	0.25

[a] Some transformations of coordinates have been made to values reported in the literature to produce the same coordinates as those reported for $Cs_2[IrCl_5(H_2O)]$

[b] Parameters containing no errors (in parentheses) are fixed by the nature of the special positions on which they are located.

Table 4.2.3(b): Thermal Parameters ($Å^2$) for $Cs_2[IrCl_5(H_2O)]$

Atom	U(or U_{11})	U_{22}	U_{33}	U_{12}	U_{13}	U_{23}
Ir	0.0172(5)	0.0223(5)	0.0117(5)	0.0	0.0	0.0
Cs(1)	0.043(1)	0.046(1)	0.0193(8)	0.0	0.0	0.0
Cs(2)	0.0358(9)	0.0361(9)	0.043(1)	0.0	0.0	0.0
Cl(1)	0.029(3)	0.026(3)	0.043(4)	0.0	0.0	0.0
Cl(2)	0.033(1)	0.042(2)	0.028(2)	0.007(1)	-0.011(1)	-0.002(1)
O	0.05(1)	0.04(1)	0.009(8)	0.0	0.0	0.0

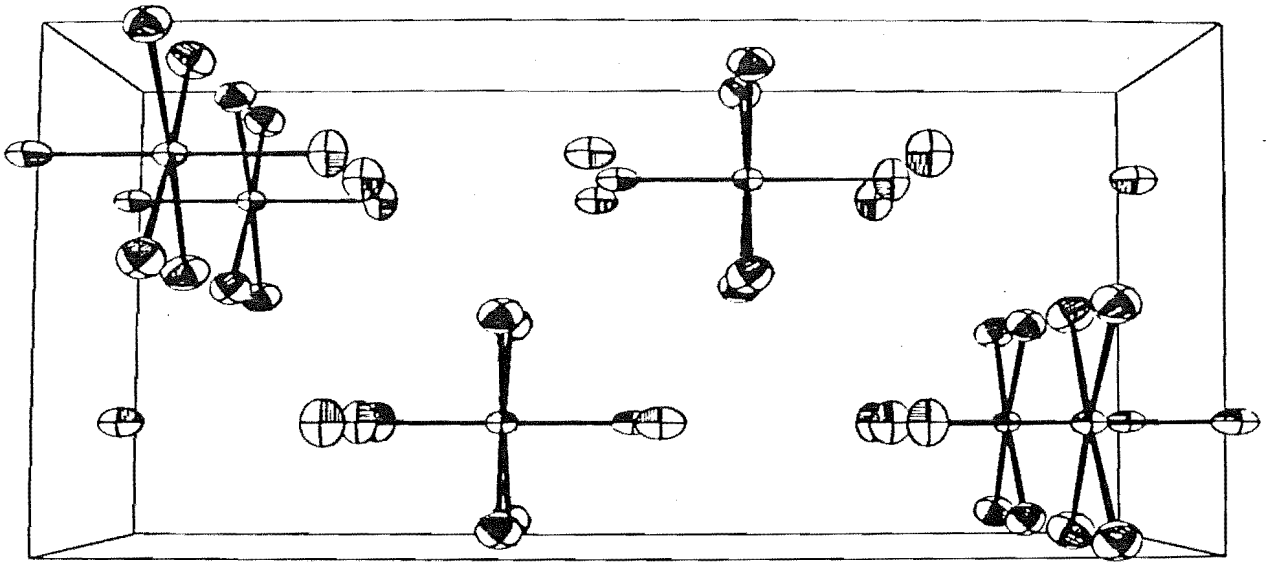

Figure 4.2.1: Projection diagram of the unit cell contents of $Cs_2[IrCl_5(H_2O)]$ viewed down an axis nearly parallel to the a axis.

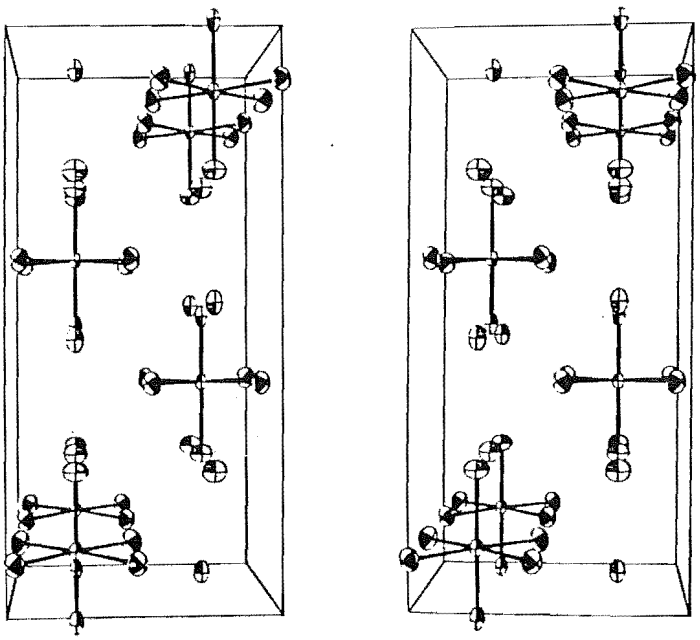

Figure 4.2.2: Stereoscopic view of the unit cell contents of $Cs_2[IrCl_5(H_2O)]$.

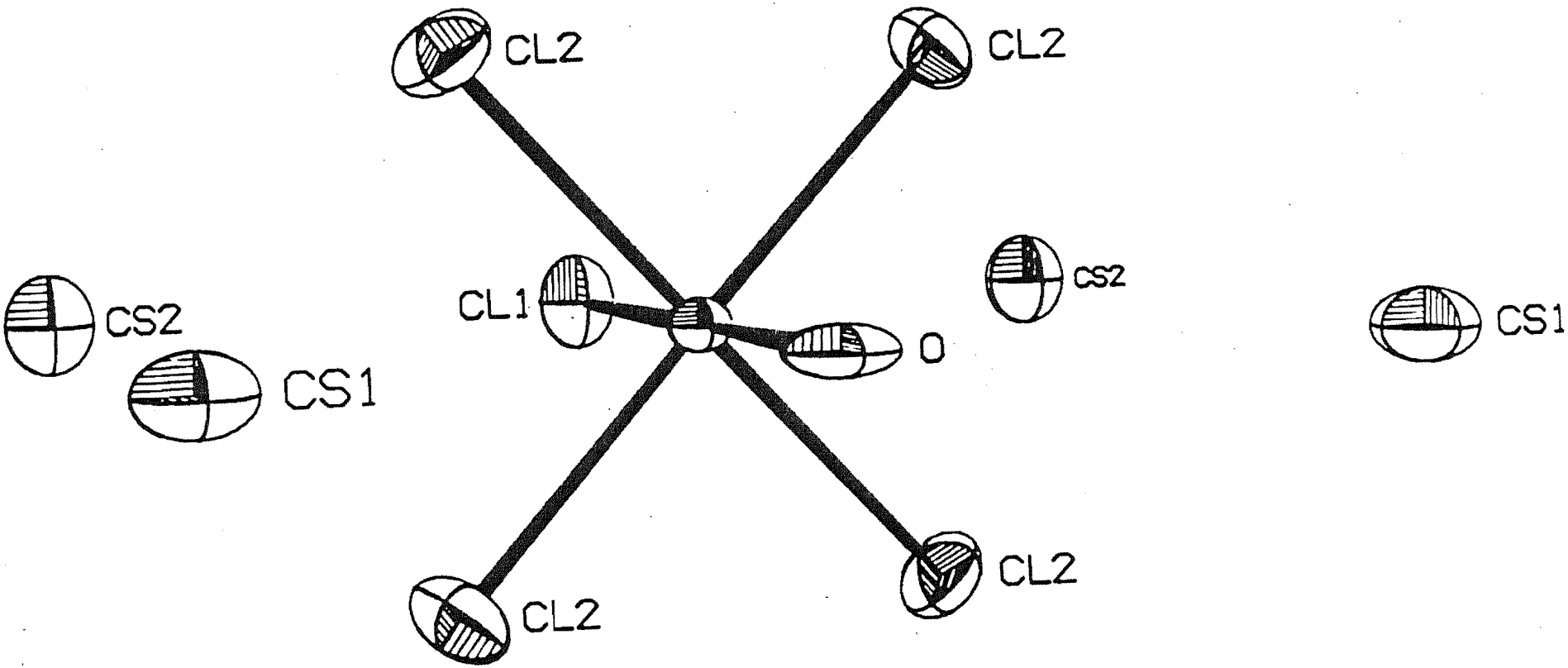

Figure 4.2.3: Environment of the iridium atom in $Cs_2[IrCl_5(H_2O)]$. The atoms Cs(1), Cs(2), Ir(unlabelled), Cl1 and O shown lie in one of the xy mirror planes at z = 1/4, 3/4. The Cl1, Ir, O atoms shown also lie in one of the yz mirror planes at x = 0, 1/2 thus giving rise to two possible orientations for the hydrogen atoms attached to the oxygen atom (assuming no disorder). These hydrogen atoms will preferably lie in the yz mirror planes.

Table 4.2.4: Bond Lengths (Å) and Angles (degrees) in $[MCl_5(H_2O)]^{2-}$ Anions in $Cs_2[MCl_5(H_2O)]$, where M is Ir, Ru, Rh.

(a) Bond lengths

	$Cs_2[IrCl_5(H_2O)]$		$Cs_2[RuCl_5(H_2O)]$	$Cs[RhCl_5(H_2O)]$
M-O	2.091(23)	2.098(23)[a]	2.104(28)	2.096(13)
M-Cl(1)	2.315(7)	2.324(7)[a]	2.311(8)	2.300(5)
M-Cl(2)	2.350(4)	2.360(4)[a]	2.353(4)	2.337(3)

(b) Angles

	$Cs_2[IrCl_5(H_2O)]$	$Cs_2[RuCl_5(H_2O)]$	$Cs_2[RhCl_5(H_2O)]$
O-M-Cl(1)	180.0	180.0	180.0
O-M-Cl(2)	88.7(1)	88.3(1)	89.09(8)
Cl(1)-M-Cl(2)	91.3(1)	91.7(1)	90.91(8)
Cl(2)-M-Cl(2)	88.8(2)	88.7(2)	88.72(13)
Cl(2)-M-Cl(2)	91.1(2)	91.2(2)	91.25(13)
Cl(2)-M-Cl(2)	177.3(2)	-	178.19(15)

[a] Bond lengths averaged over t nal motion

0.07Å, and 0.04Å for the Ir(III), Rh(III) and Ru(III) complexes respectively. Thus, the M-Cl(1) bond is significantly shorter than that of the M-Cl(2) bond.

The root-mean-square amplitudes of vibration along the principal axes of the thermal vibration ellipsoids of the various atoms in $Cs_2[IrCl_5(H_2O)]$ are reported in Table 4.2.5. The anisotropic thermal motion of the chlorine atoms and oxygen atom in the $[IrCl_5(H_2O)]^{2-}$ anion shows the major vibration components are at right angles to their respective bonds to the iridium atom. The oxygen atom does have one major vibration component along the Ir-O bond, which is somewhat unusual. However, this does not appear to be the result of any disorder (of Cl(1) and O atomic positions) in the structure, as no evidence for such a hypothesis was found in the final difference electron density map. Calculated corrections to bond lengths to allow for thermal motion (using a riding model) for atoms Cl(1), Cl(2) and O bonded to Ir indicated no significant changes. The Ir-Cl(2) bond length of 2.350(4)Å is essentially the same as that observed in other compounds containing distorted $[IrCl_6]^{3-}$ octahedra (e.g. $K_3[IrCl_6]$ and $(NH_4)_3[IrCl_6]H_2O$). Furthermore, although the bond Ir-Cl(1) (2.315(7)Å) is significantly shorter than that of Ir-Cl(2), a bond length of this order has been found in a distorted $[IrCl_6]^{3-}$ anion in $K_3[IrCl_6]H_2O$ (see Section 3.3). The mechanism causing the differences in bond lengths within a compound for these two compounds probably has different origins.

Table 4.2.5: Root-Mean-Square Components (Å) of the Thermal Vibration Ellipsoids of Selected Atoms Along Their Principal Axes and Angles (degrees)[a] Between These Principal Axes of the Anisotropic Chlorine Atoms and Their Respective Ir-Cl Vectors in $Cs_2[IrCl_5(H_2O)]$

Atom	Axis 1	Angle	Axis 2	Angle	Axis 3	Angle
Ir	0.108(2)		0.131(2)		0.150(2)	
Cs(1)	0.139(3)		0.208(2)		0.215(2)	
Cs(2)	0.189(2)		0.190(2)		0.209(3)	
Cl(1)	0.1605(9)	0.0	0.171(9)	90.0	0.207(10)	90.0
Cl(2)	0.137(5)	7(2)	0.189(5)	91(4)	0.220(4)	83(2)
O	0.094(40)	90.0	0.197(28)	0.0	0.224(28)	90.0

[a] Angles with no errors (in parentheses) are constrained by virtue of the atom they are associated with being located on a special position.

Table 4.2.6: Selected Interatomic Non Bonded Contacts (Å) less than 5.0 Å in $Cs_2[IrCl_5(H_2O)]$.

Cs(1)...Cl(2)	3.39	Cs(2)...Cl(2)	3.62
...Cl(2)	3.60	...Cl(1)	3.69
...O	3.71	...Cl(2)	3.69
...Cl(1)	3.83	...Cl(1)	4.01
...Cs(1)	4.14	...O	4.14
...Ir	4.45	...Ir	4.41
...Cs(2)	4.91	...Ir	4.62
Cl(1)...Cl(2)	3.34	Cl(2)...O	3.11
...Cl(2)	3.95	...Cl(2)	3.29
		...Cl(2)	3.36
		...O	3.37

No plausible hydrogen atomic sites were located in the final difference electron density map although some residual density did remain in the mirror planes at x=0, ½ at suitable O-H bonding distances. Unless the hydrogen atoms of the coordinated water molecule are disordered, the only other positions they may occupy are on the mirror planes at z = 1/4, 3/4. However, as can be seen in Figure 4.2.3, repulsive $H^{\delta+}...Cs^{+}$ interactions would arise for hydrogen atoms located on such sites and thus occupancy of such sites would be unlikely. As suggested by Hopkins et al.[5] location of hydrogen atoms on the mirror planes at x = 0,½ probably accounts for the distortion of the Cl(2) atoms from four fold rotational symmetry. The $Cl^{\delta-}...H^{\delta+}$ interactions between atoms Cl(2) and hydrogen atoms in the planes x = 0,½ would be greater (as the H...Cl(2) distances are smaller) than those between atoms Cl(2) and hydrogen atoms located in the planes at z = 1/4, 3/4.

4.3 THE CRYSTAL STRUCTURE OF CAESIUM HEXACHLOROIRIDATE(IV), $Cs_2[IrCl_6]$

4.3.1 Preliminary Study and Data Collection

Red crystals of this compound were isolated during recrystallisation of $Cs_3[IrCl_6]H_2O$ from concentrated hydrochloric acid. A preliminary study using both Weissenberg and precession camera techniques revealed the compound crystallised in the cubic space group Fm3m. Relevant crystal data are recorded in Table 4.3.1.

Table 4.3.1: Crystal Data for $Cs_2[IrCl_6]$

Formula	$Cs_2[IrCl_6]$
Formula weight	670.728
Crystal system	cubic
Space group	$Fm3m$ (O_h^5, No. 225)
a,b,c	10.2119(8) Å
α,β,γ	90°
V	1064.9 Å^3
z	4
d calculated	4.18 gcm^{-3}
measured	> 3.33 gcm^{-3}
F(000)	1156
μ(MoKα)	215.10 cm^{-1}

A refined cubic unit cell parameter as follows was obtained :

$a = 10.2119(8)\text{Å}$.

Using Zr filtered MoKα radiation, the intensities of 1560 reflections were measured using the θ-2θ scan technique in the positive octant of reciprocal space ($h,k, \ell \geq 0$) out to a Bragg angle of 45°. Because of the small size of the crystal and the consequent low ratio of peak to background scattering total scan times were increased to 200 seconds per reflection (per 0.5° scan range) with 100 seconds total background count. At higher angles (i.e. for θ in the range 35° to 45°), the scan range and scan times were further increased, the former to ensure correct collection of the α_1,α_2 doublet, whose splitting in the diffracted beam is proportional to tan θ. No attenuation of any reflections was required.

Equivalent reflections in the data set were averaged for use in initial structure solution. Before final refinement was executed, corrections for absorption were made using an analytical technique. After final averaging of equivalent reflections, there were 187 reflections such that $F^2_{obs} \geq 3\sigma(F^2_{obs})$ and these were used in final structural refinement. Experimental parameters for data collection are given in Table 4.3.2.

4.3.2 Structure Solution and Refinement

A three dimensional Patterson function was calculated (vector space group Fm3m). The expected isomorphism of this

Table 4.3.2: Experimental Parameters for $Cs_2[IrCl_6]$ Data Collection.

Temperature	$22^{\circ}C$ ($\pm$ $1^{\circ}C$)
Radiation	MoKα (λ=0.7107Å for MoKᾱ]
Scan range	0.50° and 0.60° (see section 4.3.1)
Scan time	200 seconds (and 240 seconds)
Total background time	100 seconds (and 120 seconds)
Bragg angle limit	45°
Incident beam collimator	1 mm (diameter)
Diffracted beam collimator	5 mm (diameter)
Tube take off angle	3°
Crystal dimensions	0.2 mm x 0.2 mm x 0.2 mm
Crystal volume	0.016915 mm^3
Mosaicity	0.2°
Total independent reflections	364
Reflections used in refinement	187 such that $F^2_{obs} \geqslant 3\sigma(F^2_{obs})$
Radio observations to variables in least squares refinements	187:7 $\approx$ 26:1
Range of transmission factors	0.1894 (for 1 17 11) to 0.1160 (for 0 0 2)
No. equivalent forms of data	1
Weighting parameter p	0.05

compound with $K_2[PtCl_6]$ was then immediately obvious from the simple Patterson map (which essentially contained only six unique vectors). Using coordinates reported for $K_2[PtCl_6]$[81] , a trial least squares refinement (with all atoms isotropic) was made. A residual of 0.065 was produced after 4 cycles of refinement, thus confirming the isomorphism of $Cs_2[IrCl_6]$ with $K_2[PtCl_6]$. With the chlorine atom assigned anisotropic thermal parameters (and suitable constraints placed on some of these thermal parameters), the residual dropped to 0.061.

After absorption corrections were made, the above refinement was continued. Close examination of the magnitude of observed and calculated structure factors for strong low angle reflections indicated the necessity of an extinction correction, and with this parameter included and anomalous dispersion corrections applied to all three atom types, the model converged producing a residual, R, of 0.020 (R_w was 0.021). Including a further 48 reflections such that $1\sigma(F^2_{obs}) \leqslant F^2_{obs} \leqslant 3\sigma(F^2_{obs})$ in final refinement produced a final residual, R, of 0.025 with R_w at 0.023. The error in an observation of unit weight was 0.493. An analysis of the errors produced in this final refinement indicated the weighting scheme with the chosen p factor of 0.05 was satisfactory.

A list of final parameters obtained from the least squares refinement is given in Table 4.3.3. Calculated and observed structure factors for the 235 reflections used in final refinement are given in Appendix F.

Table 4.3.3: Positional and Thermal Parameters ($Å^2$) for $Cs_2[IrCl_6]$[a]

(a) Positional parameters

Atom	x	y	z
Ir	0.0	0.0	0.0
Cs	0.25	0.25	0.25
Cl	0.2283(1)	0.0	0.0

(b) Thermal parameters

Atom	U(or U_{11})	U_{22}	U_{33}	U_{12}	U_{13}	U_{23}
Ir	0.0184(1)					
Cs	0.0292(1)					
Cl	0.0209(4)	0.0305(7)	0.0305[b]	0.0	0.0	0.0

[a] Parameters with no errors are fixed by symmetry

[b] For atom Cl, $U_{22} = U_{33}$

4.3.3 Description of the Structure

$Cs_2[IrCl_6]$ contains discrete $[IrCl_6]^{2-}$ anions located on sites of O_h(m3m) symmetry. Table 4.3.4 contains a number of structural parameters for $Cs_2[IrCl_6]$. The Ir-Cl bond length of 2.332(2)Å agrees within limits of error with that of 2.307(8)Å reported for the $[IrCl_6]^{2-}$ anion in $K_2[IrCl_6]$[76]. However, it is significantly shorter than the average bond length of about 2.360 Å found in many $[IrCl_6]^{3-}$ anions. This is presumably a function of a stronger bond interaction possible in the $[IrCl_6]^{2-}$ species (as the formal charge on the Ir^{4+} ion has increased from that of the Ir^{3+} ion) and Cl → Ir π bonding is now possible in the $[IrCl_6]^{2-}$ species, as a consequence of the change in the d electron configuration of the iridium ion (from t_{2g}^6 in Ir^{3+} to t_{2g}^5 in Ir^{4+}).

The two major components of anisotropic motion of the chlorine atoms occur at right angles (these angles are constrained by symmetry to exactly 90°) to the Ir-Cl bond vector as expected.

4.4 A CRYSTAL STRUCTURE INVESTIGATION OF TRI-TETRAMETHYLAMMONIUM TRI-μ-BROMOHEXABROMODIRHODATE(III), $[N(CH_3)_4]_3[Rh_2Br_9]$

4.4.1 Preliminary Study and Data Collection

A preliminary study on suitable crystals of hexagonal morphology revealed the compound crystallised in the hexagonal space group $P6_3/mmc$ (or $P6_3mc$, $P\bar{6}2c$) with

Table 4.3.4: Structural Parameters for $Cs_2[IrCl_6]$

(a) Root-Mean-Square Components (Å) Along the Principal Axes of the Thermal Vibration Ellipsoids of the Chlorine Atoms in $Cs_2[IrCl_6]$ and the Angles (degrees) made by their Axes and the Ir-Cl Bond Vector.

Atom	Axis 1	Angle	Axis 2	Angle	Axis 3	Angle
Cl	0.144(1)	0.0	0.175(2)	90.0	0.175(2)	90.0

(b) Bond Length (Å) of the Ir-Cl Bond in the $[IrCl_6]^{2-}$ in $Cs_2[IrCl_6]$

Ir-Cl	2.3315(15)

(c) Interatomic Contacts (Å) less than 4.0 Å in $Cs_2[IrCl_6]$

Cl...Cl	3.303(2)
Cs...Cl	3.617(4)

systematic absences of the form hhℓ for ℓ = 2n+1. Relevant crystal data are given in Table 4.4.1.

Most of the plate-like crystals examined for data collection were found to be a collection of crystallites, often containing as many as six crystallites in the one crystal, all showing slight misalignment with respect to one another about the unique hexagonal c axis. Finally a very small crystal which showed no evidence of twinning was located and mounted on the diffractometer. The mosaicity of this crystal was found to be quite acceptable (no greater than 0.12^{o}). Refined cell dimensions were as follows:

$$a(=b)=9.3892(6)\text{Å},\ c = 21.402(1)\text{Å},\ \alpha = \beta = 90^{o},\ \gamma = 120^{o}.$$

These are in reasonable agreement with those previously reported[14].

The intensities of 1078 reflections were then measured in the portion of reciprocal space with $h,k,\ell \geqslant 0$ with Ni filtered CuKα radiation to a Bragg angle of 57^{o}. Relevant experimental and other parameters are recorded in Table 4.4.2. Greater than normal scan times were used because of the small size of the crystal.

The final data set, after correcting for absorption and averaging equivalent reflections yielded 344 reflections such that $F^2_{obs} \geqslant 3\sigma(F^2_{obs})$ for use in all calculations.

Table 4.4.1: Crystal Data for $(N(CH_3)_4)_3[Rh_2Br_9]$

Formula	$(N(CH_3)_4)_3[Rh_2Br_9]$
Formula weight	1147.39
Crystal system	hexagonal
Space group	$P6_3/mmc$ (D^4_{6h}, No. 194)
a,b	9.389(1)Å
c	21.402(1)Å
α,β	90°
γ	120°
V	1633.7 Å^3
z	2
d calculated	2.33 gcm^{-3}
measured	2.29(5) gcm^{-3}
F(000)	1068
μ(MoKα)	228.75 cm^{-1}

Table 4.4.2: Experimental Parameters for $(N(CH_3)_4)_3[Rh_2Br_9]$ Data Collection.

Temperature	$22^{\circ}C(\pm 1^{\circ}C)$
Radiation	CuKα (λ = 1.5418Å for CuKᾱ)
Scan range	0.50° (in 0.01° steps)
Scan time	200 seconds
Total background time	100 seconds
Bragg angle limit	57°
Incident beam collimator (diameter)	1.2 mm
Diffracted beam collimator (diameter)	5.0 mm
Tube take-off angle	3°
Crystal dimensions (maximum)	0.1 mm x 0.06 mm x 0.03 mm
Crystal volume	0.20985×10^{-3} mm^3
Mosaicity	0.12°
Total independent reflections	1078
Reflections used in refinement	344 (such that $F^2_{obs} \geqslant 3\sigma(F_{obs}{}^2)$)
Ratio observations to variables in least squares refinements	344:24 $\approx$ 14:1
Range of transmission factors	0.5429 (for 1 0 23) to 0.1857 for (0 0 2)
No. of equivalent forms of data	1
Weighting parameter p	0.05

4.4.2 Attempted Structure Solution and Refinement

A trial set of atomic coordinates were obtained from an isomorphous structure (that of $Cs_3[Cr_2Br_9]$[82] crystallising in space group $P6_3/mmc$) and, with suitable isotropic temperature factors chosen, six cycles of least squares refinement yielded a residual of 0.25. Only parameters for the unique bromine and rhodium atoms were included in this refinement. At this stage the refinement had essentially converged, and in view of the bulk of the diffracting power of the crystal apparently now located, the residual was rather high. A difference electron density synthesis at this stage revealed suitable density indicating the presence of tetramethylammonium cations. These cations are located on two types of special positions. One has point symmetry $D_{3d}(\bar{6}m2)$, which must confer disorder on the orientation of the tetrahedral anion located on this site, and the other has point symmetry $C_s(m)$.

After absorption corrections were made further refinements were carried out using the SHELX76 programme. Initially refinement was attempted with the tetramethylammonium cation carbon and nitrogen atoms constrained as rigid tetrahedral groups with suitable N-C bond lengths (1.52Å) chosen from the literature.[83,84] A further six cycles of least squares refinement with both the rhodium and bromine atoms given anisotropic thermal parameters were executed. This refinement included corrections for anomalous dispersion by the heavy atoms and individual isotropic thermal parameters

assigned to each atom type within the rigid group cations. This model refined to produce a residual of 0.169.

However, further refinement with group constraints released and extinction catered for produced no improvement in the R factor. A difference electron density map was featureless and, in particular, no high density peaks were found near any known atomic positions. An analysis of the weighting scheme showed no systematic dependence of the errors between calculated and observed structure factors on particular indices of reflections or structure factor magnitudes.

Attempts at further refinement were finally abandoned with the conclusion that some inadequacies in the data set were preventing structure elucidation. A list of observed and calculated structure factors for the data used in final refinement are listed in Appendix G. Table 4.4.3 contains a list of positional and thermal parameters for the model at the present stage of refinement.

4.4.3 Description of the Partially Solved Structure

The model discussed here was that obtained with a residual of 0.169 (R_w was 0.20) where no parameter shifts divided by the e.s.d. of that parameter were greater than 0.34. Although the refinement is unsatisfactory there are some significant facts that have emerged from the

Table 4.4.3: Positional and Thermal Parameters ($Å^2$) for $[N(CH_3)_4]_3[Rh_2Br_9]$ (at the present stage of refinement)

Atom	x	y	z	U(or U_{11})	U_{22}	U_{33}	U_{23}	U_{13}	U_{12}
Rh	0.3333	0.6667	0.8271(4)	0.050(4)	0.050(4)	0.064(5)	0.0	0.0	0.025(2)
Br(1)	0.7905(6)	1.5810(11)	0.1092(4)	0.158(7)	0.075(7)	0.078(5)	0.023(4)	0.012(2)	0.038(3)
Br(2)	0.5497(7)	1.0974(13)	0.25	0.118(7)	0.057(7)	0.077(7)	0.0	0.0	0.028(3)
N(1)	0.0	0.0	0.25	0.17(6)					
C(11)	0.0	0.0	0.3210	0.17(6)					
C(12)	0.0915(42)	0.1830(85)	0.2353(130)	0.17(6)					
N(2)	0.3333	0.6667	0.0901(70)	0.15(3)					
N(21)	0.3333	0.6667	0.1611(70)	0.15(3)					
N(22)	0.2508(49)	0.5017(98)	0.0566(60)	0.15(3)					

present analysis that warrant discussion.

The determination of the space group as one of $P6_3/mmc$, $P6_3mc$ or $P\bar{6}2c$ on the basis of systematic absences in the data set has been confirmed. The cell dimensions have been determined accurately. Furthermore, at the present stage, it can be stated with some certainty that the dimeric anion, $[Rh_2Br_9]^{3-}$, in this compound, contains no metal-metal bonding interaction. This will be discussed in more detail in Section 4.6.

In Figure 4.4.1 a projection diagram of the unit cell contents of $[N(CH_3)_4]_3[Rh_2Br_9]$ is given, and in Figure 4.4.2 the atomic arrangement in the dimetallate anion is depicted, showing clearly the bridging bromine atoms and the terminal bromine atoms forming an octahedral environment around each rhodium atom.

The dimeric anions are located on sites of $D_{3d}(\bar{6}m2)$ point symmetry with the Rh-Rh bond vector aligned parallel to the unit cell c axis. Table 4.4.4 contains a number of bond lengths and bond angles for the dimeric anion obtained in the present analysis. The coordination in the bioctahedron shows a number of deviations from ideal octahedral coordination around each equivalent rhodium atom. The Rh-Br(bridge) bond is significantly (10σ) longer than the Rh-Br (terminal) bond, consistent with other reported structures. The geometry of such anions will be discussed more fully in Section 4.6. The bond lengths compare favourably with those found in $(H_3O)K_8[RhBr_6]_3{}^9H_2O$[4] (where the average Rh-Br bond length is 2.50 Å) especially when the precision

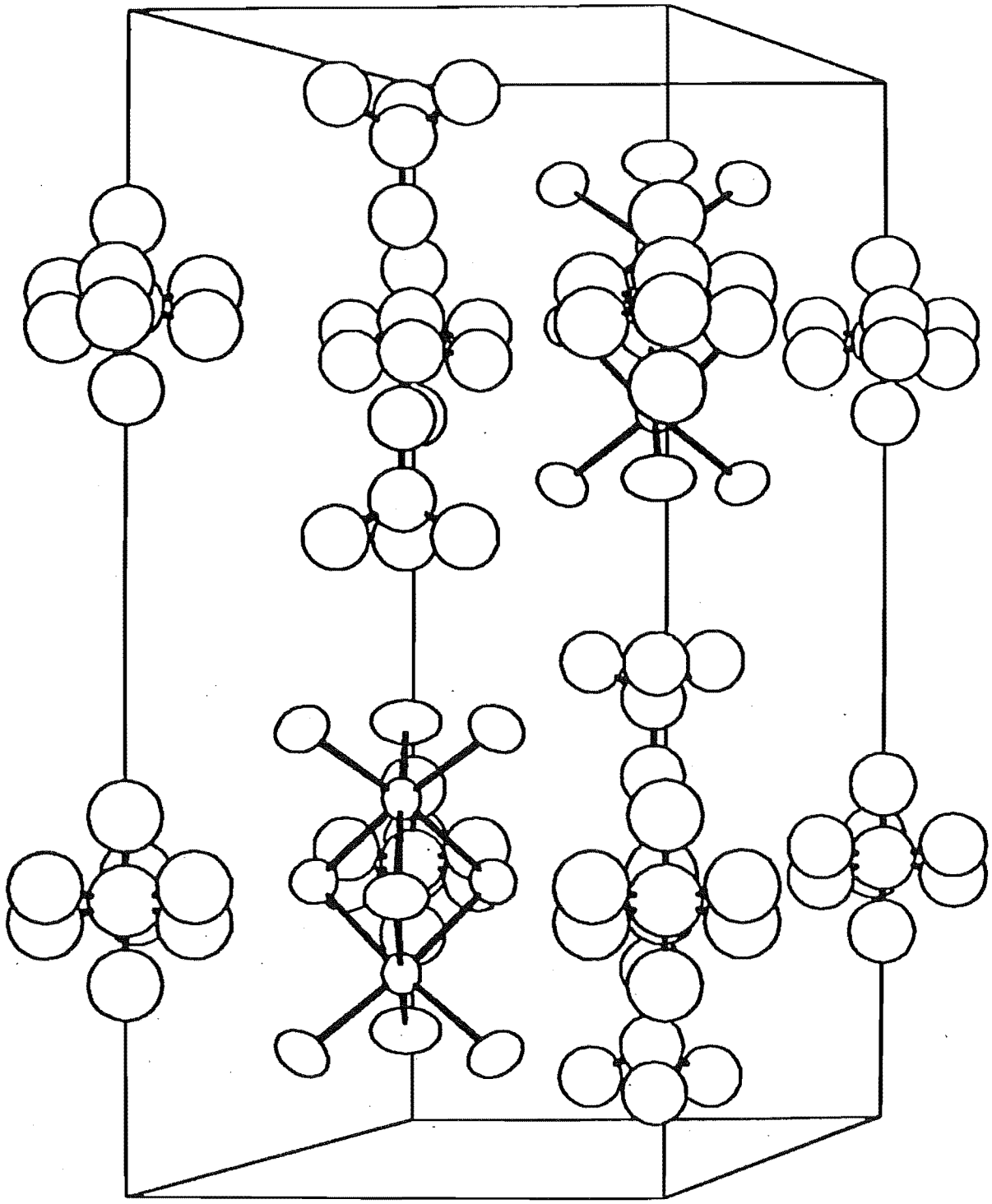

Figure 4.4.1: Projection diagram of the unit cell contents of $[N(CH_3)_4]_3[Rh_2Br_9]$ viewed into the ac face of the unit cell. The disorder of the tetrahedral $[N(CH_3)_4]^+$ cations on sites of symmetry D_{3d} ($\bar{6}m2$) on the c axis (vertical axis) is illustrated.

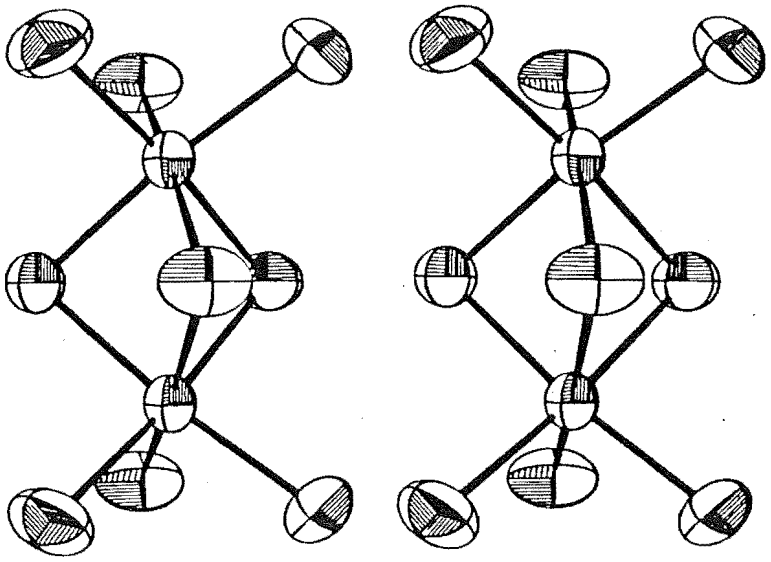

Figure 4.4.2: Stereoscopic view of the dirhodate(III) anion, $[Rh_2Br_9]^{3-}$.

Table 4.4.4: Bond Lengths (Å), Non Bonding Interactions (Å) and Angles (degrees) in the $[Rh_2Br_9]^{3-}$ Anion in $[N(CH_3)_4]_3[Rh_2Br_9]$ (at the present stage of incomplete structural analysis).

(a) Bond lengths

Rh(1)-Br(1)[a]	2.432(9)
Rh(1)-Br(2)[a]	2.531(7)

(b) Non-bonding interactions (< 3.4 Å)

Rh(1)-Rh(2)[b]	3.302(12)
Br(2)-Br(2)[b]	3.323(14)

(c) Bond angles

Br(1)-Rl(1)-Br(1)[b]	91.6(3)	Rh(1)-Br(2)-Rh(2)[b]	81.4(3)
Br(2)-Rh(1)-Br(1)	93.0(3)	Br(1)-Rh(1)-Rh(2)[b]	124.1(2)
Br(2)-Rh(1)-Br(1)[b]	173.4(2)	Br(2)-Rh(1)-Rh(2)[b]	49.3(2)
Br(2)-Rh(1)-Br(2)[b]	82.0(2)		

[a] Atoms Br(1) are terminal bromine atoms and atoms Br(2) are bridging bromine atoms.

[b] Symmetry related atoms.

of the model is considered. Non bonding contacts between atoms in the cations and anions in the unit cell are all in acceptable ranges.

The reason for the unsatisfactory refinement of the structure remains unknown. On the basis of the degree of accuracy of the refined cell dimensions, it would seem unlikely that twinning was present in the crystal, when the magnitude of the errors in the cell dimensions for a twinned crystal of $(NH_4)_3[IrCl_6]H_2O$ are recalled (Section 3.4). However, this does not completely exclude twinning as a possible reason for the unsatisfactory refinement. It simply reinforces the fact that if the crystal were twinned, then in the present analysis only reflections from one crystallite were examined on the diffractometer in the determination of cell dimensions. As was established in the initial attempt to determine the structure of $(NH_4)_3[IrCl_6]H_2O$, data from a twinned crystal yielded the overall geometry of the complex $[IrCl_6]^{3-}$ anion and other atomic positions but did not permit refinement to a satisfactory conclusion beyond a residual of 0.16. The same problem could be occurring in the present study. Relatively large errors in intensity data (consequent on the very small crystal size) could also be a contributing factor.

Unfortunately lack of any other suitable crystals of $[N(CH_3)_4]_3[Rh_2Br_9]$ prevented recollection of the data set.

4.5 THE CRYSTAL STRUCTURES OF HALOGENOMETALLATES OF IRIDIUM(III), IRIDIUM(IV) AND OTHER TRANSITION METAL IONS

4.5.1 The Crystal Structure of Rubidium Pentachloroaqua-Iridate(III), $Rb_2[IrCl_5(H_2O)]$, and Related Compounds

A single crystal X-ray diffraction study of $Rb_2[IrCl_5(H_2O)]$ revealed the compound crystallised in the orthorhombic space group Pnma with unit cell dimensions as reported in Table 4.5.1. Powder photography suggested this compound was isomorphous with its rhodium analogue. The above data suggested both compounds were isomorphous with a wide ranging series of transition metal and non transition metal pentachloroaqua salts of the $K_2[FeCl_5(H_2O)]$ type[85], which crystallise with a variety of cations (e.g. K^+, Rb^+, NH_4^+, ND_4^+, and in some cases Cs^+) in the same space group and with similar cell dimensions. This series includes salts of Ti[86], V[87,88], Cr[14], Fe[85], Ru[6, 13, 89], Rh[14], In[90, 91] and Tl[92], and presumably many other pentachloroaqua salts reported in the literature (e.g. Mo, W, Mn), but for which no structural data are reported. Unit cell parameters for some of these compounds are reported in Table 4.5.1. The salts of some pentabromoaqua complexes have also been reported to be isomorphous to this series[93].

Pentachloroaquametallate(III) salts of the $K_2[FeCl_5(H_2O)]$ type mentioned above, all contain $[MCl_5(H_2O)]^{2-}$ (M is a tervalent metal ion) anions of idealized symmetry C_{4v}(4m) (excluding hydrogen atoms) located on sites of symmetry C_s(m) in the unit cell. There are usually differences in

Table 4.5.1: Crystal Data for Pentachloroaquametallate(III) salts

Compound	Space Group[a]	Anion site symmetry	Axial cell parameters a(Å)	b(Å)	c(Å)	Reference
$Rb_2[CrCl_5(H_2O)]$	Pnma	C_s(m)	13.74(4)	9.70(3)	7.26(6)	14
$K_2[FeCl_5(H_2O)]$[b]	"	"	13.75	9.92	6.93	85,89
$(NH_4)_2[FeCl_5(H_2O)]$[b]	"	"	13.78(3)	9.85(5)	7.09(3)	89
$K_2[RuCl_5(H_2O)]$[b]	"	"	13.53(3)	9.55(5)	6.96(3)	6,89
$K_2[RhCl_5(H_2O)]$	"	"	13.55(2)	9.48(3)	7.02(2)	14
$(NH_4)_2[RhCl_5(H_2O)]$	"	"	13.63(7)	9.80(5)	7.11(8)	14
$Rb_2[RhCl_5(H_2O)]$	"	"	13.70(6)	9.69(5)	7.25(8)	14
$Rb_2[IrCl_5(H_2O)]$[c]	"	"	13.845(30)	9.668(20)	7.232(20)	this work
$(NH_4)_2[InCl_5(H_2O)]$[b]	"	"	14.10(5)	10.17(5)	7.16(5)	90
$Cs_2[TlCl_5(H_2O)]$[b]	"	"	14.36	10.61	7.38	92
$Cs_2[RuCl_5(H_2O)]$[b,d]	Cmcm	C_{2v}(mm)	7.400(4)	17.289(8)	7.986(5)	5
$Cs_2[RhCl_5(H_2O)]$[b,d]	"	"	7.353(4)	17.271(10)	8.023(3)	7
$Cs_2[IrCl_5(H_2O)]$[b]	"	"	7.372(1)	17.283(2)	8.014(2)	this work

[a] All space groups are in the orthorhombic system and therefore have $\alpha=\beta=\gamma = 90^o$.

[b] Crystal structures have been reported for these compounds.

[c] Cell data from single crystal zero level precession photographs.

[d] The cell parameters reported for these compounds have been rearranged to give values consistent with those of $Cs_2[IrCl_5(H_2O)]$ whose structure was solved using the space group Cmcm (unlike those of the Ru and Rh analogues which were solved in the non standard setting of this space group, Amam).

M-Cl bond lengths (particularly between that chlorine atom trans to the oxygen atom and those cis to the oxygen atom) and deviations of interbond angles from 90°. The distortions are presumably associated with the unequal sizes of the H_2O and Cl groups coordinated to the metal ion.

The above series of pentachloroaquametallate(III) salts is unlike the corresponding series of caesium salts, of which structures have been reported for ruthenium, rhodium and (in this work) iridium compounds. These salts all crystallise in the orthorhombic space group Cmcm. Cell parameters are listed in Table 4.5.1. Presumably some cation effect is operating here, as has been invoked previously to explain the differences between the crystal structures of some hexahalogenometallates (III) e.g. $K_3[IrCl_6]H_2O$ and $(NH_4)_3[IrCl_6]H_2O$. This is reinforced by the observation that the structures of $Cs_2[TlCl_5(H_2O)]$ [92] and $Cs_2[InCl_5(H_2O)]$ [91] are reported to be of the $K_2[FeCl_5(H_2O)]$ type. Some relevant structural data are given in Table 4.5.2.

Examination of the radius ratio, r_a/r_c, for these compounds, reveals that the value for thallium compounds is closer to that value for $Rb_2[IrCl_5(H_2O)]$ than that of $Cs_2[IrCl_5(H_2O)]$ and hence offers an explanation as to why the $K_2[FeCl_5(H_2O)]$ structural type is preferred. In the case of $Cs_2[InCl_5(H_2O)]$, the radius ratio is actually closer to that of $Cs_2[IrCl_5(H_2O)]$, but being relatively close to that value for $Cs_2[TlCl_5(H_2O)]$ the compound again prefers to crystallise in the $K_2[FeCl_5(H_2O)]$ structural type.

Table 4.5.2: Comparison of the Ionic Radii of Component Ions in Compounds $A_2[MCl_5(H_2O)]$ (where A = Rb, Cs; M = Ir, In, Tl)

Compound	Radius M^{3+} (Å)	Radius anion (Å), r_a [a]	Radius cation (Å), r_c	r_a/r_c
$Rb_2[IrCl_5(H_2O)]$	≈ 0.68	3.0	1.48	2.03
$Cs_2[InCl_5(H_2O)]$	0.81 - 0.92	3.2	1.69	1.89
$Cs_2[TlCl_5(H_2O)]$	0.95 - 1.05	3.3	1.69	1.95
$Cs_2[IrCl_5(H_2O)$	≈ 0.68	3.0	1.69	1.78

[a] Estimated value for the $[IrCl_5(H_2O)]^{2-}$ anion (and others) from thermochemical radii for other octahedrally coordinated ions in reference [77] (taking into account the differences in the M^{3+} ionic radii).

4.5.2 The Crystal Structures of Salts of Stoichiometry $A_2[MX_6]$ (where A is a Univalent Cation, M is a Tetravalent Transition Metal and X a Halogen) and Related Hexahalogenoiridates(IV)

A large number of $A_2[MX_6]$ hexahalogenometallate salts of tetravalent transition metal ions crystallise with alkali metal ions (or univalent cations of a similar size) in the face centred cubic space group Fm3m[81,89,94] and are isostructural with $K_2[PtCl_6]$[89]. The potassium, ammonium, rubidium and caesium hexachloro and hexabromo-iridates(IV) whose cell data have been reported in the literature[76,95-100] all crystallise in this space group. Crystal data for some iridium(IV) hexahalogenometallates and related compounds are given in Table 4.5.3.

However, in some cases, where either very small or rather large counter cations are used, the cubic antifluorite structure is no longer retained. A few examples of iridium (IV) compounds which show such effects have been reported. Gmelin[101] reports $Na_2[IrCl_6]6H_2O$ to be isostructural to $Na_2[PtCl_6]6H_2O$ and $Na_2[PtBr_6]6H_2O$, which both crystallise in a triclinic space group. The sodium ion must be too small to be satisfactorily located in the cation lattice site in the cubic structure, and, as is common for small cations (e.g. lithium, sodium), the compound crystallises in some lower symmetry space group with water of crystallisation in the crystal lattice. Also a recent paper by Urushiyama et al.[102] gives structural

Table 4.5.3: Crystal Data for Iridium (IV) Hexahalogenometallates and Related Compounds.

Compound	Crystal class	Space Group	Anion site symmetry	Cell parameters a(Å)	b(Å)	c(Å)	α(°)	β(°)	γ(°)	Reference
$K_2[IrCl_6]$[c]	cubic[a]	Fm3m	$O_h(m3m)$	9.719						11
$K_2[IrCl_6]$	"	"	"	9.761						97
$(NH_4)[IrCl_6]$	"	"	"	9.860						95
$Rb_2[IrCl_6]$	"	"	"	9.910						96
$Cs_2[IrCl_6]$[c]	"	"	"	10.2119(8)[b]						this work
$Cs_2[IrCl_6]$	"	"	"	10.205						98
$K_2[IrBr_6]$	"	"	"	10.19						99
$Rb_2[IrBr_6]$	"	"	"	10.40						100
$Rb_2[IrBr_6]$	"	"	"	10.42						99
$Cs_2[IrBr_6]$	"	"	"	10.53						99
$K_2[PtCl_6]$[c]	"	"	"	9.745						81
$Na_2[IrCl_6]6H_2O$	triclinic	P1 or $P\bar{1}$	$C_1(1)$ or $C_i(\bar{1})$							101
$(CH_3NH_3)_2[IrCl_6]$	trigonal	R3m	$D_{3d}(\bar{3}m)$							102
$(CH_3)_2NH_2)_2[IrCl_6]$	orthorhombic	Pnn2 (or Pnnm)	$C_1(1)$ or $C_i(\bar{1})$ or $C_2(2)$							102
$((CH_3)_3NH)_2[IrCl_6]$	cubic	Pa3	$D_{3d}(\bar{3}m)$							102
$K_2[TcCl_6]$	cubic	Fm3m	$O_h(m3m)$	9.89						94
$H_2[TcCl_6]9H_2O$[c]	triclinic	$P\bar{1}$	$C_1(1)$	8.30(4)	7.35(4)	8.04(4)	95(.5)	98(.5)	117.5(.5)	103
$K_2[ReCl_6]$	cubic	Fm3m	$O_h(m3m)$	9.84						105
$(CH_3C_6H_4NH_3)_2[ReCl_6]$[c]	monoclinic	$P2_1/c$	$C_1(1)$	7.01(2)	25.04(5)	11.54(2)	90.0	90.0(1)	90.0	104
$K_2[TiF_6]$	cubic	Fm3m	$O_h(m3m)$	8.22						89
$Li_2[TiF_6]2H_2O$[c]	monoclinic	C2/m	$C_{2h}(2/m)$	10.294(1)	5.934(2)	4.8032(5)	90.0	90.13(8)	90.0	106

[a] Where reported, compounds of cubic space groups have $a = b = c$ and $\alpha = \beta = \gamma = 90^\circ$.

[b] Where possible, errors of cell dimensions are given in parentheses.

[c] Crystal structures are reported for these compounds.

details for a number of $[IrCl_6]^{2-}$ salts of methylammonium cations, determined from their apparent isomorphism (on the basis of their powder photographs) with their tin analogues. The cations in this case are too large to be satisfactorily located on the cation sites in the cubic structure (and would require disordering for their location on these sites of symmetry $T_d(\bar{4}3m)$). Thus, they crystallise in different spatial arrangements and space groups.

With the crystallisation of these compounds in different space groups that no longer confer $O_h(m3m)$ site symmetry on the $[IrCl_6]^{2-}$ anions, the possibility of distortion of the anions from idealised octahedral symmetry arises. No structures of iridium compounds containing $[IrCl_6]^{2-}$ anions in such space groups have been reported to date. However, in view of structures reported for iridium (III) hexahalogenometallates, none of which crystallise in a cubic space group confering O_h symmetry upon the $[IrCl_6]^{3-}$ anion, it seems reasonable to assume that in these cases the $[IrCl_6]^{2-}$ anions will also show distortion from ideal octahedral symmetry. As discussed previously, the distortion will arise from crystal packing effects.

An example supporting this hypothesis is available in the reported crystal structure of $H_2[TcCl_6]9H_2O$[103], which is said to crystallise in the triclinic space group P1, with the $[TcCl_6]^{2-}$ anion located on a site containing no symmetry at all. The compound contains extensive hydrogen bonding and a $[TcCl_6]^{2-}$ anion showing significant distortion

from O_h symmetry. However, other technetate (IV) compounds, such as $K_2[TcCl_6]$ and $Rb_2[TcCl_6]$, crystallise in the cubic $K_2[PtCl_6]$ structural type [94]. The reported crystal structure of bis(p - toluidinium) hexachlororhenate(IV) [104] also reveals significant distortion from O_h symmetry of the $[ReCl_6]^{2-}$ anion in the solid state. The Re-Cl bond lengths in the anion are essentially all equivalent but the interbond angles show significant deviations from 90^o. The simple salts of univalent alkali metal cations and the $[ReCl_6]^{2-}$ anion all crystallise in the cubic $K_2[PtCl_6]$ [105] type.

Further evidence for the distortion of anions in non cubic space groups due to crystal packing effects comes from the hexafluoro analogues of some tetravalent transition metals. Although there is some disagreement in the literature over the structures of alkali metal salts containing the hexafluorotitanate (IV) anion [89,99] the lithium salt $Li_2[TiF_6]2H_2O$, is certainly not cubic. It crystallises in the monoclinic space group C2/m, and like its tin analogue [106], contains significantly distorted anions (from idealised octahedral geometry), which are involved in hydrogen bonding. Again, like the $Na_2[IrCl_6]6H_2O$ compound, the salt contains a degree of hydration associated with the small lithium cation.

4.6 THE CRYSTAL STRUCTURES OF SALTS OF STOICHIOMETRY $A_3[M_2X_9]$ (WHERE A IS A UNIVALENT CATION, M IS A TERVALENT TRANSITION METAL AND X A HALOGEN)

The recent work of Greenaway[13] and Sherlock[14] has seen the isolation and characterisation of a number of compounds of stoichiometry $A_3[M_2X_9]$, where A is a univalent cation, X is a halogen, and M is a tervalent ruthenium or rhodium ion. This thesis reports the successful preparation of a number of iridium (III) analogues. These compounds are isomorphous with a wide ranging series of similar compounds of both tervalent transition metals and non transition metals including Zr, Ti, Fe, Cr, Nb, Mo, Ru, Rh, In, As, W, Tl, Sb and Bi. A number of crystal structures have been reported for these compounds, and in some cases these have shown significant metal-metal bonding interactions in the dimetallate $[M_2X_9]^{3-}$ anions as their most important structural feature.

Before the results of the present studies of iridium(III) compounds are discussed, details on a number of crystal structures of compounds containing these dimetallate anions will be surveyed. Emphasis will be placed on the discussion of the structural types in which these compounds form and the bonding within the $[M_2X_9]^{3-}$ dimetallate anion.

4.6.1. A Survey of the Crystal Structures of Compounds Containing the Dimetallate $[M_2X_9]^{3-}$ Anion (where M is a tervalent element and X is a halogen).

4.6.1(i). Compounds Crystallising in the Hexagonal Space Group $P6_3/mmc$.

The majority of tri-μ-halogenohexahalogenodimetallate(III) salts crystallise in the hexagonal space group $P6_3/mmc$. Compounds crystallising in this space group and containing the following metals have been reported; Nb [107], Cr [82,108,109,110], Mo [82,110,111,112], W [113,114]*, Ti [109,115], V [109], Rh [14], Ru [13] and Bi [116]. Unit cell parameters for a number of these compounds are listed in Tables 4.6.1 and 4.6.4. These compounds all contain dimetallate anions comprising a bi-octahedral unit of two $[MX_6]$ units sharing a common trigonal face (see Figure 4.6.1).

The reported crystal structures of $Cs_3[Cr_2Cl_9]$ [109] and $K_2[W_2Cl_9]$ [113] have revealed metal-metal distances of 3.12 Å and 2.41 Å in the dimeric $[Cr_2Cl_9]^{3-}$ and $[W_2Cl_9]^{3-}$ anions respectively. The very short W-W distance of 2.41 Å (compared to 2.52 Å for the W-W separation in tungsten metal) has been interpreted, in conjunction with the observed diamagnetism of $K_3[W_2Cl_9]$ [113,117], as being indicative of a metal-metal bond. This has been verified by the persistence of the tungsten-tungsten bond in the products resulting from chemical reactions of this dimeric complex [118] and tungsten-182 Mössbauer measurements performed on

* The reported crystal structure of $K_3[W_2Cl_9]$ [113] was refined in the space group $P6_3/m$. However, the same spatial arrangement of ions and hexagonal cell as those of compounds crystallising in the space group $P6_3/mmc$ means the choice of space group is irrelevant to the arguments presented here.

Table 4.6.1: Cell Parameters and Other Data for $A_3[M_2X_9]$ Complexes Crystallising in the Hexagonal Space Group $P6_3/mmc$

Compound	a(Å)	c(Å)	c/a	d(M-M) (Å) (where given)	d(M-M) (Å) in metal[b]	Reference
$Cs_3[Ti_2Cl_9]$	7.32	17.97	2.45		2.64	109
$Cs_3[V_2Cl_9]$	7.24	17.94	2.48		2.44	109
$K_3[Cr_2Cl_9]$	6.88	17.52	2.51	3.05	2.39	110
$Rb_3[Cr_2Cl_9]$	6.99	17.65	2.52	3.07	2.39	110
$Cs_3[Cr_2Cl_9]$	7.22(1)	17.93(2)	2.48	3.12[a]	2.39	109
$(Et_4N)_3[Cr_2Cl_9]$	9.66	22.35	2.31	3.89	2.39	110
$Cs_3[Nb_2Cl_9]$	7.404	17.578	2.37	2.70	2.68	107
$K_3[Mo_2Cl_9]$	7.11	16.63	2.34	2.53[a]	2.59	110
$Rb_3[Mo_2Cl_9]$	7.18	16.98	2.36	2.59	2.59	110
$Cs_3[Mo_2Cl_9]$	7.357(5)	17.545(12)	2.38	2.66(1)[a]	2.59	82
$Cs_3[Mo_2Cl_9]$	7.346(3)	17.506(14)	2.38	2.68[a]	2.59	110
$(Me_4N)_3[Mo_2Cl_9]$	9.27	20.50	2.21	3.13	2.59	110
$(Et_4N)_3[Mo_2Cl_9]$	10.08	22.45	2.23	3.43	3.59	110
$K_3[W_2Cl_9]$	7.16	16.16	2.26	2.41[a]	2.61	113
$(NH_4)_3[W_2Cl_9]$	7.16	16.17	2.26			114
$Tl_3[W_2Cl_9]$	7.15	16.33	2.28			114
$Rb_3[W_2Cl_9]$	7.24	16.95	2.34			114
$Cs_3[W_2Cl_9]$	7.35	17.06	2.32			114
$Rb_3[Nb_2Br_9]$	7.594	17.993	2.37			107
$Cs_3[Nb_2Br_9]$	7.704	18.313	2.38	2.77(3)	2.68	107
$Cs_3[Cr_2Br_9]$	7.51	18.72	2.49	3.26	2.39	110
$Cs_3[Cr_2Br_9]$	7.507(6)	18.680(15)	2.49	3.317(21)[a]	2.39	82
$(Et_4N)_3[Cr_2Br_9]$	10.18	23.03	2.26	4.00	2.59	110
$Cs_3[Mo_2Br_9]$	7.648(3)	18.339(16)	2.40	2.816(9)[a]	2.59	82
$(Et_4N)_3[Mo_2Br_9]$	10.30	23.13	2.25	3.53	2.59	110
$Rb_3[W_2Br_9]$	7.6	17.5	2.30			124
$Cs_3[Cr_2I_9]$	7.90	19.60	2.48			108
$Cs_3[Nb_2I_9]$	8.249	19.529	2.37	2.96(9)	2.68	107
$Cs_3[Bi_2I_9]$	8.4116(7)	21.182(2)	2.52	4.051(5)[a]	3.02	116

[a] Metal-metal distance within dimeric anion determined from a complete X-ray crystal structure determination. Other M-M bond lengths quoted are those calculated from isostructural compounds assuming the given cell dimensions.

[b] Single bond metallic radii calculated by Pauling and obtained from Reference 77.

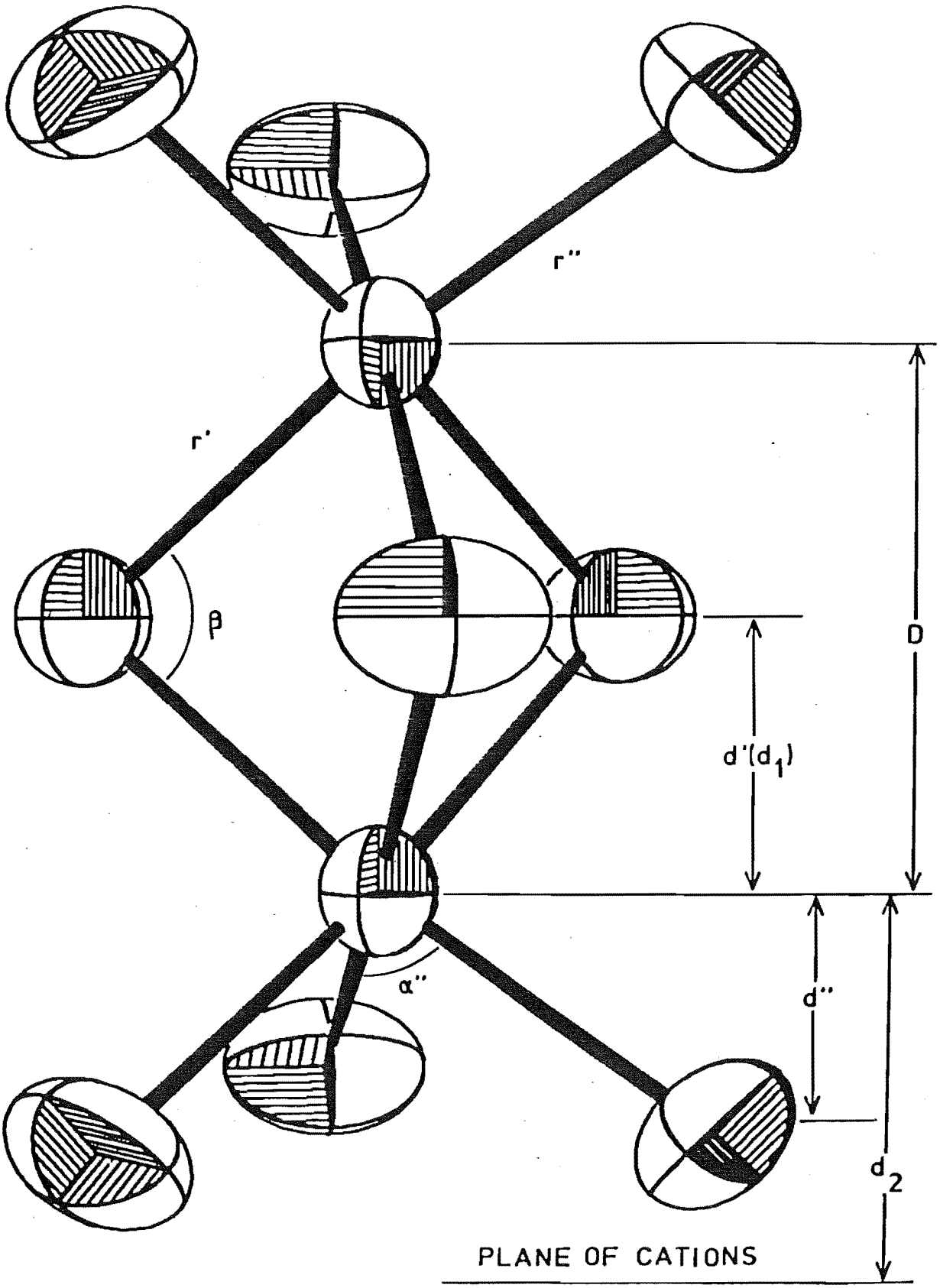

Figure 4.6.1: Diagram illustrating the bonding within a dimetallate $[M_2X_9]^{3-}$ anion and a number of structural parameters.

$K_3[W_2Cl_9]$[119]. On the other hand, magnetic data for $Cs_3[Cr_2Cl_9]$[109,120] (the magnetic moment is 3.82 μ_B compared with the theoretical value of 3.87 μ_B for a Cr^{3+} ion with three unpaired d electrons) and the larger Cr-Cr separation in the $[Cr_2Cl_9]^{3-}$ anion, indicates the absence of any metal-metal bonding interaction in this compound. The magnetic data and reported crystal structures of a number of molybdenum compounds[110,121,122] suggest that metal-metal bonding in the $[Mo_2Cl_9]^{3-}$ anions is intermediate between these two extremes.

The extent of metal-metal bonding in the complex ions of these compounds has been studied by a number of workers[11,13,14,111,112,110,123]. In particular Kepert[123] and Sherlock[14] have made use of c/a ratios (a(=b) and c are the axial hexagonal unit cell dimensions) for indicating the possibility of metal-metal bonding. For chloro compounds having a ratio of c/a less than 2.40, a metal-metal bond is predicted. Thus, niobium, molybdenum and tungsten chloro dimetallates (see Table 4.6.1) have some metal-metal bonding (as has been verified by X-ray crystal structure analysis for compounds of the latter two metals).

The hexagonal cell of these compounds can be visualised as layers of closest packed cations and halogen atoms of stoichiometry AX_3, stacked perpendicular to the unique hexagonal axis in the order ABACBCAB... throughout space. Occupying suitable octahedral interstices in this arrangement will be tervalent metal ions, thus completing the octahedral halogen coordination sphere of each metal ion. When some

degree of metal-metal bonding occurs within a dimetallate anion, two changes are observed in the hexagonal crystal lattice. On close approach of the two metal atoms the bridging halogen atoms, which are located in the AX_3 closest packed layers, expand outwards from one another (but are retained within their AX_3 plane). This is a consequence of the necessity to maintain suitable M-X bond lengths. On the other hand for the terminal halogen bond lengths to remain satisfactory, the halogen atoms concerned must move out of the planes of the anions and cations (or the whole AX_3 layer move), and move closer to the metal atoms. The nett result of these two effects is expansion of both the hexagonal a and b axes and contraction of the unique c axis. The data in table 4.6.1 for the triad $Cs_3[M_2Cl_9]$ (M = Cr, Mo, W) illustrate this effect.

The a (and b) cell dimension for $Cs_3[W_2Cl_9]$ is larger than that of $Cs_3[Cr_2Cl_9]$ whereas the reverse is true for the c dimension. The $[W_2Cl_9]^{3-}$ anion contains a strong metal-metal bonding interaction unlike the $[Cr_2Cl_9]^{3-}$ anion. The cell dimensions of $Cs_3[Mo_2Cl_9]$ are between these extremes, as is the metal-metal bonding interaction in this compound. The c/a ratio therefore, will be smaller for a compound exhibiting a metal-metal bonding interaction in the dimetallate anion than that of a compound having no such interactions.

However, the use of c/a ratios as a criterion for the presence of metal-metal bonding in these dimetallates is restricted to salts of K^+, Rb^+, NH_4^+ and Cs^+. As can be

seen in Table 4.6.1 a number of chloro and bromo dimetallate tetraalkylammonium salts of chromium(III) show c/a ratios less than 2.40. For these compounds the changes in cell dimensions (relative to their alkali metal cation analogues) are due mainly to the replacement of the smaller alkali metal cations by relatively large cations which will dominate the packing in the approximately closest packed AX_3 layers of cations and anions. Thus, for dimetallate compounds containing cations whose ionic radii are larger than those of the halogen atoms, a c/a ratio of less than 2.40 may no longer be a useful structural parameter for predicting the presence or absence of metal-metal bonding within the dimetallate anion. However, for alkylammonium salts of the chloro dimers a c/a ratio of less than 2.28 would seem to satisfactorily indicate the presence of some metal-metal interaction (from data in Table 4.6.1).

Cotton and Ucko[11] have considered the question of metal-metal bonding in confacial bioctahedral species. They have, using the concept of an ideal confacial bioctahedron (i.e. one in which all bond lengths are the same and inter-bond angles of 90° are maintained around each metal atom, see Figure 4.6.1), defined a number of structural parameters to evaluate and compare the degree of metal-metal attractive and repulsive interactions found in dimetallate anions. Cotton and Ucko have stated this model is purely an abstract construct, as in the real situation, in the absence of other stresses, a net repulsive potential between the metal atoms tending to elongate this bioctahedron

would exist. This arises from the coulombic repulsive potential between the tervalent metal atoms (whose nett charge may be somewhat lower than +3) and the repulsive overlapping of electron clouds of the metal ions. However, for certain electron configurations an attractive potential may be imposed. These attractive and repulsive potentials combine to give the geometries observed in these anions.

As pointed out by Greenaway[13], Cotton and Ucko's model does not accommodate the cation effect found in the hexagonal dimetallate complexes (e.g. the differences in the metal-metal bond for $K_3[Mo_2Cl_9]$ and $Cs_3[Mo_2Cl_9]$[110]).

Greenaway has suggested a slightly modified model for predicting metal-metal bonding in the dimetallate anions in hexagonal structures. In this he defines the ratio d_1/d_2, where d_1 = d' (as defined by Cotton and Ucko) but d_2 is the distance from the metal ion to the plane of cations in which the terminal bromine atoms of the dimetallate anion are approximately located (rather than to the plane of the terminal bromine atoms themselves as for Cotton and Ucko's d" parameter) (see Figure 4.6.1). However, both the model proposed by Greenaway (which is only applicable to hexagonal type structures) and Cotton and Ucko's produce essentially the same predictions of metal-metal bonding in $K_2[W_2Cl_9]$, no metal-metal bonding in $Cs_3[Cr_2Cl_9]$ and an interaction of an intermediate nature in salts containing the $[Mo_2Cl_9]^{3-}$ anion. Table 4.6.2 lists some structural parameters evaluated by Cotton and Ucko[11] and parameters evaluated for Greenaway's model for these compounds. Greenaway's model in one case

Table 4.6.2: Structural Data and Moduli of Distortion from Ideal Confacial Bioctahedron[a]

Complex anion	$[Cr_2Cl_9]^{3-}$	$[Cr_2Br_9]^{3-}$	$[Mo_2Cl_9]^{3-}$	$[Mo_2Br_9]^{3-}$	$[W_2Cl_9]^{3-}$	$[Bi_2I_9]^{3-}$
D(Å)	3.12	3.317(21)	2.655(11)	2.816(9)	2.41(10)	4.051(5)
r'(Å)	2.52	2.577(9)	2.487(22)	2.624(5)	2.5(2)	3.249(5)
r"(Å)	2.34	2.417(5)	2.384(6)	2.544(3)	2.4(3)	2.923(4)
α"	93.3(3)	93.7(3)	91.0(3)	90.73(15)	91(14)	90.11(11)
β	76.4	80.0(4)	64.5(3)	64.88(15)	58(6)	77.12(15)
d'(Å)	1.56	1.66	1.33	1.41	1.21	2.02
d"(Å)	1.27	1.30	1.35	1.45	1.35	1.56
d_2	1.54	1.60	1.75	1.84	1.70	1.53
d'/d"	1.23	1.28	0.98	0.97	0.90	1.29
d_1/d_2	1.01	1.04	0.76	0.77	0.71	1.32
reference	109	82	82	82	113	116

[a] Errors where quoted are given in parentheses.

(the $[Bi_2I_9]^{3-}$ anion) also shows a marked deviation of the calculated d_1/d_2 value from those values found for the chloro and bromo dimetallates showing no metal-metal bonding. Thus, his model may only be applicable to the latter two types of dimers, or, on the other hand, as bismuth is not a transition metal, may only apply to transition metal dimetallate complexes. The d_1/d_2 ratio for $[N(CH_3)_4]_3[Rh_2Br_9]$ at 0.93 is also lower than those values reported for $Cs_3[Cr_2Cl_9]$ and $Cs_3[Cr_2Br_9]$ (1.01 and 1.04 respectively) and could indicate the inability of the model to accommodate structures containing large cations (see Section 4.6.2, page 181).

The d'/d" parameters vary from 1.29 for $[Bi_2I_9]^{3-}$ to 0.90 for $[W_2Cl_9]^{3-}$. The cation effect mentioned earlier yields d'/d" values for $K_3[Mo_2Cl_9]$ and $Cs_3[Mo_2Cl_9]$ of 0.93 and 0.99 respectively but still shows, relative to the $[Cr_2Cl_9]^{3-}$ anions, appreciable attraction between the molybdenum atoms in these compounds.

4.6.1(ii) Compounds Crystallising in Other Space Groups

There are a number of other compounds of stoichiometry $A_3[M_2X_9]$ which crystallise with the same spatial arrangement of anions and cations as those crystallising in the hexagonal space group $P6_3/mmc$ but differ slightly in their reported space group assignments. These include compounds of the tervalent metals Tl[61,125], As[126], In[127], Sb[128,129], Bi[129] and Fe[130,131]. Some of these reported structures are not at all accurately determined and some of the compounds

(e.g. Sb^{129}, Fe^{131}) exhibit polymorphism. Furthermore, some of these compounds no longer contain the dimeric $[M_2X_9]^{3-}$ anion, but have been shown in some cases (e.g. Fe compounds[130,131]) to be best described as aggregates of $FeCl_3$ molecules and Cl^- anions. Except for the iron(III) and arsenic(III) compounds, the majority of the other compounds reported above contain tervalent metal ions that are somewhat larger than their transition metal ion counterparts, and this probably accounts for the structural differences.

The crystal structures have also been reported for a number of compounds that have packing arrangements of anions and cations bearing no relation to those of the hexagonal structures. Often these compounds contain very large cations which make the formation of closest packed AX_3 layers (as for the hexagonal structures) difficult.

The following compounds whose structures have been determined, pyridinium nonabromodiantimonate(III) dibromide, $(C_5H_5NH)_5[Sb_2Br_9]Br_2$[132], trimethylphenylammonium nonachlorodirhodate, $((CH_3)_3(C_6H_5)N)[Rh_2Cl_9]$[11] and tetraphenylarsonium nonachlorodirhodate, $[(C_6H_5)_4As]_3[Rh_2Cl_9]$[12] all contain discrete dimetallate anions. Using average bond length and bond angle data reported for these compounds, and relevant data from the partially solved crystal structure of tri-tetramethylammonium tri-μ-bromohexabromodirhodate in this work, some structural parameters (as defined by Cotton, see Figure 4.6.1) have been calculated and are listed in Table 4.6.3. This data will be discussed in more detail in Section 4.6.2.

Table 4.6.3: Structural Data and Moduli of Distortion from Ideal Confacial Bioctahedron

Complex anion	$[Sb_2Br_9]^{3-}$	$[Rh_2Cl_9]^{3-}$	$[Rh_2Cl_9]^{3-}$	$[Rh_2Br_9]^{3-}$ [a,c]
D(Å)	4.008(13)	3.121(5)	3.11(1)	3.302(12)
r'(Å)	3.013(29)	2.397(10)	2.36(2)	2.531(7)
r"(Å)	2.653(5)	2.291(10)	2.32(2)	2.432(9)
α"	91.0(5)	92.5(3)	91(1)	91.6(3)
β	84(1)	81.3(3)	82(1)	81.4(3)
d'(Å)	2.00	1.56	1.56	1.65
d"(Å)	1.50	1.23(1.27)[b]	1.32	1.36
d'/d"	1.33	1.27(1.23)[b]	1.18	1.21
reference	132	11	131	this work

[a] Real errors for this structure will be greater than those reported, because of the unsatisfactory nature of the final refinement of this structure.

[b] Recalculated in this work. Cotton and Ucko may have accidentally transposed these two figures.

[c] d_2=1.77, d_1/d_2 = 0.93

The preparation of some tetravalent rhenium[134], titanium[135,136] and zirconium[135] nonachlorodimetallate (IV) complexes have also been reported, and the crystal structure of a titanium complex, $[PCl_4][Ti_2Cl_9]$, has been determined[136]. With the change in stoichiometry of this complex from that of its tervalent metal analogues, the compound no longer crystallises in the hexagonal crystal system (although the large size of the counter cations required to allow isolation of the $[Ti_2Cl_9]^-$ anion would probably preclude crystallisation in this space group if it were at all possible). The d'/d" ratio for the $[Ti_2Cl_9]^-$ anion in the compound $[PCl_4][Ti_2Cl_9]$ is 1.62 which reflects the large formal charge on the titanium atom and the repulsive forces exerted between these two metal ions.

4.6.2 The Crystal Structures of Compounds Containing the Dimetallate $[Ir_2X_9]^{3-}$ Anions (where X = Cl, Br)

Compounds of stoichiometry $A_3[Ir_2X_9]$ (A = Rb, Cs, $N(CH_3)_4$; X = Cl, Br) have been isolated in the present work and have been found to be isomorphous with their rhodium analogues as revealed by their near identical powder photographs.[63] Hexagonal cell dimension data have been determined for the iridium compounds prepared in this work by using an X-ray powder diffractometer (see Section 9.3.5). Table 4.6.4 contains cell parameters determined for these iridium compounds and those for isostructural rhodium[14] and ruthenium[13] complexes.

Table 4.6.4: Unit Cell Parameters for Compounds Containing the Dimetallate $[M_2X_9]^{3-}$ Anion (M = Ru, Rh, Ir; X = Cl, Br) Crystallising in the Hexagonal Crystal System.

Compound	a(Å)	c(Å)	c/a	Reference
$Cs_3[Ru_2Cl_9]$	7.22	17.58	2.43	133
$K_3[Ru_2Br_9]$	7.293	17.94	2.46	13
$Rb_3[Ru_2Br_9]$	7.344	18.031	2.46	13
$Cs_3[Ru_2Br_9]$	7.526	18.363	2.44	13
$K_3[Rh_2Cl_9]$	6.880(5)	17.25(3)	2.51	14
$(NH_4)_3[Rh_2Cl_9]$	6.935(5)	17.35(5)	2.50	14
$Rb_3[Rh_2Cl_9]$	6.972(4)	17.42(7)	2.50	14
$Cs_3[Rh_2Cl_9]$	7.183(5)	17.77(2)	2.47	14
$[N(CH_3)_4][Rh_2Cl_9]$	9.12(2)	20.92(5)	2.29	14
$K_3[Rh_2Br_9]$	7.28(1)	18.20(4)	2.50	14
$Rb_3[Rh_2Br_9]$	7.303(6)	18.41(2)	2.52	14
$Cs_3[Rh_2Br_9]$	7.500(7)	18.69(3)	2.49	14
$[N(CH_3)_4]_3[Rh_2Br_9]$	9.50(1)	21.44(4)	2.26	14
$[N(CH_3)_4]_3[Rh_2Br_9]$	9.389(1)	21.402(1)	2.28	This work
$Rb_3[Ir_2Cl_9]$	7.018(4)	17.12(1)	2.43	This work[a]
$Cs_3[Ir_2Cl_9]$	7.204(2)	17.615(5)	2.45	" "
$Rb_3[Ir_2Br_9]$	7.308(2)	18.546(5)	2.54	" "
$Cs_3[Ir_2Br_9]$	7.465(6)	18.56(2)	2.49	" "
$[N(CH_3)_4]_3[Ir_2Br_9]$	9.375(5)	21.55(2)	2.30	" "

[a]Cell dimension data for this compound and the remaining dimetallate iridium(III) compounds were obtained from X-ray powder diffractometer determined data. The errors reported in parentheses (in the least significant digits) are those arising from the least squares refinement of the cell dimensions but real errors could be greater.

With all low angle lines observed in the X-ray powder diffractograms (to 50°) satisfactorily indexed on the basis of a hexagonal unit cell and refinement of cell parameters producing values of the correct magnitude, the compounds were assumed to be isostructural with other hexagonal compounds of the same stoichiometry reported in the literature.

The data reported in Table 4.6.4 show both the rhodium and iridium compounds have similar cell dimensions and that the chloro dimetallate anions of both metals probably contain no metal-metal bonding interactions (on the basis of the c/a ratios being greater than 2.40 and the metal-metal distances predicted by the method of Fergusson and Sherlock[8], from a c/a versus M-M distance plot for related compounds). Both the rhodium(III) and iridium(III) metal ions have a t_{2g}^6 d electron configuration. As suggested by Cotton and Ucko[11], these metal ions will tend to repel one another in a dimetallate anion, as individual t_{2g} orbitals (d_{xy}, d_{yz}, d_{xz}) will be oriented towards one another, and, as these orbitals are fully occupied, cannot interact in an attractive manner. This has been verified in two crystal structures of compounds containing dimeric $[Rh_2Cl_9]^{3-}$ anions reported to date (see Table 4.6.3). The rhodium-rhodium distances in both structures are 3.11 Å, and the geometry within both anions is the same (within experimental error). The $[Rh_2Cl_9]^{3-}$ anions also show similar geometry to the $[Cr_2Cl_9]^{3-}$ anion reported in $Cs_3[Cr_2Cl_9]$ [109] (the latter anion contains no

metal-metal bonding interaction) with d'/d" ratios and other moduli of distortion similar for all three compounds.

Although there is some uncertainty about the crystal structure of $[N(CH_3)_4]_3[Rh_2Br_9]$ because of unsatisfactory refinement of parameters (Section 4.4), some features of the structure as determined deserve some comment. The rhodium-rhodium separation in the $[Rh_2Br_9]^{3-}$ anion agrees, within limits of error, with that reported for the $[Cr_2Br_9]^{3-}$ anion in $Cs_3[Cr_2Br_9]$.[82] This is analogous to the situation found for the rhodium and chromium chloro dimetallate compounds, where the metal-metal separation is also the same. Furthermore, the geometry within the $[Rh_2Br_9]^{3-}$ and $[Rh_2Cl_9]^{3-}$ anions is very similar, as is evident when the structural data and moduli of distortion from an ideal confacial bioctahedron listed in Tables 4.6.3 and 4.6.4 are examined. Re-examination of the d" and d'/d" structural data reported by Cotton and Ucko[11] for the $[Rh_2Cl_9]^{3-}$ anion suggests these figures may have been accidentally transposed, and that the d'/d" value should be 1.23. Thus, d'/d" values for the chromium(III) and rhodium(III) dimetallate bromo and chloro anions are all within the range 1.18 to 1.28, and compared with those values reported for molybdenum compounds[11] indicate no metal-metal bonding interaction in the former dimetallate anions.

One point that arises out of this work concerns some predictions made by Grey and Smith[110] on the metal-metal separations in dimetallate anions for a series of isostructural

hexagonal compounds. Where a change over from a hexagonal cell dominated by the size of the halogen atoms to one dominated by the cations occurs, use of coordinates of isostructural compounds (containing the larger halogen atoms) and the cell dimensions of the compound containing the larger cations no longer yields correct predictions of the geometry within the dimetallate anion. For example, assuming $[N(CH_3)_4]_3[Rh_2Br_9]$ shows no metal-metal bonding interaction in the dimetallate anion and is therefore isostructural with $Cs_3[Cr_2Cl_9]$, use of the cell dimensions of the former compound and the Cr-Cr separation of 3.12Å yields a Rh-Rh separation of 3.72Å. This is significantly larger than the value of 3.30(1)Å found in the present incomplete structural analysis. Thus, a number of metal-metal distances for alkyl ammonium salts of the dimetallate anions reported in reference 110 (see Table 4.6.1) may be in error.

However, with the structure of a compound such as $[N(CH_3)_4]_3[Rh_2Br_9]$ established, it seems reasonable to calculate structural parameters for other isomorphous (as opposed to isostructural) compounds, such as the iridium(III) analogue, using the relevant coordinates of the determined structure and the cell dimensions of the other compound. The close similarity of the cell dimensions determined by X-ray powder diffraction techniques for both the iridium(III) and rhodium(III) bromo tetramethylammonium salts implies the compounds are isomorphous. Thus the iridium-iridium separation in the tri-μ-bromo-hexabromodiiridate(III) anion in this tetramethylammonium

salt would be expected to be of the order of 3.32Å i.e. no metal-metal bonding.

A molecular orbital bonding scheme for dimeric anions, involving use of non bonding d orbitals on the metal ions, has been discussed by Cotton and Ucko[11] and Crozat and Watkins[137]. In the isolated dimeric anion, the metal ion sites have C_{3v} point symmetry. The three d orbitals not involved in the σ bonding framework of the anion (d_{xy}, d_{xz}, d_{yz}), form bases for two irreducible representations of hybrid orbitals formed on each metal atom whose functional forms are as follows

$$\psi(A_1) = \frac{1}{\sqrt{3}} [d_{xy} + d_{yz} + d_{xz}]$$

$$\psi_1(E) = \frac{1}{\sqrt{2}} [d_{xy} - d_{yz}] \qquad \psi_2(E) = \frac{1}{\sqrt{6}} [2d_{xz} - d_{xy} - d_{yz}]$$

The two $\psi(A_1)$ metal orbitals, which will have maximum overlap along the metal-metal internuclear axis, essentially form a σ bond. The two degenerate metal $\psi_1(E)$ and $\psi_2(E)$ orbitals, whose overlap in formation of molecular orbitals is not as great as that for the $\psi(A_1)$ orbitals, combine to form two degenerate π molecular orbitals. The formation of the bonding (A_1,E) and anti-bonding (A_1*,E*) molecular orbitals is illustrated schematically in Figure 4.6.2.

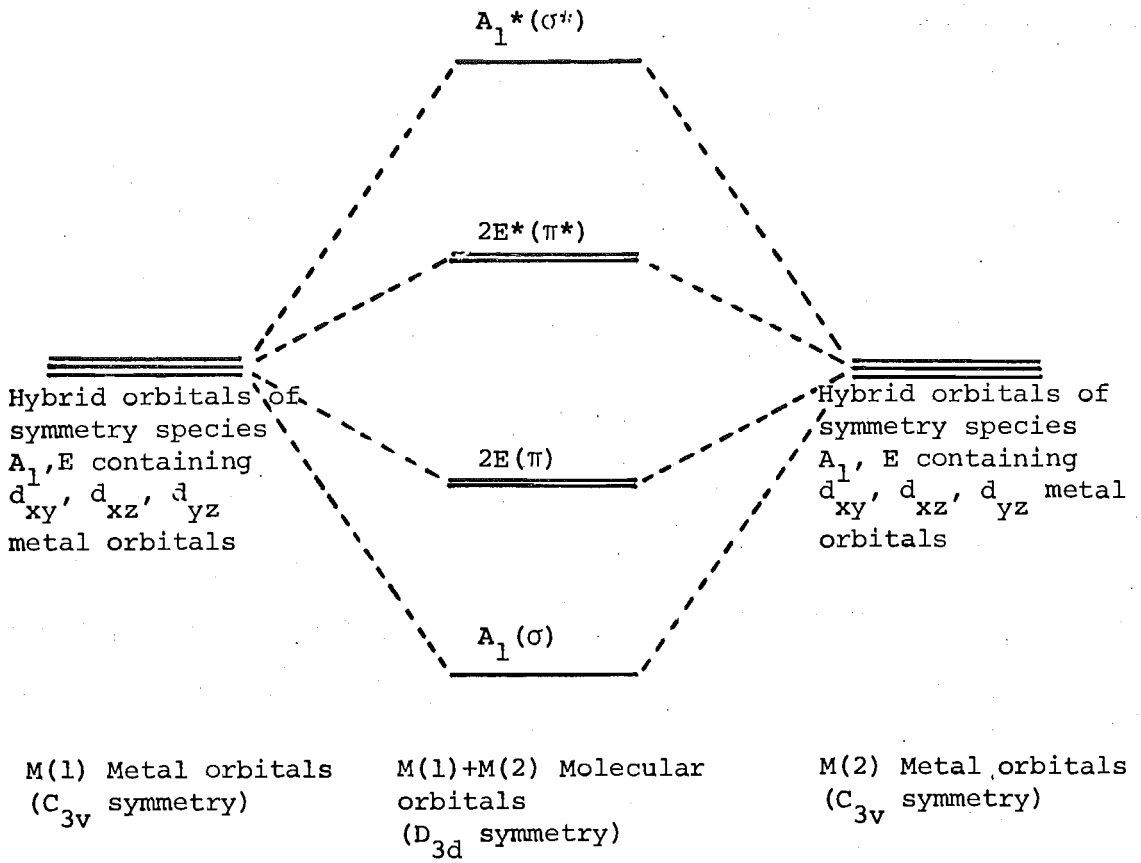

Figure 4.6.2: A possible molecular orbital bonding scheme for the $[M_2X_9]^{3-}$ anion to explain metal-metal bonding interactions in such anions.

However, this scheme completely fails to predict the magnitude of the metal-metal bonding interaction observed for the three anions $[Cr_2Cl_9]^{3-}$, $[Mo_2Cl_9]^{3-}$ and $[W_2Cl_9]^{3-}$. The metal ions in these compounds all have t_{2g}^3 d electron configurations which should, according to the above molecular orbital scheme, give rise to one σ and two π bonds. This situation is perhaps realised for the tungsten dimeric anion (tungsten-tungsten bond length is 2.41 Å) but only partially for the molybdenum case and not at all for the

chromium dimer (where the chromium-chromium separation is 3.12 Å). Thus, some fundamental difference between the metal ions (such as size) must be causing the different degree of participation of their d electrons in formation of these molecular orbitals. Another reason is that these metal orbitals may not be involved in the formation of a metal-metal bonding molecular orbital. This does not seem plausible, especially in view of the fact that when one of the bridging ligands is replaced by a hydride ion in formation of the $[Mo_2Cl_8H]^{3-}$ anion, the steric factor maintained by the three bridging atoms, which essentially establishes the geometry of the dimeric anions, has been decreased and molybdenum-molybdenum interaction can increase. This is observed to be the case, with a molybdenum-molybdenum bond length of 2.38(1)Å being produced and the Mo-$Cl_{bridging}$-Mo angle collapsing to 56.8(9)° in the $[Mo_2Cl_8H]^{3-}$ anion[138] (cf. 2.665(10)Å and 65.6(4)° in the $[Mo_2Cl_9]^{3-}$ anion). Compounds containing the $[Mo_2Cl_8H]^{3-}$ anion are found to have magnetic moments near zero, indicating a strong bonding interaction between the metal atoms. Thus, the more diffuse nature of the metal d orbitals of the tungsten(III) ion, and the fact that they extend further out into space than their first row transition metal chromium(III) ion counterparts, must play an important role in the presence or absence of metal-metal bonding in compounds containing the dimeric $[M_2X_9]^{3-}$ anion.

The above molecular orbital scheme does offer a logical explanation for the absence of any metal-metal bonding in the rhodium and iridium chloro and bromo dimers. Both these metal ions have t_{2g}^6 d electron configurations (i.e. each d_{xy}, d_{yz}, d_{xz} metal orbital is filled) and as a result all the bonding and antibonding orbitals in the above scheme will be occupied. Thus, there will be no contribution to any metal-metal bonding interaction in these compounds from the metal ion d electrons.

CHAPTER 5

INFRARED AND RAMAN VIBRATIONAL SPECTROSCOPIC STUDIES OF HALOGENOIRIDATE(III) SALTS

5.1 INTRODUCTION

The low frequency infrared spectra of many hexahalogenometallate(III) complexes have been reported. Many of these spectra show "anomalous" absorption bands (compared with the analogous series of cubic hexahalogenometallate(IV) complexes) which in some cases have been attributed to distortion from cubic symmetry of the complexes. The low frequency infrared spectra of hexahalogenoiridate(III) and other compounds recorded in the present work show similar effects and an interpretation has been made with the assistance of factor group analysis. The analysis requires a knowledge of the crystal structures of the compounds many of which contain halogenoiridate(III) anions significantly distorted from their ideal molecular point symmetry.

Before discussing the observed vibrational spectra a brief introduction to the theoretical approaches available for the prediction of vibrational selection rules in the solid state will be made. Results of factor group analyses for some complexes are listed in an appendix to this chapter.

5.2 INFRARED AND RAMAN SPECTROSCOPY IN THE CRYSTALLINE STATE

The spectra of polyatomic molecules in a crystal lattice differ from those of free molecules (i.e. in the gaseous or liquid state) in two ways. Firstly, the selection rules are determined by both crystal and molecular symmetry and secondly new modes of motion of the crystal lattice (translational or librational modes) appear. These latter modes are often called external modes to distinguish them from internal modes of the molecular species within the crystal lattice.

Two approaches have been developed for prediction of the number and type of symmetry species which represent the normal vibrational motions of compounds in the crystalline state. They are based on the vibrational potential energy of the crystal as expressed by Hornig[139] (equation (5.2.1)).

$$V = \sum_{n} V_n + \sum_{n} \sum_{k} V_{nk} + V_{\ell} + V_{\ell n} \qquad (5.2.1)$$

The four terms in this equation represent the potential energies due to internal vibrations, interaction between internal vibrations, lattice modes and interaction between lattice and internal modes respectively. The site group approximation uses the first term in this potential energy expression whereas the factor group approximation also takes the second term into account.

5.2.1 The Site Group Approximation

The site group approximation, first developed by Halford[140], considers the symmetry of some molecular species to be modified by and become that of the crystallographic point symmetry of the site at which the molecular species is located in the unit cell. The irreducible representations of such site groups corresponding to those of the molecular point group are found using correlation tables (e.g. by Ross[141], Fateley et al.[142]). The most important result of such an analysis is the prediction of a greater number of modes of vibration (and therefore absorptions in the Raman and infrared spectrum) for species in the solid state than in solution or the gaseous state. This is often a consequence of the removal of degeneracy of certain vibration species as the site group symmetry is normally lower than that of the point group of the molecular species. Such effects have been observed for a number of complexes e.g. $[PO_4]^{3-}$ [143] $[ClO_3]^-$ [144,145] but are not always found when predicted.

5.2.2 The Factor Group Approximation

This approximation was first developed by Bhagavantum and Venkatarayudu[146,147] and extended by Adams and Newton[148] and Fateley et al.[142]. This method treats the interaction of incident radiation with a complete unit cell of a compound and requires a knowledge of the crystal structure of the compound under consideration. The species of the factor group representing the irreducible representation of the

vibrational modes of the contents of the Bravais unit cell are found from either a correlation method[142], by consideration of the reducible representation of the unit cell contents[146,147] or by use of Adams and Newton's tables[148]. Each method yields the same results.

Normally factor group analysis predicts a greater number of vibrational modes than the number predicted by the site group approximation, due to the inclusion of the interaction term (2nd term) in equation (5.2.1). The weak interactions result in small "correlation splitting" of the frequencies of vibrational modes predicted by the site group approximation. This is normally of the order of 1-2% of the observed mode frequency.

5.2.3 Factor Group Analyses

The characterisation of the crystal structures of the halogenometallate complexes prepared in this work has allowed a full factor group analysis to be carried out for each compound and therefore prediction of the number of infrared and Raman active fundamentals that may be observed.

In the present studies on powdered samples where resolution of broad bands has not normally been achieved (even for infrared spectra recorded at 179 K) the number of vibrational absorption bands in both the recorded Raman and infrared spectra is less than predicted. As suggested previously, powdered crystalline samples do not normally allow observation of correlation splitting[141], but it is

assumed that the frequencies of the vibrational modes contribute to, and form the broad band envelopes observed.

The broad absorption bands present in far infrared spectra often showed "fine" structure some of which was not reproducible. The origin of this structure is uncertain but in some cases probably arises from errors in the recorded interferogram function as has been previously reported[149] rather than from real absorption effects. It is unlikely that the structure is arising from correlation splitting effects as in many cases the number of individual shoulders or small peaks observed on a broad absorption exceeds the number of infrared active modes predicted by a factor group analysis for the compound under study.

Thus, interpretation of recorded spectra has been made rather cautiously. Only in cases where absorption bands are well separated and resolved and reproducible are their individual frequencies reported. In cases where a broad absorption band contains structure, the centre of the band is taken as the mean frequency of the vibrations contributing to such an absorption.

Factor group analyses for the different complexes studied in this thesis are summarised in an appendix to this chapter (see Section 5.7).

5.3 THE INFRARED AND RAMAN SPECTRA OF HEXAHALOGENOMETALLATES OF IRIDIUM(III) AND IRIDIUM(IV)

Numerous vibrational studies of hexahalogenoiridates(IV) using both low frequency infrared and Raman techniques have been reported[2,28,53,99,102,150-158] and some studies include force constant calculations.

Studies on hexahalogenoiridates(III) are less common although the low frequency infrared and Raman spectra of a number of chloro and bromoiridates(III) have been reported [2,44,53,154,159-161]. A normal coordinate analysis for the $[IrBr_6]^{3-}$ species has been reported by Sanyal et al.[162].

Reported vibrational data which are relevant to the present discussion are listed in Table 5.3.1 and the data recorded in the present work are listed in Tables 5.3.2 and 5.3.3. The results obtained in this work will be discussed in two parts; firstly in the normal frequency range 4000 cm^{-1} to 400 cm^{-1} and secondly in the low frequency range 400 cm^{-1} to 40 cm^{-1}.

5.3.1 Infrared Absorption Spectra in the Region 4000 cm^{-1} to 400 cm^{-1}

The infrared active vibrational modes occurring in the range 4000 cm^{-1} to 400 cm^{-1} of some iridium(III) hexahalogenometallates arise from either water of crystallisation (lattice water) or in some cases the cations (e.g. ammonium or cobaltic hexaammine cations) present in these salts.

Table 5.3.1: Reported Vibrational Frequencies (cm^{-1}) for Hexahalogenoiridates of Iridium(III) and Iridium(IV).

Complex	Temperature (K)	ν_1	ν_2	ν_3	ν_4	ν_5	$2\nu_6$	ν_7	Reference
$K_2[IrCl_6]$	300	352		333	182	188		87	53
				323					27
				332					150
				332	182			86	152
				334	183			85	2
$[IrCl_6]^{2-}(aq)$[a]		346	293			160			158
$(NH_4)_2[IrCl_6]$				325-330					178
				326	187			132	156
				316					27
		320	235	326	187	181		132	155
$Rb_2[IrCl_6]$				327	187			74	156
				310					27
$Cs_2[IrCl_6]$				321	183			71	156
				308					27
	300	341		321	182	177		72	53
$[R_4N][IrCl_6]$				311	180				28
$K_2[IrBr_6]$				235	82				156
	300	216	178	233	124			80	53
				230					99
$Rb_2[IrBr_6]$	300	213	177	230	123			65	53
				227					99
$Cs_2[IrBr_6]$	300	207	173	225	123			63	53
				223					99
$[R_4N][IrBr_6]$[b]				220					28
$K_3[IrCl_6]$				296	200			86	153
	300	323	303	309 281	200 184	161	288	112	53
				310	185			110	2
$K_3[IrCl_6]H_2O$				299	184			110	2
$(NH_4)_3[IrCl_6]$				303	200			131	2
$(NH_4)_3[IrCl_6H_2O$				303 292	197			132	2
				302					160
$Ag_3[IrCl_6]$		331	311	293 306	221	162		108	53

Table 5.3.1 Continued

Complex	Temperature (K)	ν_1	ν_2	ν_3	ν_4	ν_5	$2\nu_6$	ν_7	Reference
$[N(CH_2CH_2NH_3)_3][IrCl_6]3H_2O$				305					44
$K_3[IrBr_6]$	300	200	184	219	140		178	94	53
$Ag_3[IrBr_6]$	300	198	186	222	143			86	53
$[N(CH_2CH_2NH_3)_3][IrBr_6]H_2O$				220					44
$[IrCl_6]^{3-}$ (aq)[a]		315	296						158

[a] Raman measurements performed in aqueous solution.

[b] Infrared measurements performed in benzene solutions (R is A336S or n-heptyl).

Table 5.3.2: Normal Frequency Vibrational Data (cm^{-1}) for Hexahalogenometallates of Iridium(III)

Complex	Frequencies (cm^{-1})
$K_3[IrCl_6]H_2O$	3510, 1630, 510
$(NH_4)_3[IrCl_6]H_2O$	3550, 3480, 2900-3300, 1590,1350-1440
$Rb_3[IrCl_4]H_2O$	3580, 3500, 1593
$Cs_3[IrCl_6]H_2O$	3600, 3520, 1635, 1585
$[Co(NH_3)_6][IrCl_6]$	3050, 1580, 1315, 840, 480
$(H_3O)K_8[IrBr_6]_3 9H_2O$	3450, 1615, 545
$(NH_4)_3[IrBr_6]H_2O$	3440, 3000, 1655, 1400
$Rb_3[IrBr_6]H_2O$	3450, 1618, 1586
$Cs_3[IrBr_6]H_2O$	3570, 3500, 1620, 1587
$[Co(NH_3)_6][IrBr_6]$	3200, 1600, 1320, 832, 480

Table 5.3.3: Vibrational Data (cm^{-1}) for Hexahalogenometallates of Iridium(III) and Iridium(IV) Determined in this Work.

(a) Infrared Data[a]

Complex	Temperature (K)	$\nu_3(F_{1u})$	$\nu_4(F_{1u})$	$\nu_7(F_{1u})$
$K_2[IrCl_6]$	296	333	183	83
	179	340	182	83
$(NH_4)_2[IrCl_6]$	296	329	195	133
	179	333	195	135
$Rb_2[IrCl_6]$	296	330	183	72
$Cs_2[IrCl_6]$	296	323	182	69
	179	326	183	72
$K_2[IrBr_6]$	296	233	124	77
$Rb_2[IrBr_6]$	296	230	122	68
$Cs_2[IrBr_6]$	296	227	122	66
$K_3[IrCl_6]$	296	293,317	193	100
$K_3[IrCl_6]H_2O$	296	336,310	215,183,160	102
	179	341,312	228,180	105
$(NH_4)_3[IrCl_6]$	296	324,332	218,227	136,100,78
$(NH_4)_3[IrCl_6]H_2O$	296	300	200	130
	179	308	204	130,80
$Rb_3[IrCl_6]H_2O$	296	298	195,180	80
	179	325,309,294	199,182,170	96,78
$Cs_3[IrCl_6]H_2O$	296	316,290	190,177	72
	179	320,304,292	194,179,171	78
$[Co(NH_3)_6][IrCl_6]$[c]	296	304,290	(334)193,170	95
	179	305,294	(338)197,190,170	95
$(H_3O)K_8[IrBr_6]_3 9H_2O$	296	232,221,208	147,134	90
	179	232,224,210	140	97
$(NH_4)_3[IrBr_6]H_2O$	296	220	155	106,71
	179	220	168	107,78
$Rb_3[IrBr_6]H_2O$	296	216	132	72
	179	224,196,200,190	145,134	87,70
$Cs_3[IrBr_6]H_2O$	296	226, 213	130	60
	179	228,222,193	123,133	78,62
$[Co(NH_3)_6][IrBr_6]$[c]	296	214,224	(328)133	98,77,70
	179	217,228	(325,331)137	103,98,78

Table 5.3.3 Continued

(b) Raman Data[b]

	$\nu_1(A_{1g})$	$\nu_2(E_g)$
$K_3[IrCl_6]$	315	290
$(NH_4)_3[IrCl_6]$	322	290
$(NH_4)_3[IrCl_6]H_2O$	323	292
$Cs_3[IrCl_6]H_2O$	316	287

[a] Because of the structure on and in some cases split nature of many of these absorption bands frequencies reported have an error of approximately $\pm$ 5 cm^{-1}.

[b] Errors assigned to these frequencies are of the order of $\pm$ 4 cm^{-1}.

[c] Bands frequencies given in brackets refer to cation modes.

Lattice Water

For those complexes containing water of crystallisation (see Table 5.3.2) the number of fundamental vibrations expected for the water molecules can be derived from a factor group analysis. Their frequencies will be similar to those of the fundamental vibrations for gaseous water i.e. ν_1, symmetric stretch at 3650 cm^{-1}; ν_3, asymmetric stretch at 3750 cm^{-1} and ν_2 bending mode at 1595 cm^{-1}. In some instances using high resolution infrared single crystal techniques correlation splitting has been observed[163,164] although in another study[165] and in the present work such effects have not normally been observed.

All the hydrated complexes contain symmetric and asymmetric O-H stretching modes in the regions 3200 cm^{-1} to 3600 cm^{-1} and bending modes in the regions 1580 cm^{-1} to 1630 cm^{-1} as found in other complexes containing water of crystallisation[164-167]. The lower frequency bands at 510 cm^{-1} and 545 cm^{-1} in the potassium salts of the $[IrCl_6]^{3-}$ and $[IrBr_6]^{3-}$ anions respectively may result from some librational mode of the water molecule in the crystal lattice. A feature of the spectra of $Cs_3[IrCl_6]H_2O$, $Rb_3[IrBr_6]H_2O$ and $Cs_3[IrBr_6]H_2O$ is the appearance of two frequencies in the water molecule bending mode region (with peak separations of 50 cm^{-1}, 32 cm^{-1}, 33 cm^{-1} respectively). Splitting of the bending vibrational mode frequency has been previously observed in $[FeCl_2(H_2O)_4]$[168] and in $[Co(H_2O)_4Cl_2]2H_2O$[169]; in the former case attributed to the two different types of Fe-O bond lengths of the

water molecules coordinated to the iron atom and in the latter case due to the presence of both coordinated water and water of crystallisation. However, neither of these explanations is applicable in the present case as only lattice water is present. Factor group analysis predicts two infrared active bending modes (B_{1u} and B_{3u}) of the water molecules in these compounds assuming the hydrogen atoms (whose positions were not determined in single crystal X-ray structural studies) lie on the mirror planes perpendicular to the y axis or on general positions. It is possible that this is the explanation though the location of the hydrogen atoms are unknown and it is unclear why the analogous isostructural $A_3[IrX_6]H_2O$ (X = Cl, A = NH_4, Rb; X = Br, A = NH_4) compounds do not show a similar effect. The fact that these differences exist could indicate some cation effect is operating. The magnitude of the difference in frequency between the peaks is of the order of that normally expected for correlation splitting (15 cm^{-1} to 30 cm^{-1}) [141].

Complex Cation Vibrational Modes

Other absorptions occurring in the infrared region 4000 cm^{-1} to 400 cm^{-1} in the complexes studied arise from the vibrations of the $[NH_4]^+$ and $[Co(NH_3)_6]^{3+}$ cations.

Both $(NH_4)_3[IrCl_6]H_2O$ and $(NH_4)_3[IrBr_6]H_2O$ show asymmetric and symmetric N-H stretching modes in the region ~~2900~~ ~~1350~~ cm^{-1} to ~~3400~~ ~~1450~~ cm^{-1}, and bending modes in the region 1350 cm^{-1} to 1450 cm^{-1}

The complex cation $[Co(NH_3)_6]^{3+}$, on the other hand, contains additional frequencies including vibrations associated with Co-N stretching modes and N-Co-N angle deformations. Thus, the frequencies recorded for $[Co(NH_3)_6][IrCl_6]$ and $[Co(NH_3)_6][IrBr_6]$ are assigned as follows; 3100 cm^{-1} region N-H stretching modes, 1600 cm^{-1} region degenerate bending mode of the NH_3 species, 1320 cm^{-1} region symmetric bending deformation, 835 cm^{-1} region $Co-NH_3$ rocking mode and the band at 480 cm^{-1} to a Co-N stretching mode. This latter assignment has also been ascribed to the N-Co-N bending mode[144]. However, the weight of evidence is in favour of the absorption arising from a Co-N stretching with the N-Co-N bending mode occurring in the region of 300 cm^{-1} (see Section 5.3.2). This is in agreement with infrared active stretching modes occurring at a higher wavenumber (energy) than associated bending modes.

5.3.2. Raman and Infrared Absorption Spectra in The Region 400 cm^{-1} to 40 cm^{-1}

The low frequency data listed in Tables 5.3.1 and 5.3.3 arise from internal and lattice vibrations involving the hexahalogenometallate species in each complex salt. The vibrational modes have been labelled after Herzberg[170] but strictly refer only to the cubic $K_2[IrCl_6]$ structural type complexes which contain hexahalogenometallate anions of regular octahedral symmetry.

Absorption Spectra of Hexahalogenoiridates(IV)

All iridium(IV) complex salts listed in Table 5.3.3(a) crystallise in the cubic $K_2[PtCl_6]$ structural type and factor group analysis predicts for these compounds two Raman and one infrared active metal halogen stretching modes ($\nu_1(A_{1g})$, $\nu_2(E_g)$ and $\nu_3(F_{1u})$), one Raman, one infrared active and one inactive bending mode ($\nu_5(F_{2g})$, $\nu_4(F_{1u})$ and $\nu_6(F_{2u})$), one Raman and one infrared active lattice vibration ($\nu_8(F_{2g})$ and $\nu_7(F_{1u})$) and one inactive anion libration mode ($\nu_9(F_{1g})$).

Examples of the observed spectra of hexahalogenoiridates (IV) reported in Table 5.3.3 are illustrated in Figures 5.3.1 to 5.3.6. These spectra contain three bands arising from the infrared active ν_3, ν_4 and ν_7 fundamentals and ignoring slight structure on some of these peaks are all essentially single peaks. The spectra of $K_2[IrCl_6]$ and $Rb_2[IrCl_6]$ also contain peaks at 142 cm^{-1} and 128 cm^{-1} respectively which are due to KCl and RbCl impurities (from their transverse optic modes[141]). The recorded frequencies agree well with those reported in the literature (see Table 5.3.1) and show cation effects similar to those observed in a series of $[PtCl_6]^{2-}$ alkali metal salts[171] and $[MoCl_6]^{2-}$ and $[WBr_6]^{2-}$ salts[172] where the ν_3 stretching mode frequency decreases as the alkali metal cation size increases. There is some disagreement over the values for ν_2 reported in the literature, but, after the studies of Bosworth and Clark[158], this problem now seems resolved. The assignment of ν_7 as a lattice mode appears correct especially

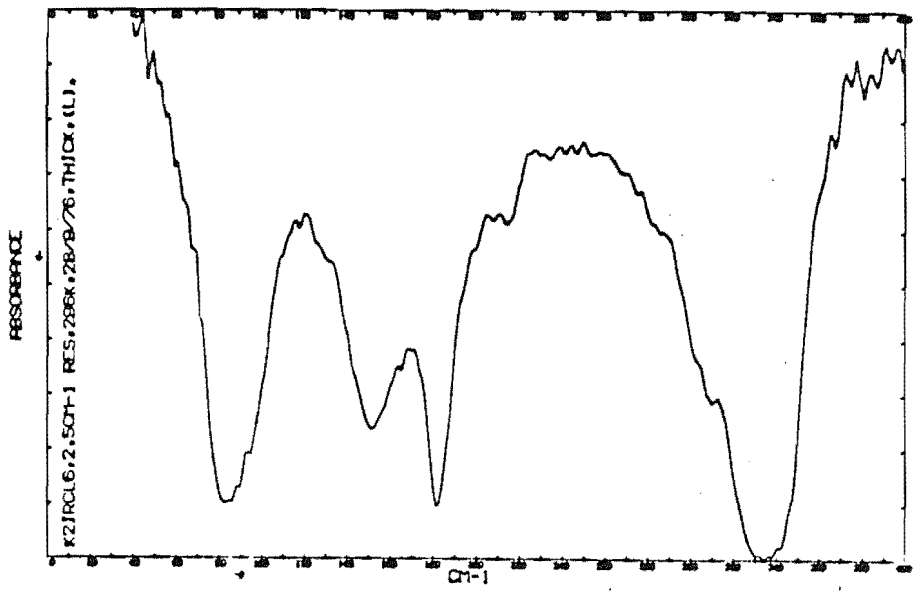

Figure 5.3.1

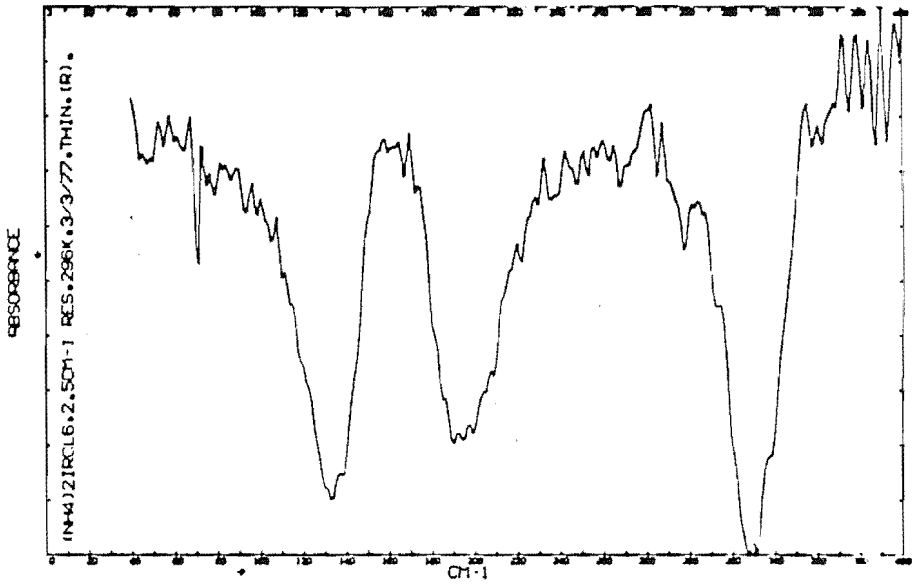

Figure 5.3.2

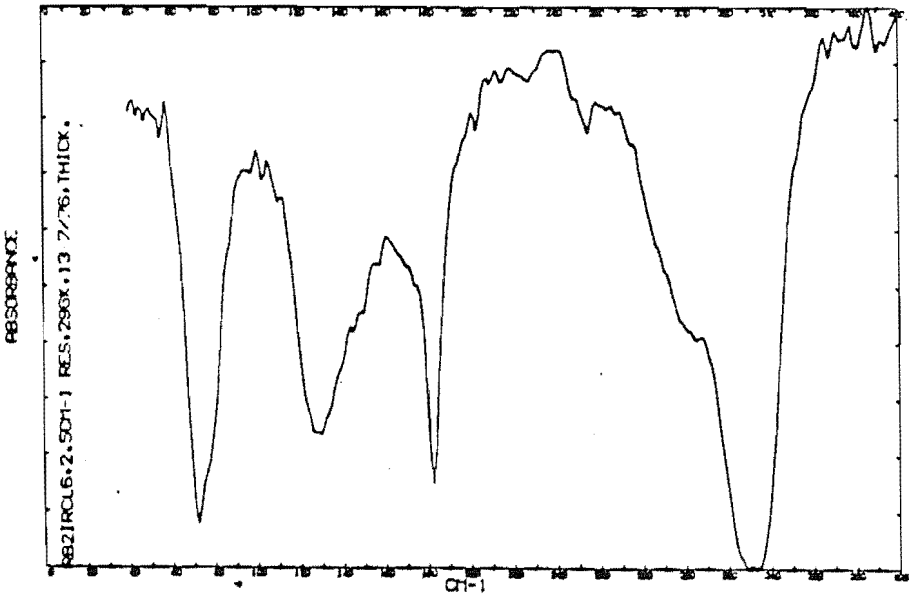

Figure 5.3.3

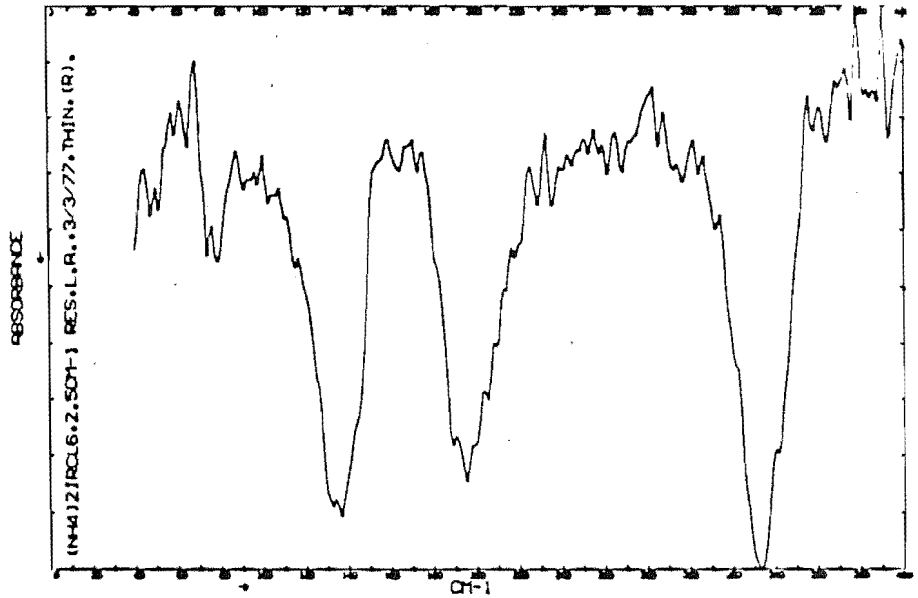

Figure 5.3.2

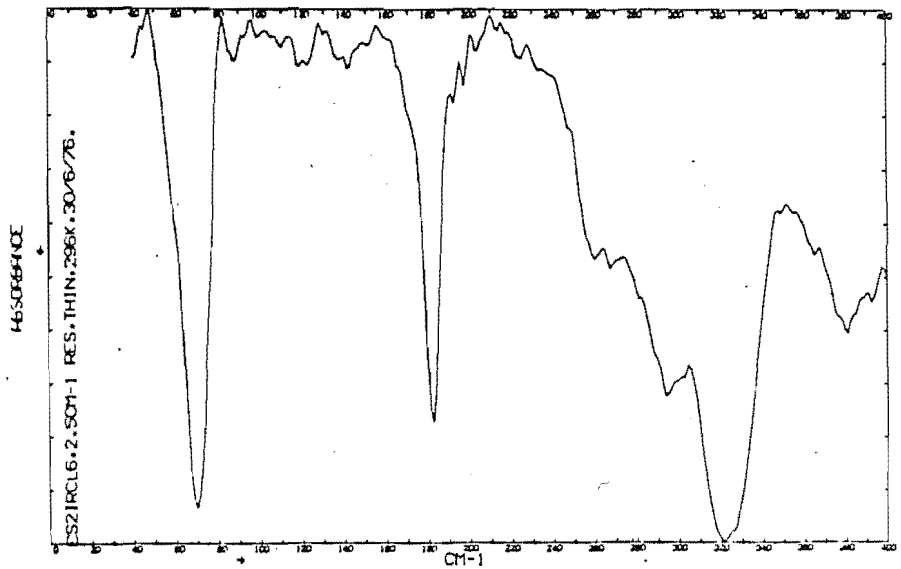

Figure 5.3.4

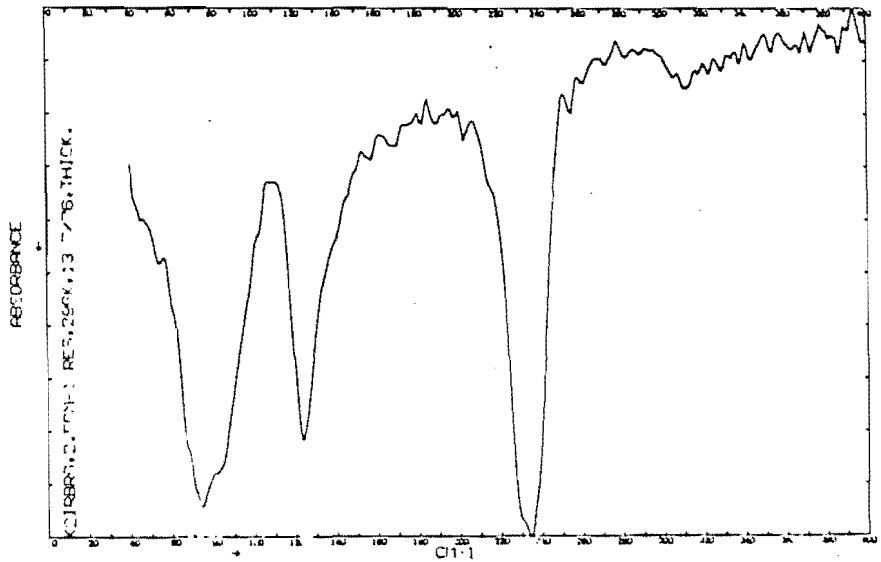

Figure 5.3.5

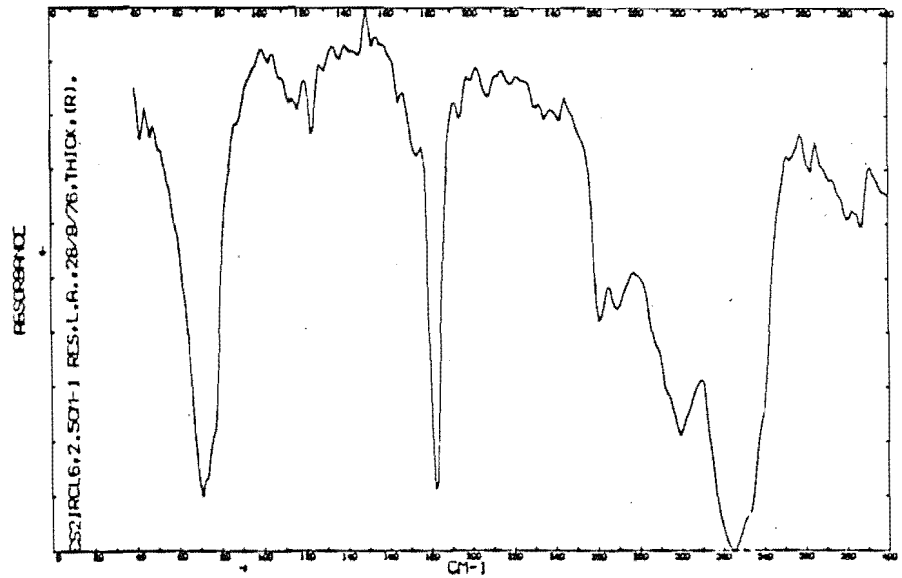

Figure 5.3.4

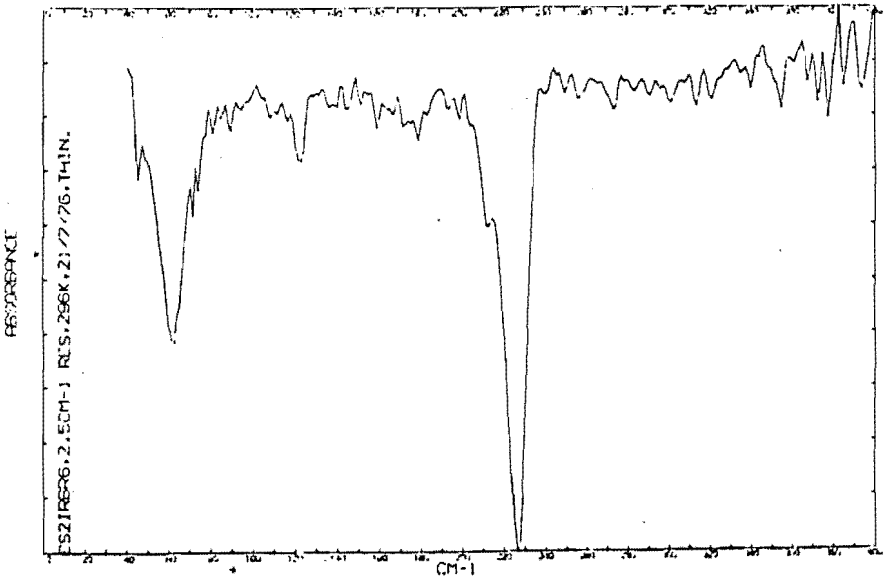

Figure 5.3.6

when the expected decrease in frequency for the series of NH_4^+, K^+, Rb^+ and Cs^+ salts is observed.

A normal coordinate analysis using three different force field approximations has been made for the $[IrCl_6]^{2-}$ species by Rai et al.[157]. However, their results will be somewhat in error because of their assumed ν_2 frequency of 225 cm^{-1} (which has since been observed at 295 cm^{-1} [158]).

Absorption Spectra of Hexahalogenoiridates(III)

As a consequence of the lower than octahedral site symmetry of the hexahalogenoiridate(III) ions found in the complexes examined in the present study, the low frequency infrared spectra of these compounds show significant differences to their iridate(IV) counterparts. The most notable difference is the greater broadness of the absorption bands for the iridate(III) complexes. In some instances these bands are split into a number of distinct bands which are better resolved at low temperature. The lattice and bending mode regions in particular often display a number of absorptions where only one band is predicted and observed for the cubic iridium(IV) complexes.

The complexity of the infrared spectra of many other hexahalogenometallate(III) complexes has been reported[2,53,69,111,154,160,161,173-175] but little attempt has been made to explain the spectra.

$K_3[IrCl_6]$

The infrared spectrum obtained in this work (Figure 5.3.7) was essentially in agreement with those previously reported

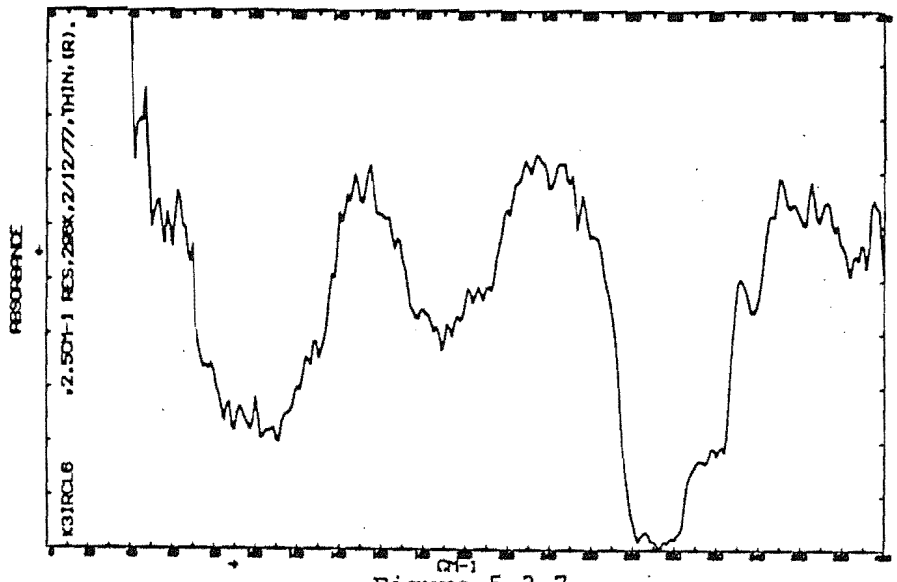

Figure 5.3.7

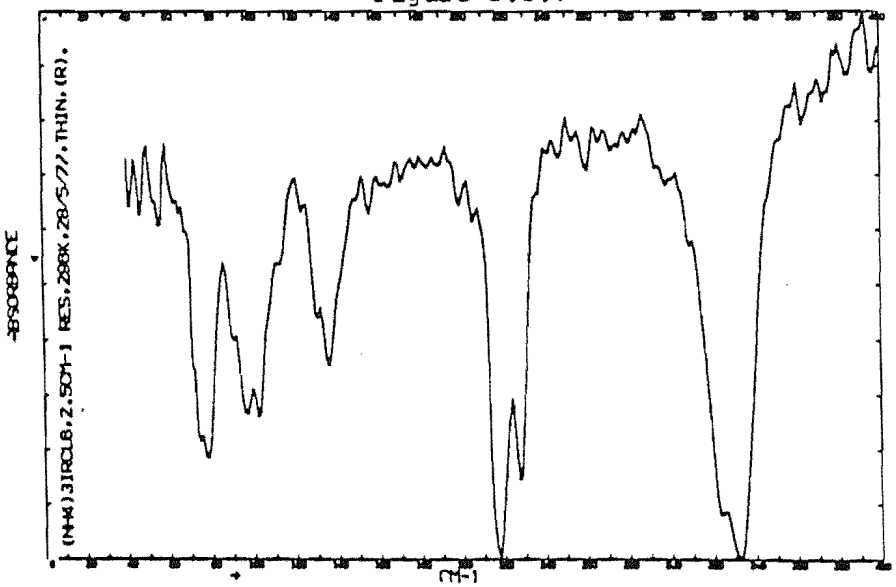

Figure 5.3.9

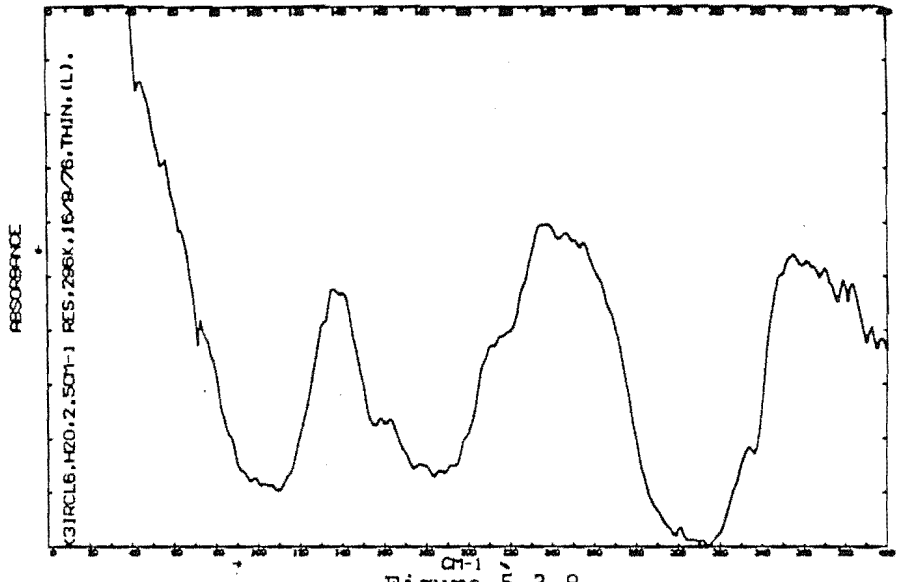

Figure 5.3.8

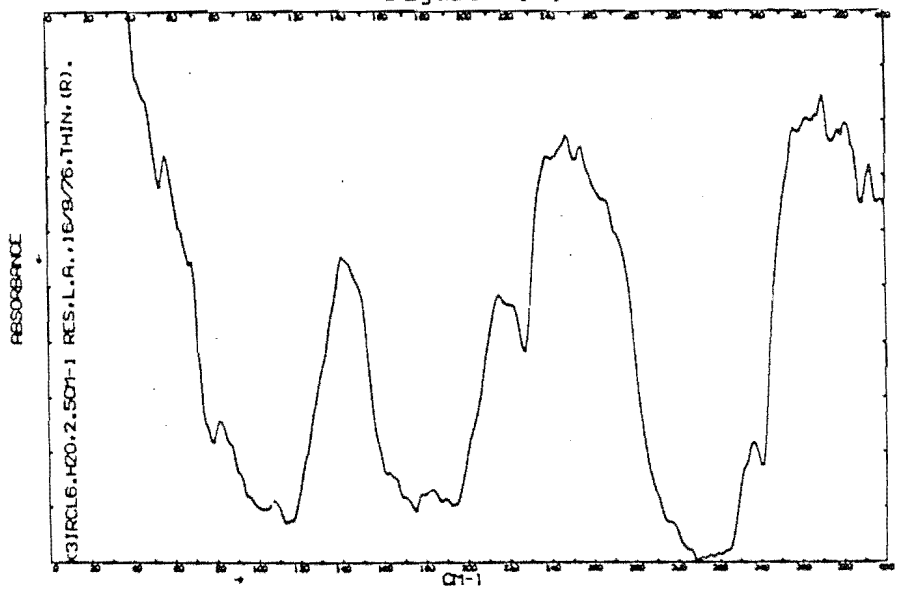

Figure 5.3.8

for $K_3[IrCl_6]$ [2, 53, 153]. The Raman spectrum obtained was essentially the same as that reported by Bottger and Salwin[53] but could not be reproduced exactly. However, the assignment of some vibrational modes by these authors has been reconsidered.

The Raman frequencies reported by Bottger and Salwin at 323, 303, 288 and 161 cm^{-1} were assigned to an A_{1g}, E_g, an overtone of the infrared and Raman inactive F_{2u} species and an F_{2g} vibrational mode respectively. Their far infrared spectrum contains a number of absorption bands; bands at 309, 281 cm^{-1} and 200, 184 cm^{-1} have been assigned to the $\nu_3(F_{1u})$ stretching mode and the $\nu_4(F_{1u})$ bending mode.

Bottger and Salwin have stated *a priori* that the removal of the degeneracy of the bands observed in the infrared spectrum probably results from site or factor group effects and that the hexohalogenoiridate(III) ions are undistorted from octahedral symmetry. This statement poses problems in that if the anion retains octahedral symmetry then site group effects cannot explain removal of the degeneracy of the ν_3 and ν_4 F_{1u} vibrational modes. These authors also comment on a "structural similarity" between $K_2[IrCl_6]$, $K_3[IrCl_6]$, $K_3[IrBr_6]$ and other compounds on the basis of X-ray powder photographs. This has not been confirmed in the present studies.

A factor group analysis for $K_3[IrCl_6]$ predicts a total of six A_g Raman active stretching modes which includes removal of the degeneracy of the $\nu_2(E_g)$ Raman active mode.

Thus rather than assign a band at 288 cm^{-1} in the Raman spectra to a ν_6 overtone (e.g. see reference[176]) it could equally well be assigned to the $\nu_2(E_g)$ mode together with a band at 303 cm^{-1}. The band at 323 cm^{-1} would remain assigned to the $\nu_1(A_{1g})$ mode. Both the infrared spectrum reported by Bottger and Salwin[53] and that recorded in this work reflect removal of the degeneracy of the ν_3 and ν_4 vibrational modes in agreement with the $6A_u$ stretching and 12 A_u bending modes predicted by a factor group analysis. Thus, both absorptions present in the infrared and Raman spectrum could reflect site or factor group effects as a consequence of the low $[IrCl_6]^{3-}$ anion site symmetry and the actual distortion of these anions from octahedral symmetry in the solid state.

The Raman spectrum recorded in this work contained peaks as follows: 315 cm^{-1} (A_{1g} stretching vibration) and 290 cm^{-1} (E_g stretching vibration). These values are close to the frequencies observed for the $[IrCl_6]^{3-}$ species measured in aqueous solution[158] where ν_1 occurs at 315 cm^{-1} and ν_2 occurs at 296 cm^{-1}. The spectrum recorded in this work was not of sufficient resolution to separate the A_g components of the doubly degenerate $\nu_2(E_g)$ vibrational modes as was observed by Bottger and Salwin[53] .

$\underline{(NH_4)_3[IrCl_6]}$

The far infrared spectrum illustrated in Figure 5.3.9 is the same as that observed by Cresswell et al.[2] although

the present spectra contains more structure in some bands. Both the ν_3 stretching mode and ν_4 bending mode bands show split character. The ν_4 bending mode band centred on 220 cm^{-1} is significantly higher in frequency than that in $(NH_4)_3[IrCl_6]H_2O$ (200 cm^{-1}) and $K_3[IrCl_6]H_2O$ (185 cm^{-1}) and may reflect significant differences in hydrogen bonding between the former and latter two compounds. Hydrogen bonding may well restrict the bending deformation of the $[IrCl_6]^{3-}$ anion thus influencing the frequency of the vibration. The absorptions at 131, 100 and 78 cm^{-1} are assigned to lattice modes. The Raman spectrum contains only two absorptions at 312 cm^{-1} and 290 cm^{-1} which are assigned to the $\nu_1(A_{1g})$ and $\nu_2(E_g)$ stretching vibrational modes respectively. The split nature of the bands observed in the infrared spectrum may be accounted for by a factor group analysis for $(NH_4)_3[IrCl_6]$ which is the same as that for $K_3[IrCl_6]$ as the compounds are isostructural.

$\underline{A_3[IrCl_6]H_2O\ (A = K, NH_4, Rb, Cs)}$

The far infrared spectra of these complexes are illustrated in Figures 5.3.8, 5.3.10, 5.3.11 and 5.3.12, respectively. All show absorption bands in the same regions except for the ν_4 and ν_7 modes for $(NH_4)_3[IrCl_6]H_2O$ which are at higher frequencies than those of other complexes. The position of the ν_4 bending mode band may be determined by hydrogen bonding which is also suggested by NQR results (see Section 6.4). The ν_7 lattice mode is at a similar

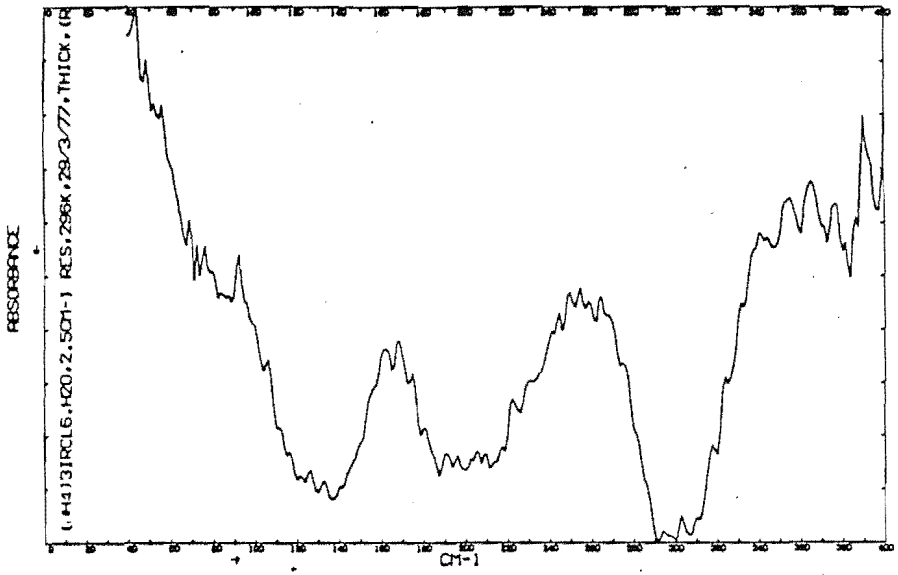

Figure 5.3.10

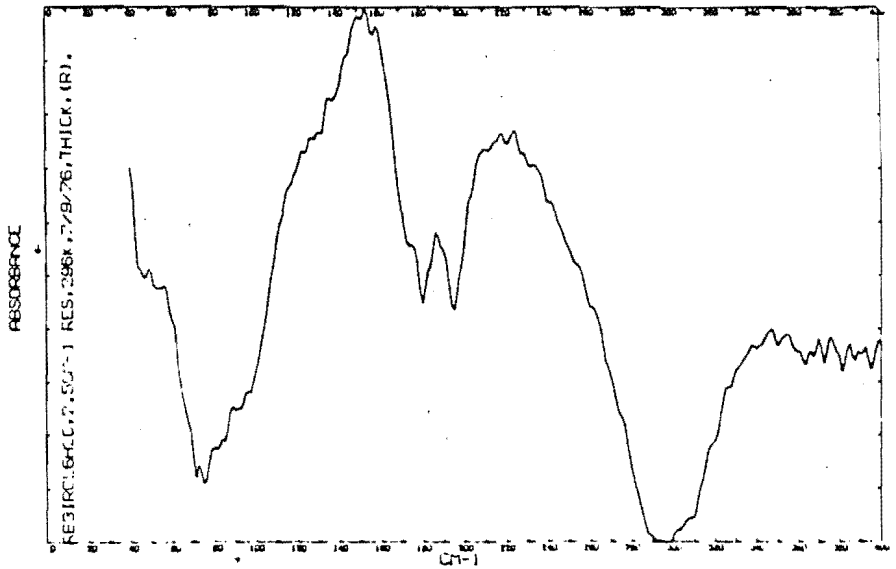

Figure 5.3.11

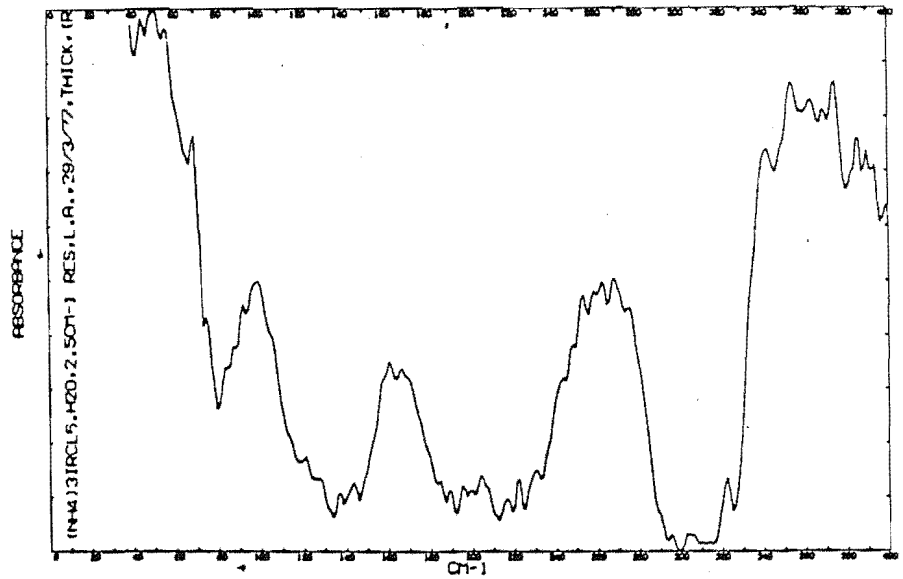

Figure 5.3.10

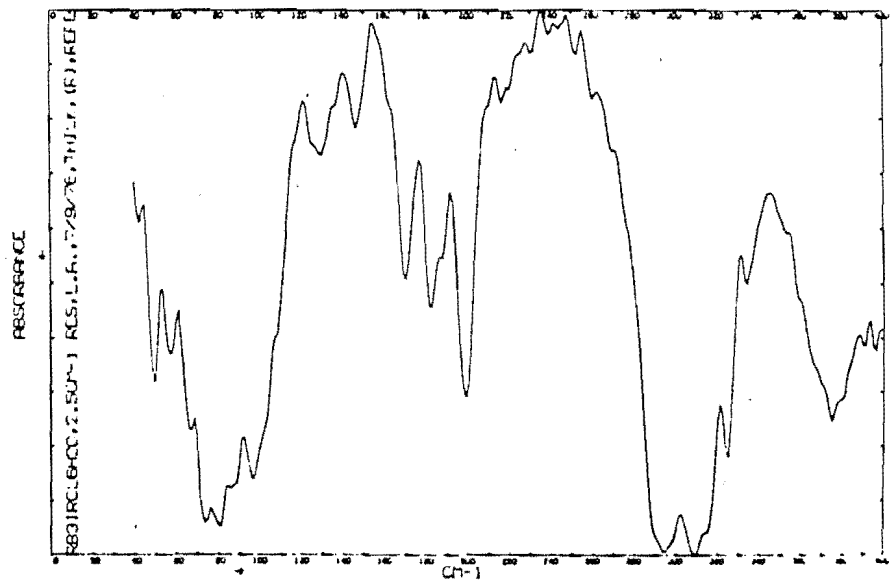

Figure 5.3.11

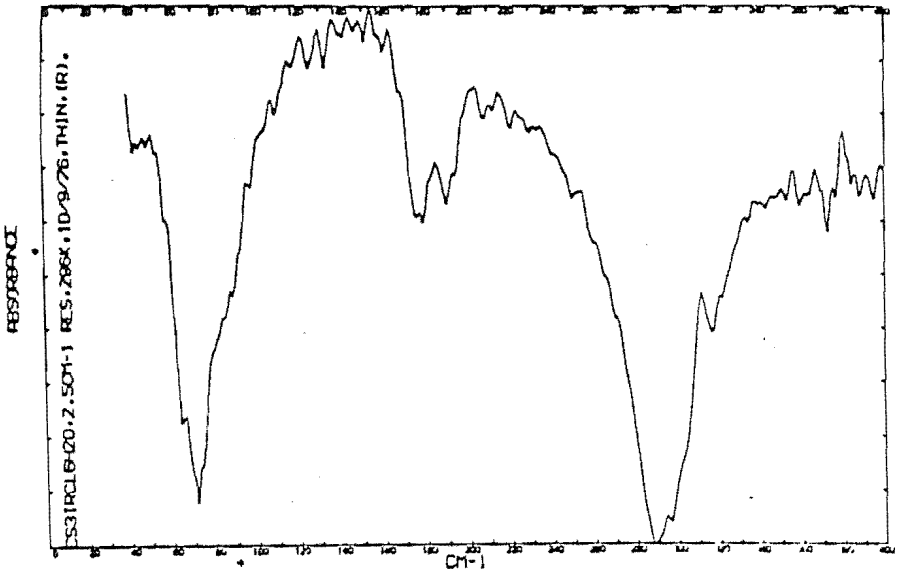

Figure 5.3.12

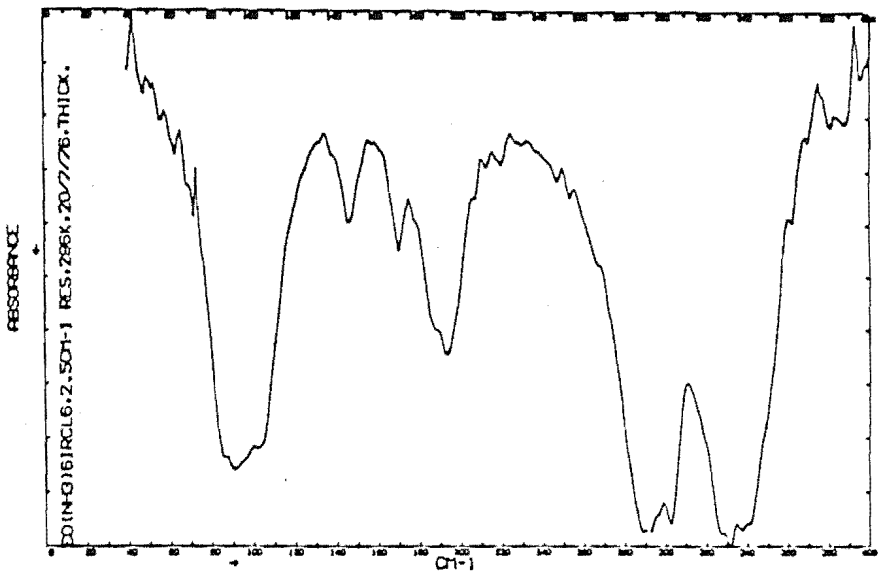

Figure 5.3.13

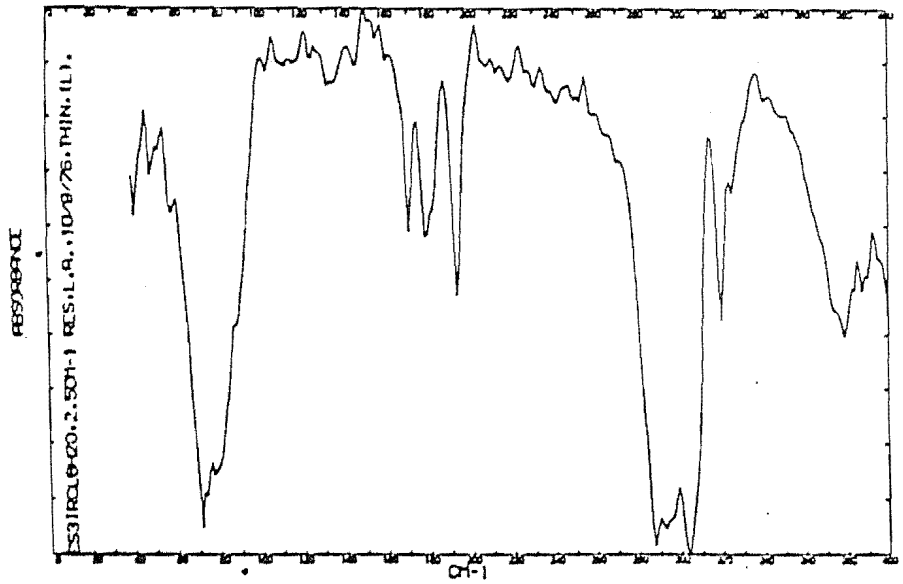

Figure 5.3.12

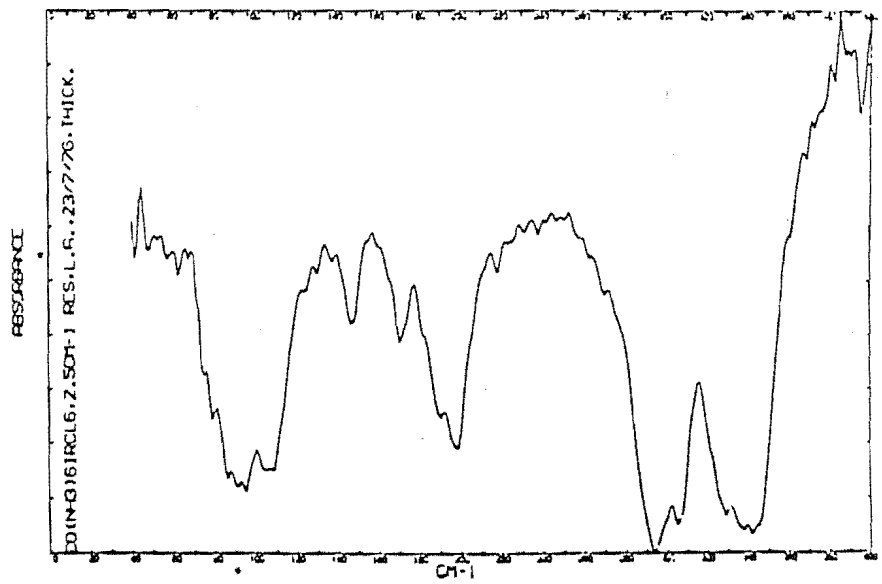

Figure 5.3.13

frequency to a similarly assigned band of $(NH_4)_3[IrCl_6]$.

The overall broadness of the bands observed reflects the 18 stretching modes ($6B_{1u}$, $6B_{2u}$, $6B_{3u}$) 27 bending modes ($9B_{1u}$, $9B_{2u}$, $9B_{3u}$) and 42 lattice modes predicted for the $[IrCl_6]^{3-}$ species in $K_3[IrCl_6]H_2O$ and the 10 stretching modes ($4B_{1u}$, $4B_{3u}$, $2B_{2u}$), 14 bending modes ($5B_{1u}$, $4B_{2u}$, $5B_{3u}$) and 25 lattice vibrational modes ($10B_{1u}$, $5B_{2u}$, $10B_{3u}$) predicted for the $[IrCl_6]^{3-}$ species in the isostructural compounds $A_3[IrCl_6]H_2O$, where A is NH_4, Rb, Cs. In both $Rb_3[IrCl_6]H_2O$ and $Cs_3[IrCl_6]H_2O$ two bands are observed for the ν_4 bending mode at 296 K. At 179 K these bands are further resolved into three bands in total thus realising complete removal of the degeneracy of the ν_4 F_{1u} species as predicted by factor group analysis.

Raman spectra recorded for $(NH_4)_3[IrCl_6]H_2O$ and $Cs_3[IrCl_6]H_2O$ contained peaks at 323, 292 and 316, 287 cm^{-1} respectively. Each pair has been assigned to the $\nu_1(A_{1g})$ and $\nu_2(E_g)$ Raman active stretching modes respectively which represent the $4A_g$, $2B_{1g}$, $4B_{2g}$ and $2B_{3g}$ Raman active vibration modes predicted by factor group analysis. The $\nu_5(F_{2g})$ Raman active bending mode was not observed.

$[Co(NH_3)_6][IrCl_6]$ and $[Co(NH_3)_6][IrBr_6]$

Both these compounds crystallise in the cubic space group Pa3 and the iridate(III) anions are located on sites of C_{3i} symmetry. The site group approximation predicts removal of the degeneracy of the infrared active F_{1u} bending and stretching cation internal vibrational modes (e.g. see the

correlation table for the Raman and infrared selection rules in reference[73]). This is observed as (see Figure 5.3.13) two absorption bands in the stretching mode region of the $[IrCl_6]^{3-}$ species at 289 cm^{-1} and 304 cm^{-1}, assigned to the A_u and E_u C_{3i} site symmetry species. The results are similar to those found for the $[FeCl_6]^{3-}$ species in $[Co(NH_3)_6][FeCl_6]$[177]. The band assigned to the $\nu_4(F_{1u})$ bending mode of the $[Co(NH_3)_6]^{3+}$ cation appears as a broad band at a similar frequency (331 cm^{-1}) to absorption bands reported in the literature for this complex cation[73] The ν_4 (F_{1u}) $[IrCl_6]^{3-}$ species bending mode occurs at 193 cm^{-1} and 170 cm^{-1} and the previously inactive $\nu_6(F_{2u})$ bending mode, which is now infrared active (see summary of factor group analysis and correlation table in reference[73]) as A_u, E_u and F_u species may possibly be assigned to the peak at 145 cm^{-1}.

The far infrared spectrum of $[Co(NH_3)_6][IrBr_6]$ (see Figure 5.3.18) shows similar character to that of the chloroiridate(III) analogue with the removal of the degeneracy of the ν_3 stretching vibration of the $[IrBr_6]^{3-}$ species illustrated by the observation of two bands at 214 and 224 cm^{-1}. The $\nu_4(F_{1u})$ $[Co(NH_3)_6]^{3+}$ species bending vibration occurs at 328 cm^{-1} and the ν_4 bending vibration of the $[IrBr_6]^{3-}$ species occurs at 133 cm^{-1}. The ν_7 lattice mode is as expected at a frequency (77 cm^{-1}) lower than that of the chloroiridate(III) analogue (94 cm^{-1}). The band at 98 cm^{-1} could possibly be assigned to the previously inactive $\nu_6(F_{2u})$ bending mode as in the assignment made for

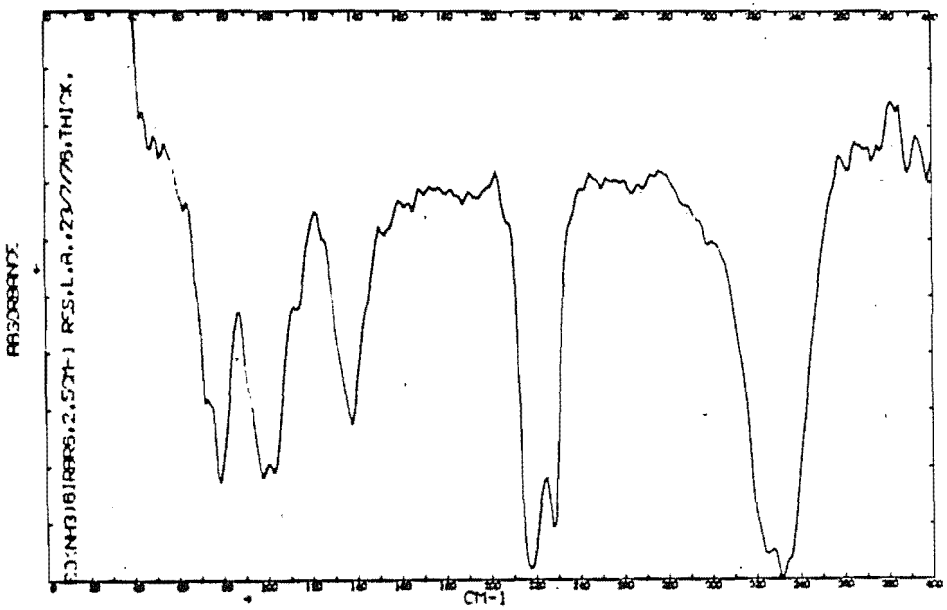

Figure 5.3.18

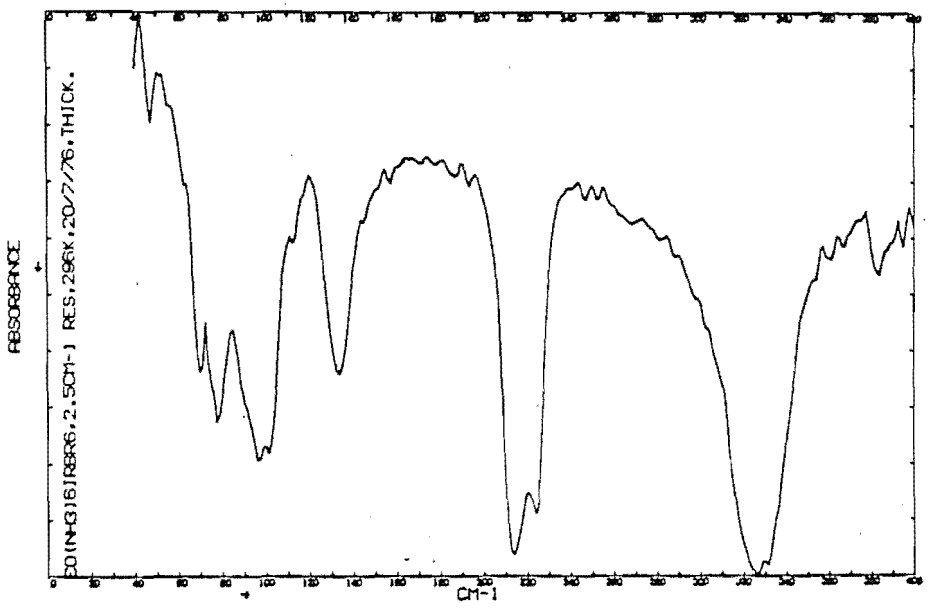

Figure 5.3.18

the $[Co(NH_3)_6][IrCl_6]$ salt. It is unlikely that this band is due to a lattice mode as the former compound has such a vibration band centred at 94 cm^{-1} and therefore a lower frequency could be expected.

$\underline{(H_3O)K_8[IrBr_6]_3 9H_2O}$

A factor group analysis for this compound predicts 16 stretching and 24 bending modes of the $[IrBr_6]^{3-}$ anion and 48 lattice vibrational modes (all infrared active). The bands observed at 221 cm^{-1}, 142 cm^{-1} and 94 cm^{-1} are assigned to these three types of modes respectively (see Figure 5.3.14). The frequencies are in agreement with those reported by Bottger and Salwin[53] for $K_3[IrBr_6]$ and $Ag_3[IrBr_6]$ and Zipp and Madan[44] for $[N(CH_2CH_2NH_3)_3][IrBr_6]H_2O$. No Raman spectrum could be obtained for $(H_3O)K_8[IrBr_6]_3 9H_2O$. However, the Raman spectrum for $K_3[IrBr_6]$, reported by Bottger and Salwin[53], has a shoulder at 178 cm^{-1} on a peak at 184 cm^{-1} (assigned to a $\nu_2(E_g)$ stretching mode). The shoulder assigned to a $2\nu_6$ (F_{2u}) overtone could be reinterpreted (as discussed above for the spectrum of $K_3[IrCl_6]$) together with the 184 cm^{-1} absorption as the $\nu_2(E_g)$ mode, the degeneracy being removed because of low site symmetry of the $[IrBr_6]^{3-}$ anion. There is no direct evidence to suggest that $K_3[IrBr_6]$ contains a distorted octahedral anion. However, it was impossible to prepare this compound by the method outlined by Bottger and Salwin[53]; in all attempts the salt $(H_3O)K_8[IrBr_6]_3 9H_2O$ was produced

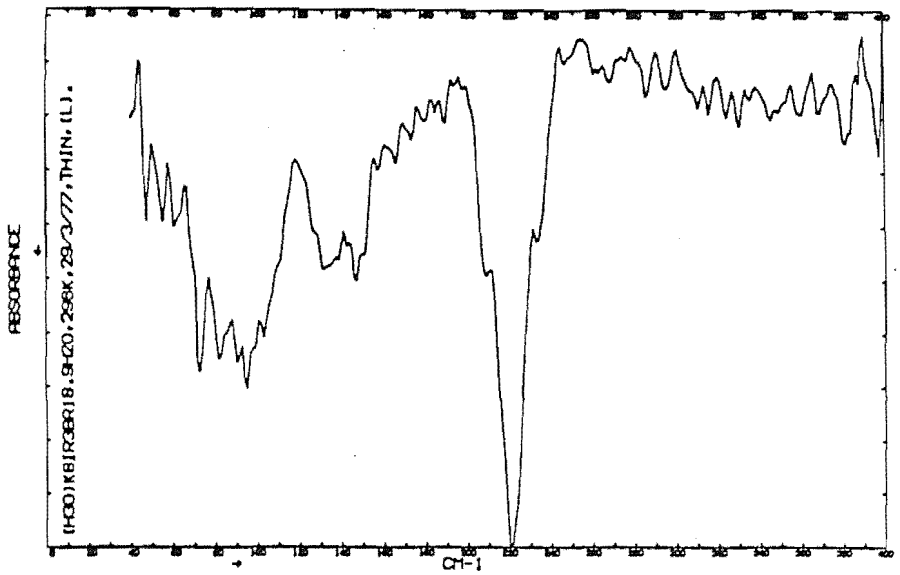

Figure 5.3.14

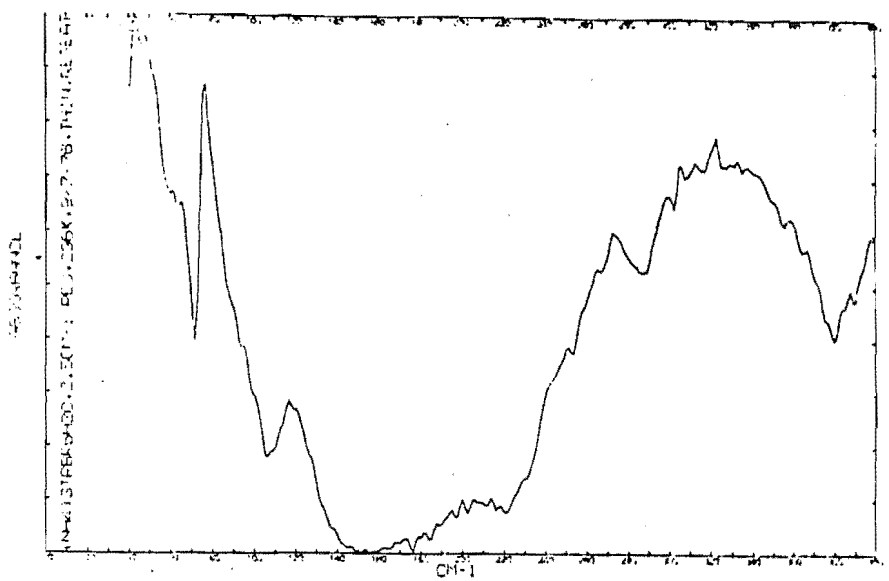

Figure 5.3.15

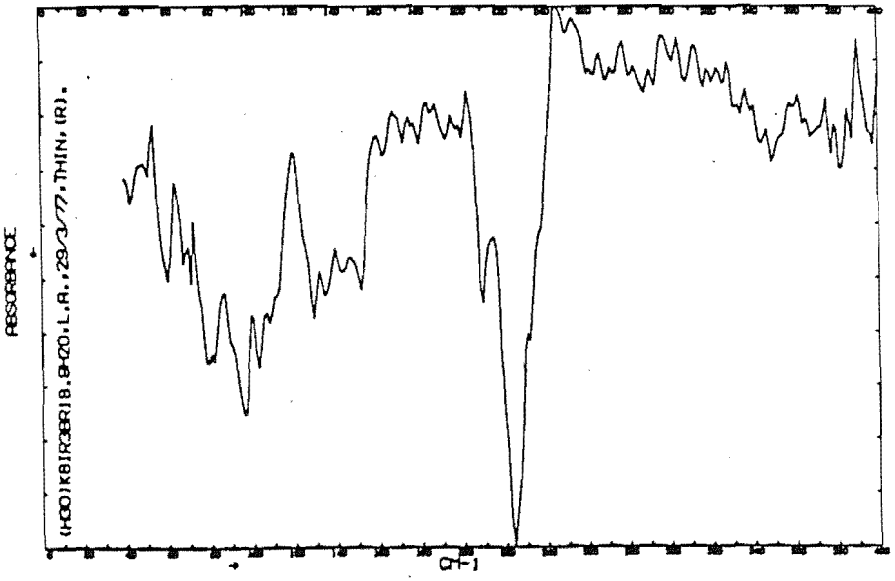

Figure 5.3.14

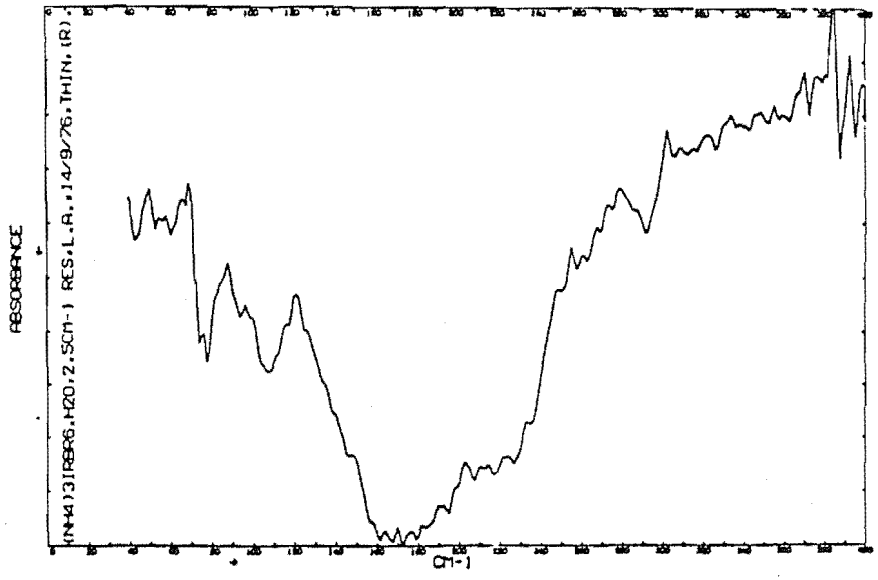

Figure 5.3.15

giving rise to some doubt as to the stoichiometry of the complex originally studied[53] . The isomorphous rhodium compound $(H_3O)K_8[RhBr_6]_3 9H_2O$ does contain $[RhBr_6]^{3-}$ anions distorted from regular octahedral symmetry and therefore the iridium analogue would be expected to contain $[IrBr_6]^{3-}$ ions showing similar distortion.

$\underline{A_3[IrBr_6]H_2O (A = NH_4, Rb, Cs)}$

The far infrared spectra of these complexes are recorded in Figures 5.3.15, 5.3.16 and 5.3.17 respectively. The absorption spectrum of $(NH_4)_3[IrBr_6]H_2O$ is quite different to that of the other two complexes presumably because of the close proximity of the ν_3, ν_4 and ν_7 absorption bands. Factor group analysis predicts the same vibrational species as for their isostructural hexachloroiridate(III) counterparts and the broad bands which in some cases are resolved into a number of smaller bands reflect this situation. The three complexes have similar ν_3 stretching mode frequencies but the ν_4 bending mode frequencies and lattice modes (as expected in this latter case) show some dependence on the cation type. Mean frequencies for the ν_4 mode vary from 156 cm^{-1} to 125 cm^{-1} for the ammonium and caesium salts respectively. This is probably a function of some hydrogen bonding present in the ammonium salt as discussed above for $(NH_4)_3[IrCl_6]H_2O$.

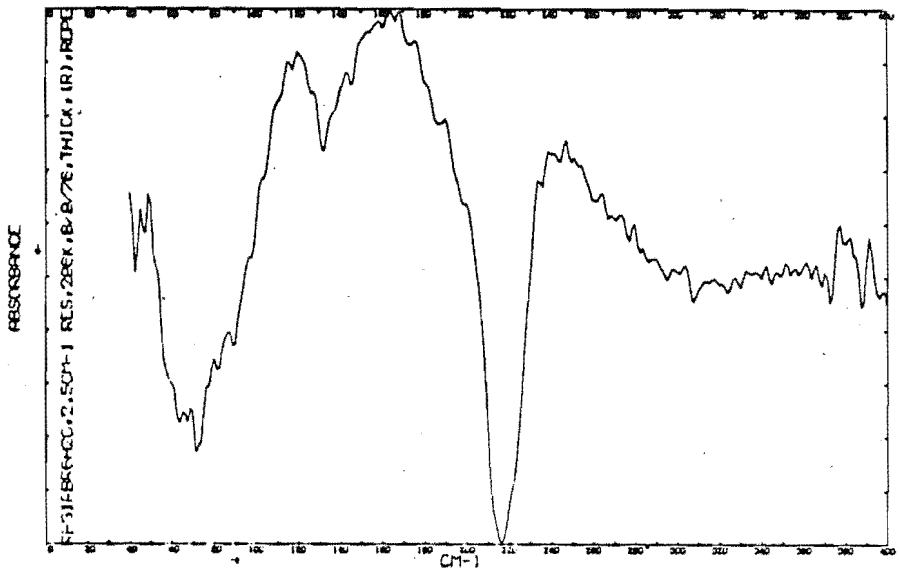

Figure 5.3.16

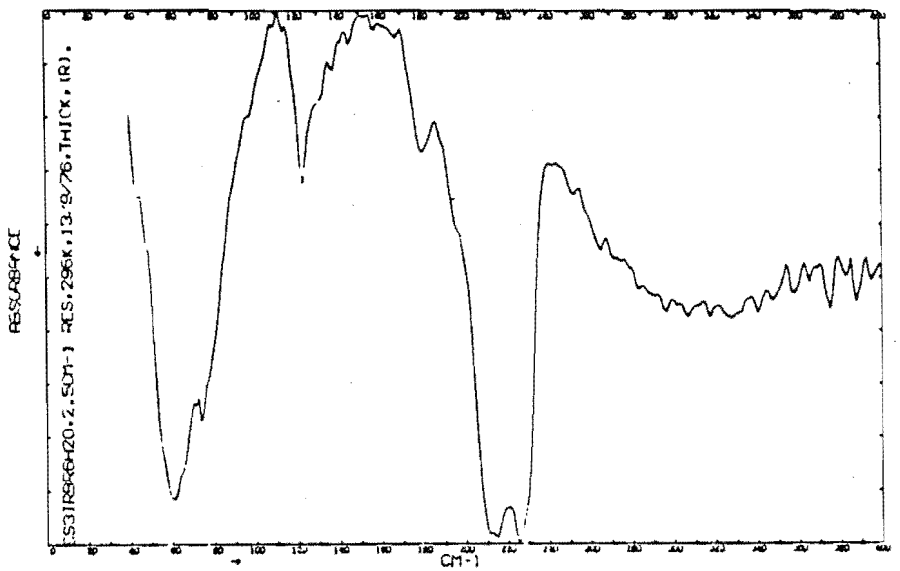

Figure 5.3.17

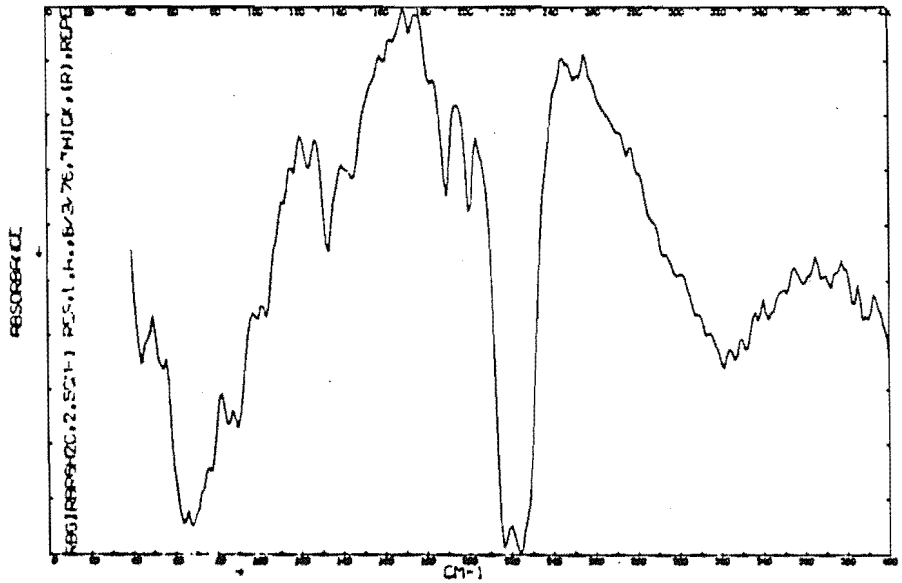

Figure 5.3.16

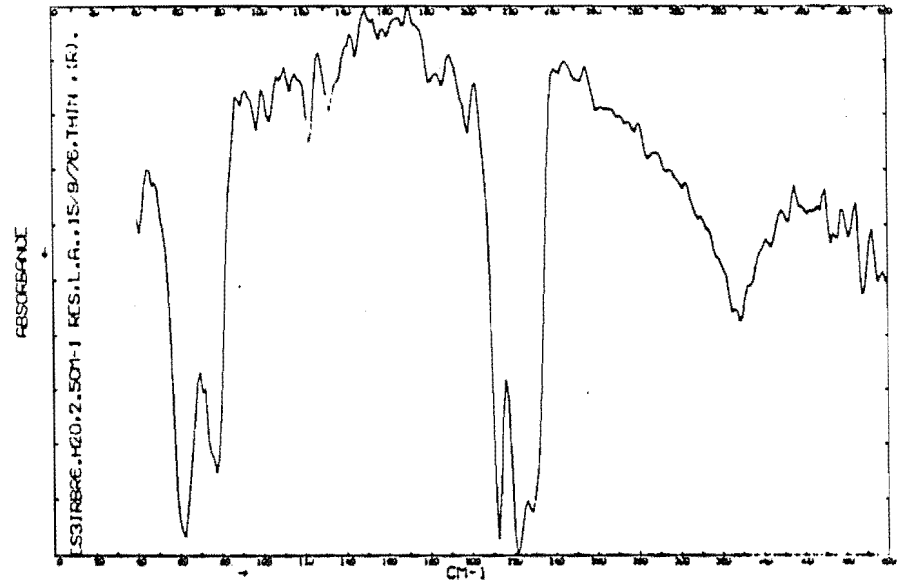

Figure 5.3.17

Force Constant Calculations

Approximate force constant calculations have been carried out for both the $[IrCl_6]^{3-}$ and $[IrBr_6]^{3-}$ species by Bottger and Salwin[53]. They have calculated metal halogen force constants using the Raman ν_1 and ν_2 vibrational frequencies and two force constants in a generalised force field approach outlined by Pistorius.[179] The trends in the calculated force constants agree with a more rigorous study by Sanyal et al.[162]. The results of these and other relevant studies are summarised in Table 5.3.4.

Table 5.3.4: Force Constants for Hexahalogenoiridate Anions (mdyn/Å)

Anion	Chloride		Bromide		Reference
	f_r	f_{rr}	f_r	f_{rr}	
$[IrX_6]^{2-}$	2.07	0.13[a]	1.73	0.12	53
	1.67	0.26[b]			157
$[IrX_6]^{3-}$	2.01	0.04	1.69	0.05	53
	1.77	0.04	1.56	0.05	162

[a] These values were estimated by Bottger and Salwin and predicted a ν_2 frequency of 295 cm^{-1}. This has since been observed to be correct and therefore these force constants are now comparable to those other values calculated by these authors.

[b] Calculated from data given in reference[157] by the author. These data will be in error (especially f_{rr}) because of the incorrectly chosen ν_2 frequency of 225 cm^{-1}.

The data suggests that the Ir-Cl bond is somewhat stronger than the Ir-Br bond. Furthermore with f_r being greater for $[IrCl_6]^{2-}$ ($[IrBr_6]^{2-}$) than for $[IrCl_6]^{3-}$ ($[IrBr_6]^{3-}$) it is evident that with a decrease in the formal charge on the central iridium atom (in changing the oxidation state of iridium from +4 in $[IrX_6]^{2-}$ to +3 in $[IrX_6]^{3-}$) in the hexahalogenoiridate anions the degree of bonding interaction decreases. While approximate, the calculations are normally sufficiently accurate to establish force constant trends.[151]

In the normal coordinate analysis reported by Sanyal et al.[162] it is assumed that the $[IrCl_6]^{3-}$ species in the solid state (in the potassium salt) has regular octahedral symmetry. This is not correct. The frequencies used have been chosen in a rather random fashion (with no explanation given) and no account is made in the model for the removal of the degeneracy of the various infrared active vibrational modes or for any cation effect which will influence the observed frequencies. Irrespective of these short comings the analysis[162] is more complete than that of Bottger and Salwin[53].

Some elementary force constant calculations in this work using a simple Valence Force Field (SVFF) (see Chapter 9) have been carried out for the $[IrCl_6]^{3-}$ species in the solid state, using structural parameters for the $[IrCl_6]^{3-}$ anion derived from the crystal structure of $K_3[IrCl_6]$ determined in this work. Initial calculations using three force constants (f_r bond stretch, f_{rr} adjacent bond stretch

interactions, f_α bond angle deformation) and mass weighted cartesian coordinates of a regular octahedron (with an Ir-Cl bond length of 2.356 Å) gave poor agreement between the calculated and observed ν_1 and ν_2 frequencies of $K_3[IrCl_6]$ but reasonable agreement for other frequencies. This is attributed to the exclusion in the SVFF approximation of non bonded interaction force constants which are catered for in other potential fields (e.g. the Urey Bradley force field). The results of the above calculations are summarised in Table 5.3.5 Section A.

To examine the effect of the distortion of the anions in the solid state on the calculated infrared and Raman frequencies, calculations were also made using the same set of force constants as above and mass weighted cartesian coordinates of each of the three distorted $[IrCl_6]^{3-}$ anions contained in crystalline $K_3[IrCl_6]$. The results are listed in Table 5.3.5 Section B. As expected most of the degenerate vibrational modes of the regular octahedral anion show a removal of degeneracy when calculations are made using mass weighted cartesian coordinates of the distorted anions. However, the magnitude of the difference between the frequencies of these now non degenerate modes of a particular type of vibration (e.g. a $\nu_3(F_{1u})$ stretching mode type) is smaller than the differences observed i.e. 6-7 cm^{-1} as compared with 16-18 cm^{-1}. This could suggest that the magnitude of the differences between the observed component ν_3 and ν_4 frequencies does not entirely arise from distortion of the anion (for example correlation effects have yet to be considered).

Table 5.3.5: Results from SVFF Force Constant Calculations for the $[IrCl_6]^{3-}$ Anion in the Solid State (in $K_3[IrCl_6]$).

	Frequencies (cm^{-1})[a]					
Section A	$\nu_1(A_{1g})$	$\nu_2(E_g)$	$\nu_3(F_{1u})$	$\nu_4(F_{1u})$	$\nu_5(F_{1g})$	$\nu_6(F_{2g})$
Observed Frequencies[b]	323	303,288	309,281 (average 300)	200,184 (average 193)	161	-
Calculated Frequencies	264(1)	242(2)	301(3)	191(3)	163(3)	135(3)

Section B (Calculated Frequencies)

Force Constants

Anion	f_r	f_α	f_{rr}						
						302	193	164	137
1	0.65	0.53	0.02	264	242(2)	302	192	163	135
						299	190	163	135
							194	164	137
						304	191	162	135
2	0.65	0.53	0.02	264	242(2)	301	187	161	132
						298			
						304	194	164	137
3	0.65	0.53	0.02	264	242(2)	301	191	162	135
						298	188	162	132

[a] Where given in brackets, numbers refer to the degeneracy of particular vibrational modes.

[b] From reference [53] and this work

However, other factors may affect the results, such as the exclusion of non bonding interaction constants including those arising from chlorine atoms and potassium ions in the solid state and the assumption that all the Ir-Cl bond force constants are equal. At present, refinement of the above model by including such variables is not possible because of the lack of sufficient spectroscopic data.

5.4 THE RAMAN AND INFRARED ABSORPTION SPECTRA OF PENTACHLOROAQUAIRIDATES(III)

No vibrational data has previously been reported for pentachloroaquairidates(III) although a number of infrared and Raman spectroscopic studies have been reported for complexes containing pentachloroaquametallate(III) species of Ti(III)[180], Cr(III)[14], Fe(III)[93,177,181,182,183], Ru(III)[13, 173], In(III)[93, 177, 181], Rh(III)[14, 183]. Greenaway has reported a normal coordinate analysis for the $[RuCl_5(H_2O)]^{2-}$ anion[13]. Results of studies on $Rb_2[IrCl_5(H_2O)]$ and $Cs_2[IrCl_5(H_2O)]$ are now reported and the data are recorded in Table 5.4.1.

5.4.1 Infrared Absorption Spectra in the Region 4000 cm^{-1} to 400 cm^{-1}

The normal frequency infrared absorption spectra of both $Rb_2[IrCl_5(H_2O)]$ and $Cs_2[IrCl_5(H_2O)]$ have three bands

Table 5.4.1: Vibrational Data.(cm^{-1}) for Pentachloro-aquairidates(III)

(a) Infrared Data

(i) Normal Frequency

Complex	Frequencies (cm^{-1}, $\pm$ 5 cm^{-1})
$Rb_2[IrCl_5(H_2O)]$	3350, 1600, 595
$Cs_2[IrCl_5(H_2O)]$	3320, 1600, 618

(ii) Low Frequency

Complex	Temperature (^oK)	Frequencies (cm^{-1})
$Rb_2[IrCl_5(H_2O)]$	296	308, 214, 176, 75
	179	336, 310, 218, 175, 104, 73
$Cs_2[IrCl_5(H_2O)]$	296	316, 228, 173, 73
	179	314, 232, 210, 173, 73

(b) Raman Data

Complex	Frequencies (cm^{-1}, $\pm$ 4 cm^{-1})
$Rb_2[IrCl_5(H_2O)]$	313, 294

that can be assigned as follows; 3320 and 3350 cm^{-1} asymmetric and symmetric O-H stretching modes, 1600 cm^{-1} H-O-H bending mode and 595 and 618 cm^{-1} wagging modes[184]. The H-O-H bending mode at 1600 cm^{-1} appears as a sharp peak in both spectra which is a characteristic of such salts[177]. The assignment of the frequencies of 595 cm^{-1} and 618 cm^{-1} to a wagging mode of the coordinated water molecule follows that of Adams and Lock[177]. The rubidium and caesium compounds crystallise with different crystal structures and it is possible that the wagging modes are cation sensitive and a function of the different structures (unlike H_2O rocking and bending modes which are not expected to show any dependence on structural type). It is unlikely that the lowest frequencies could be assigned to a ν(Ir-O) stretching mode as studies on deuterated complexes of Fe(III)[177] and $Cs_2[RhCl_5(H_2O)]$[183] indicate these normally occur below 400 cm^{-1}.

5.4.2 Raman and Infrared Absorption Spectra in the Region 400 cm^{-1} to 40 cm^{-1}

The isolated $[IrCl_5(H_2O)]^{2-}$ anion has C_{4v} symmetry giving rise to $4A_1$, 4E, $2B_1$ and B_2 vibrational symmetry species of which $4A_1$ and 4E are infrared active and $4A_1$, 4E, $2B_1$ and B_2 are Raman active. The vibrational modes that these symmetry species represent are listed in a table by Adams and Newton[181] and in a diagram by Greenaway[13]. Full factor group analyses (see Section 5.7) predict $4B_{1u}$, $1B_{2u}$ and $4B_{3u}$ Ir-Cl stretching modes, $1B_{1u}$ and $1B_{3u}$ Ir-O stretching modes and $5B_{1u}$, $4B_{2u}$ and $5B_{3u}$ bending modes

of the $[IrCl_5(H_2O)]^{2-}$ anion (all infrared active) for $Rb_2[IrCl_5(H_2O)]$, and $1B_{1u}$, $2B_{2u}$ and $1B_{3u}$ Ir-Cl stretching modes, $1B_{2u}$ Ir-O stretching mode and $3B_{1u}$, $2B_{2u}$ and $3B_{3u}$ bending modes of the $[IrCl_5(H_2O)]^{2-}$ anion (all infrared active) for $Cs_2[IrCl_5(H_2O)]$.

The low frequency infrared spectra of both complexes contain a great deal of structure as well as background noise (see Figures 5.4.1 and 5.4.2). The principal bands observed in the spectra at 296 K may be assigned to the following vibrational modes; 310 cm^{-1} Ir-Cl stretching modes, 218 and 228 cm^{-1} anion bending modes (mainly involving Ir-O wagging motion), 176 and 173 cm^{-1} anion bending modes (mainly involving Ir-Cl bond angle deformations) and finally 100 cm^{-1} to 40 cm^{-1} lattice vibrations. These assignments are the same as those made by Greenaway for the $[RuCl_5(H_2O)]^{2-}$ anion[13]. The bending mode involving Ir-O wagging motion in $Cs_2[IrCl_5(H_2O)]$ shows interesting behaviour on lowering the temperature. This absorption at 228 cm^{-1} (assigned to the degenerate E mode (in C_{4v} symmetry)) observed at room temperature, splits into two components at 179 K with bands now at 232 cm^{-1} and 210 cm^{-1}. The difference between the frequencies of these two components (22 cm^{-1}) is much larger than that calculated for similar modes in $Cs_2[RuCl_5(H_2O)]$ by Greenaway[13] (3.7 cm^{-1}). An absorption which could be assigned to the ν(Ir-O) stretching frequency was not observed.

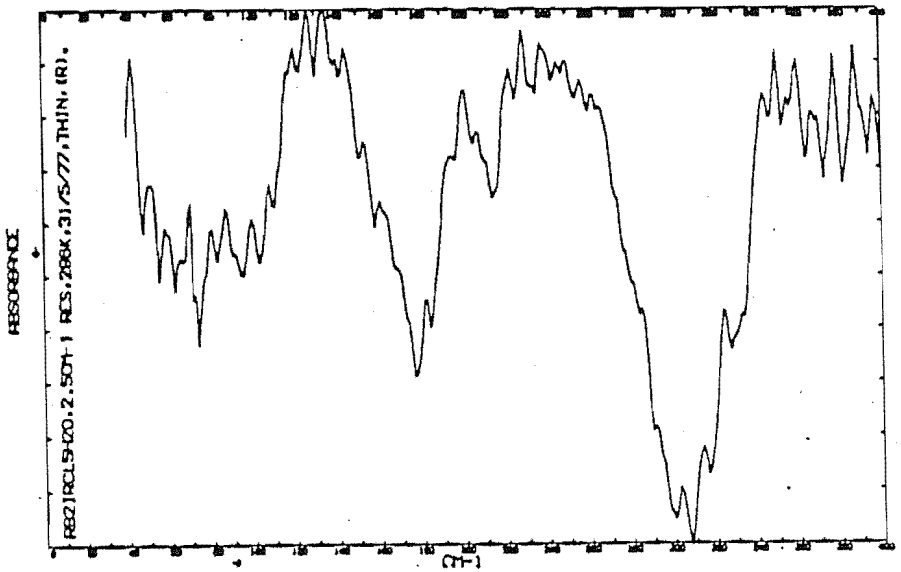

Figure 5.4.1

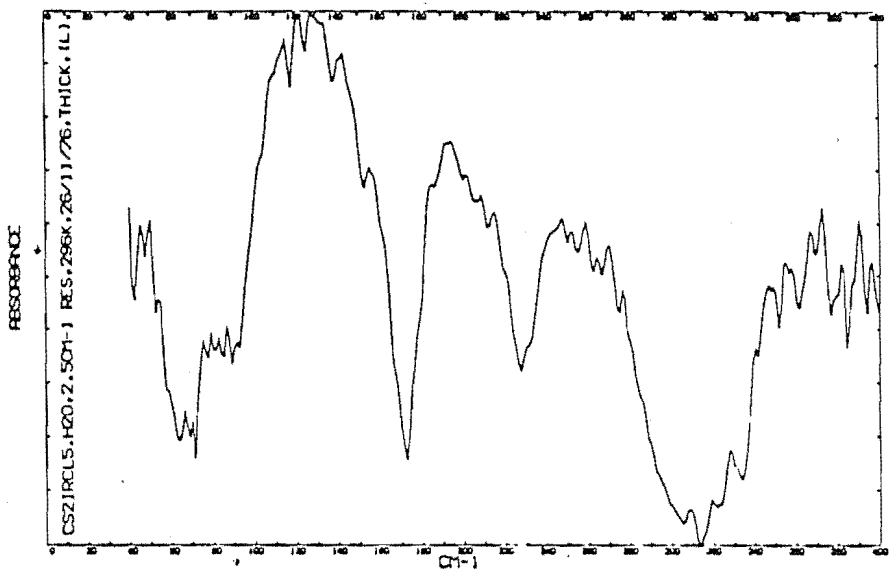

Figure 5.4.2

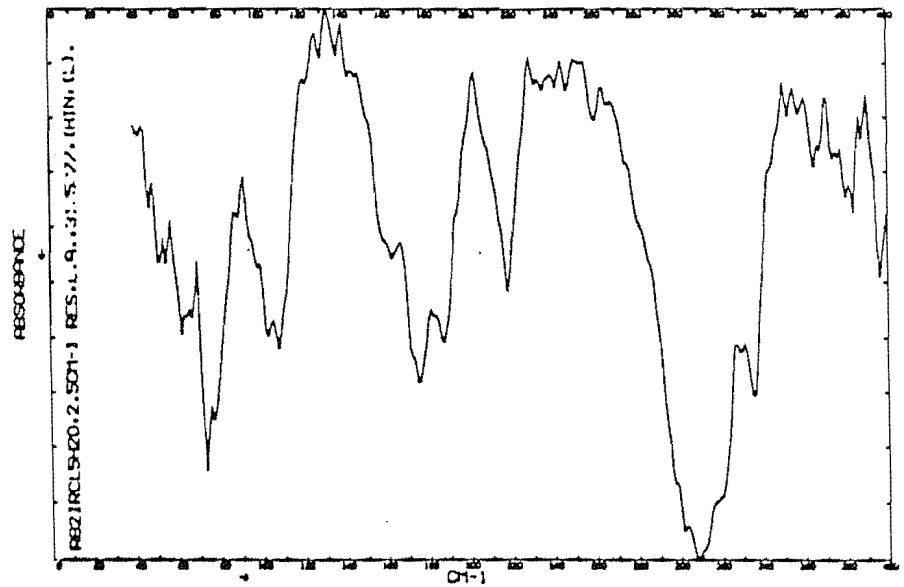

Figure 5.4.1

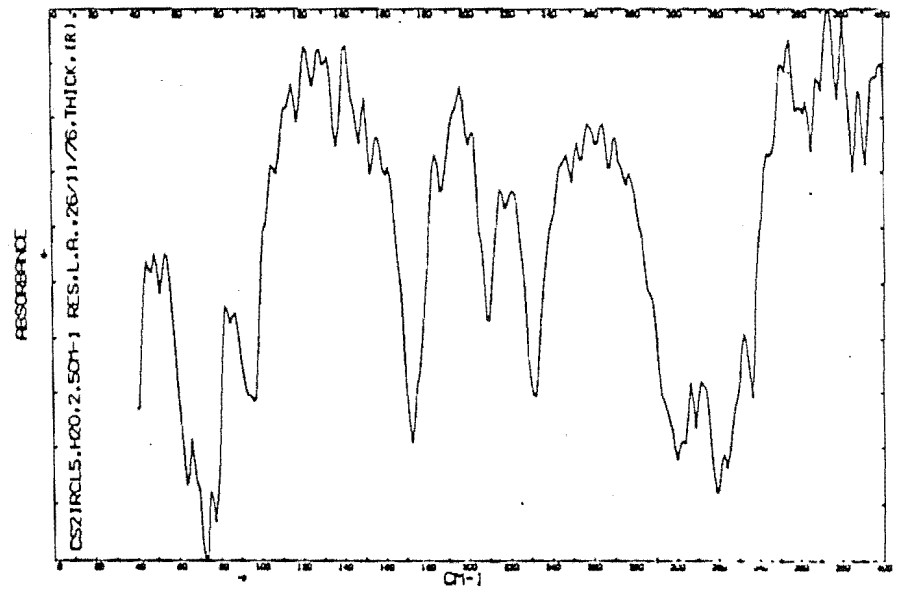

Figure 5.4.2

The two Raman frequencies observed for $Rb_2[IrCl_5(H_2O)]$ could be assigned to any of the number of the predicted Raman active Ir-Cl stretching modes (i.e. $4A_g$, B_{1g}, $4B_{2g}$, B_{3g}) as these frequencies occur in the same region as the Raman active Ir-Cl stretching (A_{1g}, E_g) modes of the $[IrCl_6]^{3-}$ species.

5.5 THE INFRARED ABSORPTION SPECTRA OF TRI-μ-HALOGENO-HEXAHALOGENODIIRIDATES(III)

A number of Raman and infrared vibrational studies have been reported for a variety of transition metal and non transition metal tri-μ-halogenohexahalogenodimetallate(III) (primarily chloro and bromo complexes) species including the tervalent metal ions of Cr, Mo, Ti, V, Zr, Rh, Ru, Tl, In and Sb[12-14,111,127,128,130,135,185-193]. Three detailed single crystal infrared and Raman studies of the $[Cr_2Cl_9]^{3-}$, $[W_2Cl_9]^{3-}$ and $[Tl_2Cl_9]^{3-}$ ions[185,186,188] have been reported to date. Normal coordinate analyses have been included in these studies.

The infrared spectra of a number of tri-μ-halogeno-hexahalogenodiiridates(III) prepared in this work are illustrated in Figures 5.5.1 to 5.5.5 and the frequency data are recorded in Table 5.5.1.

Table 5.5.1: Vibrational Data (cm^{-1}) for Tri-μ-halogenohexahalogenodiiridates(III)

Complex	Temperature (°K)	Frequencies (cm^{-1})			
		$\nu(Ir-X_t)$ terminal stretching modes	$\nu(Ir-X_{br})$ bridging stretching modes	Bending modes	Lattice modes
$Rb_3[Ir_2Cl_9]$	296	342,331	269,260	183,100	72
$Cs_3[Ir_2Cl_9]$	296	334,329	267	112	65
$Rb_3[Ir_2Br_9]$	296	232,220	182	121,95	72
	179	236,224	189,182	124,100	72
$Cs_3[Ir_2Br_9]$	296	227,219,213	178	123	65
	179	231,224,213	180	123	78,65
$[N(CH_3)_4]_3[Rh_2Br_9]$	296	222,209	181		65

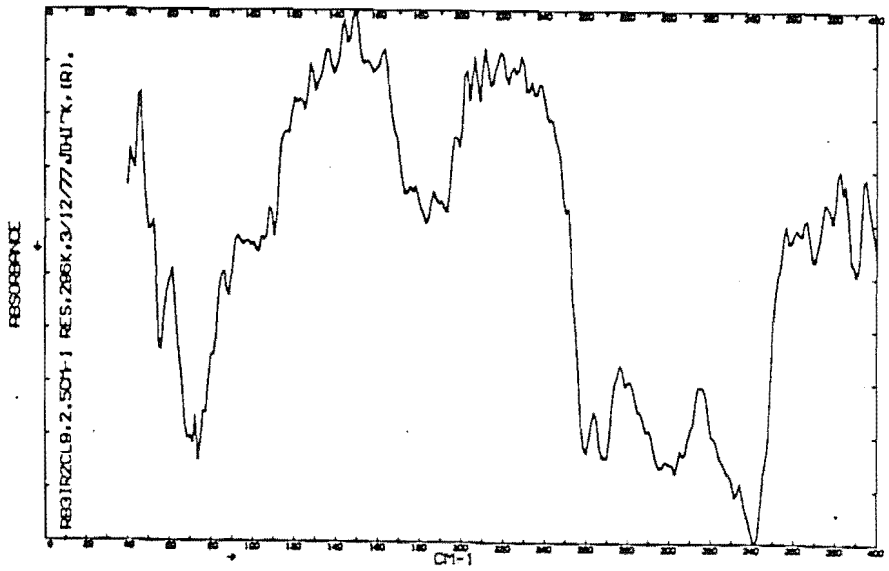

Figure 5.5.1

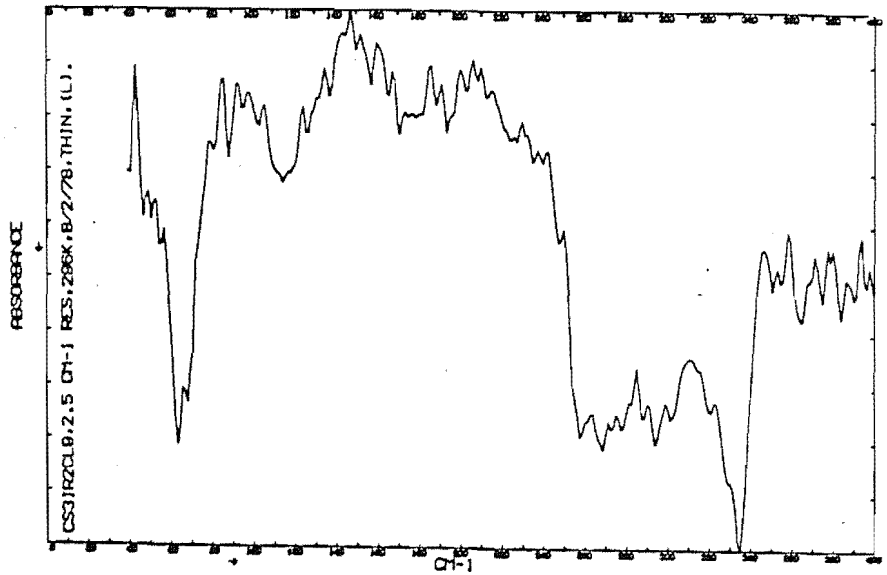

Figure 5.5.2

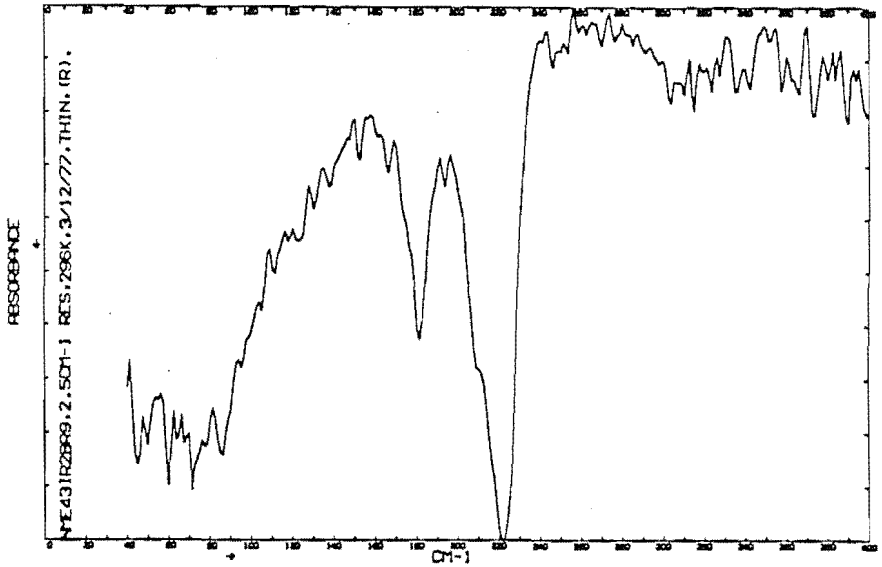

Figure 5.5.5

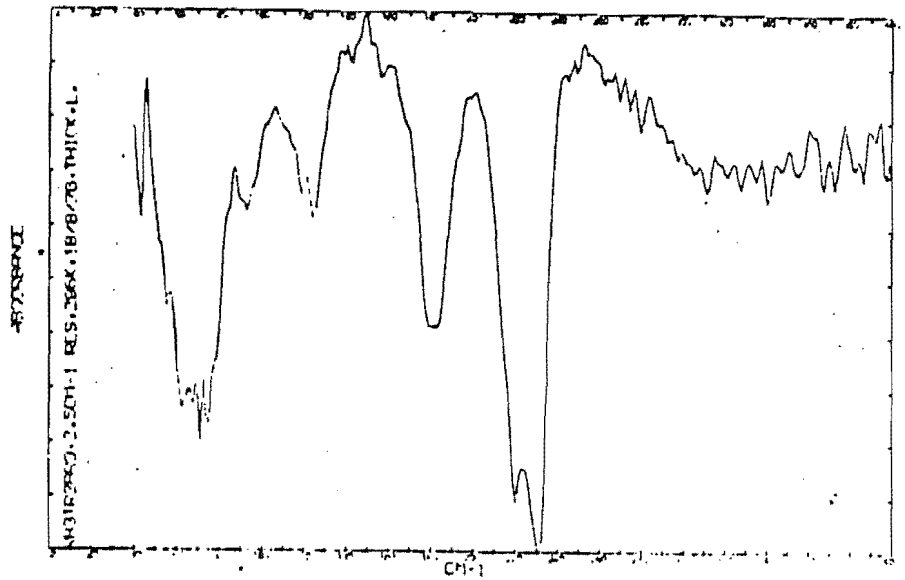

Figure 5.5.3

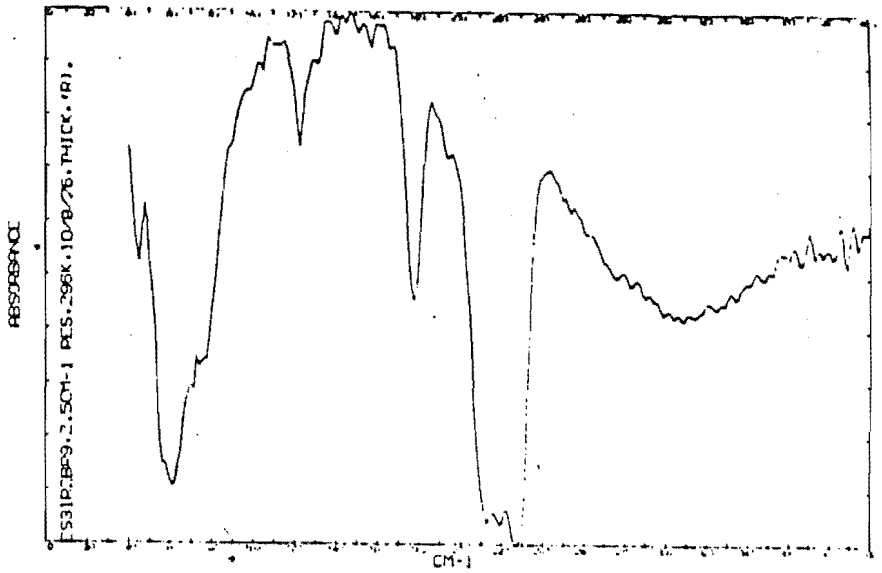

Figure 5.5.4

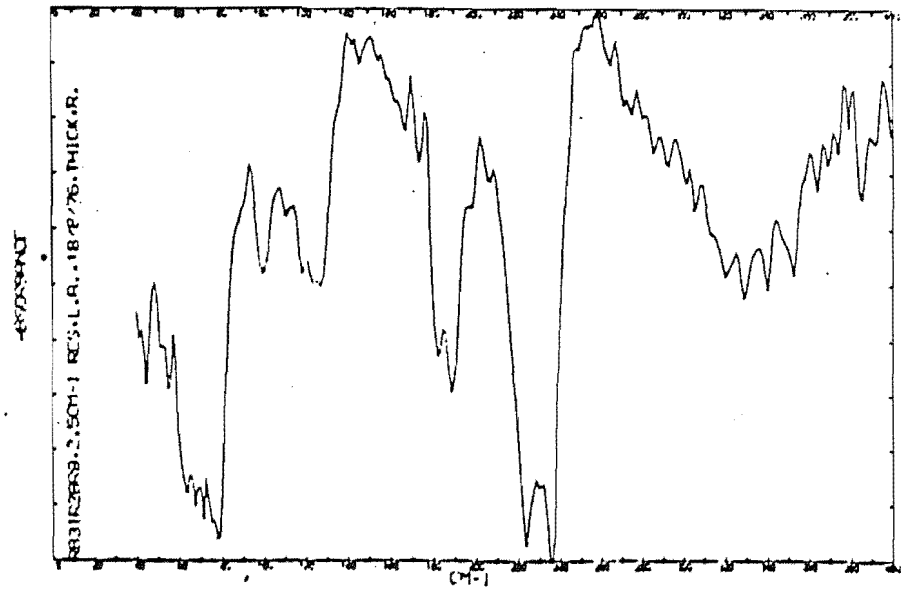

Figure 5.5.3

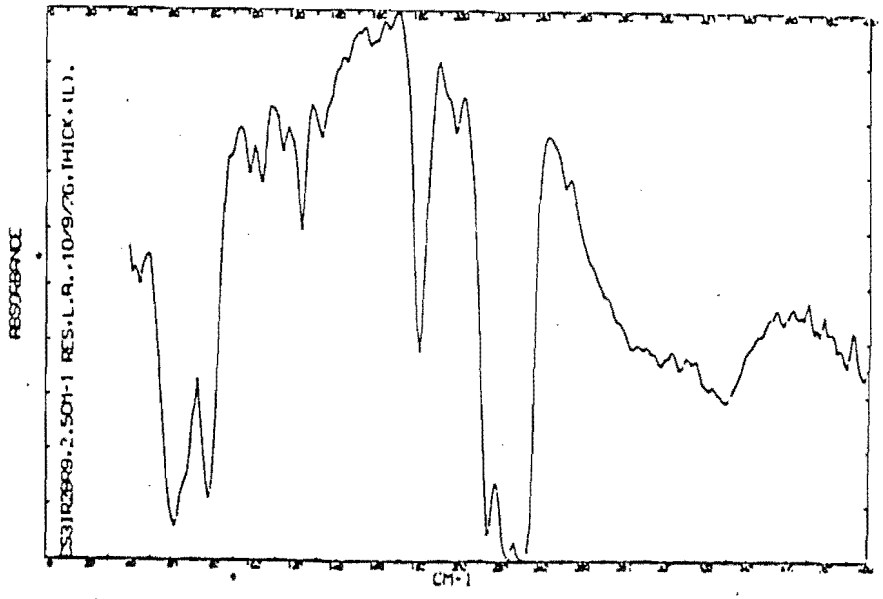

Figure 5.5.4

Of the irreducible representation of the normal vibrational modes of the isolated $[Ir_2X_9]^{3-}$ anion, which has D_{3d} point symmetry,

$$\text{i.e. } \Gamma_{\text{internal vibration}} = 4a_1' + a_1'' + a_2' + 3a_2'' + 5e' + 4e''$$

the a_1' and e" modes are Raman active, the e' modes are both Raman and infrared active and the a_2'' modes are infrared active only. The site symmetry of the $[Ir_2X_9]^{3-}$ species (X = Cl,Br) in the solid state in the compounds $A_3[Ir_2X_9]$, assuming isomorphism to $A_3[Cr_2X_9]$ (see Section 4.6), is D_{3d}. However, crystallisation of two of these anions per unit cell means the vibrational selection rules will change (these are summarised in section 5.7). Thus, $3A_{2u}$ and $5E_{1u}$ infrared active internal modes of the $[Ir_2X_9]^{3-}$ anion and $2A_{2u}$ and $2E_{1u}$ infrared active translatory lattice modes involving the anions and the remaining cations in the crystal lattice are predicted.

As there is some controversy in the literature over the assignment of these vibrational modes[185] to particular frequencies (in particular the order in which the A_{2u} and E_{1u} species are assigned) the spectra recorded in this work will only be discussed in general terms with observed bands assigned to the type of vibrational modes rather than specific symmetry species. Assignment of particular vibrational modes (e.g. "stretching" and "bending" modes) to specific frequencies is further complicated by observation of combination and overtone bands in some spectra and

the complicated nature of many of the vibrational modes executed by the anion (i.e. they are not pure terminal or bridging atom stretch or bending motions but often complicated mixtures of a number of motions[185]).

5.5.1 The Infrared Absorption Spectra of Tri-μ-chloro-hexachlorodiiridate(III) Salts of Rubidium and Caesium

In $Rb_3[Ir_2Cl_9]$ a band at about 340 cm^{-1} can be assigned to $\nu(Ir\text{-}Cl_t)$ (Cl_t-terminal chlorine) stretching vibrations and that at 265 cm^{-1} to $\nu(Ir\text{-}Cl_{br})$ (Cl_{br}-bridging chlorine) stretching vibrations. The band at 300 cm^{-1} in $Rb_3[Ir_2Cl_9]$ probably arises from either monometallate $Rb_3[IrCl_6]H_2O$ (Ir-Cl stretching modes at about 300 cm^{-1}) impurity or some combination or overtone band. The band at 183 cm^{-1} can be assigned to bending mode vibrations of the $[Ir_2Cl_9]^{3-}$ anion as can the band at 100 cm^{-1}. However, this latter assignment may be more correctly made to a lattice vibration together with a band at 72 cm^{-1} (although bending modes of such a low frequency have been observed for the $[Cr_2Cl_9]^{3-}$ species[185]).

The spectrum of $Cs_3[Ir_2Cl_9]$ is similar to that of the rubidium salt particularly in the Ir-Cl stretching mode region but some bending mode absorptions are very weak. Furthermore, the stretching mode absorptions contain more structure than expected. The band at 334 cm^{-1} can be assigned to a $\nu(Ir\text{-}Cl_t)$ stretching vibration and that at 267 cm^{-1} to $\nu(Ir\text{-}Cl_{br})$ stretching vibrations. The band

centred approximately at 292 cm^{-1} probably arises from monometallate $Cs_3[IrCl_6]H_2O$ impurity or some combination or overtone band. The band at 112 cm^{-1} has been assigned to a bending mode and that at 65 cm^{-1} to a lattice mode.

A number of similarities exist between the spectra of the iridium compounds and chromium and rhodium compounds in which no metal-metal bonding interaction within the dimetallate $[M_2Cl_9]^{3-}$ anion exists. The spectra of the rhodium[14] and chromium[111] dimetallates(III) have been analysed in terms of an assumed D_{3d} site symmetry of the $[M_2Cl_9]^{3-}$ anions and the terminal and bridging stretching modes have been assigned as the $a_2"$ and e' species after that of Beattie et al.[186] . Grey and Smith[111] have examined both cation effects and the influence of metal-metal bonding on the spectra of the dimetallate Mo(III) species. They conclude that the frequency separation between the two $\nu(M\text{-}Cl_{br})a_2"$ and $\nu(M\text{-}Cl_{br})e'$ modes may be used as an indication of metal-metal bonding in a dimetallate anion. Table 5.5.2 contains some relevant data.

The $[Mo_2Cl_9]^{3-}$ anion, which does have some metal-metal bonding present, shows a significantly larger separation of the two $\nu(M\text{-}Cl_{br})$ frequencies than those of $[Cr_2Cl_9]^{3-}$ in which no Cr-Cr bonding is present. On this basis the low value of the frequency difference for $[Ir_2Cl_9]^{3-}$ salts could indicate no metal-metal bonding. The data reported by Sherlock[14] is apparently inconsistent with Grey and Smith's hypothesis (it would indicate metal-metal bonding in the $[Rh_2Cl_9]^{3-}$ anion) as the $[Rh_2Cl_9]^{3-}$ anion contains no

Table 5.5.2: Frequencies (cm^{-1}) of the $\nu(M\text{-}Cl_{br})$ Stretching Modes in $A_3[M_2Cl_9]$ Complexes (M = Ir, Rh, Cr, Mo; A = K, Rb, Cs)

Complex	$\nu(M\text{-}Cl_{br})$	Frequencies (cm^{-1})[a]	$\Delta\nu$ (cm^{-1})	Reference
$K_3[Cr_2Cl_9]$	268	244	24	111
$Rb_3[Cr_2Cl_9]$	265	240	25	111
$Cs_3[Cr_2Cl_9]$	258	234	24	111
$K_3[Mo_2Cl_9]$	283	236	47	111
$Cs_3[Mo_2Cl_9]$	277	238	39	111
$Rb_3[Rh_2Cl_9]$	332	270	62	14
$Cs_3[Rh_2Cl_9]$	313	268	45	14
$Rb_3[Ir_2Cl_9]$	269	260	9	this work
$Cs_3[Ir_2Cl_9]$	268	258	10	this work

[a] Because of the uncertainty of the order of assignation of the a_2'' and e' (or A_{2u} and E_u) modes[185] such assignments of these species to particular frequencies have not been made here.

metal-metal interaction. However, if the data is reassigned, with the higher of the two $\nu(Rh\text{-}Cl_{br})$ vibrational frequencies being associated with a $\nu(Rh\text{-}Cl_t)$ stretching mode, the data is then in agreement with Grey and Smith's hypothesis.

On the basis of force constant calculations for the $[Ru_2Br_9]^{3-}$ anion using a SVFF approximation and force constants chosen from Black et al.[185] but including a Ru-Ru force constant, Greenaway[13] has suggested the separation between the two infrared active $\nu(M\text{-}X_t)$ frequencies may be used in a similar fashion to predict the presence of metal-metal bonding in $[M_2X_9]^{3-}$ anions. However, the number of force constants used by Greenaway to calculate the two observed stretching frequencies (whose separation seemed dependent on the Ru-Ru bonding force constant) puts the validity of these calculations in doubt. No such effects have been observed elsewhere[111], and it seems more intuitive to expect bridging halogeno stretching frequencies to be more affected by M-M bonding than terminal halogen stretching frequencies. The magnitude of the difference in frequency between the average of the $\nu(M\text{-}Cl_t)$ components and the $\nu(M\text{-}Cl_{br})$ components (70 cm^{-1}) is smaller for the $[Ir_2Cl_9]^{3-}$ species than that of $[Cr_2Cl_9]^{3-}$ (98 cm^{-1}) as could be expected on the basis of mass effects.

5.5.2 The Infrared Absorption Spectra of Tri-μ-bromohexabromodiiridate(III) Salts

In the spectra of $Rb_3[Ir_2Br_9]$ (Figure 5.5.3), bands centred on 226 cm^{-1} and 182 cm^{-1} can be assigned to terminal

and bridging iridium bromine stretching modes respectively, the two bands at 121 cm^{-1} and 95 cm^{-1} are most probably bending modes and the broad band centred on 71 cm^{-1} can be assigned to a lattice mode(s). The low temperature spectrum of $Rb_3[Ir_2Br_9]$ shows resolution of the absorption occurring at 182 cm^{-1} at room temperature with two bands at 189 cm^{-1} and 182 cm^{-1}. The usual shifts to higher frequencies of the other terminal bromine stretching modes occurs with the temperature change. The spectrum of the caesium salt (Figure 5.5.4) does not show this resolution of the $\nu(Ir\text{-}Br_{br})$ absorption at 179 K, and in addition a bending mode absorption at 95 cm^{-1} is absent and the $\nu(Ir\text{-}Br_t)$ stretching mode band is composed of three distinct peaks rather than the two expected on the basis of a factor group analysis. The additional peak could be attributed to an interferogram error[149] and therefore not be real or it could result from some overtone or combination mode as has been observed in other spectra.[185] Additional absorptions have also been observed previously for chlorodichromate(III) species and in these cases (at times contrary to their known structures) have been attributed to the lowering of the site symmetry of the $[M_2X_9]^{3-}$ anions from D_{3d} symmetry[111]. However, for the spectra recorded in this work this explanation is untenable (as the compounds are assumed to crystallise in the space group $P6_3/mmc$ with the anions located on sites of D_{3d} symmetry) and so the additional band (one of the three) must arise from some other source.

The spectrum of $[N(CH_3)_4]_3[Ir_2Br_9]$ does not contain any resolved bending modes; these may, along with lattice modes, be contained in a broad absorption from 40 cm^{-1} to 130 cm^{-1}. The spectra for the three compounds at 296 K show a decrease in terminal bromine stretching mode frequencies with an increase in ionic radius of the counter cation. Such an effect has been observed in a series of salts containing the $[Ru_2Br_9]^{3-}$ anion[13] .

The spectra of $[Ru_2Br_9]^{3-}$ salts reported by Greenaway[13] and analogous rhodium salts reported by Sherlock[14] are similar to those of the diiridates(III) recorded in this work although no bridging halogen stretching modes or bending modes were observed for the ruthenium complexes. The assignments of some bridging bromine stretching modes for the rhodium complexes seem doubtful and if both the $\nu(Rh\text{-}Br_{br})$ frequencies were in fact at 175 cm^{-1} the interpretation of the spectra would be more in line with that made for the bromodiiridates(III). This is not entirely unreasonable considering the similarities between the structures and spectra of many halogenometallate(III) salts of rhodium and iridium although the latter do contain differences due to mass and bonding effects. The similar frequencies of the A_{2u} and E_{1u} modes would then reflect the absence of metal-metal bonding in the $[Ir_2Br_9]^{3-}$ anion if in fact the theory developed by Grey and Smith[111] was applicable to bromodimetallate(III) complexes as well as chlorodimetallate(III) complexes.

5.6 SUMMARY

The use of factor group analysis to allow prediction of selection rules for the Raman and infrared spectra of compounds in the solid state has made it clear why a number of the bands occur with more than one maxima (or as broad absorption bands). Since these studies were performed on crystalline powders, rather than oriented single crystals, assignment of symmetry species to particular absorptions remains impossible, unless assignments can be made in simple cases such as the hexahalogenoiridates(IV) where there is a wealth of conclusive data from other studies of related compounds to aid assignments.

The examination of low frequency spectra at 179 K has in some cases improved resolution of spectra. However, in the absence of low temperature structural data this needs to be treated with caution, as phase transitions which are known to occur for $K_3[IrCl_6]$ and $(NH_4)_3[IrCl_6]H_2O$ for example (see Section 6.4.2) may lead to a change in the spectra. In general absorptions associated with stretching vibrational modes in the low temperature spectra occur around 5 cm^{-1} higher in frequency than at 296 K. This is presumably associated with contraction of the unit cell with the result that stretching vibrations, which involve an increase in the anion or cation volume, must be at a higher energy than those for the same structure at room temperature.

Low frequency infrared spectra have proved useful in characterisation of types of complexes, especially

in the identification of the tri-μ-halogenohexahalogenodi-iridate(III) complexes whose infrared spectra bear little resemblance to those of related hexahalogeniridate(III) complexes.

5.7 APPENDIX: SUMMARY OF FACTOR GROUP ANALYSES FOR IRIDIUM(IV) AND IRIDIUM(III) HALOGENOMETALLATE COMPLEXES

$K_2[IrCl_6]$ (and $A_2[IrX_6]$, A = NH_4, Rb, Cs; X = Cl, Br) Space Group: Fm3m, z = 4 (NH_4^+ cation hydrogen atoms not included in analysis).

Factor Group Species, O_h	Lattice Vibrations	Acoustical Vibration	Rotation Libration	$[IrX_6]^{2-}$ Anion Vibrations: Stretching Modes	Bending Modes	Activity
A_{1g}				1		R
A_{2g}						
E_g				1		R
F_{1g}			1			none
F_{2g}	1				1	R
A_{1u}						
A_{2u}						
E_u						
F_{1u}	1	1		1	1	IR
F_{2u}					1	none

$K_3[IrCl_6]$ (and $(NH_4)_3[IrCl_6]$) Space Group: $P\bar{1}$, z = 2 (NH_4^+ cation hydrogen atoms not included in analysis).

Factor Group Species, C_i	Lattice Vibrations	Acoustical Vibrations	$[IrCl_6]^{3-}$ Anion Stretching Modes	Vibrations Bending Modes	Librations	Activity
A_g	9	0	6	6	6	R
A_u	12	3	6	12	0	IR

$K_3[IrCl_6]H_2O$ Space Group: Pbcn, z = 8

Factor Group Species, D_{2h}	Lattice Vibrations	Acoustical Vibrations	$[IrCl_6]^{3-}$ Anion Rotational	Libration	Stretch	Bend	H_2O molecule Rotational	Libration	Stretch	Bend	Activity
A_g	15	0	3		6	9	3		2	1	R
B_{1g}	15	0	3		6	9	3		2	1	R
B_{2g}	15	0	3		6	9	3		2	1	R
B_{3g}	15	0	3		6	9	3		2	1	R
A_u	15	0	3		6	9	3		2	1	none
B_{1u}	14	1	3		6	9	3		2	1	IR
B_{2u}	14	1	3		6	9	3		2	1	IR
B_{3u}	14	1	3		6	9	3		2	1	IR

$(NH_4)_3[IrCl_6]H_2O$ (and $A_3[IrX_6]H_2O$, A = NH_4, Rb, Cs; X = Cl, Br) Space Group Pnma, z = 4. (NH_4^+ cation hydrogen atoms not included in analysis).

Factor Group Species	Lattice vibrations	Acoustical vibration	$[IrX_6]^{3-}$ Anion Stretch	Bend	Libration	H_2O molecule Strecth	Bend	Libration	Activity
A_g	10	0	4	5	1	2(1)	1(1)	1(1)	R
B_{1g}	5	0	2	4	2	0(1)	0(0)	2(2)	R
B_{2g}	10	0	4	5	1	2(1)	1(1)	1(1)	R
B_{3g}	5	0	2	4	2	0(1)	0(0)	2(2)	R
A_u	5	0	2	4	2	0(1)	0(0)	2(2)	none
B_{1u}	9	1	4	5	1	2(1)	1(1)	1(1)	IR
B_{2u}	4	1	2	4	2	0(1)	0(0)	2(2)	IR
B_{3u}	9	1	4	5	1	2(1)	1(1)	1(1)	IR

(species in brackets refer to the situation with hydrogen atoms on sites d, otherwise sites c)

$[Co(NH_3)_6][IrCl_6]$ (and $[Co(NH_3)_6][IrBr_6]$) Space Group Pa3, z=4 (Hydrogen atoms not included in analysis)

Factor Group Species, T_h	Lattice Vibrations	Acoustical Vibrations	$[IrX_6]^{3-}$ Anion Stretch	Bend	Libration	$[Co(NH_3)_6]^{3+}$ Cation Stretch	Bend	Libration	Activity
A_g	0	0	1	1	1	1	1	1	R
E_g	0	0	1	1	1	1	1	1	R
F_g	0	0	3	3	3	3	3	3	R
A_u	2	0	1	2	0	1	2	0	IR
E_u	2	0	1	2	0	1	2	0	IR
F_u	5	1	3	6	0	3	6	0	IR

$(H_3O)K_8[IrBr_6]_3 9H_2O$ Space Group Pbam, z = 2 (Hydrogen atoms not included in analysis)

Factor Group Species, D_{2h}	Lattice Vibrations	Acoustical Vibrations	$[IrBr_6]^{3-}$ Anion Vibrations			
			Stretch	Bend	Libration	Activity
A_g	16	0	8	6	2	R
B_{1g}	16	0	8	6	2	R
B_{2g}	14	0	1	6	4	R
B_{3g}	14	0	1	6	4	R
A_u	15	0	2	6	2	none
B_{1u}	14	1	2	6	2	IR
B_{2u}	17	1	7	9	1	IR
B_{3u}	17	1	7	9	1	IR

$Rb_2[IrCl_5(H_2O)]$ Space Group Pnma, z = 4 (Hydrogen atoms included in analysis for two possible sites. Species given normally are for hydrogen atoms on sites c, those in brackets for hydrogen atom sites on d.)

Factor Group Species, D_{2h}	Lattice vibrations	Acoustical vibrations	$[IrCl_5(H_2O)]^{2-}$ Anion Vibrations						
			Ir-Cl Stretch	Ir-O Stretch	Bend	O-H Stretch	O-H Bend	Libration	Activity
A_g	5	0	4	1	5	2(1)	0(2)	1	R
B_{1g}	4	0	1	0	4	0(1)	4(2)	2	R
B_{2g}	5	0	4	1	5	2(1)	0(2)	1	R
B_{3g}	4	0	1	0	4	0(1)	4(2)	2	R
A_u	4	0	1	0	4	0(1)	4(2)	2	none
B_{1u}	4	1	4	1	5	2(1)	0(2)	1	IR
B_{2u}	3	1	1	0	4	0(1)	4(2)	2	IR
B_{3u}	4	1	4	1	5	2(1)	0(2)	1	IR

$Cs_2[IrCl_5(H_2O)]$ Space Group Cmcm, z = 4 (Hydrogen atoms included in analysis and located on Wyckoff sites f).

Factor Group Species, D_{2h}	Lattice Vibrations	Acoustical Vibrations	$[IrCl_5(H_2O)]$ Anion Vibrations						
			M-Cl Stretch	M-O Stretch	Bend	O-H Stretch	O-H Bend	Libration	Activity
A_g	3	0	2	1	2	1	1	0	R
B_{1g}	3	0	1	0	3	0	1	1	R
B_{2g}	0	0	1	0	1	0	1	1	R
B_{3g}	3	0	1	0	3	1	1	1	R
A_u	0	0	1	0	1	0	1	1	none
B_{1u}	2	1	1	0	3	1	1	1	IR
B_{2u}	2	1	2	1	2	1	1	0	IR
B_{3u}	2	1	1	0	3	0	1	1	IR

$Cs_3[Ir_2Cl_9]$ (and $A_3Ir_2X_9$ where A = Rb, Cs, $N(CH_3)_4$; X = Cl, Br) Space Group $P6_3/mmc$, z = 2 ($N(CH_3)_4^+$ cation hydrogen atoms are not included in this analysis).

Factor Group Species, D_{6h}	Lattice Vibrations	Acoustical Vibrations	$[Ir_2X_9]^{3-}$ Anion Vibrations Stretch	Bend	Libration	Activity
A_{1g}	1	0	2	2	0	R
A_{2g}	0	0	0	1	1	none
B_{1g}	3	0	1	2	0	none
B_{2g}	0	0	0	1	0	none
E_{1g}	1	0	1	3	1	R
E_{2g}	3	0	2	3	0	R
A_{1u}	0	0	0	1	0	none
A_{2u}	2	1	1	2	0	IR
B_{1u}	0	0	0	1	1	none
B_{2u}	1	0	2	2	0	none
E_{1u}	2	1	2	3	0	IR
E_{2u}	1	0	1	3	1	none

CHAPTER 6

INTERPRETATION OF THE NUCLEAR QUADRUPOLE RESONANCE IN HEXAHALOGENOMETALLATES

6.1 INTRODUCTION

In this chapter the nuclear quadrupole resonance (NQR) spectra of iridium (III) hexachlorometallates as reported by Cresswell et al.[2] will be discussed in the light of the determination of a number of crystal structures of iridium (III) hexachlorometallates in this present study. No new NQR spectra are reported in this present study. The NQR results provide further evidence for the distortion of the anions in the hexachlorometallates in the solid state from octahedral symmetry (as found in the full crystal structure analyses). Phase transitions also reported by Cresswell et al. for some of the hexachlorometallate compounds have been examined further, and the results of these studies are also reported here.

A brief description of the theory of NQR will be given and a simplified mathematical treatment to show how the effect arises will be outlined (largely as an appendix to this chapter). A short review of the two aspects of NQR spectroscopy of hexahalogenometallates which are relevant to the present discussion will then be given, followed by an interpretation of NQR spectra reported by Cresswell et al. Finally a short summary of important points that

arise out of this reinterpretation will be given.

6.2 AN INTRODUCTION TO THE THEORY OF NUCLEAR QUADRUPOLE RESONANCE

Nuclear quadrupole resonance is a sensitive radio-frequency spectroscopic technique which gives detailed information about the charge distributions surrounding certain nuclei that have a nuclear spin greater than or equal to unity. The technique has found wide application in both organic and inorganic chemistry since its discovery in 1950 by Dehemlt and Krüger[194].

The frequency of the magnetic transition possible between the two spin states resulting from quantisation of nuclear spin along the principal axis of the field gradient for nuclei such as ^{35}Cl or ^{37}Cl having $I = \frac{3}{2}$ is given by

$$\nu_Q = \frac{eQq}{2h} (1 + \eta^2/3)^{\frac{1}{2}} \qquad (6.2.11)$$

This relation defines the interaction between the nuclear quadrupole moment, eQ, and the field gradient, q, at a particular nucleus. ν_Q is the NQR frequency, η is the asymmetry parameter and h is Planck's constant. The quantity $\frac{eQq}{h}$ is known as the quadrupole coupling constant (see Section 6.6).

In atoms, a contribution is made to the quadrupole coupling constant through the field gradient, by the electrons distributed in their various orbitals. Electrons in s orbitals or closed shells will not give rise to any

field gradient (ignoring polarisation effects) at a nucleus possessing a nuclear quadrupole moment, because of the spherical symmetry of the electron distribution. Thus, as far as atoms are concerned, only p, d, and f electrons contribute to the field gradient.

In molecules the situation is more complex, as the field gradients at a particular nucleus are now determined by both the charge distribution close to the nucleus in question and by the charge distribution in the remainder of the molecule.

In solids (e.g. crystals) containing molecular entities, the field gradients at atomic (nuclear) sites within these molecular species are determined by the two factors mentioned for molecules as well as the distribution of ions within the lattice, which has been shown to give a finite contribution to the field gradient[195].

For ions with completely closed shells, the electric field gradient will be zero, and hence no quadrupole coupling constant will be observed (e.g. KCl ^{35}Cl eQq/h = 0.04 MHz). However, in a free atom, for example a chlorine atom, a large electric field gradient may result because of a p electron hole in the outer valence shell. For such an atom the quadrupole coupling constant has been calculated to be -109.74 MHz.

Thus in molecules and solids, the variation in nuclear quadrupole coupling constants from values of zero to -109.74 MHz can give an indication of the type of bonding

involved in a compound, be it ionic or covalent or of an intermediate nature. Furthermore, as NQR frequencies can be determined with a great degree of precision, the technique is a useful tool for distinguishing crystallographic environments of atoms within crystal lattices.

In hexahalogenometallates studied by NQR, η has generally been found to be reasonably small[196] (of the order of 0.05). The range of NQR frequencies observed for hexachlorometallates is 10 MHz to 30 MHz (corresponding coupling constants are 20 MHz to 60 MHz). These non zero values reflect and reinforce the concept of a covalent contribution to the bonding in such coordination compounds; in some studies such covalent bonding has been examined in detail and related to both σ and π components, the latter of which can arise in some cases[2,151,197].

6.3 A BRIEF SURVEY OF SOME ASPECTS OF NQR SPECTRA OF HEXAHALOGENOMETALLATES

A large number of studies[196,198] have been made on a variety of transition metal and non transition metal hexahalogeno compounds, principally of the stoichiometry $A_2[MX_6]$, where A is a univalent cation, M is a tetravalent transition metal (or a non transition metal) and X is a halogen. Only a few studies of tervalent hexahalogenometallate complexes have been reported to date[2,151].

6.3.1 The Inter-relation between Crystal Structure and the Number of Observed NQR Frequencies in Hexahalogenometallates in the Crystalline State

The study of NQR spectra of complex halogenometallate salts in the solid state yields detailed information on the crystallographic environment of particular nuclei under study. This arises from fundamental considerations of the site symmetry of the particular species containing the atom(s) whose NQR are being observed. Two examples will serve to clarify this point.

(i) The ^{35}Cl NQR spectra of $K_2[IrCl_6]$

This compound crystallises in the cubic space group Fm3m (and is isomorphous to $K_2[PtCl_6]$[89]), with the $[IrCl_6]^{2-}$ anion located on a site of octahedral symmetry, O_h (m3m). As a result each chlorine atom within this anion is crystallographically equivalent and each chlorine atom has an identical environment. The environment is made up of the remainder of the $[IrCl_6]^{2-}$ octahedron and the K^+ and $[IrCl_6]^{2-}$ ions making up the remainder of the crystal lattice. Thus calculation of the field gradient at any chlorine atom site (which will necessarily involve contributions from the internal electron distribution within the $[IrCl_6]^{2-}$ anion containing the chlorine atom chosen, and contributions from the remaining ions within the crystal lattice) will yield the same value of q as any other chlorine atom used in the calculation. This being

the case, it can be seen that as far as the NQR experiment is concerned, only one resonance frequency will be expected. One resonance is observed at 20.73 MHz[197, 199], in agreement with this argument.

(ii) The ^{35}Cl NQR spectra of $K_3[IrCl_6]H_2O$

In this compound, which contains $[IrCl_6]^{3-}$ anions, K^+ cations and a water molecule of crystallisation, the situation is somewhat different to that above for $K_2[IrCl_6]$. $K_3[IrCl_6]H_2O$ crystallises in the space group Pbcn and the anions $[IrCl_6]^{3-}$ are located on sites of symmetry C_1 i.e. no symmetry at all. Furthermore, the anion is significantly distorted from octahedral symmetry (see Section 3.3), with bond angles deviating significantly from 90^o. Thus, the six crystallographically inequivalent chlorine atoms in the $[IrCl_6]^{3-}$ anion are inequivalent as far as NQR is concerned. The environment around each chlorine atom within an anion is different. Although there are eight $[IrCl_6]^{3-}$ anions in each unit cell, only the chlorine atoms within the asymmetric unit need be considered, as the remaining octahedra within the unit cell can be generated from the one octahedra in the asymmetric unit by the symmetry operations applicable to the space group Pbcn. Calculation of the field gradient at the six inequivalent chlorine atom sites should yield (unless there is some accidental equivalence) six different values. Thus, interaction of these individual field gradients with the

nuclear quadrupole moment, eQ, at each chlorine nucleus, should give rise to, at most, six NQR frequencies. Six resonances are actually observed at 16.754, 16.939, 17.505, 18.109, 18.251 and 18.800 MHz at 298 K [2].

Thus, the relationship between the crystal structure of the solid under scrutiny and the number of NQR frequencies expected is established. As can be seen in the two examples given, the number of resonance frequencies observed reflects the number of crystallographically independent resonant nuclei in the anions concerned.

However, in many cases the full complement of resonance frequencies expected on the basis of structural considerations is not found. Some authors have attributed this to complex relaxation effects [2]. It may also be the case that in some circumstances accidental equivalence of NQR frequencies, unresolvable by the NQR spectrometer, could be present. The most important point is that in no case has the number of resonances detected, exceeded the number of resonances expected on the basis of the known structure of the compound under consideration.

Table 6.3.1 lists the NQR frequencies of a number of halogenometallates. Most of the compounds in this table of stoichiometry $A_2[MX_6]$ crystallise in the cubic space group Fm3m (in the $K_2[PtCl_6]$ structural type [89]) and hence exhibit one resonance frequency. Those compounds of stoichiometry $A[MX_6]$ do not normally adopt a cubic structure[200], and, as a consequence of the low site symmetry of these anions, more than one resonance frequency

Table 6.3.1: ^{35}Cl NQR Frequencies at 300 K for a Number of Hexachlorometallate Salts.

Compound	NQR Frequencies [a] (MHz)	No. NQR Frequencies Observed	No. NQR Frequencies Expected [b]	Metal Oxidation State	No. d_π Holes	Reference
$[WCl_6]$	10.54	1	1	+6	6	151
$K[WCl_6]$	11.46,11.34(11.40)	2	>1	+5	5	151
$Rb[WCl_6]$	11.56,11.32(11.44)	2	>1	+5	5	151
$Cs[WCl_6]$	11.75,11.60,11.28(11.54)	3	>1	+5	5	151
$K_2[WCl_6]$	10.19	1	1	+4	4	151
$Rb_2[WCl_6]$	10.58	1	1	+4	4	151
$Cs_2[WCl_6]$	10.91	1	1	+4	4	151
$MoCl_5$	14.08	1	-	+5	5	151
$Cs_2[MoCl_6]$	10.34	1	1	+4	4	151
$K_3[MoCl_6]$	9.83,9.54(9.69)	2	6	+3	3	151
$K_2[IrCl_6]$	20.73	1	1	+4	1	2
$K_3[IrCl_6]$	16.639,17.690,17.845,			+3	0	2
	18.435(17.65)	4	9			
$Cs_2[RhCl_6]$	21.859	1	1	+4	1	2
$K_3[RhCl_6]H_2O$	18.292,18.497,19.463			+3	0	2
	(18.75)	3	6			

[a] Frequencies in parentheses are unweighted mean values at 300 K.

[b] Expected on the basis of the crystal structures of these compounds.

is observed. This correlation, between the number of NQR frequencies observed and the number expected on structural grounds, is adhered to in a number of more complex compounds such as tetrahalogenodiaquoaurates[201-203]. It is also observed in a number of non transition metal halogeno complexes, for example in the $[Sb_2X_9]^{3-}$ anion (X = Br,I)[204], and the $[InCl_5(H_2O)]^{2-}$ anion[195]. It is interesting to note that in reference[151] two NQR frequencies are reported for the complex $K_3[MoCl_6]$ which is consistent with the observed monoclinic space group[205] in which the compound is said to crystallise.

6.3.2 The Occurrence of Phase Transitions in Hexahalogenometallates as Revealed by NQR Spectroscopy

The occurrence of phase transitions, both above and below room temperature, has been well established for hexahalogenometallate compounds of stoichiometry $A_2[MX_6]$[196,198,206-210,212].

The transitions have been observed by recording NQR signals over a range of temperatures, and in some cases confirmatory evidence has been obtained from differential thermal analysis (DTA)[2] and accurate specific heat capacity determinations[211] over a range of temperatures. Phase transitions have also been recorded for a number of tervalent hexachlorometallates $A_3[MCl_6]H_2O$, $A_3[MCl_6]$[2] and also for some compounds of stoichiometry $A_3[MX_6]$, where M is a non transition metal[213]. The majority of these phase transitions are of the second order type, that is

transitions involving a discontinuous reconstruction of the crystal lattice.

Phase Transitions in $K_2[ReCl_6]$

The compound $K_2[ReCl_6]$, which displays phase transitions[206,209,211,212] will be briefly discussed, as the physical changes occurring are probably the same as in some of the compounds studied by Cresswell et al.[2]. The discussion will be based on the theory proposed by O'Leary and Wheeler[206,209].

Where phase changes occur in compounds, discontinuities in the frequency versus temperature plot may occur in their NQR spectra as well as new resonances possibly emerging, depending on the nature of the phase transition i.e. whether more or fewer crystallographically inequivalent resonant nuclei arise as a result of the phase transition. Discontinuities in the NQR spectrum of $K_2[ReCl_6]$ were observed at 76 K, 103 K and 110.9 K, and independent measurements of expansivity, cell dimensions and heat capacity[211] confirmed the discontinuities as being indicative of phase transitions.

In conjunction with some low frequency vibrational spectroscopy data, O'Leary and Wheeler concluded the phase transitions occurring in $K_2[ReCl_6]$ essentially involved rotation of the $[ReCl_6]^{2-}$ anion, the anion remaining as a rigid group during these phase transitions. These rotations were postulated to occur in a smooth fashion i.e. rotation occurs in an ever increasing angle about some

axis (axes), from the transition temperature, as the temperature is lowered.

O'Leary and Wheeler found $K_2[ReCl_6]$ underwent a change from a high temperature cubic form ($K_2[PtCl_6]$ antifluorite structure) to a tetragonal form at 110.9 K (formed by rotation of the anions about one of the original cubic axes (see Figure 6.3.1)). The phase transition to a lower symmetry monoclinic form at 103 K could result from combined rotations of the anion about two of the original cubic axes. The number of NQR frequencies observed within the three temperature ranges are one, two and three respectively; consistent with the structures observed.

Nakamura et al.[214] have found similar phase transitions occurring in a number of non-transition metal hexahalogenometallates (IV). For example, the structure of $K_2[TeBr_6]$ at room temperature[215] is not of the cubic $K_2[PtCl_6]$ type, but above room temperature a phase transition to the cubic system occurs. The NQR spectrum of $K_2[TeBr_6]$ reflects this situation with three resonances being observed at room temperature and one resonance observed above the transition point.

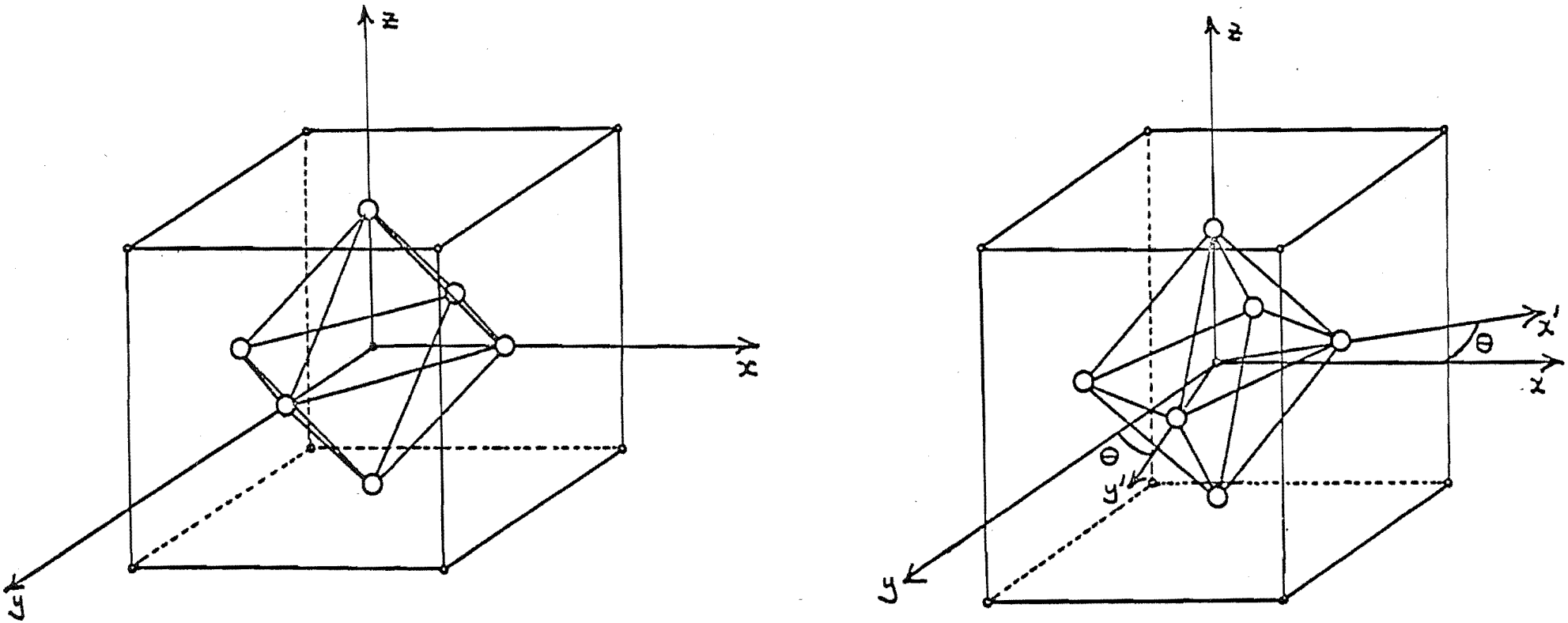

Figure 6.3.1: Orientation of the $[ReCl_6]^{2-}$ anion in the cubic (left) and tetragonal (right) crystalline forms of $K_2[ReCl_6]$ (the angle, θ, through which the anion moves in the phase transition between these structural forms, via rotation of the $[ReCl_6]^{3-}$ anion about the z axis, is shown).

6.4 NUCLEAR QUADRUPOLE RESONANCE STUDIES OF HEXACHLOROIRIDATES (III)

6.4.1 Examination of the Determined Crystal Structures and NQR Spectra of a number of Iridium (III) Hexachlorometallates

The ^{35}Cl NQR spectra reported by Cresswell et al.[2] for a number of tervalent hexachlorometallates of stoichiometries $A_3[MCl_6]$, $A_3[MCl_6]H_2O$ and other hydrated species all show complex character, both in terms of the number of lines observed and the appearance of phase transitions. Their data are recorded in Table 6.4.1. The number of resonances observed in these NQR spectra has been suggested to be indicative of low site symmetries of the $[IrCl_6]^{3-}$ anions. This has been verified both by a structure reported by Cresswell et al., and by three further crystal structures reported in this work.

The NQR Spectrum of $K_3[IrCl_6]H_2O$

The crystal structure of $K_3[IrCl_6]H_2O$ completed in this work was found to be isomorphous to that of $K_3[RhCl_6]H_2O$ as suggested in reference 2. The NQR spectra contains six lines consistent with the six crystallographically independent chlorine atoms contained in the distorted $[IrCl_6]^{3-}$ anion. Furthermore, all six resonances showed negative temperature coefficients, $\left(\frac{\partial \nu_Q}{\partial T}\right)_P$, as are expected for compounds showing no gross covalent character or hydrogen bonding[196,198,201,202,203,213,216].

Table 6.4.1: ^{35}Cl NQR Frequencies (MHz) for Hexachlorometallates of Iridium (III) and Rhodium (III)[a]

$K_3[IrCl_6]H_2O$						
298 K	16.754	16.939	17.505	18.109	18.251	18.800
243 K	16.773	16.968	17.533	18.144	18.289	18.863
201 K	16.739	16.998	17.562	18.179	18.323	18.927
$\frac{d\nu}{dT}$ (kHz deg^{-1} at 298 K)	-0.3	-0.5	-0.5	-0.6	-0.7	-1.1
$K_3[IrCl_6]$						
298 K	16.639			17.690	17.845	18.435
273 K	16.648			17.712	17.864	18.468
243 K				17.733	17.874	18.502
222 K		17.378	17.508	17.753	17.890	18.527
201 K		17.403	17.521			18.558
$\frac{d\nu}{dT}$(kHz deg^{-1})[b]	-0.4	-1.2	-0.6	-0.9	-0.8	-1.3
$(NH_4)_3[IrCl_6]H_2O$						
298 K		17.526		17.758	18.038	
273 K	17.559	17.610	17.704	17.847	18.069	
243 K	17.539	17.672	17.780	17.902	18.084	
222 K	17.527	17.722	17.831	17.954	18.096	
201 K	17.522	17.773	17.868	18.016	18.102	
77 K	17.498	18.056	17.165	17.283		
$\frac{d\nu}{dT}$ (kHz deg^{-1} at 298 K)	+0.7	-3.4	-3.8	-3.6	-1.2	
$K_3[RhCl_6]H_2O$						
298 K	18.292	18.497	19.463			
273 K	18.314	18.514	19.493			
243 K		18.525	19.536	18.331		
231 K		18.536				
204 K		18.551				
201 K		18.555				
$\frac{d\nu}{dT}$(kHz deg^{-1} at 298 K)	-0.8	-0.6	-1.2			

[a] Data obtained from reference 2.

[b] At 298 K or nearest temperature to where line appears.

However, a few points need clarification, especially in relation to the comparison of the observed three line spectrum of $K_3[RhCl_6]H_2O$ and the six line spectrum of $K_3[IrCl_6]H_2O$ as reported by Cresswell et al.[2]. Cresswell et al. emphasise the apparent isomorphism between these two complexes, but in order to explain the difference between the two NQR spectra, suggest that two independent $[IrCl_6]^{3-}$ octahedra are present in $K_3[IrCl_6]H_2O$, each contributing three lines of the six line resonance spectrum. However, this statement contradicts the concept of structural isomorphism. As was found in the present work, $K_3[IrCl_6]H_2O$ does indeed contain only one kind of distorted $[IrCl_6]^{3-}$ anion, and this anion maintains the same position and orientation within the unit cell (as do the other ions and water molecules) as the $[RhCl_6]^{3-}$ anion (and other components of the crystal lattice) in $K_3[RhCl_6]H_2O$. Hence the reason for the $K_3[RhCl_6]H_2O$ spectrum containing only three resonances, instead of the six expected, must be sought elsewhere (see Section 6.3.1 (ii)).

Cresswell et al. also state "that in view of the complex environment of the anion and the presence of the water molecule it is not meaningful to calculate the intermolecular forces and their effect on each chlorine atom and hence the field gradient". This comment is a little puzzling. One can only presume Cresswell et al. were trying to point out that in view of a number of such calculations that have been reported in the past[195,217,218], which have revealed that only a small portion of the electric field

gradient at each chlorine nucleus arises from effects due to charge distributions external to such anions, there would be little point in carrying out such calculations. Molecular orbital calculations for a series of $K_2[MCl_6]$ hexachlorometallates, where M = Re, Os, Ir, Pt[219], have verified that the major contribution to the field gradient does arise from charge distributions internal to the anion. However, all these calculations show that the precise determination of NQR frequencies for atoms at different sites within crystals are beyond the scope of present computational methods.

The NQR Spectrum of $K_3[IrCl_6]$

This compound crystallises in the space group $P\bar{1}$ (Section 3.2). However, because of disorder at one of the anion sites (and subsequent disorder of two of the potassium ions), determination of the number of possible inequivalent sites from which different NQR frequencies will arise is complex. The disorder must be random (if it were "regular" a new unit cell could be chosen), and therefore, each chlorine atom in every $[IrCl_6]^{3-}$ anion will strictly speaking have a different environment, when the distribution of ions external to such anions is considered. Each chlorine atom in the crystal would therefore give rise to a different NQR frequency (excepting accidental equivalence of frequencies). However, as the field gradient at each chlorine atom in the crystal is dominated by the internal charge distribution

of the anion it is associated with, there are essentially nine independent chlorine atoms as far as the NQR experiment is concerned. This is because each of the three independent $[IrCl_6]^{3-}$ anions contains only three independent chlorine atoms (as the anions in all cases contain a centre of inversion). Thus, one could possibly expect, at most, nine resonances in the NQR spectrum, with some line broadening caused by the disorder problem mentioned earlier.

The NQR spectrum contains only four resonance frequencies at 298 K and shows complex behaviour with variation in temperature with the emergence (and disappearance of one resonance) of two new resonances at 222 K. The four line spectra recorded at 298 K is consistent with the crystal structure determined at that temperature.

The NQR Spectrum of $(NH_4)_3[IrCl_6]H_2O$

At room temperature (297 K) $(NH_4)_3[IrCl_6]H_2O$ crystallises in the space group Pnma (Section 3.4). As the anions are located in a particular fashion on the mirror planes at y=¼, 3/4 in the unit cell, only four independent chlorine atoms are found and thus, at most, four NQR frequencies would be expected. Therefore, the three observed resonances at 298 K are consistent with the determined structure at 297 K. Below a phase transition, which occurs between 298 K and 273 K, two new resonances emerge (making a total of five), one of which has a positive temperature coefficient (see Table 6.4.1). This positive temperature

coefficient* may result from some hydrogen bonding interaction, as has been postulated for a number of other compounds studied[198,201,202,203,216]. As no such effects were observed in $K_3[IrCl_6]H_2O$ or $K_3[RhCl_6]H_2O$, this could suggest that the hydrogen bonding involves interaction between the ammonium cation and one of the chlorine atoms in the $[IrCl_6]^{3-}$ anion or water molecule oxygen atoms rather than the water molecule and the $[IrCl_6]^{3-}$ anion.

Comparison of the NQR Spectra of $K_2[IrCl_6]$ and $K_3[IrCl_6]$

The one NQR frequency observed for $K_2[IrCl_6]$ occurs at 20.73 MHz at 300 K. The unweighted mean of the four resonances observed at 298 K for $K_3[IrCl_6]$ is 17.65 MHz (the range is 16.639 MHz to 18.435 MHz).

The magnitude of the observed NQR frequencies suggests some covalent bonding is present in both complexes. Also the NQR frequency of $K_2[IrCl_6]$ is greater than the average resonance frequency of $K_3[IrCl_6]$ by some 3.08 MHz. This may be explained in terms of differences between the covalent bonding modes in the $[IrCl_6]^{2-}$ and $[IrCl_6]^{3-}$ anions.

* This assumes that the resonances observed and labelled in Table IV, reference 2 , always arise from the same ^{35}Cl site over the temperature range considered. If this is not so, then discussion of temperature coefficients would be meaningless, as the origin of a particular NQR frequency, as labelled in Table IV, is no longer confined to one particular chlorine atom.

The NQR spectra of a series of isostructural hexachlorometallate salts of the metals Re, Os, Ir, Pt (all in the +4 oxidation state) have been discussed in some detail by Kubo and Nakamura[196]. They, and others[151], have successfully related the increase in NQR frequencies for the potassium salts of these complexes to the progressive decrease in metal ← chlorine π bonding as the series is traversed from rhenium to platinum. The π-delocalisation present in $K_2[IrCl_6]$ is reported in a classic electron spin resonance study by Griffith et al.[220] The mechanism for this interaction involves back donation of filled $3p_x$ and $3p_y$ orbitals on the chlorine atoms into the electron hole in the t_{2g} orbitals of the $5d^5$ electron configuration of the iridium metal atom (see Figure 6.4.1). This assumes the filled $3p_z$ orbital on each chlorine atom is involved in the formation of the σ bond with the central metal atom. Brown et al.[151] in their analysis found the σ component of the M-Cl bond decreased in the series from Pt(IV) to Re(IV). However, both the π bonding component (increasing with the number of t_{2g} holes available on the central metal atom) and the nett metal charge, p, increased in the series from Pt(IV) to Re(IV). This latter observation was in agreement with a molecular orbital calculation performed by Cotton and Harris,[219] although these authors did not calculate such a large variation in π and σ covalent bonding components as did the former authors. Thus, if there were no π bonding

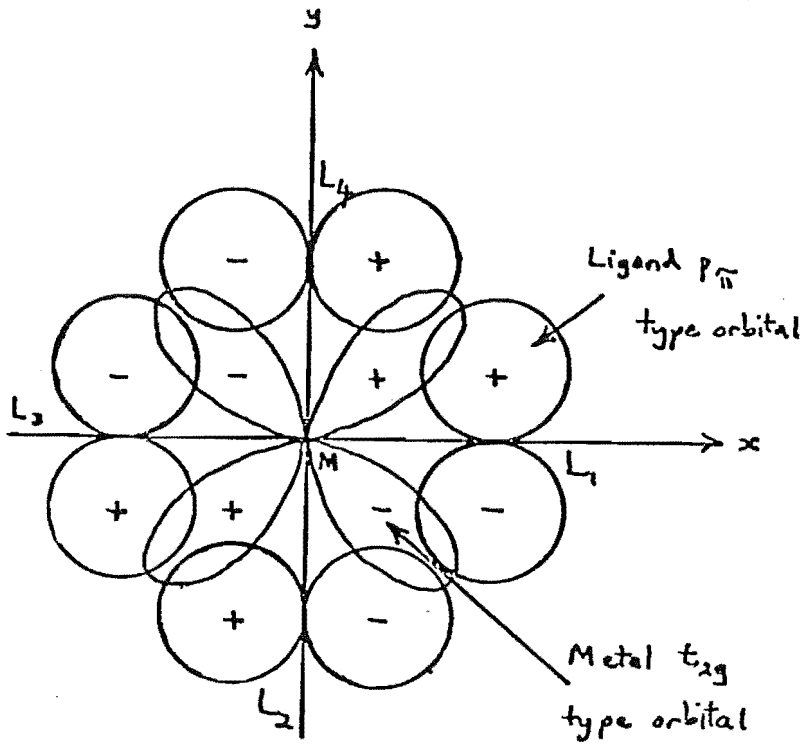

Figure 6.4.1: π-interaction of the metal t_{2g}-type orbital (here d_{xy}) with a suitable combination of ligand p_π-type orbitals (a bonding configuration is shown).

component in the Ir-Cl bond, the resonant frequency would be even greater than that of the present value of 20.73 MHz.

The π bonding component is not available to $K_3[IrCl_6]$ as the d electron configuration of the Ir^{3+} ion is t_{2g}^6 (although according to a molecular orbital approach outlined by Lucken[221], there is another π component available to both these compounds, which is essentially not used). Thus, the differences in the NQR frequencies may partially reflect a difference in the σ bonding between the two complexes, it being smaller in $K_3[IrCl_6]$ than in $K_2[IrCl_6]$ where the formal charge on the iridium atom has risen from +3 in the former to +4 in the latter.

Ignoring cation effects, similar differences observed in the NQR frequencies of $K[WCl_6]$ and $K_2[WCl_6]$; $Cs_2[MoCl_6]$ and $K_3[MoCl_6]$; and $Cs_2[RhCl_6]$ and $K_3[RhCl_6]H_2O$ (see Table 6.3.1) can be attributed to the same factors. However, because of the participation of π bonding in the former sets of complexes, the effect is less marked. Ignoring cation effects may also be invalid.

Comparison of the NQR Spectra of $K_3[IrCl_6]H_2O$ and $K_3[RhCl_6]H_2O$

The differences in NQR frequencies between $K_3[IrCl_6]H_2O$ and $K_3[RhCl_6]H_2O$ are small in comparison with those due to the change in oxidation state of related Ir(IV) and Rh(IV) hexachlorometallates, and presumably reflects subtle differences in the metal-chlorine σ bonds between the two metal ions. The mean Ir-Cl bond length in the $[IrCl_6]^{3-}$ anion in $K_3[IrCl_6]H_2O$ of 2.359Å

is somewhat longer than the mean Rh-Cl length (2.344 Å) in the $[RhCl_6]^{3-}$ anion in $K_3[RhCl_6]H_2O$. If this difference suggests a smaller degree of σ bonding in $K_3[IrCl_6]H_2O$ than in $K_3[RhCl_6]H_2O$ (which it could do, as both the Ir^{3+} and Rh^{3+} ions have ionic radii of about 0.68Å), then the NQR frequencies observed should reflect this. The NQR frequencies in fact do, with the mean frequency in $K_3[IrCl_6]H_2O$ of 17.73 MHz being 1.03 MHz lower than the mean frequency observed in $K_3[RhCl_6]H_2O$.

6.4.2 Examination of the Phase Transitions in a Number of Iridium (III) and Rhodium (III) Hexachlorometallates

Cresswell et al.[2] have deduced from NQR spectra and DTA studies that a number of phase transitions occur in both $K_3[IrCl_6]$ and $K_3[RhCl_6]H_2O$. Although their reported NQR spectrum of $(NH_4)_3[IrCl_6]H_2O$ contained anomalies consistent with phase transitions also being present over a temperature range, the above authors made no comment on this possibility nor reported any low temperature DTA study on this compound.

As an extension of their reported work, low temperature single crystal X-ray diffraction studies were carried out on $K_3[RhCl_6]H_2O$, $K_3[IrCl_6]H_2O$ and $(NH_4)_3[IrCl_6]H_2O$. A DTA study was also completed for the latter compound to clarify the possibility of phase transitions occurring.

Phase Transitions in $(NH_4)_3[IrCl_6]H_2O$

Results of a DTA study completed for this compound in this work are given in graphical form in Figure 6.4.2. A

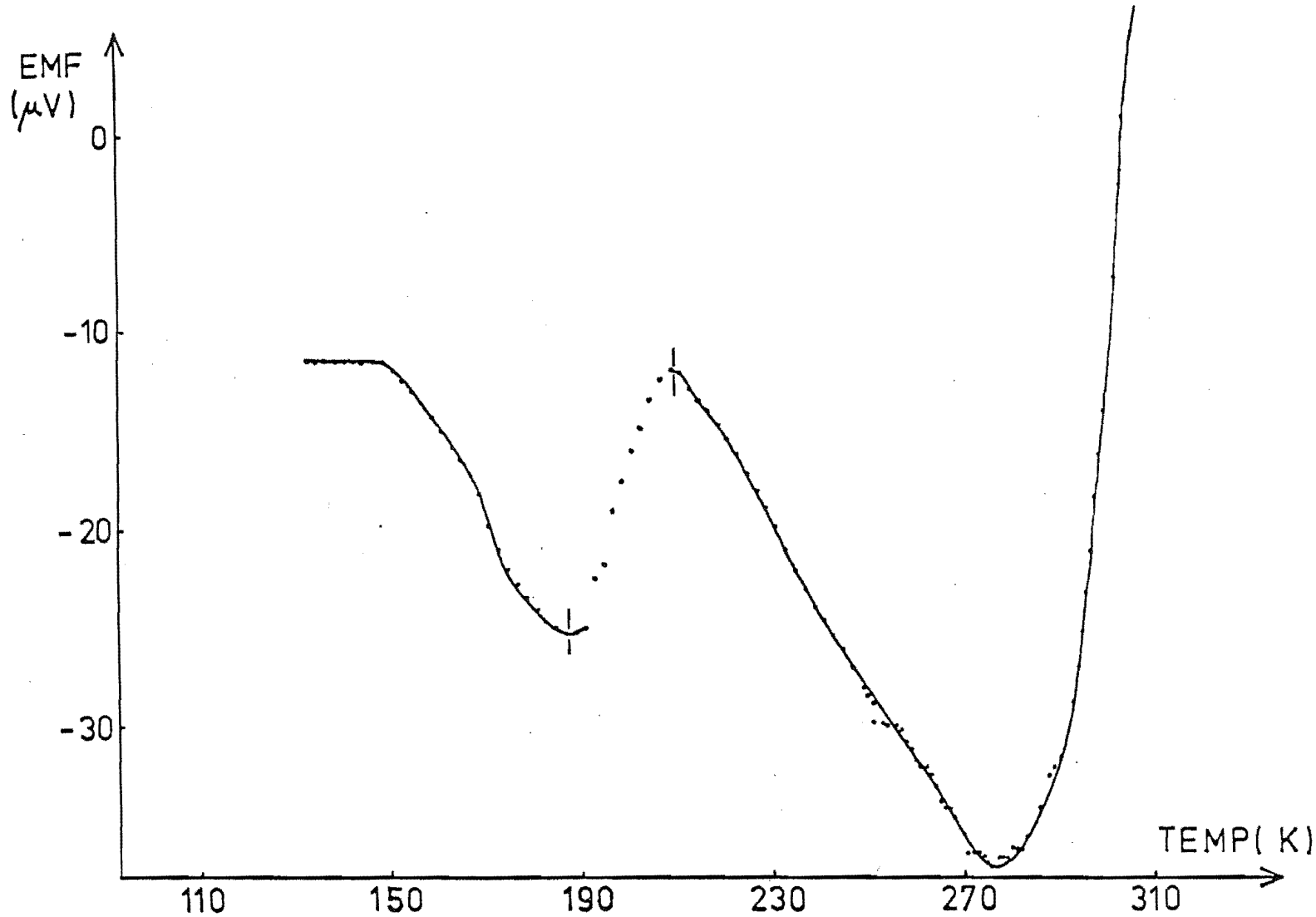

Figure 6.4.2: Low temperature differential thermal analysis (DTA) curve for $(NH_4)_3[IrCl_6]H_2O$ (The discontinuity at ≈ 190 K is a function of the low temperature cryostat (see Section 9.3.) and is not indicative of a phase transition).

phase transition occurs in the range 283 K to 273 K which is in agreement with an anomaly noted in the NQR spectrum of this compound in the range 298 K to 273 K (see Table 6.4.1). A further phase transition between 201 K and 77 K, as suggested by the reported NQR data (Table 6.4.1), was not found in the temperature range (298 K to 133 K) covered in this study.

To examine structural changes occurring in this phase transition, a study of the variation of unit cell parameters in $(NH_4)_3[IrCl_6]H_2O$ as a function of temperature was made. The reciprocal lattice was photographed using a precession camera with a special goniometer head containing a variable temperature attachment (see Chapter 9). The precession photography technique does have limitations which will now be discussed along with conclusions reached in this study.

Phase transitions have previously been examined by measurement of changes in cell dimensions using single crystal X-ray diffractometry[206] and X-ray powder diffraction[214]. The phase transitions observed in these studies involved changes from a higher symmetry crystal system (such as cubic) to a lower symmetry crystal system (such as tetragonal or monoclinic) as the temperature is decreased (for example see reference[206]). The orthorhombic crystal system of $(NH_4)_3[IrCl_6]H_2O$ at room temperature is already one of relatively low symmetry. Structural changes occurring in a phase transition may not necessarily require a change in crystal system, although, as will be discussed

for $(NH_4)_3[IrCl_6]H_2O$, these changes will require a change in space group.

Phase transitions will produce a number of changes in the intensity weighted reciprocal lattice. Reflections previously absent may become observable (i.e. intensities will change) and with changes in cell dimensions the Bragg angles of certain reflections may be slightly altered. A more fundamental change may also occur, that is a change in the symmetry of the reciprocal lattice. One problem associated with the use of photographic techniques to measure changes in the reciprocal lattice is that if the reconstruction in the crystal lattice is small then only small changes are expected in reciprocal space. This requires therefore, that the photographic technique used must be sensitive enough to detect such small changes in reciprocal space (e.g. intensities, interaxial angles etc.).

The variation in cell dimensions of $(NH_4)_3[IrCl_6]H_2O$ as a function of temperature is given in Figure 6.4.3. This may be compared with similar data for $K_3[RhCl_6]H_2O$ and $K_3[IrCl_6]H_2O$ (Figures 6.4.4 and 6.4.5 respectively). In all three compounds orthorhombic symmetry is maintained throughout the temperature ranges covered, within the limits of experimental error. The large error bars on these graphs result from uncertainty in measurement between the diffraction spots on the zero level precession photographs. It is only when temperature differences between data points are large that certain trends (e.g. positive or negative

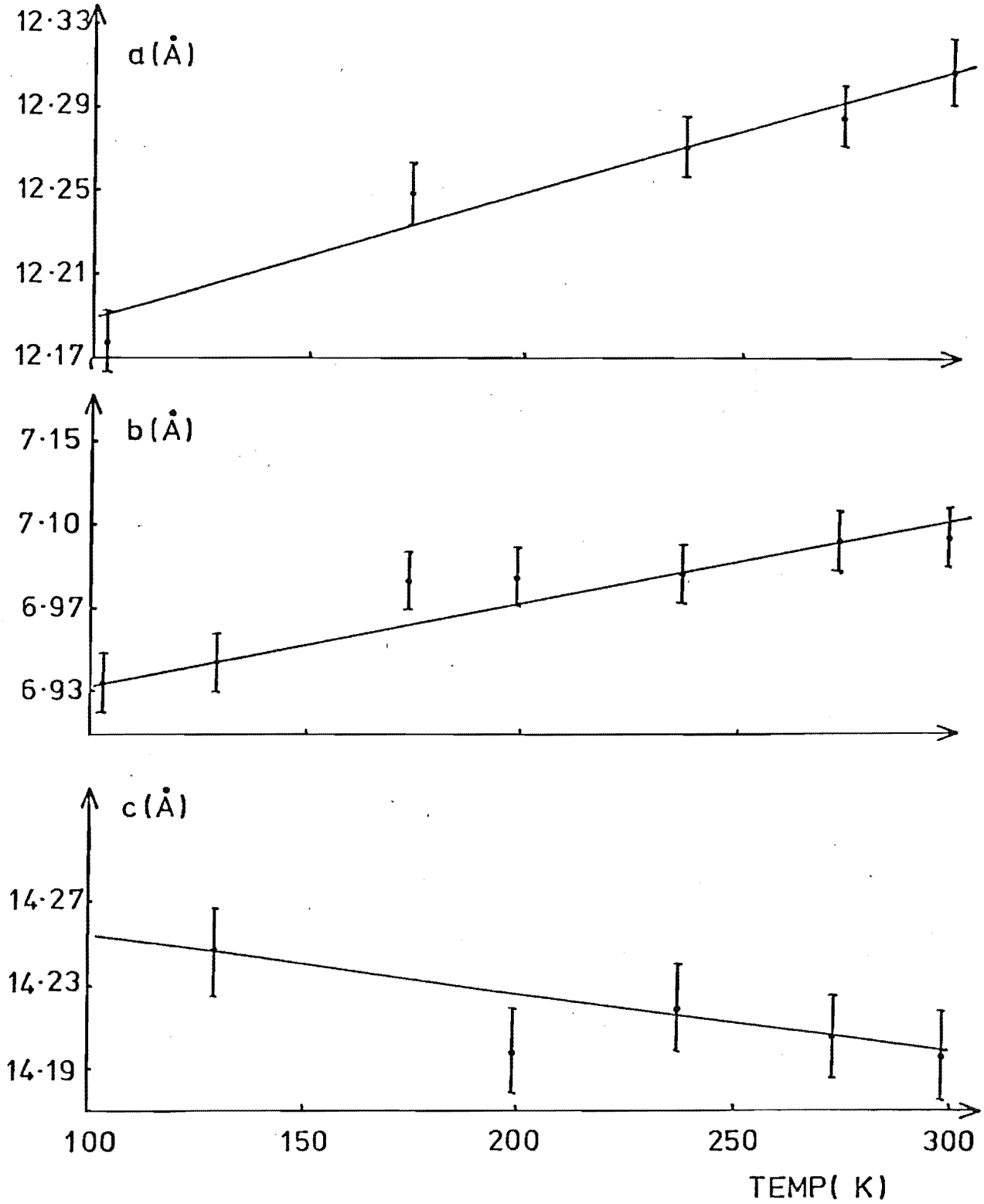

Figure 6.4.3: Temperature dependence of the orthorhombic a,b and c axial unit cell dimensions of $(NH_4)_3[IrCl_6]H_2O$.

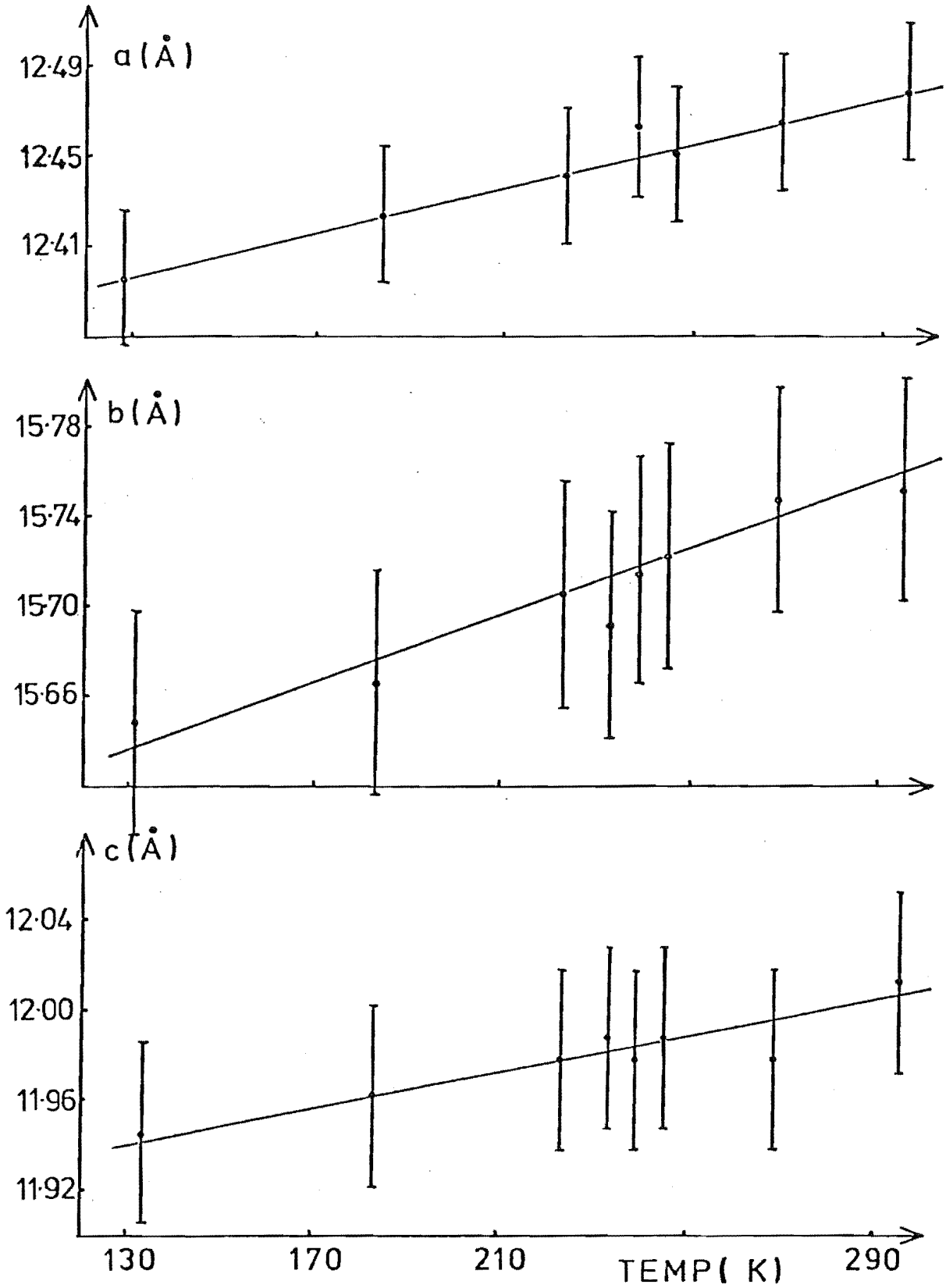

Figure 6.4.4: Temperature dependence of the orthorhombic a,b and c axial unit cell dimensions of $K_3[RhCl_6]H_2O$.

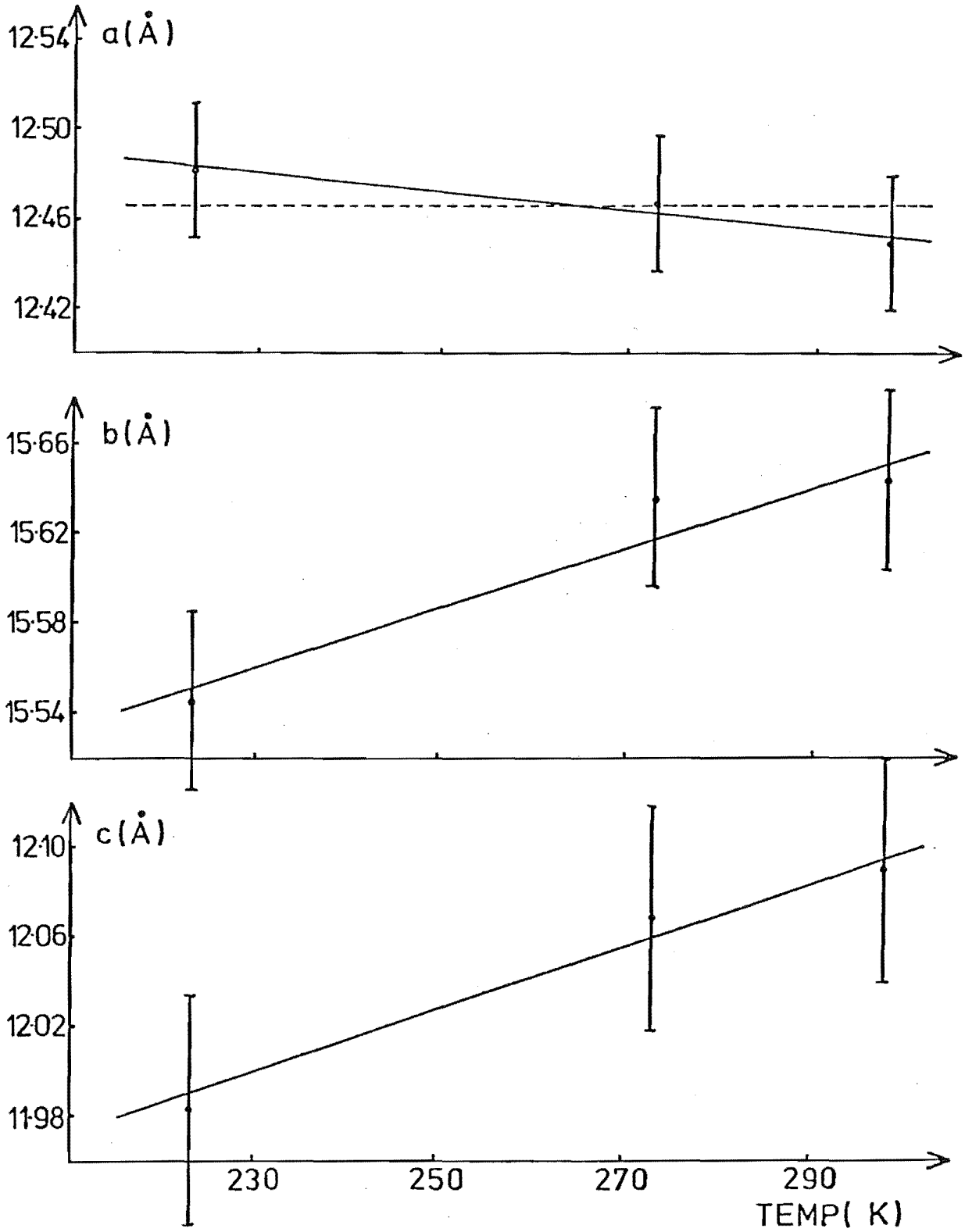

Figure 6.4.5: Temperature dependence of the orthorhombic a,b and c axial unit cell dimensions of $K_3[IrCl_6]H_2O$ (dotted line for the a axis indicates no change may be occurring in this dimension over the temperature range studied (within experimental error)).

coefficients of expansion of some of the axes) become experimentally significant. Thus,use of a more precise technique (e.g. single crystal X-ray diffractometry) would certainly improve the present results and allow a more definitive statement to be made as to whether or not the phase transitions in $(NH_4)_3[IrCl_6]H_2O$ do involve changes in the crystal system.

If one accepts that the mechanism of the phase transitions observed for compounds such as $K_2[ReCl_6]$ [206] is the same as that for those phase transitions occurring in iridium (III) hexachlorometallates, then some conclusions can be drawn about the structural changes occurring in these compounds during such transitions, especially when the apparent lack of change in crystal system is noted.

To account for the five or six crystallographically inequivalent sites suggested by the five observed NQR frequencies at 273 K for $(NH_4)_3[IrCl_6]H_2O$ (as opposed to the three resonances observed at 298 K), a rotation of the $[IrCl_6]^{3-}$ anion about the crystallographic x or z axes (or a combined rotation about all three axes) must have occurred, with subsequent loss of the mirror planes at y = ¼, 3/4. Thus, the phase transition involving a small rotation of the essentially rigid distorted octahedral $[IrCl_6]^{3-}$ anion, must see a change to another orthorhombic space group (containing no mirror planes bisecting the anions) or to a space group of a lower symmetry system. A rotation of the anion about the y axis will not see the desired change in the number of crystallographically independent

chlorine sites as two chlorine atoms still remain in the mirror plane.

Further to the observation that within experimental error orthorhombic symmetry was retained during the phase transition between 283 K to 273 K, no new reflections were observed in the two zero level precession photographs from which the cell dimensions were obtained at any temperature below 273 K. This suggested that the space group $Pn2_1a$ could be a possible orthorhombic space group that could accommodate the reconstructed lattice after the phase transition. This non centrosymmetric space group has identical extinctions to the space group Pnma and the two space groups are indistinguishable from their two diffraction patterns.

The space group $Pn2_1a$ allows retention of the "same" (as in the sense discussed below) unit cell as that before the observed phase transition and, if this space group is then adopted immediately the phase transition occurs, it also gives a satisfactory explanation for the increase in the observed number of independent chlorine atomic environments.

The fractional atomic coordinates x,y,z, of the iridium atom in the $[IrCl_6]^{3-}$ anions in $(NH_4)_3[IrCl_6]H_2O$ are approximately 0.37, 0.25, 0.05 in the space group Pnma. If during a phase transition rearrangement of the lattice was such that the space group $Pn2_1a$ was adopted, then the iridium atom could still retain the same fractional coordinates. However, because of the multiplicity of four

in the new space group (as opposed to eight in the centrosymmetric Pnma), and removal of the mirror planes at y = ¼, 3/4 present in the original space group, the number of crystallographically distinct chlorine atomic positions will become six (as opposed to four previously).

Such a hypothesis is in accord with a general theorem proposed by Landau[222] which states that for every transition involving the halving of the number of symmetry transformations of a crystal, a second order phase transition can exist. The phase transition from the room temperature space group Pnma for $(NH_4)_3[IrCl_6]H_2O$, to the below 273 K possibility of $Pn2_1a$ is consistent with observed data and Landau's general theorem.

As can be seen from the above discussion a change in crystal system is not strictly required in the phase transition between 298 K and 273 K for $(NH_4)_3[IrCl_6]H_2O$.

Phase Transitions in $K_3[RhCl_6]H_2O$

A study of the variation of cell dimensions as a function of temperature for $K_3[RhCl_6]H_2O$ is given in Figure 6.4.4. The compound has a phase transition occurring between 238 K and 240 K as shown by NQR and DTA data[2]. The variation in cell dimensions with temperature can be compared with those of the isomorphous compound $K_3[IrCl_6]H_2O$ (Figure 6.4.5), which does not undergo phase transitions below room temperature. The orthorhombic crystal system was still retained (within experimental error) below the phase transition occurring

between 238 K and 240 K, and no new reflections were observed in the zero level precession photographs taken below these temperatures. This must mean that the space group has not changed during this phase transition.

As far as the observed NQR spectrum is concerned, the phase transition involving a reorientation of the $[RhCl_6]^{3-}$ anion does not necessarily require a concurrent change in space group.

However, there are two inter-related problems associated with this interpretation. One is that this is contrary to the general rule that transitions involve changes of a more symmetrical structure to a less symmetrical structure[222]. This may mean a change in space group has occurred but has not been detected in this study. The second problem is that only three of the expected six NQR frequencies are observed in the spectrum of $K_3[RhCl_6]H_2O$ at room temperature. After the phase transition has occurred at 238 K to 240 K the number of resonances observed dropped to one. One must assume some complex relaxation phenomena is preventing observation of the remaining resonances whatever their number might be. It is highly unlikely that the one resonance line is indicative of a change to a cubic space group; it would be very difficult to accommodate a compound of such stoichiometry in a cubic space group such that all chlorine atomic sites were crystallographically equivalent. Also such a modification would involve a phase transition from a less symmetrical crystal structure to a more symmetrical structure contrary to the general rule observed by Landau[222].

Phase Transitions in $K_3[IrCl_6]$

The complex salt $K_3[IrCl_6]$ also shows a number of phase transitions below room temperature. However, as no low temperature single crystal X-ray diffraction study was performed on this compound it will not be discussed any further.

6.5 SUMMARY

The above discussions have shown that the NQR spectra reported by Cresswell et al.[2] for a number of iridium (III) hexachlorometallate salts are in agreement with the observed crystal structures at room temperature, where the $[IrCl_6]^{3-}$ anions form distorted octahedra of low site symmetry and the different crystallographic environments of the ^{35}Cl nuclei therefore give rise to a number of resolvable NQR frequencies. However, it should be emphasised here that the observation of a number of frequencies does not necessarily imply the reverse is true (i.e. that the anions are distorted). The anion site symmetry for example could be C_1 and the $[IrCl_6]^{3-}$ anion could retain octahedral geometry within the limits of experimental error (as determined by an X-ray crystal structure analysis). If this were the case, the different NQR frequencies would then result from differences in contributions to the field gradients at the ^{35}Cl nuclei from the charge distribution external to the $[IrCl_6]^{3-}$ anion under consideration (i.e. in the remainder of the

crystal lattice). These contributions must differ by virtue of the low site symmetry on which the ion is located. Therefore, with the present status of theoretical calculations of NQR frequencies, where results are not particularly accurate, no prediction can be made about the presence (or absence) of distortion in such anions from mere observation of the number and magnitude of different NQR frequencies.

The problems of not observing the complete set of NQR resonances expected for certain compounds (e.g. $K_3[RhCl_6]H_2O$, $K_3[IrCl_6]$, $(NH_4)_3[IrCl_6]H_2O$) on the basis of structural considerations also means NQR must be a limited tool for elucidating anion site symmetries of complexes of the type discussed in Section 6.4. It is obvious from data reported for a number of compounds (e.g. K_3MoCl_6, the iridium hexachlorometallates), that care is required in interpretation of the number of resonance frequencies in relation to the crystal structure and anion site symmetry. However, the appearance of more than one resonance frequency does imply the anion site symmetry in a hexahalogenometallate has been lowered from that of O_h(m3m).

NQR remains a very useful method for detecting solid state phase transitions for compounds containing nuclei accessible to the NQR technique. This has been illustrated by the study on $(NH_4)_3[IrCl_6]H_2O$ in section 6.4.2. Even if these phase transitions do not involve rotation of anions within the remaining lattice 'cage' the discussion about

changes of space groups to accommodate the observed changes in NQR spectra and structural reconstruction, is still valid for these compounds. To help elucidate the mechanism of the solid state phase transitions, a full crystal structure analysis at temperatures below the transition point for some of these compounds would at least provide the answer as to what structural modifications had occurred.

6.6 APPENDIX

The Theory of Nuclear Quadrupole Interaction.

(This account is largely taken from a review article by Sillescu[223]).

Consider the interaction between a nuclear charge cloud of density $\rho^{(n)}(R)$ and an electron charge cloud of density $\rho^{(e)}(r)$ (assume $R < r$, see Figure 6.6.1). Inside the sphere of radius R, the charge distribution $\rho^{(e)}(r)$ produces a potential, $\phi(R)$ such that

$$\phi(R) = \int \frac{\rho^{(e)}(r)\,d\tau^{(e)}}{|\underset{\sim}{r} - \underset{\sim}{R}|} \qquad (6.2.1)$$

Thus the interaction potential of the two charge clouds $\rho^{(e)}(r)$ and $\rho^{(n)}(R)$ is given by (6.2.2)

$$V = \int \phi(R)\rho^{(n)}(R)\,d\tau^{(n)}$$

$$= \iint \frac{\rho^{(e)}(r)\rho^{(n)}(R)\,d\tau^{(e)}\,d\tau^{(n)}}{|\underset{\sim}{r} - \underset{\sim}{R}|} \qquad (6.2.2)$$

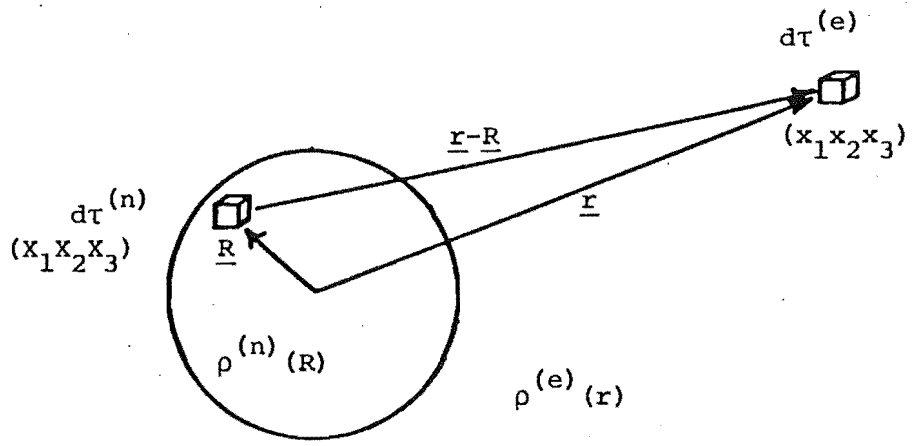

Figure 6.6.1: The interaction of two charge clouds (from reference 223). The vector from the origin to any point within a charge distribution $\rho^{(n)}(R)$ is $\underline{R}$, that to any point outside the sphere (i.e. in the region $\rho^{(e)}(r)$) is labelled $\underline{r}$.

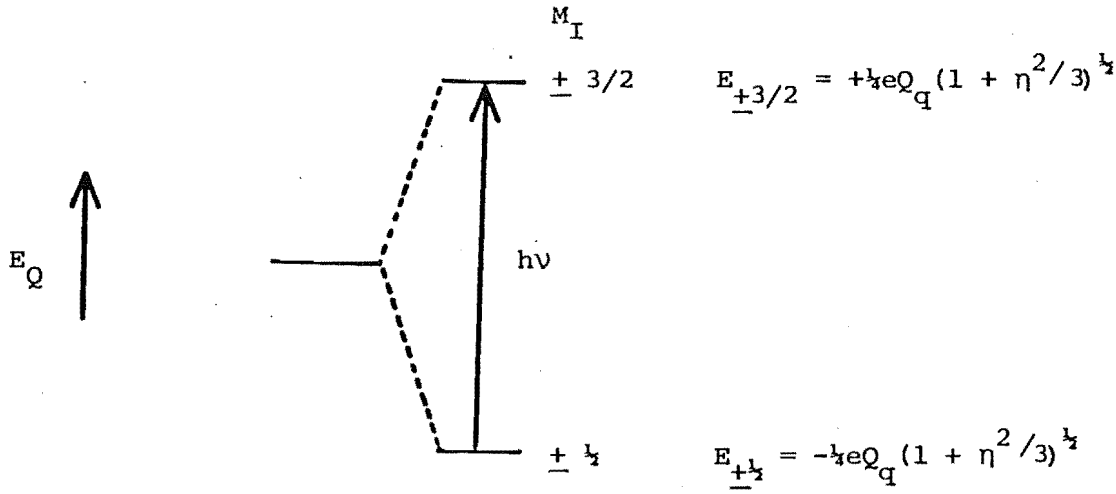

$$\nu = \frac{eQ_q}{2h}(1 + \eta^2/3)^{\frac{1}{2}} = \frac{1}{2}(\frac{eQ_q}{h}) \quad \text{(when } \eta = 0\text{)}$$

Figure 6.6.2: Energy level diagram showing the interaction of the nuclear quadrupole moment for nuclei with I = 3/2 and an inhomogeneous electric field.

It can be shown that the energy of coupling, V_Q, of the quadrupole moment of the nuclear charge (present where the nuclear spin, I, is greater than or equal to unity) and the gradient of the electric field, which makes a contribution to this expression is given by equation (6.2.3).

$$V_Q = \frac{1}{6} \sum_{j=1}^{3} \sum_{k=1}^{3} \phi_{jk} Q_{jk} \tag{6.2.3}$$

where Q_{jk} are the components of the nuclear quadrupole moment tensor $\underset{\sim}{Q}$ such that

$$Q_{jk} = \int (3X_j X_k - \delta_{jk} R^2) \rho^{(n)}(R) d\tau^{(n)} \tag{6.2.4}$$

and ϕ_{jk} are the components of the electric field gradient tensor $\underset{\sim}{\nabla E}$ such that

$$\phi_{jk} = \left(\frac{\partial^2 \phi}{\partial X_j \partial X_k} \right)_{R=0}$$

$$= \int \frac{\partial^2}{\partial X_j \partial X_k} \left(\frac{1}{|\underset{\sim}{r} - \underset{\sim}{R}|} \right) \rho^{(e)}(r) d\tau^{(e)}$$

$$= \int \left(\frac{3x_j x_k - \delta_{jk} r^2}{r^5} \right) \rho^{(e)}(r) d\tau^{(e)} \tag{6.2.5}$$

When the axes (x_1, x_2, x_3) are rotated into the principal axes x,y,z of the field gradient tensor $\underset{\sim}{\nabla E}$ the off diagonal terms ϕ_{ij} $(j \neq i)$ become identically zero and thus equation (6.2.3) reduces to

$$V_Q = \frac{1}{6}(\phi_{xx}Q_{xx} + \phi_{yy}Q_{yy} + \phi_{zz}Q_{zz})$$

Furthermore, because the electric field gradient tensor $\underset{\sim}{V}E$ obeys Laplaces equation (equation (6.2.6))

$$\Delta\phi = \sum_j \phi_{jj} = 0 \qquad (6.2.6)$$

two new variables completely defining the electric field gradient (in conjunction with the directions of the principal axes) are defined. They are q and η as expressed below (equations (6.2.7))

$$q = \phi_{zz}$$

$$\eta = |\phi_{xx}-\phi_{yy}|/|\phi_{zz}| \qquad (6.2.7)$$

η is called the asymmetry parameter and will always be less than unity as ϕ_{xx}, ϕ_{yy} and ϕ_{zz} must obey the following relation.

$$|\phi_{xx}| \leqslant |\phi_{yy}| \leqslant |\phi_{zz}| \qquad (6.2.8)$$

Thus V_Q can now be expressed as

$$V_Q = \frac{q}{6}\left[\tfrac{1}{2}(\eta-1)Q_{xx} - \tfrac{1}{2}(\eta+1)Q_{yy} + Q_{zz}\right] \qquad (6.2.9)$$

In a quantum mechanical treatment we have to obtain the Hamiltonian of nuclear quadrupole coupling. This pure nuclear

operator can be readily obtained from equation (6.2.9) and as a result for nuclei with nuclear spins of $I = \frac{3}{2}$ (such as ^{35}Cl, ^{37}Cl, ^{79}Br and ^{81}Br), two energy states arise from the quantisation of the orientations of the nuclear spin along the field gradient principal axes. These energy states are given by

$$E_{\pm\frac{3}{2}} = \tfrac{1}{4}eQq(1 + \eta^2/3)^{\frac{1}{2}}$$

$$E_{\pm\frac{1}{2}} = -\tfrac{1}{4}eQq(1 + \eta^2/3)^{\frac{1}{2}} \qquad (6.2.10)$$

where the subscripts m (in $E_{\pm m}$) refer to the case where $\eta=0$ and are magnetic quantum numbers for the nuclear states ψ_{IM}, chosen to be eigenfunctions of the nuclear spin operators $\underset{\sim}{I}^2$ and $\underset{\sim}{I}_z$ (see Figure 6.6.2).

Now magnetic transitions are possible between these two states and are detectable by an NQR spectrometer. Then the NQR frequency will be given by

$$\nu_Q = (E_{\pm\frac{3}{2}} - E_{\pm\frac{1}{2}})/h$$

$$= \frac{eQq}{2h}(1 + \eta^2/3)^{\frac{1}{2}} \qquad (6.2.11)$$

The quantity $\frac{eQq}{h}$ (or $\frac{e^{\sim}qQ}{h}$ if $\phi_{zz} = eq$ rather than q as defined in equation (6.2.7)) is known as the quadrupole coupling constant.

CHAPTER 7

VISIBLE AND ULTRAVIOLET ABSORPTION SPECTRA OF HALOGENO-IRIDATE(III) AND (IV) SALTS

7.1 INTRODUCTION

The visible and ultraviolet region absorption and reflectance spectra of a number of halogenoiridate(III) and (IV) compounds containing $[IrX_{6-n}(H_2O)_n]^{y-}$ (X = Cl, Br; n = 0,1,2,3; y = 3-n, 2-n) species have been reported[29, 38,43,44,51,54,56,58,224-230] (see Table 7.1). In general the absorption bands for compounds containing the Ir(IV) halogenometallate species have been assigned to $X(\pi) \rightarrow Ir(5d)$ charge transfer transitions. The assignments are based on the high extinction coefficients (~ 2000) of these bands giving rise to the intensely coloured solutions in a variety of solvents. The absorption bands observed for Ir(III) species are, on the other hand, largely Laporte forbidden d-d transitions. For these spin paired d^6 complexes both spin forbidden ($^3T_{1g} \leftarrow {}^1A_{1g}$; $^3T_{2g} \leftarrow {}^1A_{1g}$) and spin allowed transitions ($^1T_{1g} \leftarrow {}^1A_{1g}$, $^1T_{2g} \leftarrow {}^1A_{1g}$) [231,232] have been observed (extinction coefficients of the order of 10 and 100 respectively). Some charge transfer bands, in the ultraviolet region, have been reported. The results of the present studies will now be discussed.

Table 7.1: Reported Visible and Near Ultraviolet Region Spectra for Halogenoiridate(III) and (IV) Species and Other Metallate(III) and Dimetallate(III) Species.

Species (or Compound)	Solution and Conc. (or method)	Absorption Band Maxima (cm^{-1}) (and extinction coefficients (M^{-1} cm^{-1}))	Reference
$[IrCl_6]^{2-}$	0.0005 M $Na_2[IrCl_6]$ in H_2O or dil. HCl	17400(460) 20450(3200) 23200(2540) 24200(2480)	54
$[As(C_6H_5)_4]_2[IrCl_6]$	reflectance	17000 20000 21700sh 22700	224
" " " "	dichloromethane	17100 20100 21100sh 22700	224
$Cs_2[IrCl_6]$	reflectance	16800 19400 23100	224
$Rb_2[IrCl_6]$	"	17200 19600 23500	224
" "	" (with Al_2O_3)	17200 19300 23000	224
trans-$[IrCl_4(H_2O)_2]$	2.5 M $HClO_4$ and 1.2 M $NaClO_4$ (20-25°C)	18700(1310) 22500(2900) 28600(1090)	43
cis-$[IrCl_4(H_2O)_2]$	"	18700(1290) 22500(2790) 25600(700)sh	43
1,2,6-$[IrCl_3(H_2O)_3]^+$	"	19600(1400) 26700(1700)	43
1,2,3-$[IrCl_3(H_2O)_3]^+$	"	19500(1750) 26700(1900)	43
$[IrBr_6]^{2-}$	0.0005 M $[IrBr_6]^{2-}$ in 0.1 M HBr	13600(1550) 14300(2050) 14800(2100) 17200(3070) 18400(1500) 19600(1800)	54
$[N(n\text{-}C_4H_9)_4]_2[IrBr_6]$	reflectance	13200 14000 14500 16500 18000 18500	224
$[IrCl_6]^{3-}$	0.1M - 0.01 M $K_3[IrCl_6]$ in 4 M HCl	16300(7.5) 17900(10) 24100(76) 28100(64)	51
$[IrCl_5(H_2O)]^{2-}$	aqueous solution	18200(12) 24700(110) 28800(110)	226
trans-$[IrCl_4(H_2O)_2]^-$	2.5 M $HClO_4$ and 1.2 M $NaClO_4$ (at 20-25°C)	18900(11.3) 25500(103) 30000(115)	43
cis-$[IrCl_4(H_2O)_2]^-$	"	25400(92.8) 30100(120)	43
1,2,6-$[IrCl_3(H_2O)_3]$	"	19200(10)sh 26500(92.0) 31300(99.1)	43
1,2,3-$[IrCl_3(H_2O)_3]$	"	26300(95.5) 31300(118)	43

Table 7.1 Continued.

Species (or Compound)	Solution and Conc. (or method)	Absorption Band Maxima (cm^{-1}) (and extinction coefficients (M^{-1} cm^{-1}))	Reference
$[N(CH_2CH_2NH_3)_3][IrCl_6]3H_2O$	reflectance	19600 23200 40700	44
$[IrBr_6]^{3-}$	0.005 M to 0.015 M $[IrBr_6]^{3-}$ in 4 M HBr	16800(27 22400(232) 25800(198)	51
$[IrBr_6]^{3-}$	aqueous solution	15500(12) 17100(16) 22600(175) 26300(145) 37000(12000) 41500(20000)	226
$[IrBr_5(H_2O)]^{2-}$	"	36900(10500) 41800(17500)	226
$[N(CH_2CH_2NH_3)_3][IrBr_6]H_2O$	reflectance	17500 22700sh 37000	44
$[CrCl_6]^{3-}$	reflectance	13200 18700	108
$[Cr_2Cl_9]^{3-}$	"	12600 14000 17900	108
$[VCl_6]^{3-}$	"	11000 18000	108
$[V_2Cl_9]^{3-}$	"	11000 17900	108
$[TiCl_6]^{3-}$	"	12600	108
$[Ti_2Cl_9]^{3-}$	"	13300	108
$[(CH_3)H_3N]_3[MoCl_6]$	"	14500 19000 23600	233
$[(CH_3)H_3N]_3[Mo_2Cl_9]$	dimethylformamide	13180(28) 13800(22) 15000sh 15220(32) 18870(580) 20830sh 23200(600)	233
"	dimethylsulphoxide	13300(22) 15220(28) 18800(500) 20000sh 23100(580)	233
$[W_2Cl_9]^{3-}$	aqueous HCl	13200(50) 16300(80) 22200(2400)	234
"	"	13500(70) 16300(125) 22200(4000)	235
$K_3[W_2Cl_9]$	aqueous solution	13200(50) 15900(160) 21900(47300) 26300(120) sh	236

sh - shoulder

7.2 THE VISIBLE AND ULTRAVIOLET ABSORPTION SPECTRA OF HALOGENOIRIDATE(III) AND (IV) COMPLEXES

The majority of spectra recorded in this work have been observed using the powder reflectance technique (see data in Table 7.2) which allows studies to be made of solid state effects and avoids the problems associated with recording solution spectra such as aquation of species in aqueous solutions, finding other suitable solvents and the loss of effects in the solid state which lead to distortion of the halogenoiridate(III) anions. The main disadvantages are that the reflectance technique does not give extinction coefficients of absorption bands, it may not give the true positions of absorption band maxima compared to actual absorption spectra[237], and often the bands lose resolution.

The reflectance spectra consist of rather broad absorption bands with poorly defined maxima, with the result that actual positions of band maxima have large errors which may be as high as $\pm$ 500 cm^{-1} and not below $\pm$ 100 cm^{-1}. Resolution and improved band definition in the spectra could not be obtained by diluting samples with reference MgO. The errors preclude the observation of cation effects on band positions for a series of isostructural halogeno complexes (e.g. as in the red shift of bands observed by Jørgensen[224] for compounds containing the $[IrCl_6]^{2-}$ species and the cation effect observed by Sherlock[14] in a series of Rh(IV) monometallate

Table 7.2(a): Powder Reflectance Spectra of a Number of Halogenoiridate(III) and (IV) Salts

Compound	Reflectance Band Maxima (cm^{-1})			
$K_2[IrCl_6]$	17000 m	17200 m	22700 m	
$(NH_4)_2[IrCl_6]$	16900 m	20000 m	24300 m	
$Rb_2[IrCl_6]$	17000 m	19100 m	22700 m	
$Cs_2[IrCl_6]$	17400 m	18900 m	22600 m	
$K_2[IrBr_6]$	11000 m	15600 m		
$Rb_2[IrBr_6]$	11100 m	15700 m		
$Cs_2[IrBr_6]$	12500 m	16800 m	18200 w,sh	24100 w

	I	II	III	IV
$K_3[IrCl_6]H_2O$	18100 mw	24100 m		
$(NH_4)_3[IrCl_6]H_2O$	17800 mw	24000 m		
$Rb_3[IrCl_6]H_2O$	17900 mw	23800 m	27800 mw	
$Cs_3[IrCl_6]H_2O$	17700 mw	23600 m	27800 mw	
$[Co(NH_3)_6][IrCl_6]$	17000 mw,sh	20800 m,sh	25800 m,sh	
$Rb_2[IrCl_5(H_2O)]$	18000 mw	24000 m		
$Cs_2[IrCl_5(H_2O)]$	17400 w, sh	19400 mw	23600 m	
$(H_3O)K_8[IrBr_6]_3 9H_2O$	11700	16400	22100 m	25800 mw
$(NH_4)_3[IrBr_6]H_2O$			23800	
$Rb_3[IrBr_6]H_2O$		16500	21900 m	25600 mw
$Cs_3[IrBr_6]H_2O$	1270	16400	21900 m	25200 mw
$[Co(NH_3)_6][IrBr_6]$	11700	16800	23100 mw,sh	26400 m,sh
$Rb_3[Ir_2Br_9]$			18200 mw,sh	22800 m
$Cs_3[Ir_2Br_9]$	1270	17200	19300 mw,sh	23800 m

m - medium, mw - medium weak, w - weak, sh-shoulder.

(b) Aqueous Solution Visible and Near Ultraviolet Region Spectra for $K_2[IrBr_6]$ and $(H_3O)K_8[IrBr_6]_3 9H_2O$.

Compound	Concentration (M)	Absorption Band Maxima (cm^{-1}) (Extinction coefficients in parentheses ($M^{-1}cm^{-1}$))		
$K_2[IrBr_6]$	0.000089	13700(2700)	14490(3600)	14790(3700)
		17150(5700)	18400(2800)	19590(3300)
$(H_3O)K_8[IrBr_6]_3 9H_2O$	0.0014	23010(210)	26700(170)	

and dimetallate halogeno compounds) as the band positions observed do not show significant differences between one another.

7.2.1 The Visible and Ultraviolet Spectra of Halogenoiridates(IV)

The reflectance bands observed for the hexahalogenoiridate(IV) complexes studied in this work are assigned to $L(\pi) \rightarrow Ir(5d)$ charge transfer transitions. The results show reasonable agreement with values reported in the literature and the aqueous solution spectrum of the $[IrBr_6]^{2-}$ species agrees with that recorded by Jørgensen[54] in 0.1 MHBr. Some of the bands observed in the solution spectrum of the $[IrBr_6]^{2-}$ species were not resolved in the reflectance spectra of the K^+, Rb^+ and Cs^+ salts.

7.2.2 The Visible and Ultraviolet Spectra of Halogenoiridates(III)

The reflectance spectra of the hexachloroiridates(III) of K^+, NH_4^+, Rb^+ and Cs^+ show either two or three absorption maxima which may be assigned to the following transitions: Band I, 17000 cm^{-1} to 18100 cm^{-1}, either to the $^3T_{1g} \leftarrow {}^1A_{1g}$ transition or the $^3T_{2g} \leftarrow {}^1A_{1g}$ transition (both spin forbidden), Band II, 23600 cm^{-1} to 24100 cm^{-1} to the $^1T_{1g} \leftarrow {}^1A_{1g}$ transition and Band III, 27800 cm^{-1} to the $^1T_{2g} \leftarrow {}^1A_{1g}$ transition (the latter two transitions are both spin allowed). The assignments are based on the positions of bands and

the magnitude of extinction coefficients reported by Jørgensen[51] for $[IrCl_6]^{3-}$ in 4M HCl and other $[IrCl_{6-n}(H_2O)_n]^{3-n}$ species[226] and Co(III) d^6 low spin complexes[231]. These assignments disagree with those made by Zipp and Madan[44] for $[N(CH_2CH_2NH_3)_3][IrCl_6]3H_2O$ who assign bands at 19600 cm^{-1} and 23200 cm^{-1} to the $^1T_{1g} \leftarrow {}^1A_{1g}$ and $^1T_{2g} \leftarrow {}^1A_{1g}$ transitions respectively (although the assignments reported in Table III of their paper[44], where both bands are assigned to the $^1T_{1g} \leftarrow {}^1A_{1g}$ transition, do not agree with their text).

The reflectance spectrum of $[Co(NH_3)_6][IrCl_6]$ contains three bands as shoulders on a broad absorption in the ultraviolet region; these presumably arise from both the Co(III) and Ir(III) chromophores. Assignments have not been attempted because of the poor resolution in the spectra.

Both the Rb^+ and Cs^+ salts of the $[IrCl_5(H_2O)]^{2-}$ ion have similar reflectance spectra to the absorption spectra of the $[IrCl_5(H_2O)]^{2-}$ species in aqueous solution reported by Jørgensen[226]. The spectra are similar to those of their hexachloroiridate(III) salts which is to be expected. However, when two or more chlorine ligands in the $[IrCl_6]^{3-}$ have been substituted by water molecules the spin allowed transitions move to a higher energy (see Table 7.1).

The reflectance spectra of the bromoiridates(III) of K^+, Rb^+, NH_4^+ and Cs^+ contain both bands arising from the spin allowed $^1T_{1g} \leftarrow {}^1A_{1g}$ and $^1T_{2g} \leftarrow {}^1A_{1g}$ transitions (at approximately 22000 cm^{-1} and 25500 cm^{-1}) except in the case

of $(NH_4)_3[IrCl_6]H_2O$ where only one very broad band and a plateau are observed near 23800 cm^{-1}. The bands show the expected red shift when chlorine ligands are replaced by bromine ligands on the basis of the lower ligand field strength of the bromide ligand. The assignments are based on the band positions and extinction coefficients determined in this work for an aqueous solution of $(H_3O)K_8[IrBr_6]_3 9H_2O$ and from spectra reported in the literature[51,226]. As for the chloro complexes the assignment made by Zipp and Madan[44] for $[N(CH_2CH_2NH_3)_3][IrBr_6]H_2O$ disagrees with the above. Bands observed in the spectra around 12000 cm^{-1} and 16500 cm^{-1} in the bromoiridates (in this work) may be assigned to charge transfer bands arising from the presence of impurities of $[IrBr_6]^{2-}$ salts (for which bands are observed in the regions 11,000 cm^{-1} to 12000 cm^{-1} and 15600 cm^{-1} to 16800 cm^{-1}, also see page 29) and one of the bands i.e. the band at approximately 16500 cm^{-1} could possibly arise from a spin forbidden $^3T_{2g} \leftarrow {}^1A_{1g}$ transition which is observed at 16800 cm^{-1} for $[IrBr_6]^{3-}$ in 4M HBr[51] and at 17100 cm^{-1} for $[IrBr_6]^{3-}$ in aqueous solution[226].

7.2.3 Visible and Ultraviolet Absorption Spectra of Bromodiiridates(III)

The relationship between the electronic spectra of hexahalogenometallate(III) and nonahalogenodimetallate(III) complexes has been investigated by a number of authors[108,233-236,238].

For dimetallate(III) complexes such as $[Cr_2Cl_9]^{3-}$, $[V_2Cl_9]^{3-}$, $[Ti_2Cl_9]^{3-}$ and $[Mo_2Cl_9]^{3-}$ where some or no metal-metal bonding occurs in the dimetallate anions the spectra are found to resemble those of their hexachloro and pentachloroaquametallate(III) counterparts as regards band maxima positions (see Table 7.1). However, extinction coefficients of absorption bands of dimetallate complexes are somewhat larger than those of their monometallate counterparts (by a factor of 20 for example for Mo complexes). In the case of dimetallate complexes where there is a large degree of metal-metal bonding (e.g. in the $[W_2Cl_9]^{3-}$ species) the extinction coefficients of absorption bands of these species are even higher and assignments based on d^3 octahedral ligand field considerations are inadequate. Observed bands must result from transitions between d orbitals which are extensively delocalised between the two tungsten atoms[236].

In the bromodiiridate(III) complexes where structural data (see Section 4.6) suggest there is no Ir-Ir bonding interaction in the diiridate(III) anion, the reflectance bands at 22800 cm^{-1} and 23800 cm^{-1} for the rubidium and caesium salts respectively are similar to the bands at 21900 cm^{-1} and 21900 cm^{-1} for the Rb^+ and Cs^+ hexabromoiridate (III) salts respectively. Unfortunately extinction coefficient data is not available for these complexes, and furthermore one absorption band expected at about 25500 cm^{-1} is obscured by a strong charge transfer band whose maximum occurs at > 28000 cm^{-1}. On the basis of the band positions the present

data confirms that there is little or no Ir-Ir bonding in the diiridate(III) anions.

The foregoing assignments of the spectra of the halogenoiridate(III) complexes have been made using a simple octahedral ligand field theory model for a d^6 spin paired electronic configuration of the Ir(III) species. The small but significant distortions from regular octahedral and other ideal molecular point symmetries found in some of the halogenoiridate(III) anions in the solid state have been ignored in these first order assignations. It could be expected that distortions from ideal molecular point symmetries will be evident in the visible spectra (e.g. as has been observed in the spectra of some dimolybdate (III) species where predicted bands are split[238]) but in the present studies the effect of small distortions are not readily discernable especially in view of the broadness and poor definition of many of the absorption bands observed for the compounds in the solid state. In solution these distortions may not be occurring and therefore low temperature single crystal spectra are necessary for a detailed investigation.

CHAPTER 8

CONCLUSION

The present studies have revealed that the hexahalogeno-metallate complexes of iridium(III) and (IV) display related chemical and structural properties to analogous complexes of other transition, and in some cases, non transition metal ions. In this short summary some of the more general results that have arisen out of the present work and that have not been covered in the preceding chapters will be discussed.

Preparative studies (Chapter 2) indicate that the chemistry of Rh(III) and Ir(III) halogeno complexes in aqueous or hydrohalic acid media is similar[14] (as would be expected on the basis of their t_{2g}^6 electron configurations) although some significant differences do occur, such as the ready atmospheric oxidation of Ir(III) to Ir(IV) in aqueous solution while the corresponding oxidation of Rh(III) to Rh(IV) is difficult to achieve,[239] and the instability of $[Ir_2Br_9]^{3-}$ (i.e. reversion to the hexabromoiridate(III) species in hydrohalic acid media) compared to its rhodium analogue. The Ir(III) complexes have properties divergent to those of similar 1st row transition metal ion complexes. Such differences are exemplified by the mode of preparation of the 1st row transition metal complex ions $[MCl_6]^{3-}$ and $[M_2Cl_9]^{3-}$; these complex ions are often prepared at high temperatures ($\approx 800^{o}C$). In contrast the complex ions of

2nd and 3rd row transition metals can normally be isolated from hydrohalic solutions of sufficiently high metallate concentrations. Isolation is, in some cases, only achieved by the formation of insoluble salts with high lattice energies, and when the anion is associated with large cations (in a few cases the $[MCl_6]^{3-}$ species of 1st row transition metal ions have also been isolated in this manner[1,67,240,241]).

Both trivalent iridium and rhodium bromo dimetallate $[M_2Br_9]^{3-}$ species can be isolated in the solid state from hydrobromic acid solutions. The preparation of diiridate(III) complexes may proceed through intermediates, such as pentabromoaqua or hexabromometallate ions, as postulated for related transition metal and non transition metal ion systems[193,263,264]. To date the dimetallate anion has not been found for the first member of the triad Co, Rh and Ir and in the case of the Fe, Ru and Os triad there have been no reports of a dimetallate ion for the latter metal i.e. osmium. If such a species was to be formed it would probably have some metal-metal bonding as is found in the ruthenium bromodimetallate complexes[13].

The halogeno complexes of Ru and Ir both show complex redox equilibria between M(IV) and M(III) oxidation states in hydrohalic acid media the effect being more marked in the case of ruthenium[13]. Rhodium, on the other hand, shows no such properties. Thus, with an increase in the involvement of redox equilibria in the solution halogeno chemistries from Rh to Ru and from Rh to Ir in the tetrad of

heavy transition metals Ru, Rh, Os and Ir, it might be expected that osmium halogeno complexes in solution would show an even greater involvement in such complex redox equilibria. This could explain the difficulty encountered in attempts to isolate Os(III) complexes from electrolytic and chemically reduced Os(IV) hydrohalic acid solutions.[265]

The structural isomorphism (or isostructural relationships) between iridate(III) and iridate(IV) and other halogenometallate complexes may in some cases be attributed to the compounds containing metal ions of approximately the same size, the same valence d electron configuration and similar chemical properties (e.g. as in the case of Rh(III) and Ir(III) complexes). However, in other cases, for example the isomorphism between individual members of the three series of halogeno complexes of stoichiometry $A_2[MX_6]$, $A_2[MCl_5(H_2O)]$ and $A_3[M_2X_9]$ (A = univalent cation, M = transition or non transition metal and X = Cl, Br), this is probably "due to geometrical requirements of the structures rather than to chemical similarities of the elements" as suggested by Powell and Wells in 1935[61]. Furthermore, in these three series of salts, bonding within a series of complex anions will vary depending upon the d electron configuration of the metal ion present. For example electron spin resonance studies suggest π bonding ($Cl(p_x,p_y) \rightarrow Fe(t_{2g}^5)$) is involved in the $[FeCl_5(H_2O)]^{2-}$ anion[242] but this is not accessible to Ir(III) (t_{2g}^6) in the $[IrCl_5(H_2O)]^{2-}$ anion. In a series of $[MCl_6]^{2-}$ complexes (M = Pt, Ir, Os, Re) variations within both NQR and infrared data may be interpreted in terms of the bonding

within the $[MCl_6]^{2-}$ anions which is a function of the metal ion present and in particular of the d^n configuration[99].

The formation of the different structural types for the iridium complexes discussed in this work is dependent on a number of interrelated factors including the stoichiometry (partially dictated by oxidation state), differences in cation and anion sizes and the presence of water of crystallisation which is performing a space filling role in the crystal lattice. In contrast to the amount of structural data available for Rh(III) and Ir(III) complexes, the limited data on Ru(III) and Os(III) complexes reflects the problems in obtaining halogeno compounds of these metal ions. The M(IV) salts $A_2[MX_6]$ (X = Cl, Br; Cl only for Rh; M = Ru, Rh, Os, Ir), on the other hand, are known to be isomorphous and are readily prepared (except for rhodium complexes)[13,239,243].

The distortions found in the hexahalogenoiridate(III) anions in the crystal structures of some of the complexes prepared in this work have manifested themselves in the infrared and NQR spectra but not the ultraviolet-visible spectra. The complexity of the infrared spectra has been attributed to solid state effects. The interpretation of infrared spectra of other halogenometallate complexes[69,111, 173,174,175] have often not included consideration of such effects. This present work has indicated that this is necessary.

CHAPTER 9

EXPERIMENTAL PROCEDURES IN X-RAY STRUCTURE DETERMINATION AND PHYSIO-CHEMICAL METHODS USED

9.1 INTRODUCTION

A number of physical methods have been used to study the complexes prepared in the present work. In this chapter the experimental methods and techniques used will be briefly discussed. The first section of the chapter will outline the experimental techniques and calculation methods used in X-ray crystal structure determinations and the second section will cover the remaining physical techniques.

9.2 EXPERIMENTAL PROCEDURES IN X-RAY STRUCTURE DETERMINATION

9.2.1 (i) Preliminary Studies

Preliminary photographic studies were carried out on single crystals using Weissenberg and Buerger precession cameras and approximate cell dimensions and possible space groups were determined. Densities of crystals were determined by floatation in liquids of equal density obtained by mixing suitable pairs of pure liquids e.g. CH_2I_2, density 3.315 to 3.325 gcm^{-3} and CH_2BrCH_2Br, density 2.17 g cm^{-3}. Choice of crystals of quality suitable for data collection was on the basis of their precession photographs. Single crystals were mounted on

goniometer heads in random orientations to minimise the incidence of multiple reflections[244].

9.2.1 (ii) Intensity Data Collection

Before mounting the goniometer head on the computer controlled (PDP8/f) four circle diffractometer, precession setting photographs were recorded and two or more low angle reflections (orienting reflections) were indexed. The crystal was then mounted on the diffractometer and manually centred using the diffractometer telescope.

An approximate orientation matrix was calculated using the four circle setting angles of the orienting reflections. The four circle setting angles of twelve high angle reflections ($\theta > 10^{\circ}$ for MoKα radiation) were determined accurately using an automatic centring procedure supplied with the Hilger and Watts software. The cell dimensions and the four circle setting angles of two orientation defining reflections were refined by the method of least squares[245], using the four circle setting angles of the twelve accurately centred reflections. Refinement was continued until the errors between the calculated and observed setting angles of the twelve reflections were less than 0.03° and the estimated standard deviations of the orientation defining reflections' angles were less than 0.01°. Cell dimensions obtained in this manner usually had an error of the order of 0.015%. The orientation matrix for use in data collection was then calculated using the refined four circle angles of the two orientation defining

reflections (and their respective indices).

The mosaicity of the crystal was checked by executing a number of open counter ω scans[246] on strong low angle reflections and recording their width (in degrees) at half peak height. With a tube take off angle of 3° acceptable mosaicity values lay in the range 0.05° to 0.2°. In some structures data were collected on crystals with mosaicity values slightly higher than 0.2°.

Intensity data were collected automatically using the θ-2θ scan technique (bisecting mode geometry). These symmetric scans were executed over experimentally determined scan ranges stepping 0.02° in θ and 0.01° in ω from θ and ω values offset from their calculated positions (assuming Kα radiation) by $-0.1n^{\circ}$ and $-0.05n^{\circ}$ respectively (where n is the number of steps in the scan range). Stationary counter stationary crystal background counts were made at either end of these scans. The X-radiation used was filtered with an appropriate filter.

The intensities of three "standard reflections", well separated in reciprocal space were measured after every block of 50 reflections had been collected, to check for any systematic variations occurring during data collection e.g. crystal decomposition or crystal movement. For very strong reflections whose count rates exceeded the linear response range of the scintillation counter detector (8,000 counts per second), the incident beam was attenuated with nickel foils. Corrections were applied to observed intensities so attenuated using empirically determined

attenuator factors (normally the average attenuator factor of those measured for three different reflections).

9.2.2 Data Reduction, Structure Solution and Refinement Procedures

9.2.2 (i) Intensity Data Reduction

Intensity data recorded by the diffractometer were processed in the manner described by Corfield, Doedens and Ibers[247]. The integrated intensity, I, was given by

$$I = [C - 2(B_1 + B_2)] \times \text{attenuator factor}$$

where C is the total count for the step scan and B_1 and B_2 are the totals for the two background counts. A standard deviation $\sigma(I)$, was assigned each reflection on the basis of counting statistics such that

$$\sigma(I) = [C + (B_1 + B_2) + (pI)^2]^{\frac{1}{2}}$$

where p is an empirical factor to prevent overweighting of strong reflections[248]. Intensities were corrected for Lorentz and polarisation effects to finally yield values of F^2_{obs} and $\sigma(F^2_{obs})$, where F_{obs} is the observed structure factor amplitude.

In some structure determinations discussed in this thesis equivalent forms of data were collected. In these cases F^2_{obs} values were averaged and the standard deviations

of the averaged result calculated by taking the average of the two standard deviations of the equivalent forms, or by estimating a standard deviation based on the range of the F^2_{obs} values of the equivalent forms, whichever was the larger[247]. These estimated standard deviations were then multiplied by $(N/NEQ)^{\frac{1}{2}}$ where N was the number of equivalent sets of reflections collected and NEQ was the number of times a reflection was actually observed[249].

Corrections for crystal absorption were applied to all data sets. This was achieved using a numerical Gaussian integration method (using programme DABS) or by a more accurate analytical method (using programme ABSORB) based on that of Demeulenaer and Tompa[250].

9.2.2(ii) Structure Solution and Refinement Procedures

The crystal structures described in this thesis were solved by standard crystallographic techniques using either Patterson syntheses or direct methods combined with Fourier techniques and full matrix least squares refinements. These procedures will not be discussed in detail but reference will be made to the more important computer programmes used by the author to perform these tasks.

The majority of computing work in structures analyses was made using the X-ray crystallographic programmes developed over a period of years in the Chemistry Department at this University. Use was also made of an integrated crystallographic programme package SHELX76[251].

Fourier Syntheses Fourier syntheses were performed using the crystallographic programme FOURIER, a modified and extended version of FORDAP, written by A. Zalkin[252]. By using different functions of structure factors as coefficients in these syntheses, three dimensional Patterson maps, observed electron density maps and difference electron density (difference fourier) maps could be produced. These three dimensional syntheses were calculated with points being sampled at regular intervals of about 0.3Å, on lines parallel to unit cell axes. Peak positions and heights were then determined by an interpolation routine.

Direct Methods The automatic centrosymmetric phase determining procedure contained within SHELX76 (instruction EEES) was used to solve the crystal structure of $Rb_3[IrBr_6]H_2O$ and yielded the solution without any difficulty.

Least Squares Refinements

Two programmes were used to perform least squares refinements. The most frequently used was CUCLS, a highly modified version of ORFLS[253]. The least squares refinement programme in SHELX76 was used in some cases because of the greater flexibility it allowed in applying constraints to parameters. Both of these programmes minimise the weighted sum of the squares of the differences between the observed (F_{obs}) and calculated (F_{calc}) structure factor amplitudes (i.e. $\sum w\,[|F_{obs}| - |F_{calc}|]^2$) and produce the conventional R factors (residuals)

$$R = \sum' ||F_{obs}| - |F_{calc}|| / |F_{obs}|$$

and

$$R_w = [\sum w(|F_{obs}| - |F_{calc}|)^2 / \sum w|F_{obs}|^2]^{\frac{1}{2}}$$

where w is the weight such that

$$w = 4\ F_{obs}^2 / [\sigma(F_{obs}^2)]^2$$

The general expression for calculating the structure factor, F_{calc}, is

$$F_{calc}(S) = \sum_{j=1}^{N} f_j(S) T_j(S) \exp(2\pi i S r_j)$$

where $f_j(S)$ is the atomic scattering factor, $T_j(S)$ is a function describing the thermal motion of the jth atom, r_j is the vector (in real space) representing the position of the jth atom and S is the scattering vector (in reciprocal space). Both refinement programmes used atomic scattering factors from Cromer and Mann[254], and corrections for anomalous dispersion (both the real and imaginary components) obtained from Cromer[255] and Cromer and Liberman[256]. Atoms were assumed to be vibrating in harmonic potential fields and were assigned isotropic or anisotropic thermal parameters. The expression for the isotropic case is

$$T_j(S) = \exp(-8\pi^2 U \sin^2\theta/\lambda^2)$$

where U (or U_{iso}) is the isotropic temperature factor in $Å^2$ (the mean square amplitude of vibration). For the anisotropic case the expression for $T_j(S)$ is

$$T_j(S) = \exp[-2\pi^2(h^2a^{*2}U_{11}+k^2b^{*2}U_{22}+\ell^2c^{*2}U_{33}+2hka^*b^*U_{12} + 2h\ell a^*c^*U_{13} + 2k\ell b^*c^*U_{23})]$$

where U_{ij} are elements of the tensor U describing the anisotropic thermal motion in terms of mean square amplitudes of vibration ($Å^2$).

The necessary constraints to be applied to thermal parameters (U_{ij}) of atoms located on special positions during least squares refinement were determined using the data provided by Levy [257] and Peterse and Palm[258].

The empirical p factor (incorporated in the weighting scheme in the assignment of standard deviations of reflections) was determined on the basis of the differences between the observed and calculated structure factor magnitudes. These differences were analysed for various ranges of sin θ/λ, structure factor magnitudes and reflection indices to ensure such errors were independent of these parameters. If this was not the case the p factor was changed.

Structural diagrams were drawn using the programme ORTEP2, a highly modified version of the programme ORTEP [259].

9.3 PHYSICAL METHODS

9.3.1 Infrared Spectroscopy

(i) High Frequency Infrared Spectroscopy

The infrared spectra of compounds in the region 4000 cm^{-1} to 400 cm^{-1} were recorded using a Shimadzu IR 27G grating spectrophotometer with samples examined as nujol mulls or as KBr discs. The spectra were calibrated with polystyrene film and the experimental uncertainty was of the order of $\pm$ 5 cm^{-1}.

(ii) Low Frequency Infrared Spectroscopy

The infrared spectra of compounds in the region 400 cm^{-1} to 40 cm^{-1} were recorded using a RIIC FS720 Michelson Interferometer containing a mercury source lamp and a Golay pneumatic detector. Samples were prepared as nujol mulls (dried nujol) mounted on polythene discs. Both room temperature (296 ($\pm$ 2)^{o}K) and low temperature (179 ($\pm$ 5)^{o}K) spectra (using an apparatus described elsewhere[13]) were recorded on two samples of each compound, one containing a small amount of sample (a thin mull) and the other containing a greater quantity of sample (a thick mull). This was done primarily to check the reproducibility of the final spectra obtained.

One thousand data points (500 data points either side of the interferogram maximum) were collected for the interferogram of each sample, with a sampling interval of 8 microns giving a theoretical resolution of 2.5 cm^{-1}. The fourier transformation of this data to produce the usual absorption versus frequency

spectrum was obtained by subtracting the spectrum obtained for the background (i.e. absorption due to the mylar beam splitter and the polythene disc) from that spectrum obtained for a particular sample. The experimental uncertainty in observed frequencies was $\pm$ 5 cm^{-1}.

9.3.2 Laser Raman Spectroscopy

Powdered samples of compounds were examined by Laser Raman Spectroscopy using equipment in the Physics Department of this University. A Spectra Physics Argon Ion Laser Raman exciting source was used and the scattered Raman radiation was analysed using a Jarrell Ash Czerny-Turner Scanning Spectrometer-Spectrograph. Spectra were recorded using a number of laser lines (4727Å, 4765Å, 4965Å) primarily to check the origins of observed scattered lines (and that these lines were in fact Raman lines) as for some higher energy exciting laser lines (e.g. 4727Å) fluorescence emissions of the compounds were observed.

Samples of the powdered compound were pressed (using a hydraulic press) into a rectangular annular depression (2 mm wide and 0.5 mm deep) of diameter 37 mm on a disc 43 mm in diameter. The back surface of the annular groove was coated with a suitable varnish to aid attachment of sample material to the disc. The disc was attached to a variable speed motor mounted on a firm base, and by use of suitable adjustment slides the rotating disc was set at an angle of 45^{o} to the incident laser beam. The scattered radiation was then observed with the spectrometer

perpendicular to the direction of the beam incident on the rotating disc (and also at 45° to the disc). The sample temperature was of the order of 35°C (± 5°C). The typical experimental conditions were laser power of 0.3 W, sample rotation of the order of 1000 revolutions/minute, slits 120/120/120 microns, scanning rate of 20 cm^{-1}/minute, time constant $\tau = 1$, and a gain of 3×10^3. Plasma line filters were not used and reported spectra have been thoroughly checked to ensure such lines are not present. The assistance of Chris Tomblin in this work is gratefully acknowledged.

9.3.3 Electronic Spectra

Electronic spectra of solutions were recorded using a Varian Techtron 635 spectrophotometer (220 nm - 800 nm) and on solid samples using a Beckman DK2 spectrophotometer employing a special reflectance attachment. Solid samples were in some cases diluted with reference A.R. magnesium oxide.

9.3.4 Atomic Absorption Analyses

Atomic Absorption analyses were performed on a Varian Techtron A.A.5 instrument with experimental conditions as outlined in the manual supplied by the instrument's manufacturers.

9.3.5 X-ray Powder Diffraction

(i) Powder Photography X-ray powder diffraction photographs have been recorded for all iridium compounds

prepared in this work using a Debye-Scherrer camera of internal radius 57.30 mm. These photographs were recorded with Cu(Ni filtered) Kα radiation and were used extensively in compound characterisation. The A.S.T.M. Powder Diffraction File has also been used to examine reported powder diffraction patterns of some compounds.

(ii) Powder Diffractometry X-ray diffractograms were recorded for a number of iridium(III) compounds primarily for determination of cell dimensions of compounds crystallising in cubic or hexagonal crystal systems. A Phillips PW 1050/25 goniometer was used for this purpose with either CuKα ($K\alpha_1$, λ = 1.5405Å) or FeKα ($K\alpha_1$, λ = 1.9737 Å) radiation.

In the determination of cell dimensions a finely ground sample of compound was intimately mixed with about one eighth by volume of ground A.R. potassium chloride and distributed uniformly on a glass slide using acetone as a wetting agent. Having determined approximate reflection peak positions in a rapid scan of the spectrum, slow scans of 1/8° per minute were executed for each reflection to allow accurate measurement of the central maxima of the peak from the diffracted beam. The peak positions of the 200 and 220 reflections for KCl were accurately measured. A calibration curve was constructed (of $\Delta 2\theta$(2θ (theoretical KCl) - 2θ (experimental KCl)) versus 2θ (experimental)) to correct all reflections for any systematic errors arising in the sample thickness or instrument error, using theoretically expected 2θ values for the two KCl reflections

(for CuKα (FeKα) radiation 200 reflection, 2θ = 28.3398 (35.8281); 220 reflection, 2θ = 40.5098 (51.5704) respectively; from cell data for KCl in reference[260]). Reflections whose 2θ values lay within the 2θ angles range of the 200 and 220 KCl reflections in this linear calibration plot, were given full weight (and those outside these ranges were given half weight) in the subsequent least squares refinements.

Least squares refinements of cell dimensions (normally using cell data from isomorphous compounds as initial approximations) were then executed using the computer programme POWDER[261] with the corrected 2θ reflection angles as observed data. Refinement normally produced differences between calculated 2θ angles and observed 2θ angles of about 0.1° but in many cases errors were lower than this e.g. 0.03°. The programme also calculates estimated standard deviations for the cell dimensions, and these are reported with cell dimension data (as an error in the least significant digit(s) in parentheses) in the text.

The assistance of Dr A.J. Campbell in this work is gratefully acknowledged.

9.3.6 Low Temperature Single Crystal X-ray Diffraction

The studies reported in Chapter 6 were performed using an AC-1-101A Cryo-Tip refrigerator unit mounted on a goniometer head; the equipment being supplied by the Advanced Products Department, Air Products and Chemicals Incorporated. The small cryostat uses the Joule-Thomson effect to cool a copper

wire to which the single crystal under study was glued, and was capable of producing temperatures down to liquid nitrogen temperatures with an accuracy of $\pm$ 2°C. The gonimeter head was placed on a Stoe Buerger precession camera (F = 60 mm). Measurements for $K_3[IrCl_6]H_2O$ and $K_3[RhCl_6]H_2O$ were made using Polaroid film (Polapan 4 x 5 Land Film); the study of $(NH_4)_3[IrCl_6]H_2O$ was made using wet film (Kodak Kodirex KD54), for which no corrections for shrinkage were made. Measurements from the zero level photographs recorded were made using a Supper measuring device (Model 280).

9.3.7 Differential Thermal Analyses

(i) High Temperature The differential thermal analyses performed on $A_2[IrCl_5(H_2O)]$ complexes (reported in Chapter 2) were made using an Aminco Thermoanalyser under a nitrogen (oxygen free) atmosphere (60 ml/minute) and a heating rate of 12°C/minute. A reference sample containing 160 mg of kaolinite clay was used and the sample under study contained 50 mg of pentachloroaqua complex, 110 mg of kaolinite and 10 mg of quartz calibrant. Icewater (0°C) and the phase transition in quartz at 573°C were used to calibrate the recorded spectra. The assistance of Dr A.J. Campbell in this work is gratefully acknowledged.

(ii) Low Temperature Low temperature differential thermal analyses on $(NH_4)_3[IrCl_6]H_2O$ (reported in Chapter 6) were performed using a Newport Instruments Cryostat Controller attached to a

Variable Temperature Gouy balance. Temperatures recorded down to liquid nitrogen temperature were accurate to $\pm$ 2°C.

Approximately 1 g of finely ground sample was placed in one compartment of a two compartment sample tube (each cell approximately 10 mm x 2 mm); the other compartment was packed in a similar fashion with α-Al_2O_3 as a reference. Copper-constantan thermocouples were embedded in each sample and attached to a Keithley Instruments 155 Null Detector Microvoltmeter capable of detecting 1μV. The sample tube was suspended in the cryostat and cooled at the rate of 9°C per minute. Readings on the microvoltmeter were made every degree. At temperatures below -80°C (193°K), the vacuum in the liquid nitrogen dewar was removed, to allow maintenance of a sufficiently rapid cooling rate. This resulted in a discontinuity in the e.m.f./temperature plot as revealed in Figure 6.4.2.

9.3.8 Lattice Energy Calculations and Calculation of a Madelung Constant Function

A function of Madelung constant, f(m), given by equation (9.3.1) was evaluated for the cubic $K_2[PtCl_6]$ and $Cs_3[CoF_6]$ structural types using a point charge model.

$$f(M) = \sum_{i=1}^{N} \frac{z_i}{r_i} \qquad (9.3.1)$$

where z_i is the ionic charge of an anion or cation

r_i is the distance of the respective anion or cation from the origin $[M X_6]^{n-}$ anion.

Use of this calculated function in equation (9.3.2) yields the lattice energy, U, for the structure under consideration

$$U = \frac{-aN_A e^2}{4\pi\varepsilon_o}\left[\sum_{i=1}^{N}\frac{z_i}{r_i}\right](1 - \frac{1}{n}) \qquad (9.3.2)$$

where parameters a and n and constants N_A, e and ε_o are as defined in equation (3.7.1). The terms $\frac{z_i}{r_i}$ in equation (9.3.1) constitute an electrically neutral set of cations and anions surrounding an $[M X_6]^{a-}$ anion located at an origin. This set was composed of ions contained within a cube of 21952 (28^3) unit cells with the origin at the centre of this cube. Although a large number of ions were therefore included in these calculations (263424 for $K_2[PtCl_6]$ and 351232 for $Cs_3[KoF_6]$ structural types respectively) the summation showed poor convergence towards the theoretical value of the Madelung constant M for the $K_2[PtCl_6]$ structure in whose case M is derived from the Madelung constant function by

$$M = f(M)r_o \qquad (9.3.3)$$

where r_o is the distance from the origin to the closest potassium ion.

9.3.8 Force Constant Calculations

Force constant calculations were performed using a programme written by Dr R.G.A.R. Maclagan of this Departmnet, based on a programme reported by W.D. Gwinn[262]. The

method involves use of mass weighted cartesian coordinates and force constants of a Simple Valence Force Field (SVFF) and calculates frequencies of normal vibrations and a coefficient matrix and potential energy matrix; the coefficient matrix allows examination of the individual motions of atoms for particular vibration species.

REFERENCES

1. M.G.B. Drew, D.A. Rice and C.W. Timewell, Inorg. Chem. Letters, 7 (1971), 59.
2. P.J. Cresswell, J.E. Fergusson, B.R. Penfold and D.E. Scaife, J. Chem. Soc. Dalton Trans., (1972), 254.
3. P. Murray-Rust and J. Murray-Rust, Acta. Cryst., B31 (1975), 1037.
4. J. Coetzer, W. Robb and P. v Z. Bekker, Acta. Cryst., B28(1972), 3587.
5. T.E. Hopkins, A. Zalkin, D.H. Templeton and M.G. Adamson, Inorg. Chem., 5 (1966), 1431.
6. T.S. Khodashova, J. Struct. Chem. U.S.S.R., Eng. Transl., 1 (1960), 308.
7. C.K. Thomas and J.A. Stanko, J. Coord. Chem., 2 (1973), 231.
8. J.E. Fergusson and R.R. Sherlock, Aust. J. Chem., 30 (1977), 1445.
9. C.K. Thomas and J.A. Stanko, J. Coord. Chem., 3 (1973), 211.
10. T.E. Hopkins, A. Zalkin, D.H. Templeton and M.G. Adamson, Inorg. Chem., 5 (1966), 1427.
11. F.A. Cotton and D.A. Ucko, Inorg. Chim. Acta., 6 (1972), 161.
12. B.R. James and G. Rosenberg, Coord. Chem. Revs., 16 (1975), 153.
13. A.M. Greenaway, Ph.D. Thesis, University of Canterbury, New Zealand, 1976.
14. R.R. Sherlock, M.Sc. Thesis, University of Canterbury, New Zealand, 1976.
15. M. Delépine, Compt. Rend., 147 (1908), 118.
16. M. Delépine, Ann. Chim., 7 (1917), 277.
17. A. Joly, Compt. Rend., 110 (1890), 1131.
18. E. Leidé, Compt. Rend., 129 (1899), 1249.
19. M. Delépine, P. Boussi, Bull. Soc. Chim. France, 23 (1918), 278.
20. V. Norman and J.C. Morrow, J. Chem. Phys., 31 (1959), 455.
21. G. Brauer, 'Handbook of Preparative Inorganic Chemistry', 2nd Edition, Academic Press, New York, 1963-1965.

22. Sho-Chow Woo and D.M. Yost, J. Am. Chem. Soc., 53 (1931), 884.

23. A.D. Westland and N.C. Bhiwandker, Canad. J. Chem., 39 (1961), 2353.

24. I.A. Poulsen and C.S. Garner, J. Am. Chem. Soc., 84 (1962), 2032.

25. E.N. Sloth and C.S. Garner, J. Chem. Phys., 22 (1954), 2064.

26. G.B. Kauffman and L.A. Teter, Inorg. Synth., 8 (1966), 223.

27. G. Pannetier and D. Macarovici, J. Thermal Analysis, 4(1972), 187.

28. D.A. Kelly and M.L. Good, Spectrochimica Acta., 28A (1972), 1529.

29. J.C. Chang and C.S. Garner, Inorg. Chem., 4 (1965), 209.

30. Chem. Abstr. 73:115856h; Y.N. Kukushkin and M.S. Soboleva, Zh. Neorg. Khim., 15 (1970), 2297.

31. E.R. Birnbaum, J. Inorg. Nucl. Chem., 32 (1970), 2009.

32. G. Pannetier, D. Macarovici and M. Gaultier, J. Thermal Analysis, 4 (1972), 177.

33. E. Ogawa, J. Chem. Soc. Japan, 50 (1929), 124.

34. G.W. Watt, E.P. Helvenston and L.E. Sharif, J. Inorg. Nucl. Chem., 24 (1962), 1067.

35. F. Puche, Ann. Chim., 9 (1938), 273.

36. A.F. Trotman-Dickenson (Exec. Ed.), 'A Comprehensive Inorg. Chem.', 3 (1973) ppl265.

37. P.D.F. 22-826.

38. A.G. Sykes and R.N.F. Thorneley, J. Chem. Soc.(A), (1970), 232.

39. W.J. van Ooij and J.P.W. Houtman, Radiochim. Acta., 7 (1967), 115.

40. E. Blasius, W. Preetz and R. Schmitt, J. Inorg. Nucl. Chem., 19 (1961), 115.

41. V.I. Kravtsov and G.M. Petrova, Russ. J. Inorg. Chem., 9 (1964), 552.

42. A.J.P. Domingos, A.M.T.S. Domingos and J.M. Peixoto Cabral, J. Inorg. Nucl. Chem., 31 (1969), 2563.

43. A.A. El-Awady, E.J. Bounsall and C.S. Garner, Inorg. Chem., 6 (1967), 79.

44. S.G. Zipp and S.K. Madan, Inorg. Chim. Acta., 14 (1975), 83.

45. L. Wöhler and P. Balz, Z. Anorg. Allgem. Chem., 149 (1925), 353.

46. W.E. Bell and M. Tagami, J. Phys. Chem., 70 (1966), 640.

47. Von D. Babel and P. Deigner, Z. Anorg. Allgem. Chem., 339 (1965), 57.

48. B.D. Stepin and A.I. Chernyak, Russ. J. Inorg. Chem., 5 (1960), 1047.

49. N.I. Koblin and V.M. Samoilov, Zh. Neorg. Khim., 12 (1967), 2526.

50. M. Delépine, Bull. Soc. Chim. France, (1956), 282.

51. C.K. Jørgensen, Acta. Chem. Scand., 10 (1956), 500.

52. M. Delépine-Tard, Ann. Chim., 4 (1935), 282.

53. G.L. Bottger and A.E. Salwin, Spectrochim. Acta., 28A (1972), 925.

54. C.K. Jørgensen, Acta. Chem. Scand., 10 (1956), 518.

55. Birnbaum, Ann. der Chem., 133 (1865), 161.

56. D.A. Fine, J. Inorg. Nucl. Chem., 32 (1970), 2731.

57. D.A. Fine, Inorg. Chem., 8 (1969), 1014.

58. R.K. Broszkiewicz, J. Chem. Soc. Dalton Trans., (1973), 1799.

59. J.M. Peixoto Cabral, J. Inorg. Nucl. Chem., 26 (1964), 1657.

60. W.J. Van Ooij and J.P.W. Houtman, Radiochim. Acta., 21 (1974), 136.

61. H.M. Powell and A.F. Wells, J. Chem. Soc., (1935), 1008.

62. The Chemical Rubber Company, 'Handbook of Chemistry and Physics', 52nd Edition, 1971-1972, Table 1, D-111.

63. Powder photographs kindly supplied by R.R. Sherlock.

64. R.E. Dodd and P.L. Robinson, 'Experimental Inorganic Chemistry', Elsevier, London, 1954.

65. K. Brodersen, F. Moers and H.G. Schnering, Naturwissenshaften, 52 (1965), 205.

66. H.H. Eysel, Z. Anorg. Allg. Chem., 390 (1972), 210.

67. W.E. Hatfield, R.C. Fay, C.E. Pfluger and T.S. Piper, J. Am. Chem. Soc., 85 (1963), 265.

68. D.R. Schroeder and R.A. Jacobsen, Inorg. Chem., 12 (1973), 210.

69. E. Martineau and J.B. Milne, J. Chem. Soc. (A), (1970), 2971.

70. T. Watanabé, M. Atoji and C. Okazaki, Acta. Cryst., 3 (1950), 405.

71. K. Wieghardt and J. Weiss, Acta. Cryst., B28 (1972), 529.

72. K. Wieghardt and H. Siebert, J. Mol. Struct., 7 (1971), 305.

73. H. Siebert and H.H. Eysel, J. Mol. Struct., 4 (1969), 29.

74. W.E. Dasent, 'Inorganic Energetics', Penguin Books Ltd., England, 1970 .

75. A.F. Kapustinskii, Quarterly Reviews, Chem. Soc. London, 10 (1956), 283.

76. A.J. Lindop, J. Phys. C, Solid State Phys., 3 (1970), 1984.

77. M.C. Ball and A.H. Norbury, 'Physical Data for Inorganic Chemists', Longman Group Ltd., London, 1974.

78. B. Della Valle, E. Martineau, J.B. Milne and T. Birchall, J. Chem. Soc. (A), (1971), 1855.

79. S.L. Lawton, R.A. Jacobsen and R.S. Frye, Inorg. Chem., 10 (1971), 701.

80. S.L. Lawton and R.A. Jacobsen, Inorg. Chem., 10 (1971), 709.

81. J.D.H. Donnay and H.M. Ondik, 'Crystal Data Determinative Tables', Vol. 2, Inorganic Compounds, 3rd Edition, U.S. Department Commerce, National Bureau of Standards and Joint Committee on Powder Diffraction Standards, U.S.A., 1973.

82. R. Saillant, R.B. Jackson, W.E. Streib, K. Folting and R.A.D. Wentworth, Inorg. Chem., 10 (1971), 1453.

83. D.S. Kendal and W.N. Lipscomb, Inorg. Chem., 12 (1973), 546.

84. V.G. Albano and P.L. Bellon, J. Organomet. Chem., 19 (1969), 405.

85. O. Lindqvist, Arkiv. Kemi. Mineral Geol., 24A (1946), 1.

86. I.S. Morozov, G.M. Toptygina and N.P. Lipatova, Russ. J. Inorg. Chem., 6 (1961), 1279.

87. L.P. Podomore and P.W. Smith, Aust. J. Chem., 25 (1972), 2521.

88. H.J. Seifert and H.W. Loh, Inorg. Chem., 5 (1966), 1822.

89. R.W.G. Wyckoff, 'Crystal Structures', Vol. 3, 2nd Edition, Interscience, N.Y., 1965.

90. H.P. Klug, E. Kummer and L. Alexander, J. Am. Chem. Soc., 70 (1948), 3064.

91. P.D.F. 26-380; A. Atkinson, Ph.D. Thesis, City University London, 1968.

92. T. Watanabé and M. Atoji, J. Am. Chem. Soc., 72 (1950) 3819.

93. S.A. Cotton and J.F. Gibson, J. Chem. Soc. (A), (1971), 1693.

94. C.M. Nelson, G.E. Boyd and W.T. Smith, Jnr., J. Am. Chem. Soc., 76 (1954), 348.

95. P.D.F. 9-396.

96. P.D.F. 18-1111

97. P.D.F. 25-648

98. G. Pannetier and D. Macarovici, J. Thermal Analysis, 4 (1972), 193.

99. D.H. Brown, K.R. Dixon, C.M. Livingstone, R.H. Nuttall and D.W.A. Sharp, J. Chem. Soc.(A), (1967), 100.

100. P.D.F. 18-1110.

101. Gmelin Handbuch, 67 (1939), 92.

102. A.Urushiyama,M. Nakahara and Y. Kondo, Bull. Chem. Soc. Japan, 48 (1975), 50.

103. Chem. Abstr., 83: 69481p (1975).

104. E. Adman and T.N. Margulis, Inorg. Chem., 6 (1967), 210.

105. K. Schwochau, Z. Naturforsch., 19a (1964), 1237.

106. E.A. Marseglia and I.D. Brown, Acta. Cryst., B29 (1973), 1352.

107. A. Broll, H.G. Von Schnering and H. Schäfer, J. Less Common Metals, 22 (1970), 243.

108. R. Saillant and R.A.D. Wentworth, Inorg. Chem., 7 (1968), 1606.

109. G.J. Wessel and D.J.W. Ijdo, Acta. Cryst., 10 (1957), 466.

110. I.E. Grey and P.W. Smith, Aust. J. Chem., 24 (1971), 73.

111. I.E. Grey and P.W. Smith, Aust. J. Chem., 22 (1969), 1627.

112. I.E. Grey and P.W. Smith, Aust. J. Chem., 22 (1969), 121.

113. W.H. Watson and J. Waser, Acta. Cryst., 11 (1958), 689.

114. C. Brossett, Nature, 135 (1935), 874.

115. I.I. Kozhina and D.V. Korol'kov, Zh. Strukt. Khim., 6 (1965), 97.

116. O. Lindqvist, Acta. Chem. Scand., 22 (1968), 2943.

117. L. Pauling, Chem. Engng. News, (1947), 2970.

118. J. San Filippo and M.A. Schaefer King, Inorg. Chem., 15 (1976), 1228.

119. A.G. Maddock, R.H. Platt, A.F. Williams and R. Gancedo, J. Chem. Soc. Dalton Trans., (1974), 1314.

120. R. Saillant and R.A.D. Wentworth, Inorg. Chem., 7 (1968), 1606.

121. R. Saillant and R.A.D. Wentworth, Inorg. Chem., 8 (1969), 1226.

122. I.E. Grey and P.W. Smith, Aust. J. Chem. 24 (1971), 73.

123. D.L. Kepert, 'The Early Transition Metals', Academic Press, London, 1972.

124. J.L. Hayden and R.A.D. Wentworth, J. Am. Chem. Soc., 90 (1968), 5291.

125. J.L. Hoard and L. Goldstein, J. Chem. Phys., 3 (1935), 199.

126. J.L. Hoard and L. Goldstein, J. Chem. Phys., 3 (1935), 117.

127. F.J. Brinkman, J. Inorg. Nucl. Chem., 34 (1972), 394.

128. J.D. Donaldson, M.J. Tricker and B.W. Dale, J. Chem. Soc. Dalton Trans., (1972), 893.

129. K. Kihara and T. Sudo, Acta. Cryst., B30 (1974), 1088.

130. R.J.H. Clark and F.B. Taylor, J. Chem. Soc. (A), (1967), 693.

131. A.P. Ginsberg and M.B. Robin, Inorg. Chem., 2 (1963), 817.

132. S.K. Porter and R.A. Jacobson, J. Chem. Soc.(A), (1970), 1359.

133. D.J.W. Ijdo, Ph.D. Thesis, University of Leiden, 1960.

134. D.G. Tisley and R.A. Walton, J. Chem. Soc. Dalton Trans., (1973), 1039.

135. J.I. Bullock, F.W. Parrett and N.J. Taylor, Canad. J. Chem., 52 (1974), 2880.

136. T.J. Kistenmacher and G.D. Stucky, Inorg. Chem., 10 (1971), 122.

137. M.M. Crozat and S.F. Watkins, J. Chem. Soc. Dalton Trans., (1972), 2512.

138. F.A. Cotton and B.J. Kalbacher, Inorg. Chem., 15 (1976), 522.

139. D.F. Hornig, J. Chem. Phys., 16 (1948), 1063.

140. R.S. Halford, J. Chem. Phys., 14 (1946), 8.

141. S.D. Ross, 'Inorganic Infrared and Raman Spectra', McGraw-Hill, London, 1972.

142. W.G. Fateley, F.R. Dollish, N.T. McDevitt and F.F. Bentley, 'Infrared and Raman Selection Rules for Molecular and Lattice Vibrations: The Correlation Method', Wiley Interscience, New York, 1972.

143. A. Hezel and S.D. Ross, Spectrochim. Acta., 22 (1966), 1949.

144. K. Nakamoto, 'Infrared Spectra of Inorganic and Coordination Compounds', 1st Edition, John Wiley, New York, 1963.

145. C. Rocchiciolli, Compt. Rend., 242 (1956), 2922.

146. S. Bhagavantum and T. Venkatarayudu, Proc. Indian Acad. Sci., 9 (1939), 224; S. Bhagavantum, ibid, 13 (1941), 543.

147. S. Bhagavantum and T. Venkatarayudu, 'Theory of Groups and its Application to Physical Problems', 2nd Edition, Bangalore Press, Bangalore City, India, 1951.

148. D.M. Adams and D.C. Newton, 'Tables for Factor Group Analysis and Point Group Analysis', Beckman-RIIC Ltd., England, 1970.

149. E. Knözinger, Angew. Chem. Int. Ed. Engl. Transl., 15 (1976), 25.

150. D.M. Adams, Proc. Chem. Soc., (1961), 335.

151. T.L. Brown, W.G. McDugle and L.G. Kent, J. Am. Chem. Soc., 92 (1970), 3645.

152. J. Hiraishi and T. Shimanouchi, Spectrochim. Acta., 22 (1966), 1483.

153. D.M. Adams and H.A. Gebbie, Spectrochim. Acta., 19 (1963), 925.

154. P.J. Hendra and P.J.D. Park, Spectrochim. Acta., 23A (1967), 1635.

155. M. Debeau and A. Poulet, Spectrochim. Acta., 25A (1969), 1553.

156. M. Debeau, Spectrochim. Acta., 25A (1969), 1311.

157. S.N. Rai, S.N. Thakur and D.K. Rai, Ind. J. Pure and Appl. Phys., 9 (1971), 243.

158. Y.M. Bosworth and R.J.H. Clark, J. Chem. Soc. (A), (1974), 1749.

159. P.L. Goggin and J.R. Knight, J. Chem. Soc. Dalton Trans., (1973), 1489.

160. F. Herbelin, J.D., Herbelin, J.P. Mathieu and H. Poulet, Spectrochim. Acta., 22 (1966), 1515.

161. J.M. Jenkins and B.L. Shaw, J. Chem. Soc., (1965), 6789.

162. N.K. Sanyal, D.N. Verma and L. Dixit, Ind. J. Phys., 48 (1974), 481.

163. M. Hass and G.B.B.M. Sutherland, Proc. Roy. Soc. London, A236 (1956), 427.

164. L. Couture-Mathieu and J. Mathieu, Acta. Cryst., 5 (1952), 571.

165. J. van der Elsken and D.W. Robinson, Spectrochim. Acta., 17 (1961), 1249.

166. P.J. Lucchesi and W.J. Glasson, J. Am. Chem. Soc., 78 (1956), 1347.

167. I. Gamo, Bull. Chem. Soc. Japan, 34 (1961), 760.

168. I. Gamo, Bull. Chem. Soc. Japan, 34 (1961), 1433.

169. I. Gamo, Bull. Chem. Soc. Japan, 34 (1961), 1431.

170. G. Herzberg, 'Infrared and Raman Spectra of Polyatomic Molecules', D. Van Nostrand Company Inc., New Jersey, 1945.

171. D.M. Adams and D.M. Morris, J. Chem. Soc. (A), (1967), 1666.

172. D.M. Adams, H.A. Gebbie and R.D. Peacock, Nature, 199 (1963), 278.

173. K.I. Petrov, V.V. Kravchenko and N.M. Sinitsyn, Russ. J. Inorg. Chem., 15 (1970), 1420.

174. A.W. Atkinson, J.R. Chadwick and E. Kinsella, J. Inorg. Nucl. Chem., 30 (1968), 401.

175. T.S. Kuan, Inorg. Chem., 13 (1974), 1256.

176. H.H. Claasen, G.L. Goodman, J.H. Holloway and H. Selig, J. Chem. Phys., 53 (1970), 341.

177. D.M. Adams and P.J. Lock, J. Chem. Soc (A), (1971), 2801.

178. G. Pannetier and R. Bonnaire, J. Less Common Metals, 18 (1969), 411.

179. C.W.F.T. Pistorius, J. Chem. Phys., 29 (1958), 1328.

180. S.E. Adnitt, D.W. Barr, D. Nicholls and K.R. Seddon, J. Chem. Soc. Dalton Trans., (1974), 644.

181. D.M. Adams and D.C. Newton, J. Chem. Soc (A), (1972), 681.

182. S.K. Sharma and D.K. Pandya, J. Inorg. Nucl. Chem., 36 (1974), 1165.

183. M. Falk, Chung-Hsi Huang and O. Knop, Canad. J. Chem., 53 (1975), 51.

184. D.M. Adams, 'Metal-Ligand and Related Vibrations', Edward Arnold, London, 1967.

185. J.D. Black, J.T.R. Dunsmuir, I.W. Forrest and A.P. Lane, Inorg. Chem., 14 (1975), 1257.

186. I.R. Beattie, T.R. Gilson and G.A. Ozin, J. Chem. Soc. (A), (1968), 2765.

187. V.V. Fomichev, K.I. Petrov, G.V. Zimina and V.E. Plyushchev, Russ. J. Inorg. Chem., 18 (1973), 220.

188. R.J. Ziegler and W.M. Risen, Jnr., Inorg. Chem., 11 (1972), 2796.

189. D.M. Adams, J. Chatt, J.M. Davidson and J. Gerratt, J. Chem. Soc., (1963), 2189.

190. P.C. Crouch, G.W.A. Fowles and R.A. Walton, J. Chem. Soc. (A), (1969), 972.

191. J.A. Creighton and J.H.S. Green, J. Chem. Soc. (A), (1968), 808.

192. R.A. Work and M.L. Good, Inorg. Chem., 9 (1970), 956.

193. T.G. Spiro, Inorg. Chem., 4 (1965), 1290.

194. H. G. Dehmelt and H. Krüger, Naturwissenschaften, 37 (1950), 111.

195. S.L. Carr, B.B. Garrett and W.G. Moulton, J. Chem. Phys., 47 (1967), 1170.

196. M. Kubo and D. Nakamura, Adv. Inorg. Chem. and Radiochem., 8 (1966), 257.

197. K. Ito, D. Nakamura, K. Ito and M. Kubo, Inorg. Chem., 2 (1963), 690.

198. D. Nakamura, R. Ikeda and M. Kubo, Coord. Chem. Rev., 17 (1975), 281.

199. T.E. Haas and E.P. Marram, J. Chem. Phys., 43 (1965), 3985.

200. K.W. Bagnall and D. Brown, J. Chem. Soc., (1964), 3021.

201. A. Sasane, T. Matuo, D. Nakamura and M. Kubo, Bull. Chem. Soc. Japan, 43 (1970), 1908.

202. A. Sasane, T. Matuo, D. Nakamura and M. Kubo, J. Mag. Resonance, 4 (1971), 257.

203. C.W. Fryer, J.A.S. Smith, J. Chem. Soc. (A), (1970), 1029.

204. T.B. Brill, P.E. Garrou and G.G. Long, J. Inorg. Nucl. Chem., 33 (1971), 3285.

205. P.A. Van Dalen and M.J. Steenland, Physica, 36 (1967), 275.

206. G.P. O'Leary and R.G. Wheeler, Phys. Rev., B1 (1970), 4409.

207. A. Sasane, D. Nakamura and M. Kubo, J. Mag. Resonance, 3 (1970), 76.

208. R.L. Armstrong and H.M. Van Driel, Canad. J. Phys., 50 (1972), 2048.

209. G.P. O'Leary, Phys. Rev. Lts., 23 (1969), 782.

210. D. Nakamura and M. Kubo, J. Phys. Chem., 68 (1964), 2986.

211. R.H. Busey, H.H. Dearman and R.B. Bevan, Jnr., J. Phys. Chem., 66 (1962), 82.

212. H.W. Willemsen, R.L. Armstrong and P.M. Meincke, J. Low Temp. Phys., 26 (1977), 299.

213. T.B. Brill and G.G. Long, J. Phys. Chem., 75 (1971), 1898.

214. D. Nakamura, K. Ito and M. Kubo, J. Am. Chem. Soc., 84 (1962), 163.

215. I.D. Brown, Canad. J. Chem., 42 (1964), 2758.

216. R.A. Johnson and M.T. Rogers, J. Mag. Resonance, 15 (1974), 584.

217. P.W. Smith and R. Stoessiger, Mol. Phys., 17 (1969), 503.

218. P.W. Smith and R. Stoessiger, Private communication.

219. F.A. Cotton and C.B. Harris, Inorg. Chem., 6 (1967), 376.

220. J.H.E. Griffiths, J. Owen and I.M. Ward, Proc. Roy. Soc., Ser. A, 219 (1953), 526.

221. E.A.C. Lucken, 'Nuclear Quadrupole Coupling Constants', Academic Press, New York, 1969.

222. L.D. Landau and E.M. Lifshitz, 'Statistical Physics', 1st Edition, Pergamon Press, London, 1958.

223. H.A.O. Hill and P. Day (Editors), 'Physical Methods in Advanced Inorganic Chemistry', Interscience, London, 1968; Article by H. Sillescu.

224. C.K. Jørgensen, J. Inorg. Nucl. Chem., 24 (1962), 1587.

225. B.D. Bird, P. Day and E.A. Grant, J. Chem. Soc. (A), (1970), 100.

226. C.K. Jørgensen, Mol. Phys., 4 (1961), 235.

227. C.K. Jørgensen, Mol. Phys., 2 (1959), 309.

228. Y. Inamura and Y. Kondo, J. Chem. Soc. Japan, 72 (1951), 787, 840.

229. C.K. Jørgensen, Acta. Chem. Scand., 11 (1957), 151.

230. A.V. Babaeva and R.I. Rudyi, Zhur. Neorg. Khim., 1 (1956), 921.

231. D. Sutton, 'Electronic Spectra of Transition Metal Complexes', McGraw-Hill, London, 1968.

232. B.N. Figgis, 'Introduction to Ligand Fields', Interscience Publishers, 1967.

233. J. Lewis, R.S. Nyholm and P.W. Smith, J. Chem. Soc. (A), (1969), 57.

234. C.K. Jørgensen, Acta. Chem. Scand., 11 (1957), 73.

235. E. König, Inorg. Chem., 2 (1963), 1238.

236. R. Saillant, J.L. Hayden and R.A.D. Wentworth, Inorg. Chem., 6 (1967), 1497.

237. F.C. Jahoda, Phys. Rev., 107 (1957), 1261.

238. P.W. Smith and A.G. Wedd, J. Chem. Soc. (A), (1970), 2447.

239. I. Feldman, R.S. Nyholm and E. Watton, J. Chem. Soc., (1965), 4724.

240. J.R. Gaylor and C.V. Senoff, Inorg. Chem., 11 (1972), 2551.

241. E.W. Stout and B.B. Garrett, Inorg. Chem., 12 (1973), 2565.

242. G.M. Cole and B.B. Garrett, Inorg. Chem., 13 (1974), 2680.

243. J.E. Fergusson and P.F. Heveldt, Aust. J. Chem., 27 (1974), 661.

244. M. Renniger, Z. Krist, 97 (1937), 107.

245. W.R. Busing and H.A. Levy, ORNL-4054, Oak Ridge National Laboratory, U.S.A. (1967).

246. T.C. Furnas, 'Single Crystal Orienter - Instruction Manual', General Electric Company, Milwaukee, U.S.A. (1966).

247. P.W.R. Corfield, R.J. Doedens and J.A. Ibers, Inorg. Chem., 6 (1967), 197.

248. D.F. Grant, R.C.G. Killean and J.L. Lawrence, Acta. Cryst., B25 (1969), 374.

249. W.T. Robinson and J.A. Ibers, Inorg. Chem., 6 (1967), 1208.

250. Abstract E10, Am. Cryst. Assoc., Storrs, Conn., 1973.

251. G. Sheldrick, SHELX76, Programme for Crystal Structure Determination, Cambridge, 1975.

252. A. Zalkin, FORDAP, A Fortran Programme for Fourier Calculations, University of California, Berkeley, 1965.

253. W.R. Busing, K.O. Martin and H.A. Levy, ORFLS, Oak Ridge National Laboratory Report, ORNL-TM-305, 1963.

254. D.T. Cromer and J.B. Mann, Acta. Cryst., A24 (1968), 321.

255. D.T. Cromer, Acta. Cryst., 18 (1965), 17.

256. D.T. Cromer and D. Liberman, J. Chem. Phys., 53 (1970), 1891.

257. H.A. Levy, Acta. Cryst., 9 (1956), 679.

258. W.J.A.M. Peterse and J.H. Palm, Acta. Cryst., 20 (1966), 147.

259. C.K. Johnson, ORTEP, A Fortran Thermal-Ellipsoid Plot Programme for Crystal Structure Illustrations, Oak Ridge National Laboratory Report, ORNL-3794, 1965.

260. P.G. Hambling, Acta. Cryst., 6 (1953), 98.

261. POWDER, A Fortran Programme for Calculation of Interplanar d. Spacings and Refinement of Unit Cell Dimensions.

262. W.D. Gwinn, J. Chem. Phys., 55 (1971), 477.

263. J.A. Lingane and L.A. Small, J. Am. Chem. Soc., 71 (1949), 974.

264. J. Lewis, R.S. Nyholm and P.W. Smith, J. Chem. Soc. (A), (1969), 57.

265. J.E. Fergusson, Private communication.

266. M.J. Buerger, 'Vector Space and its Application in Crystal Structure Investigation', Wiley, New York, 1959.

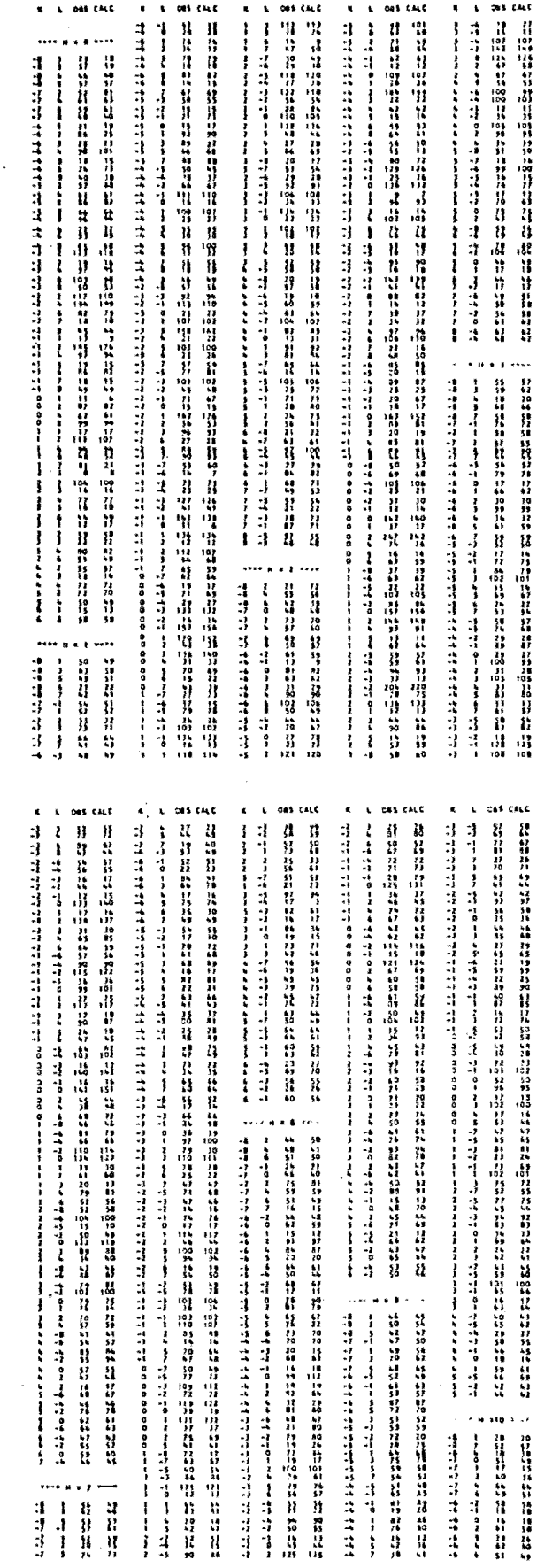

Appendix A: Calculated and Observed Structure Factors for $K_3[IrCl_6]$.

Appendix B: Calculated and Observed Structure Factors for $K_3[IrCl_6]H_2O$.

Appendix C; Calculated and Observed Structure Factors for $(NH_4)_3[IrCl_6]H_2O$.

H	L	OBS	CALC
**** K = 0 ****			
-11	7	130	126
-11	10	58	65
-10	1	99	107
-10	7	185	182
-10	9	92	84
-9	4	60	57
-8	1	223	238
-8	2	200	216
-8	3	226	242
-7	10	132	121
-7	11	88	86
-6	0	63	71
-6	6	116	114
-6	14	55	44
-5	4	168	160
-5	5	242	234
-5	7	124	112
-5	8	218	199
-4	4	245	224
-4	8	146	140
-3	5	227	200
-3	9	59	57
-3	16	53	49
-2	4	114	104
-2	6	418	398
-2	13	49	45
-1	8	204	192
-1	14	175	171
0	2	185	158
0	4	66	58
0	6	128	108
0	10	315	309
0	14	149	138
0	16	201	199
1	2	435	403
1	4	63	52
1	5	59	48
1	6	67	50
1	9	87	85
1	16	63	61
2	0	311	323
2	5	770	782
2	7	199	191
2	9	155	140
2	10	172	164
2	11	112	114
2	12	64	61
2	14	161	158
2	15	181	178
3	1	101	100
3	4	324	280
3	7	126	118
3	8	192	177
3	10	53	50
3	11	117	107
3	12	146	138
4	0	360	375
4	1	330	341
4	6	281	242
4	7	144	120
4	9	317	301
4	10	398	372
4	11	185	172
4	12	181	166
5	1	93	102
5	9	192	169
5	10	115	100
5	11	218	202
5	12	145	137
6	1	68	71
6	3	357	394
6	4	373	380
6	5	181	170
6	7	59	63
6	10	100	88
6	12	96	89
7	1	162	163
7	2	169	184
7	6	277	275
7	7	101	93
7	9	113	108
7	14	69	64
8	0	82	82
8	8	125	133
8	11	329	356
8	12	59	58
10	2	112	119
10	8	70	67
11	6	145	141
11	9	112	109
12	1	63	67
12	7	173	170
13	5	119	119
14	1	55	50
**** K = 1 ****			
-12	6	111	103
-11	6	89	86
-11	8	162	158
-10	5	117	112
-9	4	105	106
-9	12	64	64
-8	1	56	61
-8	6	112	113
-8	8	65	59
-8	10	149	149
-8	12	98	88
-7	4	187	193
-7	8	128	121
-7	9	57	52
-7	11	52	49
-7	12	89	83
-6	0	176	190
-6	1	116	125
-6	2	98	103
-6	10	129	118
-5	2	134	142
-5	5	111	101
-5	8	183	171
-5	11	151	150
-5	15	94	89
-4	8	102	88
-4	10	170	162
-3	9	124	116
-3	14	94	93
-2	4	198	174
-2	6	49	41
-2	9	139	142
0	1	235	256
0	3	301	290
0	5	44	48
0	7	198	198
0	9	46	47
0	13	217	217
1	5	325	310
1	7	101	98
1	8	76	74
1	9	56	51
1	11	164	167
1	12	77	82
1	13	48	39
1	15	72	79
2	0	151	153
2	1	100	97
2	3	189	162
2	5	93	80
2	7	253	245
2	11	49	54
2	13	180	184
2	14	78	79
3	1	258	265
3	8	115	108
3	11	86	88
3	15	104	101
4	0	82	83
4	1	142	146
4	2	156	152
4	7	192	174
4	9	152	145
4	12	48	39
5	6	101	99
5	9	186	173
6	3	204	213
6	11	65	52
7	1	55	56
7	2	141	154
7	3	116	116
7	5	103	101
8	3	77	75
8	9	100	87
8	11	103	97
9	1	81	92
9	2	206	220
9	6	76	65
10	0	136	145
10	4	61	64
10	6	174	164
10	10	85	84
11	3	68	65
12	0	210	227
13	3	56	52
**** K = 2 ****			
-12	0	98	96
-12	1	166	176
-12	3	121	118
-10	1	75	80
-10	2	80	81
-10	4	165	166
-10	6	82	83
-9	1	92	99
-9	9	145	138
-8	9	217	205
-8	10	108	106
-7	3	97	100
-7	4	112	111
-7	6	68	66
-6	1	168	174
-6	5	133	126
-6	8	54	55
-6	12	66	67
-5	6	160	144
-5	7	130	122
-4	1	55	51
-4	7	110	104
-4	10	59	54
-3	1	351	373
-3	4	147	128
-3	5	117	105
-3	6	68	59
-2	0	280	280
-2	10	130	139
-2	12	129	131
-1	7	195	204
-1	8	475	531
0	0	448	387
0	2	87	80
0	4	56	54
0	6	387	421
0	8	127	129
0	10	129	144
0	14	103	106
1	1	140	134
1	2	58	54
1	4	65	64
1	6	216	225
1	12	128	134
1	13	186	206
1	14	128	135
2	1	229	232
2	3	202	175
2	4	101	87
2	6	274	278
2	8	93	95
2	11	126	125
2	14	80	76
3	8	118	116
3	9	116	122
3	13	158	164
3	15	48	52
4	0	273	282
4	4	306	281
4	9	70	69
4	11	105	108
4	12	116	114
5	1	117	125
5	2	190	196
5	3	262	262
5	4	371	363
5	5	187	168
5	11	117	118
5	12	124	125
5	13	86	79
6	0	81	84
6	2	262	278
6	3	274	284
6	4	63	55
6	6	55	48
6	10	107	105
6	14	93	91
7	1	93	99
7	5	169	154
7	7	86	76
7	8	138	128
7	9	221	214
7	11	213	212
7	12	103	100
8	0	55	49
8	2	177	190
8	6	55	46
8	7	266	249
8	8	85	82
8	11	62	59
8	12	59	67
9	4	110	108
9	5	134	131
9	6	149	141
9	7	91	85
9	11	74	63
10	7	206	207
10	9	109	98
11	1	163	174
11	4	56	53
11	5	99	100
12	2	69	67
13	1	105	108
**** K = 3 ****			
-12	6	86	81
-11	2	89	97
-11	6	67	66
-10	4	72	68
-10	6	132	132
-9	6	54	44
-9	8	74	69
-8	6	141	131
-8	8	57	52
-8	12	83	76
-7	5	99	92
-7	8	146	145
-6	0	126	125
-6	1	64	64
-6	3	173	173
-6	10	125	122
-6	12	46	40
-5	5	89	81
-5	8	128	125
-5	11	98	104
-5	14	52	59
-4	2	111	114
-3	2	116	116
-3	14	69	69
-2	4	62	62
-2	7	192	203
0	1	118	115
0	3	186	181
0	7	207	228
0	11	55	61
0	13	179	195
1	1	127	123
1	5	248	272
1	7	88	93
1	8	56	60
1	9	74	83
1	11	152	166
1	12	66	78
1	13	45	28
2	0	103	102
2	1	109	113
2	3	156	151
2	6	79	81
2	9	101	107
2	10	46	44
2	13	143	152
3	1	269	268
3	5	154	145
3	8	72	75
3	9	65	64
3	10	60	58
3	12	54	55
4	0	149	150
4	1	157	161
4	4	74	68
4	7	104	101
4	8	62	56
4	9	87	89
4	10	99	97
5	1	81	85
5	2	152	153
5	6	127	116
5	7	80	78
5	9	134	128
6	2	45	48
6	4	177	166
6	5	73	65
6	8	52	47
6	9	57	52
6	11	82	75
7	2	95	101
7	3	61	60
7	4	141	137
7	9	77	73
7	11	57	59
7	12	81	77
8	4	120	122
8	10	161	160
8	11	80	72
9	1	56	56
9	2	148	161
9	4	112	112
10	0	149	164
10	5	128	125
11	8	95	97
12	0	211	222
**** K = 4 ****			
-10	1	92	94
-8	1	159	168
-8	2	119	125
-8	3	180	179
-8	4	55	59
-8	8	74	73
-7	5	103	97
-6	4	241	231
-6	5	143	134
-6	9	51	51
-6	10	79	80
-5	4	101	95
-5	8	134	126
-5	12	86	89
-4	3	114	113
-4	6	187	176
-4	7	90	86
-4	9	172	178
-4	10	254	261
-4	11	104	102
-3	2	109	104
-3	5	133	129
-3	7	56	56
-3	12	116	125
-2	9	97	107
-2	11	63	65
0	0	796	820
0	2	117	114
0	6	106	116
0	10	139	148
0	14	111	116
1	1	85	86
1	2	276	275
1	3	52	49
1	6	61	59
1	8	121	133
1	9	50	64
1	14	120	126
2	0	258	249
2	5	392	428
2	6	234	241
2	7	123	129
2	10	102	109
2	12	46	40
2	14	103	104
3	1	57	61
3	4	213	208
3	8	150	155
3	11	82	84
4	0	182	187
4	1	141	145
4	2	69	71
4	4	157	145
4	5	57	52
4	8	89	88
4	12	110	114
4	13	54	60
5	5	173	165
5	6	99	96
5	7	92	87
5	9	127	128
5	10	65	60
5	11	143	152
6	3	247	248
6	11	104	105
6	12	75	64
7	1	125	133
7	2	107	113
7	4	80	79
7	6	192	181
7	7	60	53
7	9	77	78
7	10	91	86
7	11	72	61
8	0	87	89
9	1	233	243
10	7	125	127
11	4	71	75
11	5	88	90
**** K = 5 ****			
-9	3	57	55
-7	3	77	75
-7	4	125	118
-7	5	66	63
-6	1	83	87
-6	3	118	118
-5	4	80	73
-5	5	87	88
-5	9	105	106
-5	11	92	93
-4	3	83	83
-3	7	50	55
-2	3	123	122
-2	4	119	120
-2	7	139	152
-1	1	199	176
0	1	172	161
0	3	199	200
0	7	75	84
1	5	159	178
1	7	51	42
1	11	92	93
2	1	82	70
2	2	62	53
2	9	82	86
3	1	101	102
3	5	127	127
3	8	85	87
3	9	110	109
3	11	89	94
4	1	49	53
4	6	80	85
4	7	155	151
4	9	122	121
4	10	98	103
5	3	70	68
5	8	135	133
6	2	99	95
6	4	69	72
6	6	58	55
6	10	90	84
7	1	57	50
7	2	145	150
8	0	115	118
8	3	70	70
8	4	110	115
9	2	129	136
9	4	71	73
**** K = 6 ****			
-6	3	145	142
-5	1	79	74
-5	3	103	106
-5	5	96	93
-4	0	145	142
-4	10	47	48
-2	4	82	87
-2	8	59	53
-2	9	70	79
0	0	158	150
0	6	215	218
0	10	111	114
1	1	76	69
1	3	140	139
1	6	110	115
1	8	232	248
2	0	180	163
2	1	109	94
2	3	68	65
2	6	119	129
2	7	52	36
2	10	74	80
3	1	148	144
3	2	231	221
3	3	113	106
3	4	79	83
3	5	27	27
4	3	161	163
4	4	142	143
5	2	129	133
5	4	156	146
6	1	77	82
6	2	132	127
6	6	56	47
7	3	65	68
7	5	97	94
**** K = 7 ****			
-6	3	74	78
-5	2	93	89
-4	0	117	110
-3	5	75	76
0	3	77	81
0	7	135	130
1	5	136	137
2	1	74	74
2	3	94	93
2	6	63	60
2	7	95	100
3	1	138	137
4	1	86	87
4	3	109	105
5	1	81	75
6	4	75	80
**** K = 8 ****			
-2	0	122	114
0	0	257	249
1	2	125	117

Appendix D: Calculated and Observed Structure Factors for $Rb_3[IrBr_6]H_2O$.

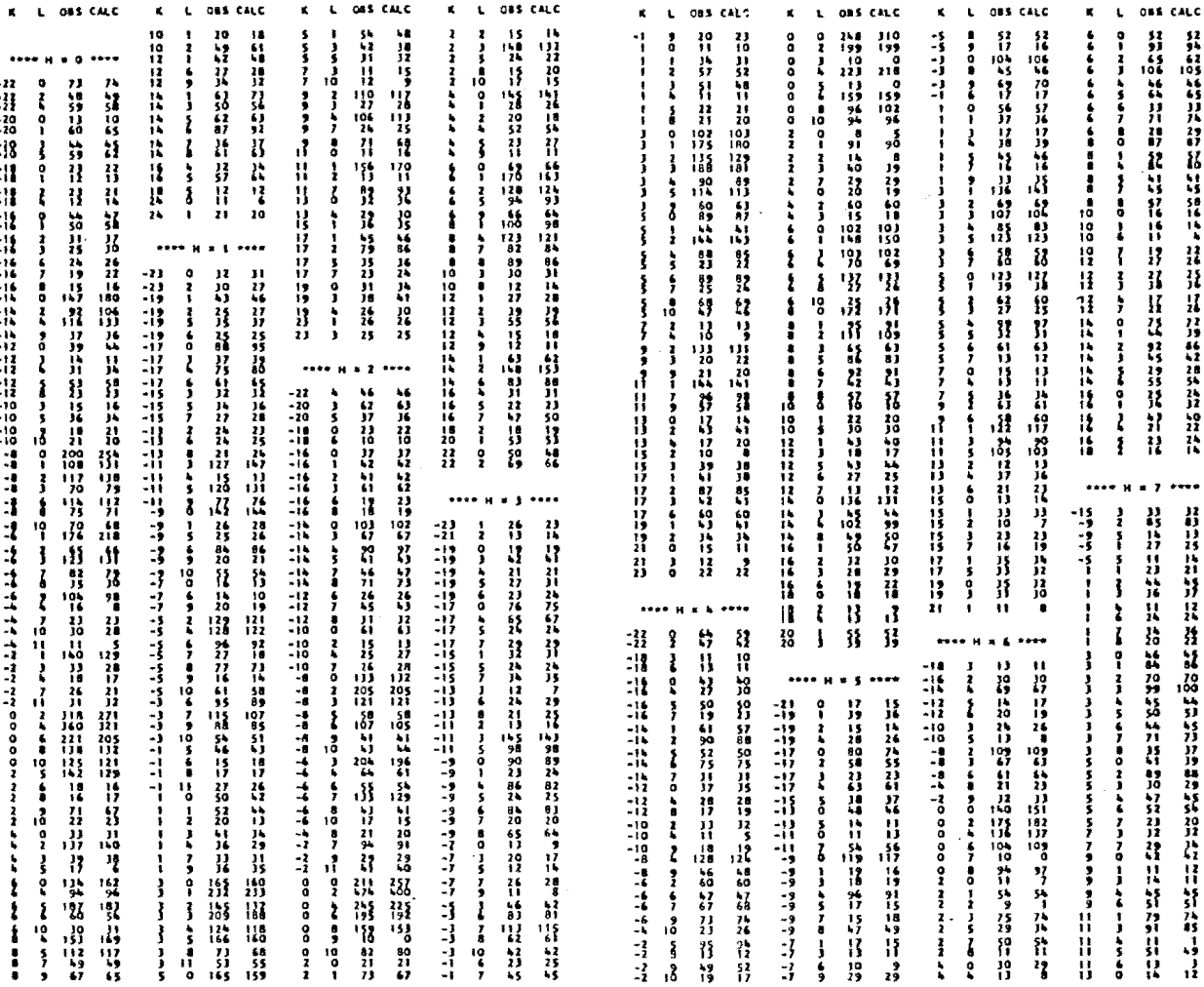

Appendix E: Calculated and Observed Structure Factors for $Cs_2[IrCl_5(H_2O)]$

H	L	OBS	CALC
**** K = 0 ****			
0	4	784	828
0	8	458	470
0	10	45	46
0	18	30	31
0	20	44	43
2	2	549	539
2	6	387	395
2	10	247	252
2	18	71	72
4	4	626	661
4	6	28	23
4	18	27	29
6	0	31	29
6	6	308	311
8	2	15	15
8	4	397	406
8	16	29	20
10	4	47	41
10	6	206	207
10	14	86	85
12	0	234	241
12	4	212	213
12	10	17	19
12	14	18	19
14	0	44	46
14	14	53	52
16	0	105	107
16	4	98	96
16	6	14	9
16	12	42	43
**** K = 1 ****			
1	1	387	337
1	3	260	243
3	3	183	179
3	5	230	227
3	13	98	99
5	1	287	285
5	5	258	254
5	13	106	107
7	1	145	145
7	9	113	114
7	13	73	73
7	15	31	31
9	1	193	194
9	9	134	135
9	13	80	81
9	15	39	41
11	1	81	83
13	1	113	114
13	11	47	47
15	1	48	49
15	5	48	50
15	13	26	28
17	1	55	57
17	7	38	38
17	9	40	41
17	11	26	26
**** K = 2 ****			
0	4	15	15
0	12	15	11
2	2	416	382
2	4	438	436
2	8	270	270
2	10	82	82
2	12	139	140
2	14	19	18
2	16	65	66
4	10	220	221
4	14	127	128
6	2	198	203
6	4	333	337
6	8	222	221
6	12	118	119
6	16	59	57
8	18	49	48
10	8	153	153
10	12	86	87
12	14	53	55
14	0	142	143
**** K = 3 ****			
1	7	111	111
1	11	65	66
1	17	49	50
3	3	131	130
3	5	183	180
3	7	82	82
3	9	137	137
3	13	83	86
3	17	40	45
3	19	20	23
5	7	117	117
5	15	41	43
7	11	36	36
7	13	63	63
9	1	165	164
9	7	96	95
9	13	72	72
9	15	37	36
9	17	37	37
11	3	51	51
11	9	60	60
11	13	41	41
13	13	47	45
15	1	40	41
15	3	38	35
15	11	21	20
17	5	47	47
**** K = 4 ****			
0	14	41	42
4	4	560	551
4	6	22	20
4	8	356	354
4	16	87	87
6	8	18	16
6	14	108	108
6	18	54	55
8	12	133	134
8	14	27	27
10	4	37	37
10	8	28	27
10	10	128	128
10	12	20	17
10	14	81	77
12	4	186	189
12	12	80	78
14	4	35	37
14	14	46	47
**** K = 5 ****			
3	5	216	211
3	11	69	71
5	5	236	231
5	11	85	85
5	13	100	100
7	1	146	145
7	7	79	79
7	11	50	51
7	15	32	32
9	1	181	181
9	5	169	168
9	9	125	125
9	11	69	69
9	13	76	75
9	15	39	39
11	1	86	86
11	13	45	45
11	15	20	23
13	3	95	94
13	13	45	46
15	5	49	49
17	1	53	53
**** K = 6 ****			
0	8	17	17
0	12	16	13
2	6	126	128
2	10	51	52
4	6	271	270
4	10	186	183
6	6	79	82
6	8	182	183
6	10	32	31
6	12	102	102
6	16	52	50
8	12	14	11
8	14	81	78
10	8	129	129
10	12	79	75
10	16	38	38
12	14	47	48
**** K = 7 ****			
1	11	47	47
3	7	60	53
3	15	24	26
3	17	34	34
5	5	143	142
7	1	72	72
7	7	39	36
7	11	28	27
7	15	23	21
9	9	88	86
9	11	44	45
9	13	57	54
9	15	26	28
11	15	19	16
13	5	69	69
13	13	33	35
17	5	38	36
17	7	24	26
**** K = 8 ****			
0	8	274	273
0	10	30	30
0	16	72	70
4	8	242	241
4	16	64	64
8	8	169	168
8	10	23	20
8	12	101	96
8	16	48	47
10	10	93	92
10	12	16	14
12	0	149	150
12	12	59	58
**** K = 9 ****			
1	11	70	70
3	5	157	155
3	9	119	118
5	7	113	110
5	17	37	38
7	7	68	68
9	9	93	93
9	11	57	54
9	15	29	31
11	11	28	30
13	9	57	57
13	11	32	35
**** K =10 ****			
0	10	144	143
2	10	24	18
2	16	44	44
6	10	17	10
8	14	59	57
10	12	58	55
**** K =11 ****			
1	11	31	32
1	15	20	23
5	11	32	35
7	11	22	21
11	3	28	27
11	13	26	22
**** K =12 ****			
0	12	09	87
4	14	17	17
**** K =13 ****			
7	7	45	47
11	7	33	32
13	1	50	50
**** K =14 ****			
2	8	92	92
**** K =15 ****			
**** K =16 ****			
**** K =17 ****			
5	5	47	49

Appendix F: Calculated and Observed Structure Factors for $Cs_2[IrCl_6]$.

OBSERVED AND CALCULATED STRUCTURE FACTORS FOR NME4)3RH2BR9

H	K	L	FO	FC	H	K	L	FO	FC	H	K	L	FO	FC	H	K	L	FO	FC	H	K	L	FO	FC
0	1	0	188	-204	-2	6	1	100	101	-1	8	2	31	-27	-3	7	4	14	-6	0	3	6	196	210
-1	2	0	182	173	-1	6	1	30	-27	-4	9	2	19	14	-2	7	4	38	-8	-2	4	6	68	77
0	2	0	86	-103	0	6	1	17	13	-5	10	2	18	-18	-1	7	4	39	18	-1	4	6	59	-59
-1	3	0	71	69	-3	7	1	43	-47	0	2	3	187	-205	-4	8	4	75	-6	0	4	6	53	-57
0	3	0	29	-19	-2	7	1	22	9	-1	3	3	109	-32	-3	8	4	36	43	-2	5	6	47	12
-2	4	0	147	192	0	7	1	37	-43	0	3	3	231	244	-2	9	4	74	-29	-1	5	6	42	57
-1	4	0	99	-83	-2	8	1	24	-22	-1	4	3	67	-55	-1	8	4	33	-25	0	5	6	40	-48
0	4	0	27	-31	-1	8	1	30	-7	-2	5	3	18	-16	-4	9	4	21	-3	-3	6	6	37	-31
-2	5	0	153	-141	0	8	1	44	55	-1	5	3	71	-73	-3	9	4	18	-19	-2	6	6	48	-9
-1	5	0	130	130	-2	9	1	40	38	0	5	3	33	43	-2	9	4	18	18	-1	6	6	51	-45
0	5	0	14	19	-1	9	1	32	-37	-2	6	3	44	9	0	1	5	84	96	0	6	6	77	97
-3	6	0	216	231	-4	10	1	26	30	-1	6	3	77	58	0	2	5	15	-17	-3	7	6	24	-22
-2	6	0	90	-46	0	0	2	206	-220	0	6	3	58	-63	-1	3	5	131	145	-2	7	6	54	68
-1	6	0	62	-24	0	1	2	40	47	-3	7	3	24	17	0	3	5	132	-148	-1	7	6	30	-32
-3	7	0	24	-25	-1	2	2	84	-86	-1	7	3	44	-9	-1	4	5	31	-35	0	7	6	22	-26
-2	7	0	33	32	0	2	2	96	-110	-3	8	3	34	-32	0	4	5	73	80	-4	8	6	64	69
-1	7	0	30	-24	-1	3	2	95	97	-2	8	3	33	-21	-2	5	5	37	34	-3	8	6	39	-37
-2	8	0	35	-6	0	3	2	37	-42	-1	8	3	35	26	-1	5	5	36	32	-2	8	6	28	-24
-1	8	0	61	64	-2	4	2	74	-80	-4	9	3	35	-4	0	5	5	76	-79	-4	9	6	25	-22
0	8	0	31	-34	-1	4	2	29	-35	-3	9	3	21	27	-2	6	5	32	-32	-3	9	6	29	39
-3	9	0	33	32	0	4	2	47	58	0	0	4	197	-194	-1	6	5	44	22	-2	9	6	21	-13
-2	9	0	35	-18	-2	5	2	43	44	0	1	4	46	40	0	6	5	31	34	-1	9	6	21	-2
-1	9	0	37	-33	-1	5	2	60	-62	-1	2	4	79	-27	-3	7	5	25	29	0	1	7	81	88
-5	10	0	32	42	0	5	2	56	67	0	2	4	215	234	-2	7	5	70	-12	0	2	7	214	234
-4	10	0	20	-15	-1	6	2	83	-87	-1	3	4	127	-124	-1	7	5	45	-42	-1	3	7	173	-177
0	1	1	233	-276	-2	6	2	53	46	0	3	4	15	-26	0	7	5	38	38	0	3	7	66	-77
0	2	1	12	-12	-1	6	2	28	-25	-2	4	4	93	-82	-3	8	5	26	-25	-1	4	7	91	89
-1	3	1	31	15	0	6	2	16	-20	-1	4	4	116	115	-2	8	5	45	48	0	4	7	106	-111
0	3	1	19	17	-3	7	2	22	21	-2	5	4	47	52	-4	9	5	39	37	-2	5	7	48	50
-1	4	1	83	90	-2	7	2	33	-28	-1	5	4	55	-42	-3	9	5	17	-15	-1	5	7	89	23
0	4	1	19	-25	-1	7	2	15	13	0	5	4	84	-98	0	0	6	245	-244	0	5	7	75	81
-2	5	1	164	-178	-4	8	2	47	-16	-3	6	4	34	-38	-1	2	6	133	143	-2	5	7	46	2
-1	5	1	84	-16	-3	8	2	17	-14	-2	6	4	18	-15	0	2	6	84	-91	-1	6	7	74	-85
0	5	1	27	30	-2	8	2	29	30	-1	6	4	82	72	-1	3	6	103	-109	-3	7	7	46	-40

OBSERVED AND CALCULATED STRUCTURE FACTORS FOR NME43RH2BR9

H	K	L	FO	FC	H	K	L	FO	FC	H	K	L	FO	FC	H	K	L	FO	FC	H	K	L	FO	FC
-2	7	7	22	-11	-1	4	9	24	5	-2	6	11	32	-12	-2	6	13	61	62	-1	3	17	34	26
-1	7	7	64	69	0	4	9	45	48	-1	6	11	57	56	-1	6	13	24	-24	0	3	17	70	-72
0	7	7	28	-26	-1	5	9	27	11	0	6	11	35	-38	-3	7	13	30	-36	0	4	17	17	19
-3	8	7	60	67	0	5	9	45	-48	-3	7	11	28	26	0	0	14	259	-267	-1	5	17	16	15
-2	8	7	40	-39	-1	6	9	22	6	-1	7	11	30	-20	0	1	14	67	67	0	5	17	19	-26
-1	8	7	39	-3	0	6	9	29	34	-3	8	11	33	-34	-1	2	14	43	-34	-2	6	17	20	-18
-4	9	7	41	-40	-1	7	9	28	-20	-2	8	11	21	-4	0	2	14	25	27	0	6	17	21	22
0	0	8	194	208	-2	8	9	22	21	-1	8	11	24	16	-1	3	14	24	-25	0	0	18	58	71
-1	2	8	125	-132	-4	9	9	23	15	0	0	12	122	109	0	3	14	16	15	-1	2	18	27	22
0	2	9	64	65	0	0	10	49	35	0	1	12	61	-61	-2	4	14	68	-68	0	2	19	60	-63
-1	3	8	89	90	-1	2	10	53	-32	-1	2	12	91	87	-1	4	14	40	27	-1	3	19	32	27
0	3	8	155	-163	0	2	10	113	-108	0	2	12	37	39	0	4	14	16	14	-2	4	18	36	34
-2	4	8	24	-22	-1	3	10	93	96	-1	3	12	70	-74	-2	5	14	62	59	-1	4	18	36	-39
-1	4	8	60	41	0	3	10	20	-25	0	3	12	49	53	-1	5	14	51	-52	-2	5	18	16	-21
0	4	8	23	13	-2	4	10	50	3	-2	4	12	50	46	-3	6	14	89	-95	-1	5	18	19	23
-2	5	8	49	-35	-1	4	10	44	-54	0	4	12	22	-25	-2	6	14	44	24	0	5	18	24	24
-1	5	8	34	-34	0	4	10	21	21	-2	5	12	24	-23	-1	6	14	28	12	-1	6	18	25	-25
0	5	8	54	58	-2	5	10	21	-13	-1	5	12	54	54	-3	7	14	17	11	0	1	19	31	-28
-3	6	8	36	35	-1	5	10	26	-1	0	5	12	56	-63	-2	7	14	16	-11	-1	3	19	46	-42
-2	6	8	47	5	0	5	10	64	74	-3	6	12	63	66	0	1	15	106	90	0	3	19	37	36
-1	6	8	50	38	-2	6	10	23	25	-2	6	12	38	-37	-1	4	15	38	-30	-1	4	19	24	25
0	6	8	69	-76	-1	6	10	50	-42	0	6	12	21	27	-2	5	15	70	68	0	4	19	26	-23
-3	7	8	28	27	-2	7	10	27	-12	-3	7	12	26	-30	-1	5	15	37	15	-2	5	19	19	-21
-2	7	8	52	-58	-1	7	10	20	2	-2	7	12	35	35	-2	6	15	38	-32	0	5	19	27	28
-1	7	8	20	13	-4	8	10	49	-12	-1	7	12	18	-4	-3	7	15	16	11	0	0	20	22	24
0	7	8	21	18	-2	8	10	73	29	-4	8	12	38	25	0	0	16	65	58	-1	2	20	31	-30
-4	8	8	58	-60	-1	8	10	20	0	-2	8	12	25	-24	0	1	16	18	-15	0	2	20	25	24
-3	8	8	25	25	-4	9	10	17	11	0	1	13	130	-133	-1	2	16	18	-5	-1	3	20	22	20
-2	8	8	29	20	0	1	11	24	-12	0	2	13	29	28	0	2	16	29	28	0	3	20	46	-45
-3	9	8	20	-25	0	2	11	125	-141	-1	4	13	36	35	-2	4	16	24	17	-2	4	20	28	-26
-2	9	8	21	13	-1	3	11	55	5	0	4	13	26	-32	-2	5	16	20	-14	-1	4	20	16	13
0	2	9	21	-14	0	3	11	152	163	-2	5	13	81	-86	-1	6	16	21	19	0	4	20	19	18
-1	3	9	81	72	-1	4	11	51	-57	-1	5	13	34	5	0	1	17	24	30	0	2	21	42	-38
0	3	9	83	-87	-1	5	11	43	-43	0	5	13	20	21	0	2	17	26	22	-1	3	21	36	31

OBSERVED AND CALCULATED STRUCTURE FACTORS FOR NME43PH2BR9

H	K	L	FO	FC	H	K	L	FO	FC	H	K	L	FO	FC	H	K	L	FO	FC	H	K	L	FO	FC
-1	4	21	21	-16	0	0	22	39	-46	-1	2	22	19	15	-1	3	22	15	-15					

Appendix G: Calculated and Observed Structure Factors for $[N(CH_3)_4]_3[Rh_2Br_9]$.